The Association of Applied Geochemists presents
the 23rd INTERNATIONAL APPLIED GEOCHEMISTRY SYMPOSIUM (IAGS)

23rd IAGS 2007
Exploring our Environment

EXPLORING OUR ENVIRONMENT

OVIEDO, ASTURIAS. SPAIN
at the PRÍNCIPE FELIPE
CONFERENCE HALL
14 – 19 JUNE 2007



Extended Abstracts

Jointly organized by the Department of Exploration and Mining of the University of Oviedo (Spain), the Geological and Mining Institute of Spain (IGME) and the Association of Applied Geochemists.

AYUNTAMIENTO DE OVIEDO

Universidad de Oviedo

THE ASSOCIATION OF APPLIED GEOCHEMISTS 1970

INSTITUTO GEOLÓGICO Y MINERO DE ESPAÑA

AUDITORIO PALACIO DE CONGRESOS

23rd International Applied Geochemistry Symposium – - IAGS -

Oviedo, 14 – 19 June 2007

IAGS 2007 – Exploring our Environment

Extended Abstracts of the Symposium

Edited by Jorge Loredo Pérez

June, 2007

University of Oviedo, Spain

Editor:
Jorge Loredo Pérez

Published by:
Departamento de Explotación y Prospección de Minas. University of Oviedo. Spain on behalf of The Association of Applied Geochemists (Vancouver, Canadá).

Aditional copies may be obtained from the Secretariat:

Dep. Explotación y Prospección de Minas
Escuela Técnica Superior de Ingenieros de Minas
C/Independencia, 13; 33004 Oviedo, Asturias, SPAIN
Phone: +34 985104205. Fax: +34 985104245

Published 2007

ISBN: 978-84-690-6462-7
Legal Deposit: AS-3015-07

PREFACE

SESION: *Mapping Geochemical Data.*

SESION: *Geochemistry in the industry sector: exploration and environmental applications.*

SESION: *Exploration case studies Symposium in honour of Dr. Eion Cameron*

SESION*: Ore Deposit-Forming Systems: A Geochemical Perspective.*

SESION: *Hydro-bio geochemistry*

SESION: *Data interpretation*

SESION: *Lithogeochemistry*

SESION: *Analytical Geochemistry*

SESION: *Geochemistry and health*

Heavy minerals in gold exploration at Petäjälehto, northern Finland

Pulkkinen Eelis, Keinänen Veikko, Sarala Pertti and V. Juhani Ojala

Geological Survey of Finland
P.O. Box 77, FIN-96101 Rovaniemi, FINLAND.
E-mail: eelis.pulkkinen@gtk.fi
Keywords: gold, heavy minerals, till geochemistry, exploration, Central Lapland, Finland

ABSTRACT

Gold exploration using till geochemical, heavy mineral and geophysical methods was done at the Petäjälehto target, northern Finland. The study area is located in the central part of the last Weichselian glaciation and the bedrock is covered by glaciogenic overburden; the thickness of glacial drift is from 2 to 6 m. Gold concentration in the fine fraction of till (<0.06 mm) is anomalous, varying from 4 to 50 ppb at the several sampling sites in the southern part of the area. In addition to geochemical anomaly, small gold nuggets which size varies from 0.1 to 0.5 mm approximately are found in the area. The number of nuggets can be more than 20 in heavy mineral concentrates. Drilling has revealed several hydrothermally altered deformation zones. The gold mineralization related alteration includes silification, carbonatization and enrichment of magnetite. Width of the intense deformation zones range from 1 to 10 m. Follow-up exploration is continuing.

INTRODUCTION

The Petäjälehto exploration target area is located ca. 80 km to the north from the centre of Sodankylä municipality in northern Finland (Fig. 1). The area is between the Paleoproterozoic Central Lapland Greenstone Belt and Lapland granulite complex and includes some Archaean rocks (Lehtonen et al.1998). The rocks have been metamorphosed at amphibolite facies conditions. Central Lapland situates in the area, which was the central part of the last Weichselian glaciation. The bedrock is covered by several metres of Quaternary glaciogenic deposits. In places, up to tens of metres thick Pre-Quarternary regolith has been preserved. However, typically the weathering crust is couple of metres thick and consists of the saprock part of the weathering profile.

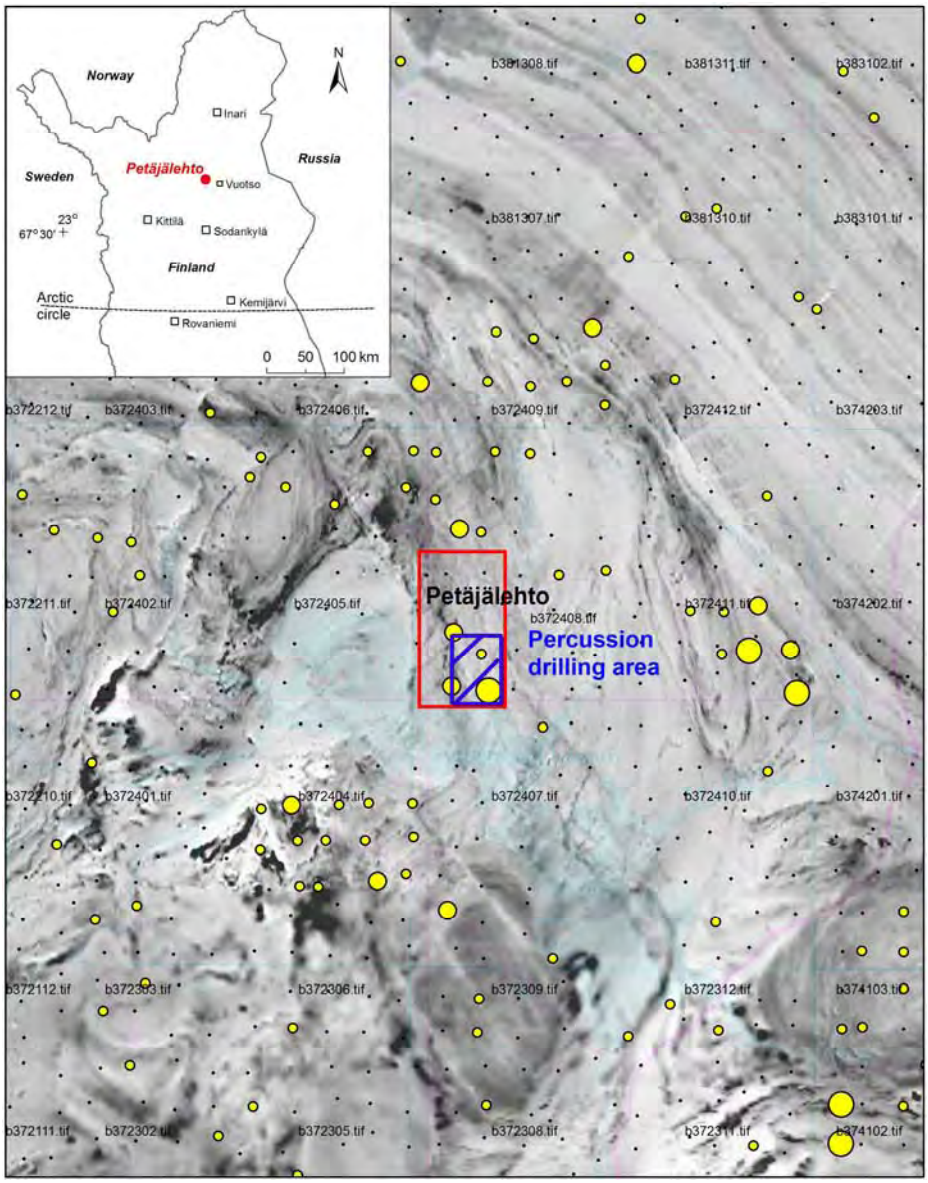

Fig. 1. Location of the Petäjälehto exploration target (red rectangle) in northern Finland and gold anomalies in till in an aeromagnetic map.

PREVIOUS STUDIES

Gold and copper anomalies revealed by the regional geochemical mapping of till, and N-S-orientated magnetic anomalies of the airborne geophysical survey encouraged starting an exploration for gold in the area. In addition, old gold prospectors have found gold nuggets from the gravels in the streams near the Petäjälehto target area. The exploration area is located on the southern part of the well-known Sotajoki-Tankavaara gold field in Finnish Lapland.

A detailed geochemical sampling in a 100 m x 100 m grid was carried out in association of the regional geochemical mapping in 1985. In total 175 till samples taken by percussion drilling were assayed (size fraction <0.06 mm) with ICP-AES and GAAS. The results showed anomalous

concentrations of As, Cu, Fe and Au (Table 1). A spatial association of gold, arsenic, copper and iron in till indicate a gold mineralization in the bedrock (Fig. 2).

Element	Max.	Mean	StD	Freq.
Au ppb	57	2.6	5.0	173
AS ppm	25	7.5	3.6	173
Cu ppm	354	84	49	173
Co ppm	42	18	5.8	173
Cr ppm	425	119	48	173
Ni ppm	207	56	23	173
Pd ppb	4.4	1.4	0.6	173
S ppm	2120	155	251	173
Te ppb	117	13.1	10	173

Table 1. Statistics of Au, As, Cu, Co, Cr, Ni, Pd, S, Te concentrations of till at Petäjälehto.

PRESENT STUDIES

The on-going exploration campaign started in 2005 in Petäjälehto. The exploration program has included 14 km^2 systematic ground geophysical VLF-R and magnetic surveys, 20 km of line gravimetric measurements, 14 diamond drill holes in total of 1460 m (assays pending), bedrock mapping, boulder tracing and excavating shallow (up to 6 m deep) test pits in till. Till was sampled for geochemical and heavy mineral analysis from the test pits. Till size fraction <0.06 mm was assayed by ICP-AES (32 elements) and GAAS (Au and Pd). Heavy mineral samples (12 litres/sample) were handled with the "Gold Hound" concentrator and the magnetic fraction was separated and removed. Minerals of the magnetite free fraction were identified using binocular microscope and XRD determinations.

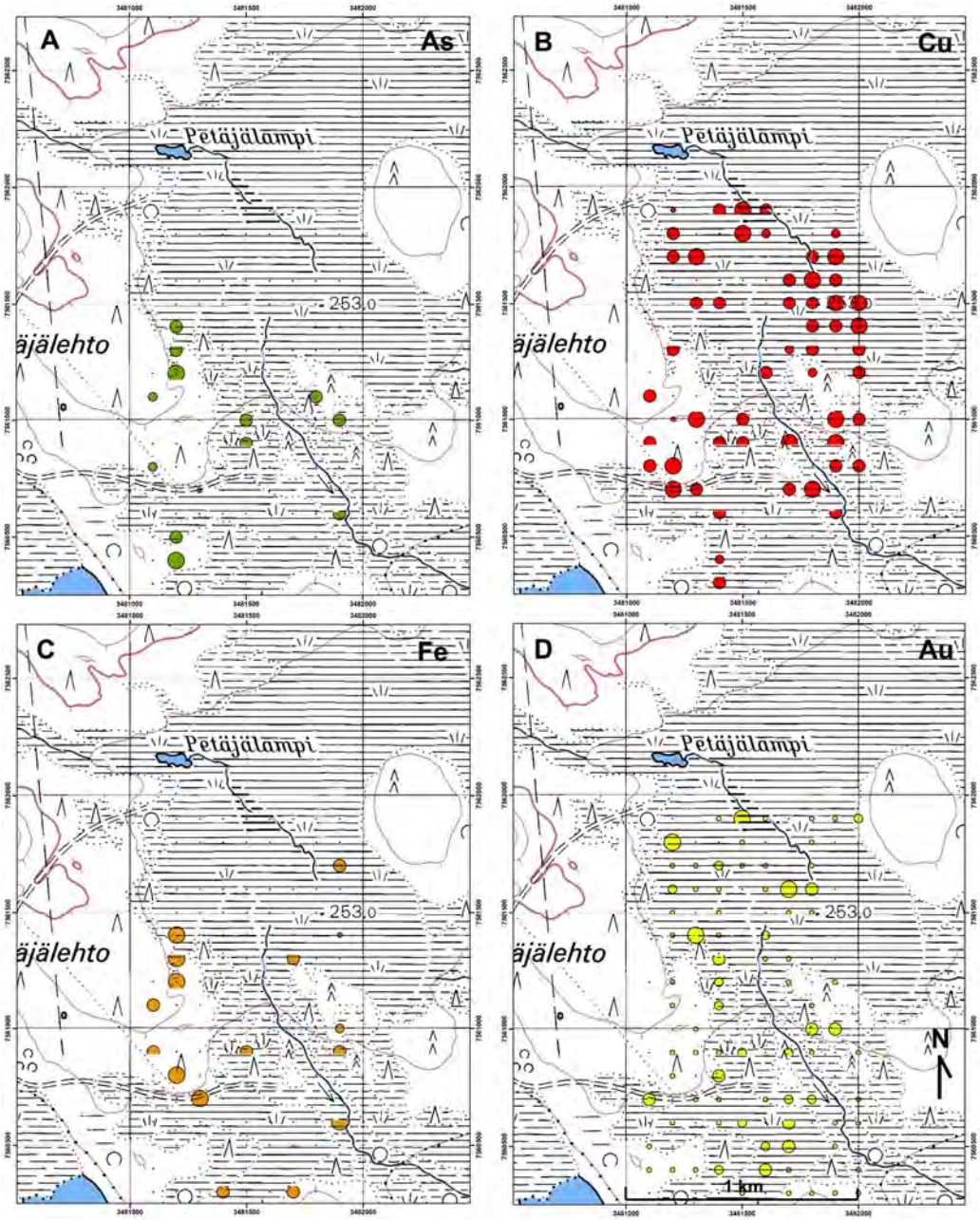

Fig.2. Distribution of A) As, B) Cu, C) Fe, and D) Au in percussion drilled till samples in the southern Petäjälehto area (Fig.1). The upper limit for the largest symbol is 20 ppm for As, 400 ppm for Cu, 1.5% for Fe and 10 ppb for Au. (Basemap © National Land Survey of Finland, license 13/MYY/07).

RESULTS

The results of till geochemistry and heavy mineral analyses indicate that the Petäjälehto has high potential for a significant gold mineralization. Gold contents in the fine till fraction (<0.06 mm) are anomalous compared to the regional background, varying from 4 to 57 ppb at the several sampling sites in the southern part of the Petäjälehto area (Table 1, Fig. 1

and 2). In all 22 test pits were excavated on the crossings of the magnetic anomalies (Fig. 3) and associated low resistivity zones, which were expected to be the most promising targets. The thickness of glacial drift vary from 2 to 6 m. In addition to anomalous gold values in the fine fraction of till, small nuggets with size varying in range from 0.1 to 0.5 mm are found from the till. The number of nuggets rises up to 22 in heavy mineral samples (12 litres/sample) (Figs. 3 and 4).

The concentrations of pathfinder elements for gold (Cu, Bi, Sb and Te) are high in lower till of the test pit 98, but gold itself is low (Fig. 4). An example of the assays and till stratigraphy is shown Fig. 5. Both high concentrations of the pathfinder elements and the number of gold nuggets in the lower till bed of the test pit M97 indicate that the gold mineralization locates 50 – 100 m to the west, which is up-ice direction from the test pit M98.

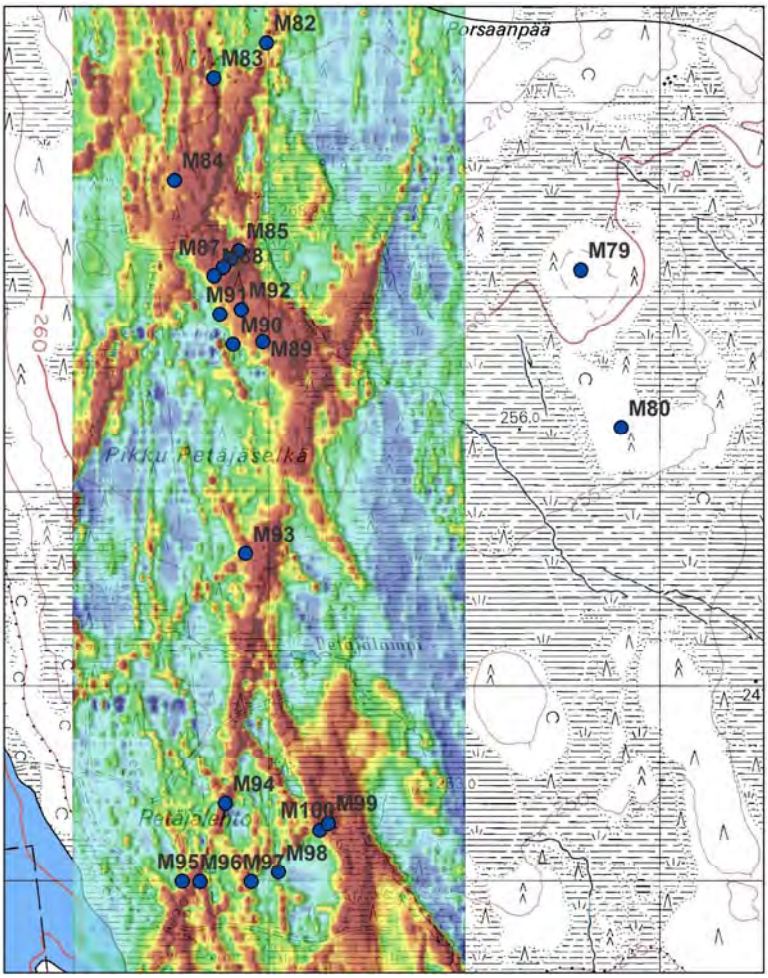

Number of gold nuggets

Test pit	Depth m	Material	Number
M79	1,0	bedrock	1
	3,0	bedrock	2
M83	1,5	till	1
M84	0,5	till	2
M85	1,5	till	1
	3,0	bedrock	22
M88	1,0	till	3
M89	1,5	till	1
M90	1,0	till	1
M93	3,0	bedrock	4
M94	2,0	till	2
M96	1,5	till	1
	2,0	till	1
M97	1,5	till	2
	1,0	till	1
	4,5	till	8

Fig. 3. Magnetic image of the exploration area with the sites of 22 test pits at Petäjälehto and the number of gold nuggets separated from the heavy mineral concentrates of till samples. (Basemap © National Land Survey of Finland, license 13/MYY/07).

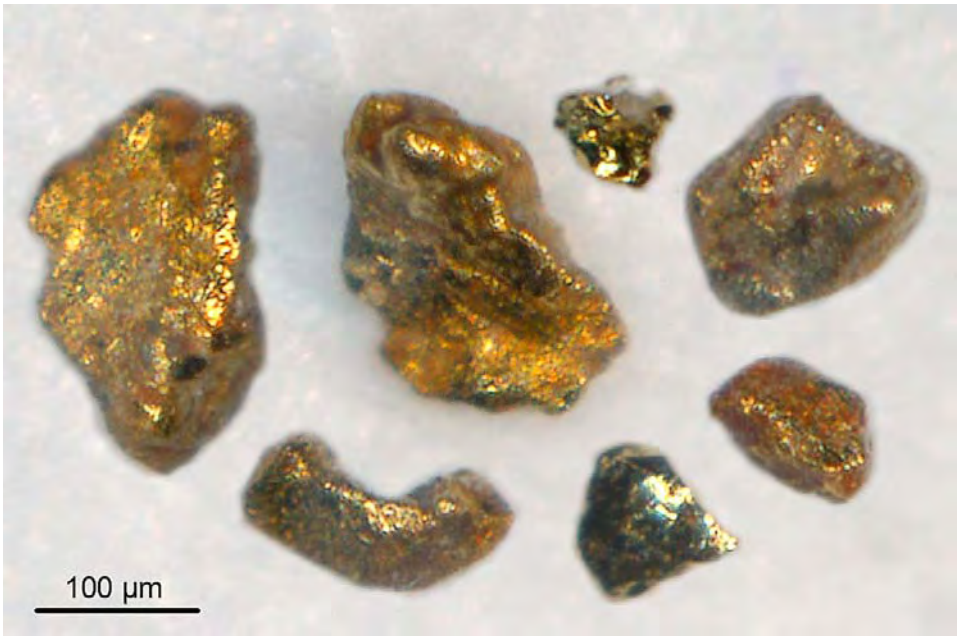

Fig. 4. Gold nuggets separated from a heavy mineral sample from the weathered bedrock in test pit M85. Photo J. Väätäinen.

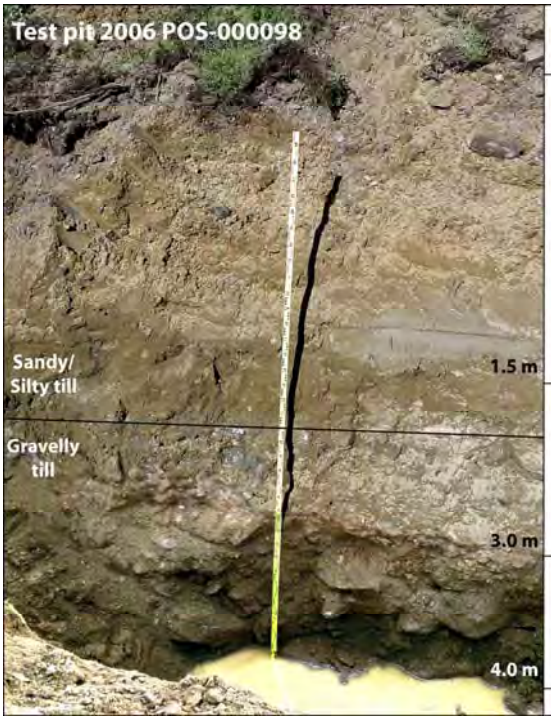

	Au ppb	Co ppm	Cu ppm	Fe %	Bi ppm	Sb ppm	Te ppb
	0.4*	14*	18*	3.1*	0.3**	0.13*	6**
1.5 m	1.6	29	99	0.6	92	30	25
3.0 m	3.6	33	184	0.5	215	40	51
4.0 m	3.1	34	128	0.7	758	59	122

Fig. 5. A vertical till profile at Petäjälehto and concentrations of Au, Co, Cu, Fe, Bi, Sb and Te in till. Topmost row shows background concentrations of the elements in till on (*) the Archaean granite gneiss terrain and (**) in soil in Finland (Koljonen 1992).

Most of the drill holes penetrate sheared rocks, which are here called as mylonite in the case the original mineralogy of the rock has altered pervasively. The alteration in the shear zones is typified by very fine-grained pyrite, magnetite and chalcopyrite dissemination. Stronger deformation is associated with contacts of ductile, mafic metavolcanic rocks and hard rock types such as quartzite, granite gneiss and quartz-epidote-feldspar breccia (Fig. 6). The deformation zones are from 1 to 10 m wide. In addition to pervasive alteration, chalcopyrite and pyrite bearing calcite veins are included in the shears. Most of the breccias are found at the intersections of the magnetic anomalies (Fig. 3). The source of the gold nuggets could be the gold mineralization related to magnetite-bearing silicified rocks.

Fig. 6. An example of the drill core R409 from Petäjälehto. Drill core from 90 m to 101.80 m, which is composed of quartz–hematite-epidote breccia associated with the contact of a monzonite dyke.

REFERENCES

Koljonen, T. 1992 (Ed). Suomen geokemiallinen atlas, osa 2: Moreeni. Thegeochemical Atlas of Finland, Part 2: Till. Geological Survey of Finland.

Lehtonen, M., Airo, M-L., Eilu, P., Hanski, E., Kortelainen, V., Lanne, E., Manninen, T., Rastas, P., Räsänen, J. ja Virransalo, P., 1998. Kittilän vihreäkivialueen geologia.Lapin vulkaniittiprojektin raportti. Summary: The stratigraphy, petrology and geochemistry of the Kittilä greenstone area, northern Finland. A Report of the Lapland Volcanite Project. Geological Survey of Finland. Report of Investigation 140, 144 p.

Exploration for gold using fluid inclusions – the acoustic decrepitation technique. With examples from Hebei, China and El Penon, Chile.

Burlinson K.

Burlinson Geochemical Services Pty. Ltd.
P.O. 37134, Winnellie NT 0821 Australian
kgb@synix.com.au
Keywords: fluid inclusions, decrepitation, epithermal, carbon dioxide, temperature

ABSTRACT

The use of fluid inclusions in exploration is frequently overlooked because conventional microthermometric measurements are slow, tedious and rarely definitive. However by using acoustic decrepitation, useful exploration data can be acquired quickly and reproducibly. The results can readily identify CO_2 rich inclusion fluids, in addition to providing relative temperatures of aqueous fluids to outline palaeo-thermal temperature gradients in hydrothermal quartz systems.

Samples from several gold mines in the Hebei province of China show that CO_2 rich fluids are quite rare in this region, in contrast with the common occurrence of very CO_2 rich fluids in typical archaean gold deposits. Because the microscopic studies on these deposits concentrated on the rare but prominent CO_2 rich inclusions, the deposits have been wrongly classified as being derived from CO_2 rich fluids, wheras acoustic decrepitation shows that those CO_2 rich fluids were merely minor phases of the overall hydrothermal system.

At the El Penon epithermal gold deposit in Chile, there are some CO_2 rich fluids present, indicating a deeper and higher pressure origin than is usual for epithermal deposits. Variations in the aqueous fluid temperatures of about 50 C suggest that mapping of palaeo-thermal gradients can be done, which may help to outline favourable mineralised zones within the quartz system.

INTRODUCTION

The fluid inclusion decrepitation method was first used in the 1940's as a method to measure homogenisation temperatures. The method was soon replaced by microthermometry which was recognized as being more accurate for determining these temperatures. However, it was not understood that much of this early decrepitation work was subject to interference caused by the presence of CO_2 rich fluid inclusions. Consequently much of the criticism of the technique, which led to its demise for academic research purposes, is now known to be inappropriate. The technique was subsequently used in Russia and China in the 1970's in exploration programmes, in which economical and rapid analyses are more important than modest inaccuracies. However, even this work failed to recognize the importance of the effects caused by the presence of CO_2 rich inclusions. It was not until 1983

(Burlinson, K., 1984) that the effect of CO_2 rich fluid inclusions upon decrepitation data was recognized. Such CO_2 rich fluid inclusions develop high internal pressures at low temperatures resulting in decrepitation long before the inclusion reaches homogenisation temperature. This behaviour is frequently observed in microthermometric studies where it is a major problem when trying to measure the homogenisation temperature. However, this decrepitation gives rise to distinctive low temperature peaks on the acoustic decrepigrams which can be used to recognize the presence of CO_2 rich fluid inclusions. This led to the recognition that CO_2 measurements by acoustic decrepitation could be used as an exploration technique for Au deposits as they are often associated with CO_2 rich hydrothermal fluids.

Confirmation of the relationship between low temperature decrepitation and CO_2 rich fluids was provided by Mavrogenes et al. (1995), who performed quadrupole mass spectrometric analyses of gases released from fluid inclusions from samples from the Cowra Creek goldfield in NSW, Australia. In this work, 5 samples with prominent low temperature acoustic decrepitation peaks were shown to give rise to CO_2 rich gases when the fluid inclusions were opened either by sequential heating or mechanical crushing of the same samples.

Following from this work, acoustic decrepitation is now a useful exploration technique for detecting CO_2 rich fluids, or in their absence, for measuring Td (temperature of decrepitation). Although it is not a high accuracy technique it is ideal for exploration because it does not require the preparation of polished thin sections and is a rapid and cheap method which has been automated using modern computers and electronics (Burlinson, 1988). Because the method uses a relatively large sample (0.5 grams) and counts many inclusions (often more than 100,000) in each sample, it provides representative and statistically meaningful data which can be difficult to match with microthermometric analyses and this is of fundamental importance in its application as an exploration tool.

EXPLANATION OF DECREPITATION BEHAVIOUR

To understand the decrepitation behaviour of aqueous CO_2 rich inclusions, it helps to realise that the unusual fluid is not actually CO_2, but water. In the 50 to 600 C temperature range and 1 bar to 3 Kbar pressure range of interest for Th (temperature of homogenisation) measurements, CO_2 does not change phase and behaves according to the Gas law (PV=nRT) with only minor variation due to non-ideallity, whereas water undergoes a phase change.

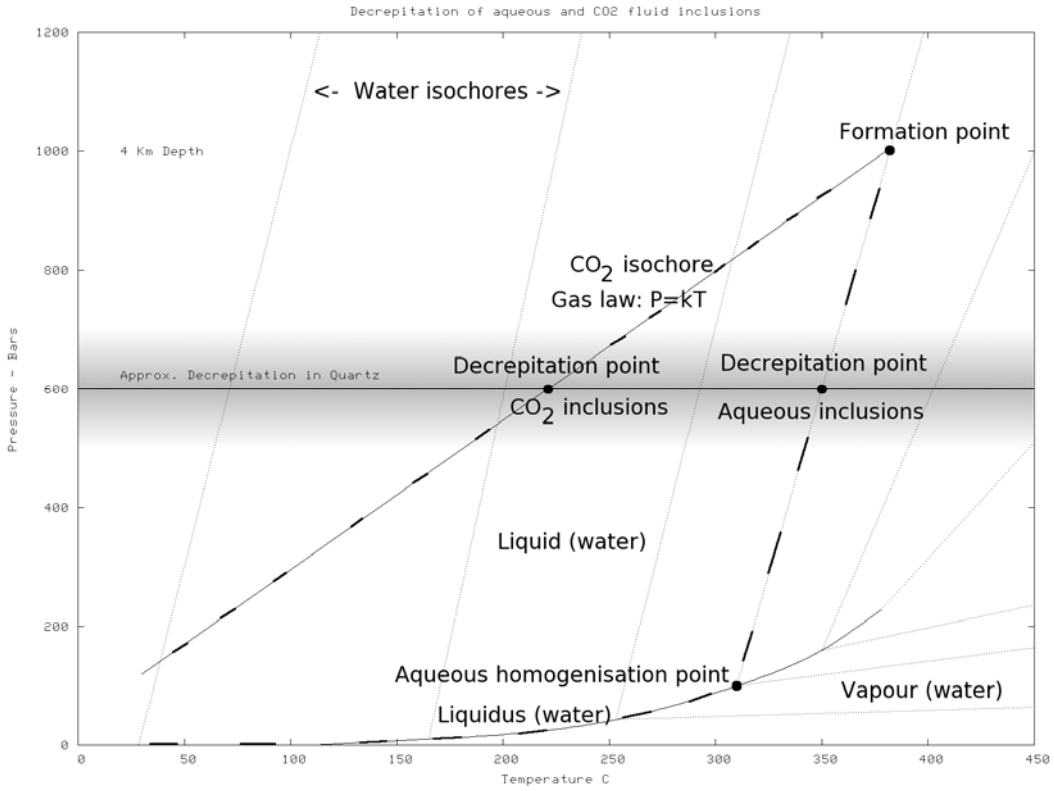

Fig. 1 PT relations and decrepitation of CO_2 and water superimposed

Figure 1 shows the behaviour of 2 hypothetical fluid inclusions of different compositions, formed at the "formation point" conditions. The pure CO_2 inclusion follows the gas law isochore, whereas the pure water inclusion follows the isochore for water, eventually reaching the liquidus curve where it nucleates a vapour phase. During cooling and exhumation the confining lithostatic pressure prevents decrepitation of the inclusions. However, when heated in the laboratory there is only one bar of confining pressure and when the inclusions generate approximately 600 bars of overpressure they can fracture the host quartz and decrepitate. During heating the CO_2 inclusion will generate high internal pressures and decrepitate at a low temperature unrelated to its formation temperature (approximately 220 C in Fig. 1), while the water inclusion will remain intact until about 350 C, close to its formation temperature.

DECREPITATION AND CO_2 IN EXPLORATION

Many workers have noted a common association between gold mineralisation and CO_2 rich forming fluids, although this relationship is indirect and due to the buffering of the fluid pH in a range which enhances the solubility of complexes of gold with reduced sulphur (Phillips, G.N. & Evans, K.A., 2004). CO_2 rich fluids are common in many gold deposit styles, particularly the archaean deposits in the Canadian Abitibi province and the West Australian Yilgarn province, as well as the turbidite hosted gold deposits in Victoria, Australia, and Nova Scotia, Canada. A detailed study of the

Timmins, Ontario region (Smith, T.J. & Kessler, S.E., 1985) has documented the relationship between CO_2 levels and the potential for Au mineralisation in that region, showing its use as a regional exploration indicator. Figure 2 shows typical decrepitation results from these types of deposits and the CO_2 rich fluids are evident from the prominent acoustic decrepitation peaks below 300 C.
In deposits formed at shallow depth, such as epithermal deposits, most of the CO_2 is exsolved from the fluid before inclusion trapping occurs. Such inclusions have low internal pressures and lack a low temperature acoustic decrepitation peak. The decrepitation observed is from dominantly aqueous inclusions and reflects the temperature of the deposition from these fluids. Variations in this temperature can be used to map out temperature gradients within the hydrothermal system as a means of identifying zones of quartz of economic interest.

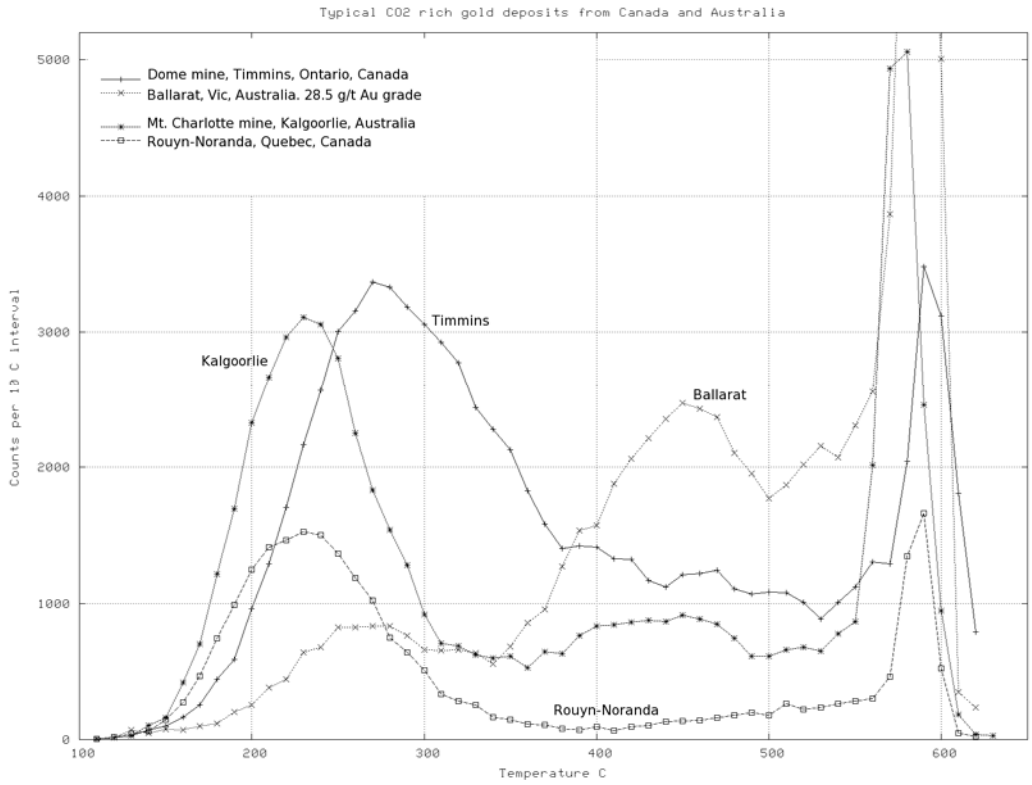

Fig. 2 Typical decrepigrams of CO_2 rich samples from Au deposits

EXPLORATION EXAMPLES

Hebei province, China

39 samples were collected from 3 mines in the Hebei province. These are from intrusion related gold deposits in structurally controlled zones, but despite the involvement of deep-seated fluids, only trace amounts of low temperature decrepitation due to CO_2 rich fluids were found in the Hougou mine, and no such CO_2 rich fluids were identified in the Dongping or Huangtuliang mines. Although other studies, using microthermometry, have suggested the formational fluids at

these mines were CO_2 rich, the acoustic decrepitation data show that such CO_2 rich fluids were volumetrically insignificant and they may not be the source of the gold mineralisation at all.

El Penon mine, Chile

20 samples were collected from the ore and waste dumps at this mine, as underground access was not possible. Of these, 12 samples showed a low temperature decrepitation peak at about 350 C, which indicates the presence of CO_2 rich inclusions. The higher than usual decrepitation temperature indicates that the inclusions had lower internal pressures than found in typical archaean gold deposits. Although this deposit is stated to be epithermal in origin, the presence of CO_2 rich inclusions indicates a formation depth much greater than usual.

The decrepitation temperature of the main peak in these samples varies from 430 C to 460 C showing that there are small temperature differences within the quartz, from which it may be possible to map out palaeo-thermal zones within the quartz, given proper spatially located samples.

CONCLUSIONS

Acoustic decrepitation is able to detect the presence of CO_2 rich fluid inclusions, due to their high internal pressures, which results in premature decrepitation at low temperatures when heated. As CO_2 rich fluids have frequently been shown to be associated with gold mineralisation in many districts, this means we can use decrepitation to quickly scan large numbers of samples as an exploration method to look for potentially mineralised quartz and to discriminate between quartz samples which are visually indistinguishable.

In addition, temperature variations of primary fluid inclusions can be used to generate palaeo-thermal maps, which can be used to identify potentially mineralised zones within quartz veins and vein systems.

Fluid inclusion information is potentially very useful in exploration, but its use has been very limited to date because collection of the information is tedious, inconvenient and expensive. The acoustic decrepitation method overcomes these limitations and provides data which is very useful in exploration, despite its accuracy being less than that from traditional microthermometric methods.

REFERENCES

Burlinson, K., 1984. Exploration for gold at Pine creek and Tennant Creek, N.T. and at Halls Creek, W.A. using the fluid inclusion decrepitation technique. *Australasian Institute of Mining and Metallurgy, Conference, Darwin, NT. August 1984.* (abstract only)

Burlinson, K., 1988. An instrument for fluid inclusion decrepitometry and examples of its application. *Bulletin de Mineralogie,* 111: 267-278.

Mavrogenes, J.A., Bodnar, R.J., Graney, J.R., McQueen, K.G. and Burlinson, Kingsley, 1995. Comparison of decrepitation, microthermometric and compositional characteristics of fluid inclusions in barren and auriferous mesothermal quartz veins

of the Cowra Creek gold district, New South Wales, Australia. *Journal of Geochemical Exploration,* 54: 167-175.
Phillips, G.N. & Evans, K.A., 2004. Role of CO_2 in the formation of gold deposits. *Nature* 429: 860-863.
Smith, Ted J. & Kesler, Stephen E., 1985. Relation of fluid inclusion geochemistry to wallrock alteration and lithogeochemical zonation at the Hollinger-McIntyre gold deposit, Timmins, Ontario, Canada. *Canadian Institute of Mining Bulletin* 78: 35-46.

The Khongor Porphyry Cu-Au Deposit: A Low Density Fine Fraction Stream Sediment Exploration Geochemistry Discovery in the Gobi Desert, Mongolia

Maopei Cui

Asia Gold Corp., 654-999 Canada Place, Vancouver, Canada V6C 3E1
Email: cuimaopei@asiagold.com
Keywords: fine fraction stream sediments, low density sampling, porphyry Cu-Au, discovery, orientation survey, Khongor, Gobi, Mongolia

ABSTRACT

In 2004, Asia Gold started a grass roots exploration program for porphyry copper and epithermal gold deposits on a 35,517 km^2 tenement block in the Gobi Desert of southern Mongolia. Asia Gold applied low density fine fraction stream sediment exploration geochemistry for evaluating the Cu and Au potential in this large and remote area.
Stream sediment orientation surveys were conducted at Yagaan (an epithermal Au prospect) and Khongor (a porphyry Cu-Au prospect) after its discovery. A test of two and three fractions (-63µm, -230µm and +1mm/-4mm) over known mineralization at both prospects was carried out to determine optimum methods for routine geochemical exploration in the West Gobi of south Mongolia. In the conditions of the Gobi Desert, the mineralized zones at both prospects can be easily detected by stream sediment surveys using fine fraction (-63µm) stream sediments at a density of 1 sample per 6 ~10 km^2 of catchment. A gold threshold of 2ppb was used and 5ppb was considered significantly anomalous. The ICP-MS analytical method with a low detection limit (Au 0.2ppb) is required.
The Khongor porphyry Cu-Au mineralization was discovered by Asia Gold during a grass root geochemical reconnaissance exploration program on the company's West Gobi properties in June 2005. Follow-up geological investigation and initial rock chip sampling of the exposed copper-oxide mineralization outcrops revealed a system in excess of 2km length and 150-200 m width. Continuous rock chip samples across outcropping copper oxide mineralization in the East Creek returned 126 meters with 0.42% Cu and 0.07g/t Au including 54m with 0.72% Cu and 0.13g/t Au and in the Central Creek, 18 meters with 1.84% Cu and 0.43g/t Au, as well as another 18 meters with 1.33% Cu and 0.55g/t Au. First phase drilling returned encouraging results including a best intercept of 50m with 1.0% Cu and 0.30g/t Au. Phase two and three drilling is ongoing.

INTRODUCTION

Asia Gold held over 35,000 km^2 of licenses in the west Gobi of Mongolia in 2004 (see Figure1).

Asia Gold Licenses in Mongolia Figure 1

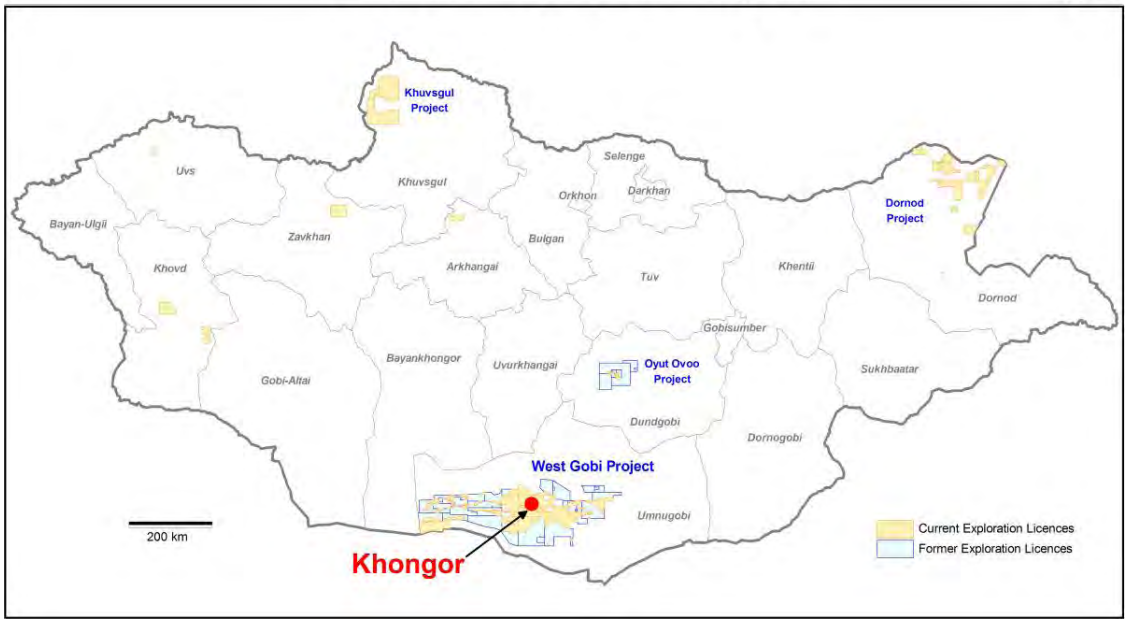

The Gobi desert of southern Mongolia is an arid, wind-swept area largely comprising broad flat areas between east-west trending small mountainous ranges. No regional systematic stream sediment sampling work is known previously in the Gobi region.

The west Gobi geological setting comprises fault bounded belts of Silurian-Devonian-Carboniferous-Permian volcanics and intrusives, narrow accretionary wedges of fore-arc sediments and later Permian-Cretaceous continental sediments in inverted basin-and-range structural settings. Major faults have approximately east-west to northwest, (assumed) arc-parallel components and northeast (assumed) transcurrent components (see Figure 2).

Regional Geology of West Gobi Property Figure 2

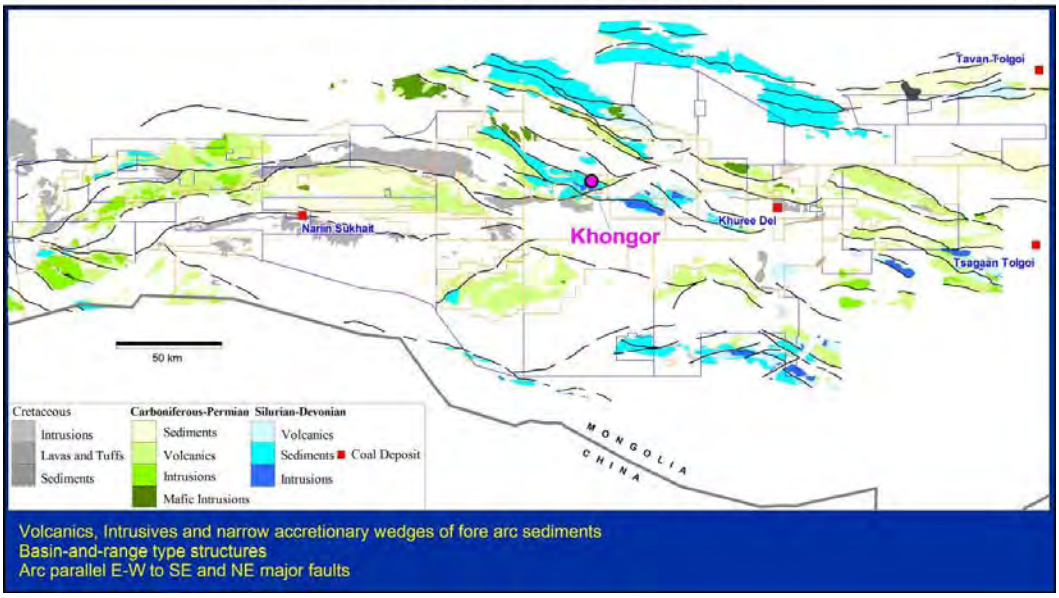

The Landsat image (Figure 3) shows that drainages are widespread in the west Gobi. All the low density stream sediment sampling was based on drainages generated from Aster and Landsat images with 15 and 30 meter resolution respectively (see Figure 3 & 4).

Landsat Image Shows the Drainage Distribution at West Gobi of South Mongolia Figure 3

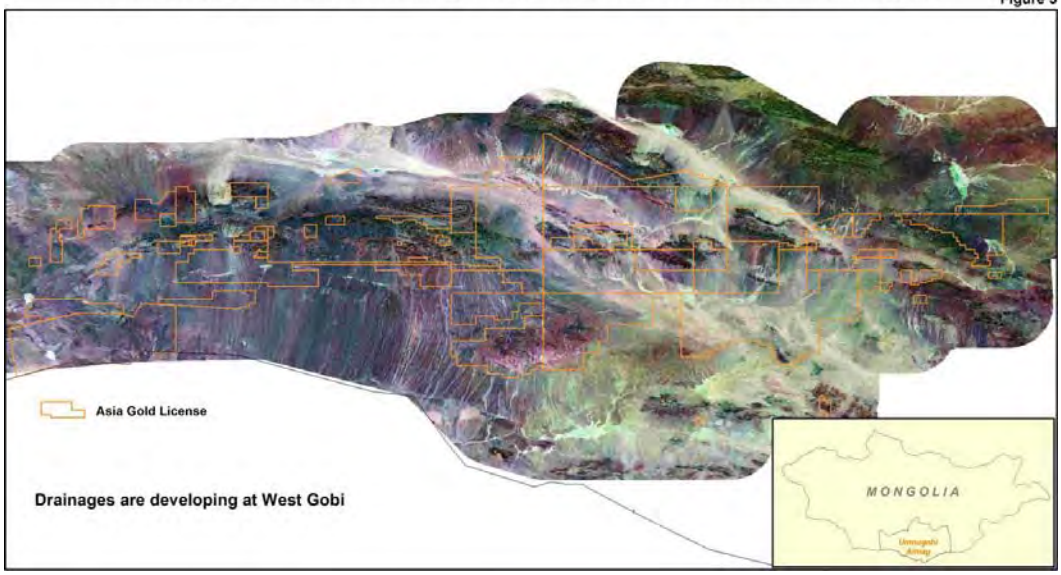

A total of 2,080 ultra fine fraction (-63µm) stream sediment samples were collected over 12,498 km^2 during 2004 and 2005 around the belts considered

prospective for porphyry Cu-Au and/or Epithermal Au mineralisation. Orientation stream sediment sampling surveys were conducted at Yagaan-Toste (before the Khongor discovery) and Khongor (after the Khongor discovery) (see Figure 4). Standards and blanks were used for Quality Control (QC) monitoring. All sampling included 10% duplicates, 5% standards and 5% blanks. The stream sediment samples were sent to ACME Vancouver for ICP-MS 53 element analysis.

Low Density Fine Fraction Stream Sediment Exploration Program in the Gobi Desert, Mongolia. 2004-2005 Figure 4

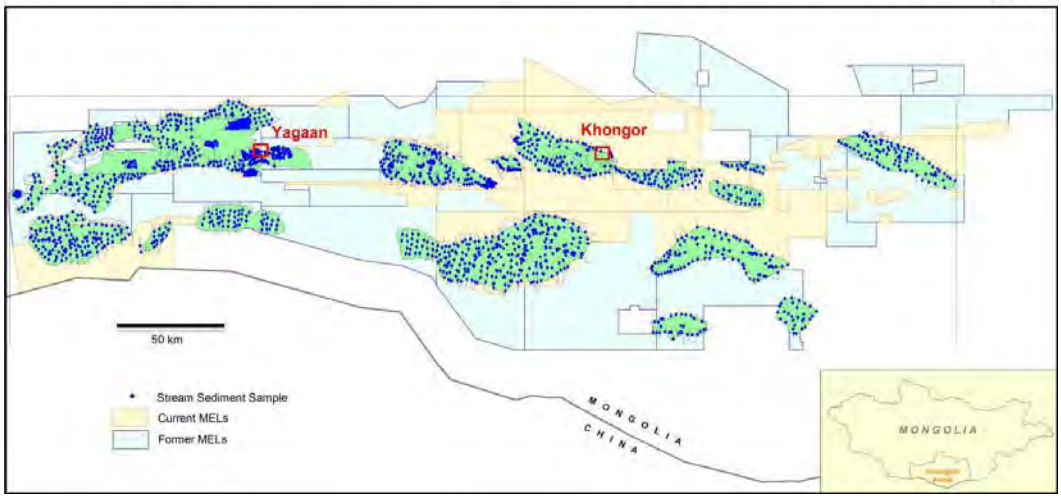

STREAM SEDIMENT ORIENTATION SAMPLING

1. Yagaan Au Prospect

The Yagaan Prospect lies along a ridge of altered andesitic to rhyolitic tuffs and breccias which are intruded by andesite dykes. A prominent andesite porphyry plug occurs immediately to the south of the target. The upper part of the Yagaan ridge is a resistive cap of intensely silica±alunite±kaolinite±sericite altered volcanics. Massive, microcrystalline, chalcedonic and vuggy quartz textures were observed. Breccias of possible hydrothermal origin are intensely hematite-goethite stained in places. Quartz-sericite-kaolinite altered andesite outcrops near the base of the ridge are stratigraphically below the silicified cap. A central 250m by 100m zone contains up to 20% sheeted and stockwocked veins of vuggy and colloform-banded quartz with up to 54.2g/t Au in rock chip samples.

An initial stream sediment sampling orientation was conducted at Yagaan in 2004. A test of two fractions (-63µm and -230µm) over known Au mineralization was carried out to determine an optimum method for routine geochemical exploration elsewhere in the west Gobi.

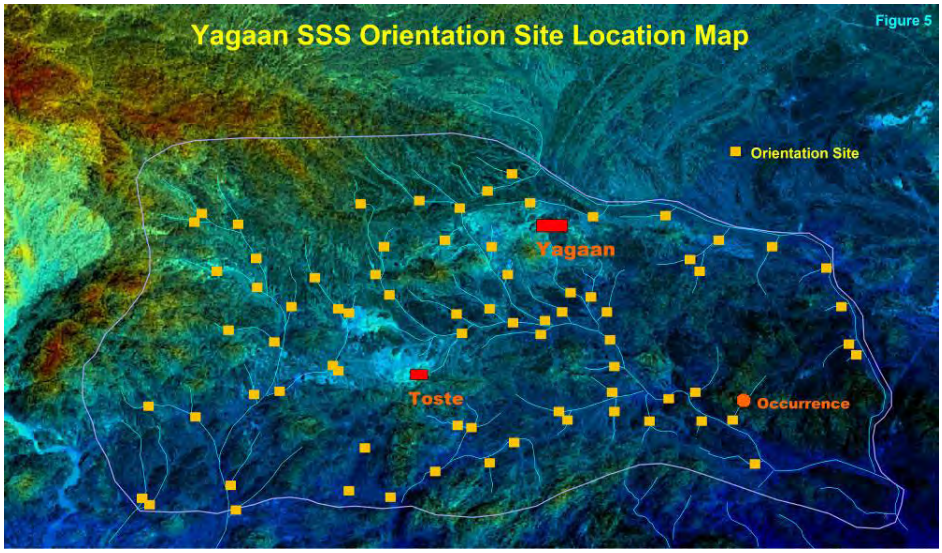

A total of 190 samples were collected in the main Yagaan-Toste drainage and adjacent tributaries (Figure 5). This stream sediment orientation survey covered 118 km^2. The test sample density was one sample per 1.5 square kilometers. All samples were sent to ACME for ICP-MS, 30g, full-suite 53 elements analysis.
The Au threshold at Yagaan was determned to be 2ppb. (see Figure 6).

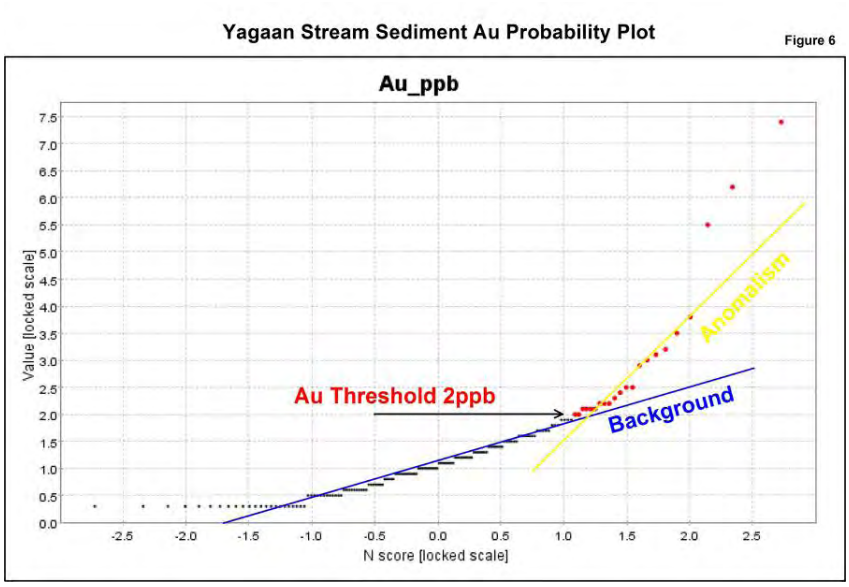

The actual Yagaan prospect was identified in both fractions. However, the fine fraction (-63µm) performed better than the coarse fraction (-230µm), and identified more anomalies and gold occurrence in the Yagaan area. The down-stream length of anomalism from the prospect was longer in the fine

fraction (2.8km) compared with the coarse fraction (1.7km). A relatively low fine fraction sampling density of 1 sample per 7 km^2 can could identify the Yagan prospect while a significantly higher coarse fraction sampling density of 1 sample per 2.89 km^2 would be required.

Yagaan Stream Sediment Orientation Gold Geochemistry Figure 7

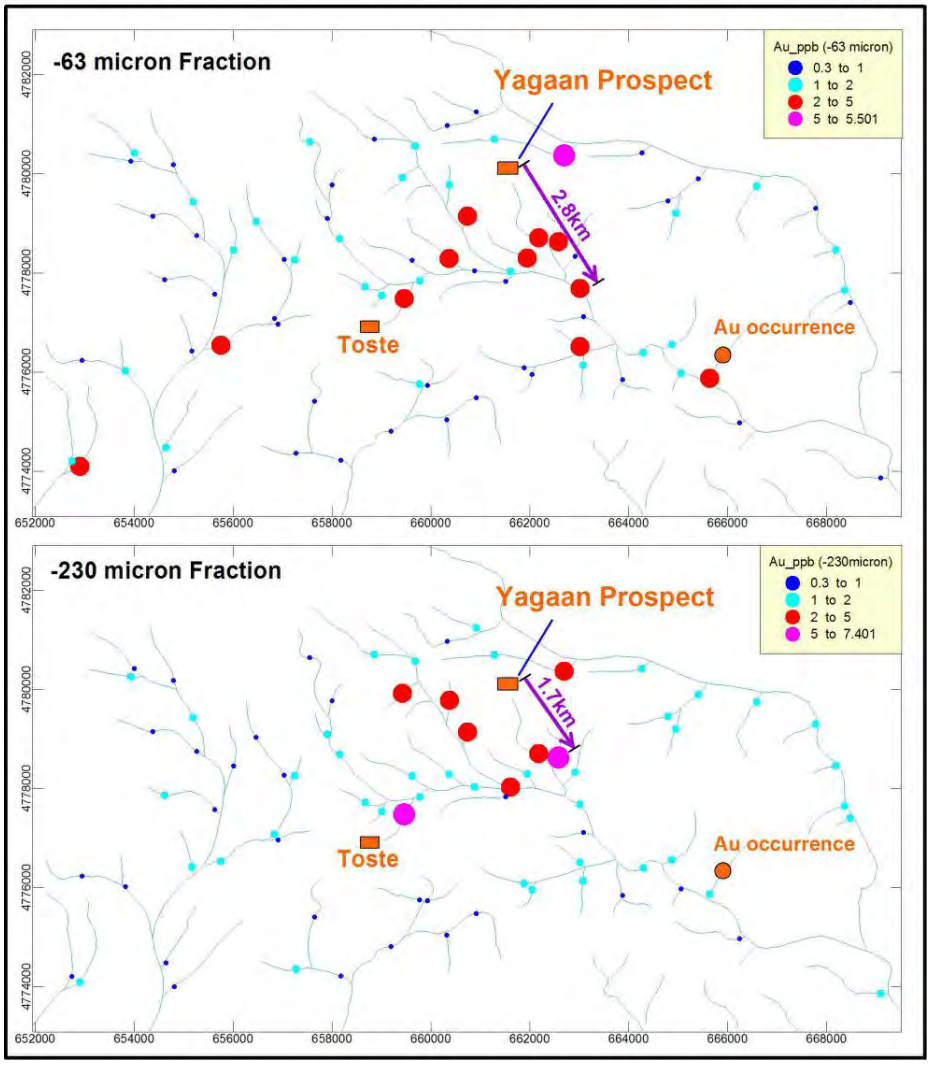

2. Khongor Cu-Au Mineralization

A comprehensive stream sediment orientation sampling study was conducted at Khongor of West Gobi in Nov 2005. A test of multiple methods over previously discovered Cu-Au mineralization was carried out to confirm that the low density, fine fraction (-63µm) stream sediment sampling is an optimum method for routine geochemical exploration in the Gobi desert of south Mongolia.

Three stream sediment fractions (-63µm, -230µm and +1mm/-4mm) orientation samples were collected at 76 sites covering 19 km^2 at Khongor. All samples were analyzed for 53 elements by ACME.
Cu, Au and Mo geochemistry for the Khongor Stream Sediment orientation program are shown in Figure 8.

Khongor Cu-Au Prospect _ Stream Sediment Orientation Sampling & Comparison of Three Fractions

Figure 8

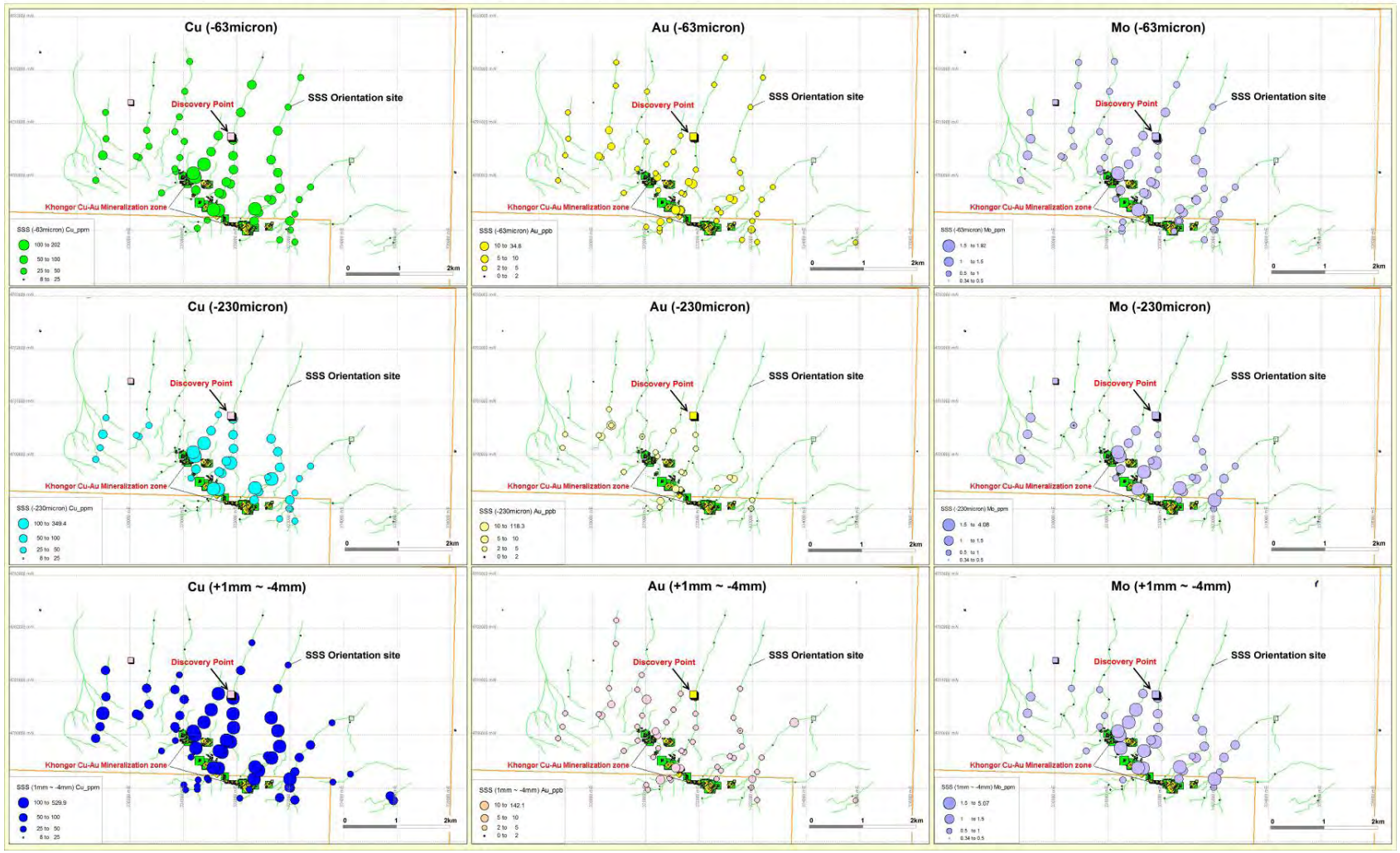

The association of anomalous elements at Khongor is: Cu-Au-Mo-(S-Se-Te)

Khongor stream sediment anomalous length

The length of down-stream anomalism from known mineralization to the termination of anomalism is shown in Table 1.

Khongor SSS Orientation Anomalous Length
Table1

Element	Anomalous Length Down Drainage (km)		
	-63µm	-230µm	+1mm ~ -4mm
Cu	2.7 ~ 3.5	1.5	2.5
Au	3.5	0.8 ~ 1.2	1.5 ~ 2.0
Mo	2.7	1.5	1.5

The length of fine fraction (-63µm) anomalism (2.7km~3.5km) is longer than coarse fractions (-230µm and +1mm/-4mm) 0.8km~2.5km

Khongor stream sediment sampling density test

The drainage spacing to the north of the Khongor range is around 1.0 to 1.5km. The orientation survey suggests that sampling of 2.7km spaced drainages could identify the Khongor porphyry Cu-Au mineralization (or any bigger deposit). (see Figure 9).

Khongor SSS Orientation Sample Density Test

Figure 9

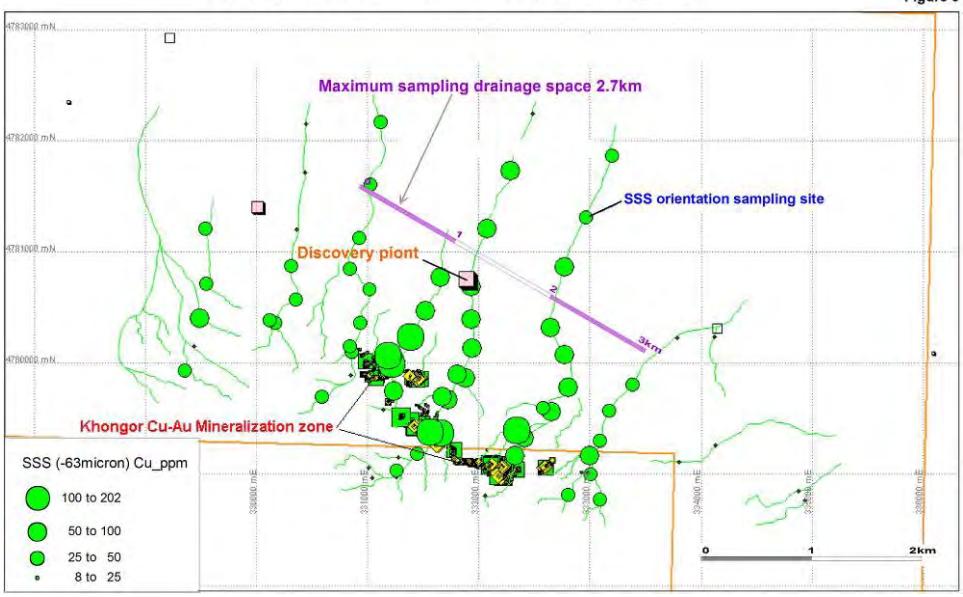

The Khongor stream sediment orientation catchment control statistics are shown in Table 2.

Khongor SSS Orientation Catchment Control Test Table 2

Element	Control Catchment Control (1samp per km^2)		
	-63µm	-230µm	+1mm ~ -4mm
Cu	7.29 ~ 12.25	2.25	6.25
Au	12.25	0.64 ~ 1.44	2.25 ~ 4.0
Mo	7.29	2.25	2.25

Therefore, one fine fraction sample for each catchment of about 7 ~ 12 km^2 is sufficient to discover Khongor, while a sample density of one per 1-6km2 is required with coarse fraction sampling.
Asia Gold has applied a stream sediment sampling density is 1 sample per 6 ~ 10km throughout the West Gobi. The Khongor porphyry Cu-Au deposit was in fact discovered by fine fraction (-63µm) low density stream sediment sampling survey in 2005 (prior to the detailed orientation survey described above).
Previous exploration work (by Company XXX) sampled 5.5km spaced drainages but didn't catch the Khongor Cu-Au anomaly although one sample point draining the east Khongor area returned <1ppb Au and 20.4ppm Cu which would not have been considered anomalous. This sample site was set behind the sandy dune in an area of heavy eolian sand accumulation and is probably heavily diluted. (see Figure 10).

Quick Bird Landsat Image Shows the Drainages cross the Gobi Desert at Khongor Figure 10

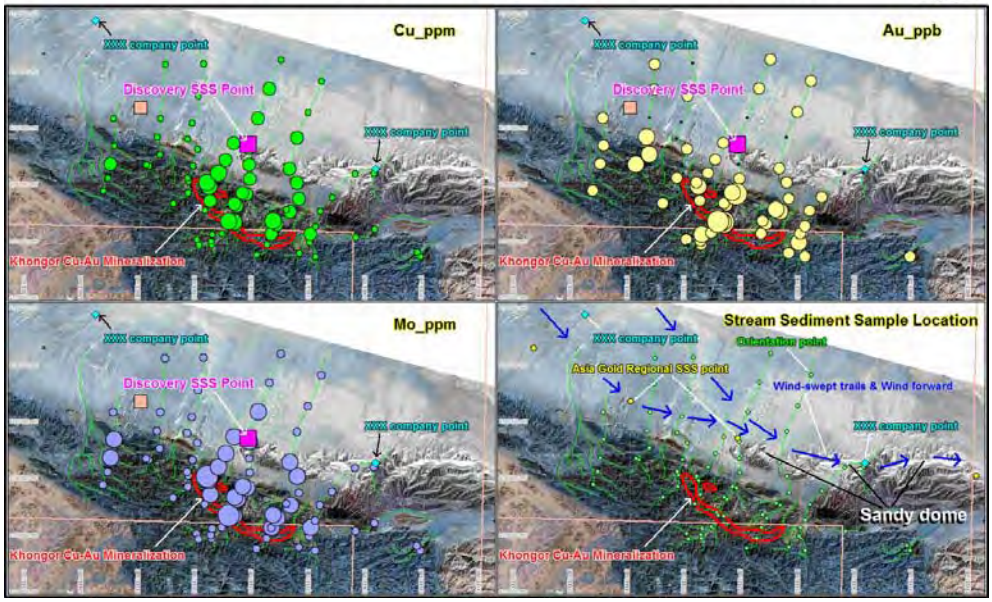

REGIONAL STREAM SEDIMENT GEOCHEMISTRY OF THE WEST GOBI

A total of 2,143 fine fraction (-63µm) stream sediment samples were collected and covered 12,498 km^2 in the west Gobi during 2004 and 2005. The Au, Cu and Mo probability plots are presented in Figure 11. The determined thresholds are: Au 2ppb, Cu 25ppm and Mo 1ppm.

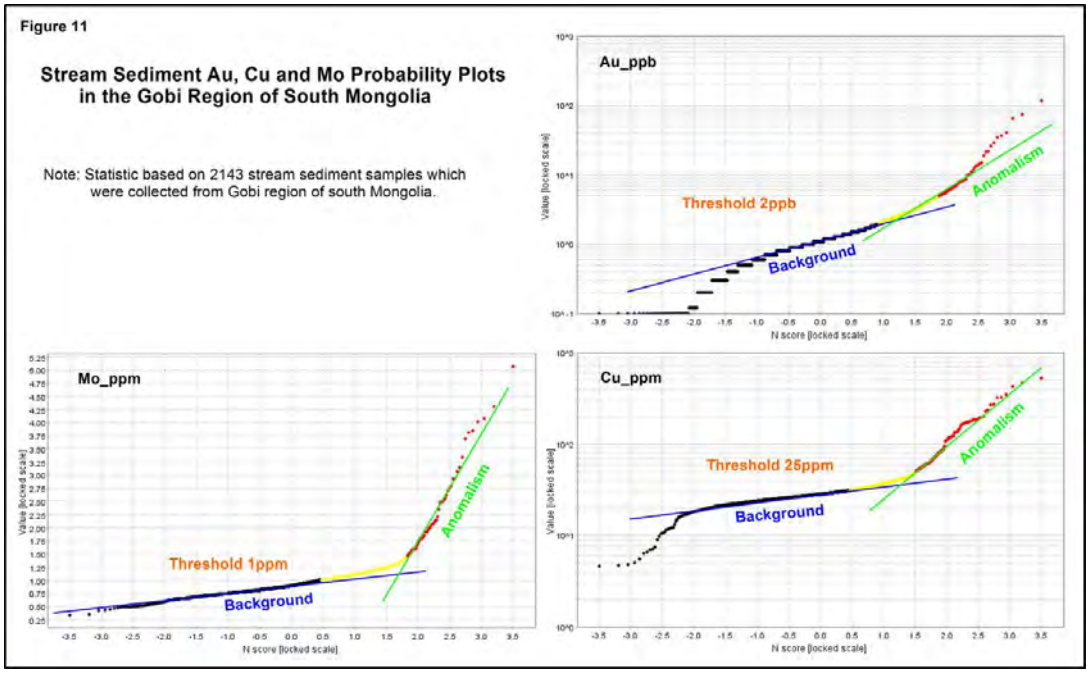

A total of 119 Cu, Au and other base metals anomalies were identified by low density, fine fraction stream sediment exploration geochemistry in this large survey. Follow up of the first batch of stream sediment anomalies lead to the discovery of the Khongor porphyry Cu-Au mineralization in June, 2005. The discovery stream sediment sample point values were 64.81ppm Cu with 12.1ppb Au. Follow up of the second batch of stream sediment anomalies generated two porphyry targets in the western parts of west Gobi in 2006. See Figures 12 & 13.

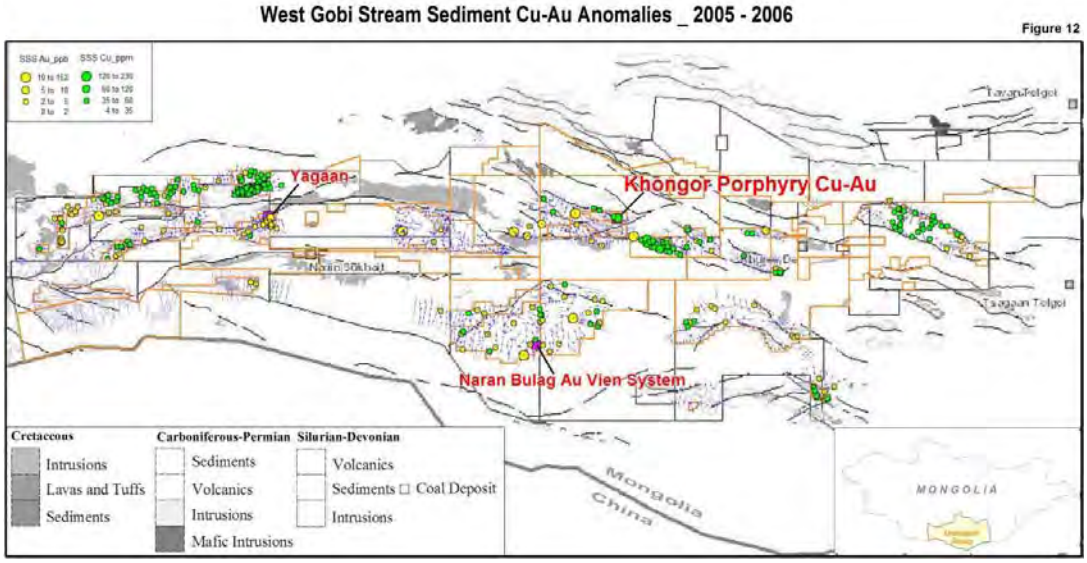

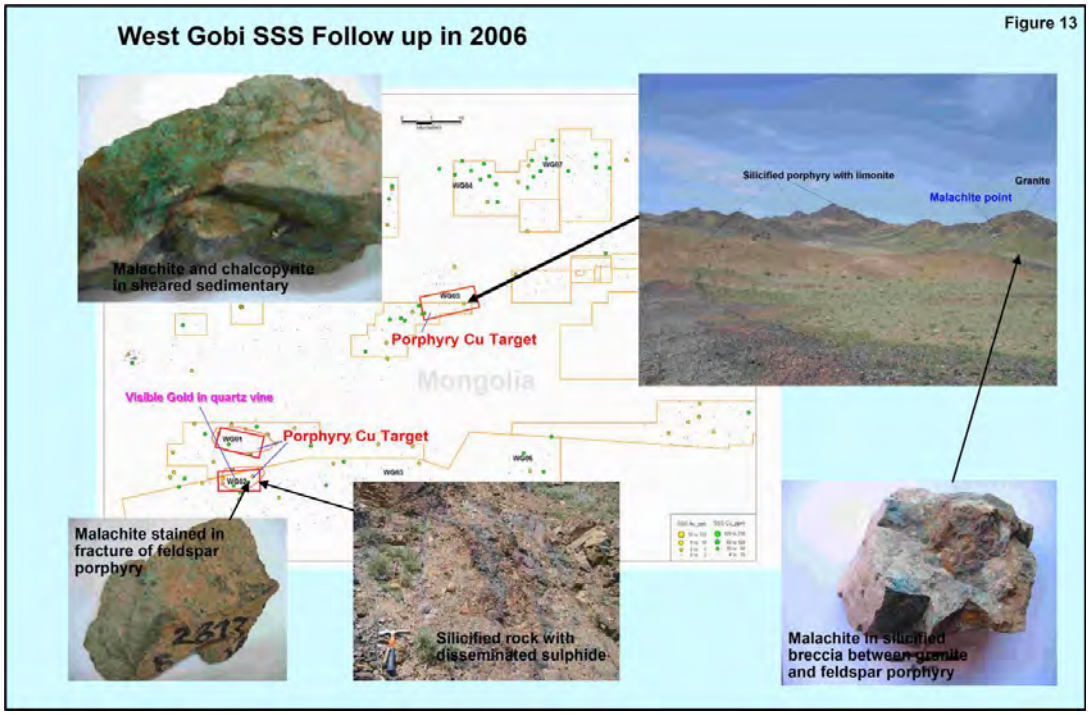

KHONGOR PORPHYRY CU-AU MINERALIZATION

Work History

No previous exploration work is known from the immediate Khongor area so it is a genuine new discovery.

Large Landsat colour anomalies (south of Khongor) reflect Advanced Argillic systems and were identified during the JICA Japan International Cooperation Association study in 1996. At Tsakhir on one of these anomalies (5km south of Khongor), some reconnaissance style sampling

was done by Harrods-Gallant during 1999-2002. Nested porphyries with UST 'Brainrock' have subsequently been identified. Moderately extensive stockworking is preserved within an advanced argillic zone with anomalously high Mo in surface rockchips. Solomon Resources did a stream sediment sampling survey around Tsakhir and two of their sample points drained Khongor but did not identify the anomaly.
The Khongor porphyry copper-gold system was identified in June, 2005 by Asia Gold during a grass roots geochemical reconnaissance exploration program on the company's West Gobi project. The discovery of outcropping mineralisation resulted from follow-up geological investigation and initial rock chip sampling of the low density, fine fraction stream sediment anomalies described above.

Geology

The geology of the Khongor area comprises Silurian-Devonian marine metasediments overlain by Carboniferous volcanics and sediments, intruded by monzogranitic to dioritic intrusives. These rocks formed in an island arc-active continental margin collisional setting. (see Figure 14).

Khongor Regional Geology Figure 14

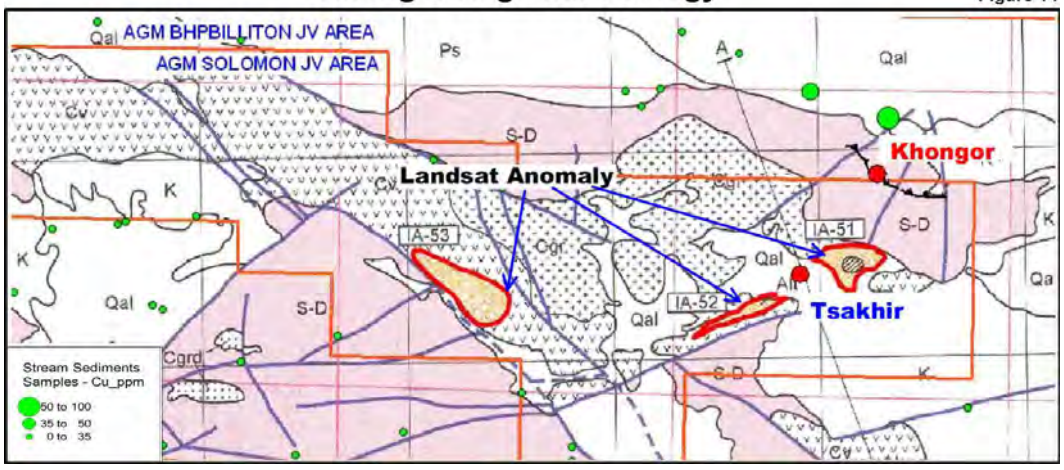

Crowded feldspar porphyry and hornfels are the host rocks for porphyry Cu-Au stockwork mineralization. A variety of multiple phases of intrusives ranging from quartz monzodiorite to diorite have been mapped crosscutting the crowded feldspar porphyry. There is a large inequigranular monzonitic intrusive complex. Younger andesite dykes cut through all lithologies.
The mineralized Khongor block is fault bounded. A transpressive thrust/reverse fault with NE movement is present on the south side. This structure has faulted Devonian sediments over Devonian sediments and intrusives. A range front fault with probably normal movement defines the north edge of the Khongor block.
The alteration assemblages and mineralization styles are similar to porphyry systems elsewhere. Alteration is dominantly K-feldspar, biotite, magnetite and sericite-quartz and silicification. Mineralization is

disseminated within the host as fracture fills and narrow veins within porphyry and the adjacent biotite-magnetite hornfelsed sediments, and locally as sheeted quartz veins and stockwork vein systems. Copper minerals include chalcopyrite, malachite, tenorite and azurite and are hosted within Crowded Feldspar Porphyry (CFP) and hornfelsed sediment throughout this system. So called, Q90-style mineralisation (massive banded high temperature quartz >90% with chalcopyrite (-magnetite) veins) occurs in a small thrust window immediately beneath the NE-directed thrust at Stockwork Gulch.
Copper values of up to 6% in 3m surface channel and grab samples have been returned. Gold shows a concentration in areas of obvious quartz stockworking.

Geochemistry
Secondary copper mineralization of the Khongor system covers an area of 4.5km^2 including the area of stream sediment anomalism. .
Geological investigation and initial rock chip sampling of the exposed copper-oxide mineralization outcrops revealed a system in excess of 2km length and 150-200m width. Continuous rock chip samples across outcropping copper oxide mineralization in the East Creek returned 126 meters with 0.42% Cu and 0.07g/t Au including 54m with 0.72% Cu and 0.13g/t Au and in the Central Creek, 18 meters with 1.84% Cu and 0.43g/t Au, as well as another 18 meters with 1.33% Cu and 0.55g/t Au (see Figure 15).

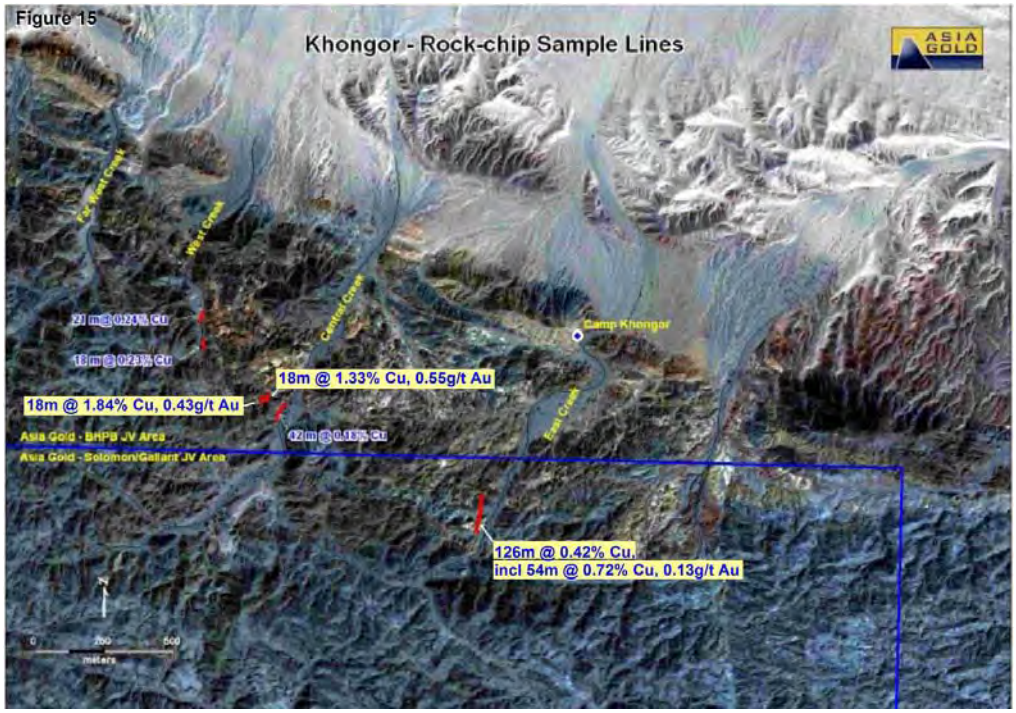

A total of 1,999 rock samples (include surface rock chips and continuous chip samples of 3m lengths) were collected at Khongor. The Cu, Au and Pb+Zn rock geochemistry are presented in Figure 16.

Rock Geochemistry at Khongor Prospect Figure 16

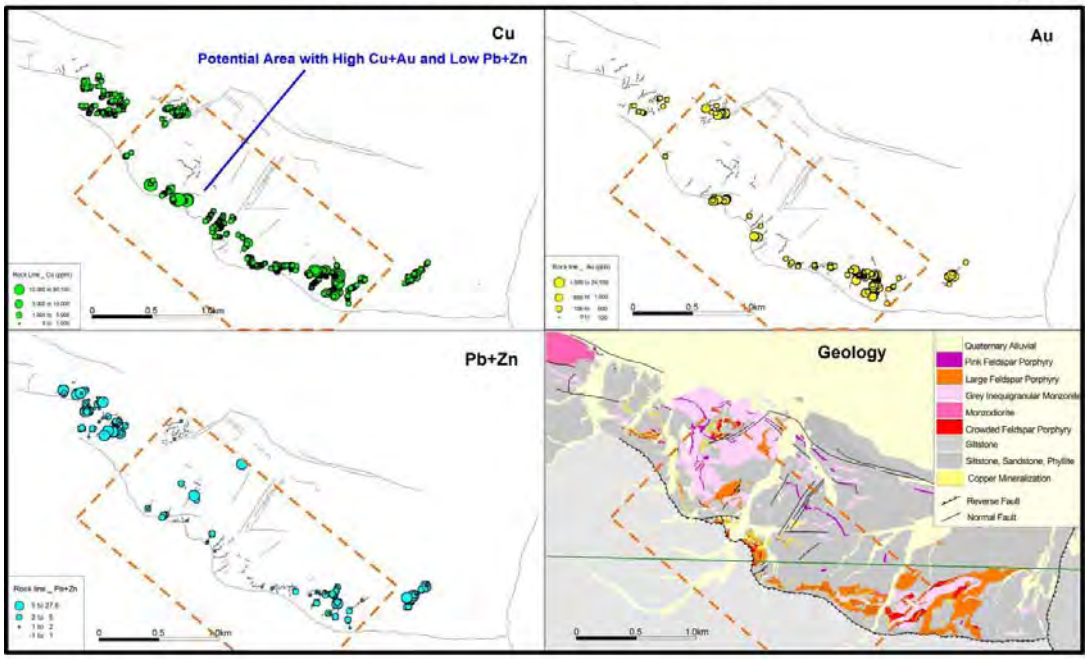

Khongor Geology:
Crowded feldspar porphyry and hornfels are the host rocks for porphyry stockwork mineralization, intrusives ranging from quartz monzodiorite to diorite mapped
Transpressive Thrust NE movement on flatter sections and vertical on EW
Alteration sequence/mineralization styles similar to porphyry systems elsewhere, including K-feldspar, biotite, magnetite and sericite-quartz alteration

The rock geochemistry shows a distinctive geochemical zonation with northwestern and southeastern extremities with higher Pb+Zn anomalism and a central area of Cu+Au mineralization which has potential for deep exploration.

Drilling

The first phase of drilling returned encouraging results including a best intercept of 50m with 1.0% Cu and 0.30g/t Au. (see Figures 17 & 18). Phase two and three drilling is ongoing.

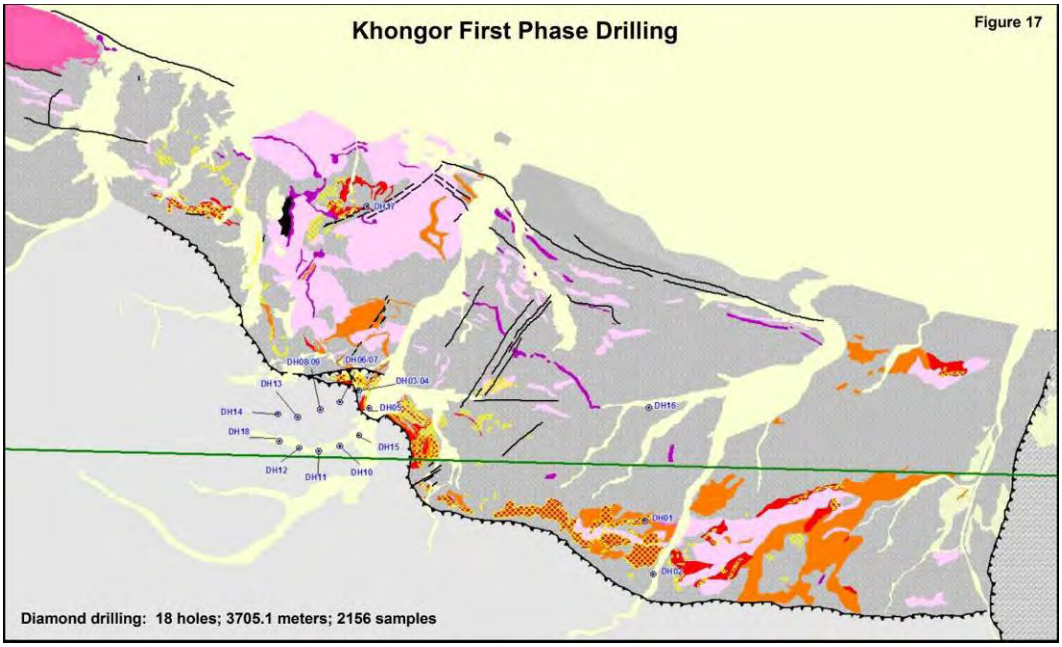

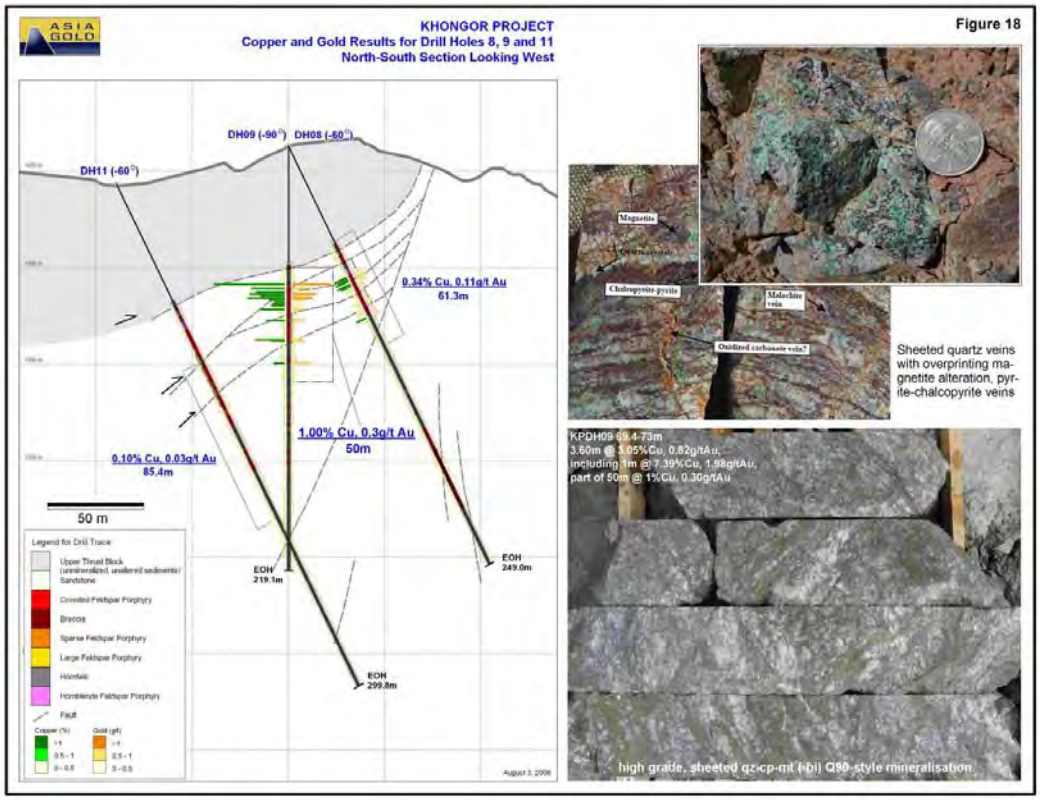

CONCLUSIONS

Exploration of large areas of the Gobi desert for Au and Cu has led Asia Gold to compare the efficiency of conventional fine-fraction (-63µm) geochemistry with coarse fraction (-230µm & +1mm/-4mm) sampling for low-density drainage surveys. Comparatitive arid region orientation test

work was carried out for different mineralization styles (epithermal Au at Yagaan & porphyry Cu-Au at Khongor). Conventional geochemistry gives broadly similar results in the test areas where Au and Cu anomalies of comparable size delineate the mineralized zones. In the conditions of the Gobi Desert, the mineralized zones at both prospects can be easily detected by stream sediment surveys using fine fraction (-63µm) stream sediments at a density of 1 sample per 6 ~10 km^2, and such a sampling density is recommended for evaluating the Au and Cu potential in large arid Gobi areas. A gold threshold of 2ppb is used and 5ppb is considered significantly anomalous.
In the test areas, the stream sediment fine fractions (<63µm) have identified more Au and Cu anomalism than the coarse fraction (-230µm & +1mm ~ -4mm) samples, despite the results being influenced by dilution of Au and Cu by barren material (eolian sands). As low detection limits (Au 0.2ppb) are required, the ICP-MS analytical method is recommended.

ACKNOWLEDGE

I wish to acknowledge Richard Gosse (Vice President of Asia Gold), Mark Hinman (Chief Geologist) and Nalin Shah (Exploration Manager of Mongolia) for their full support of the geochemical surveys and discussions of survey methodology. I also acknowledge the Asia Gold exploration group, especially Sarwanto who was the discoverer of Khongor porphyry Cu-Au deposit, Steve Enns (Consultant) for his experience in field mapping and Munkhtuya Sharav (GIS Specialist) who produced many maps for the survey and for this report, ACME (Vancouver) is thanked for their sample analysis and their consistant supply of QAQC-acceptable data.

REFERENCE

Nalin Shah. 2006. *KHONGOR a Copper Gold Porphyry Discovery***.** Conference on Discover Mongolia 2006. Ulaanbaatar, Mongolia.

Mark Hinman. 2006. *Khongor Review*. Asia Gold Corp. Internal Presentation. Ulaanbaatar, Mongolia.

C. Leduc and Y. Itard. 2003. Low sampling density exploration geochemistry for gold in arid and tropical climates: comparison between conventional geochemistry and BLEG*. Geochemistry: Exploration, Environment, Analysis*; January 2003; v. 3; no. 2; p. 121-131

Geology and geochemistry of intrusive dikes and metasedimentary rocks of Workamba area, Tigray province, northern Ethiopia

Gebresilassie, S and Marschik, R.

Department of Earth and Environmental Sciences, Ludwig-Maximilians Univeristy of Munich, Germany
Key words: Ethiopia, Workamba, trace elements, rare earth elements

ABSTRACT

The Workamba area, located in Tigray province, northern Ethiopia, is part of the Arabian-Nubian shield comprising low grade metasedimentary and volcanic rocks, monzogranites and aplitic dikes. Monzogranites and aplitic dikes, which postdate the sheared and low-grade metasedimentary rocks, are enriched in large ion lithophile elements (LILE) (Ba, Rb and Th) relative to the high field strength elements (HFSE) and show negative Nb anomaly indicating their derivation from the Pan-Afican arc related magmas. The metasedimentary rocks are enriched in light rare earth elements (LREE) as compared to heavy REE and exhibit negative Eu anomaly. Their La/Th and Eu/Eu* is 2.5 and 0.4-0.6 respectively. Such REE and element ratio characteristics suggest their derivation from felsic source, probably from the underlying Tsaliet Group metavolcanic rocks.

INTRODUCTION

The Workamba area in Tigray province, northern Ethiopia (Fig. 1), is currently explored for Au and base metals. Drilling identified mineralized zones in sheared metasediments in close vicinity to granitic dikes. The prospect rocks form part of the Neoproterozoic basement, which was studied by Beyth (1972). Further regional geologic studies have been carried out mainly after 1990 (e.g. Berhe, 1990; Stern, 1994 Tadesse et al., 1999; Alene et al., 2006). Although the knowledge on the basement rocks is continuously growing, there are many fundamental topics such as stratigraphy, geologic evolution, or tectonic setting etc. that are controversially discussed (e.g. Tadesse et al., 1999). In this paper, we present a summary of the geology of a Au-basemetal prospect near Workamba and investigate geochemical characterstics of the intrusive and metasedimentary rocks and infer their tectonic setting and link to the geologic context

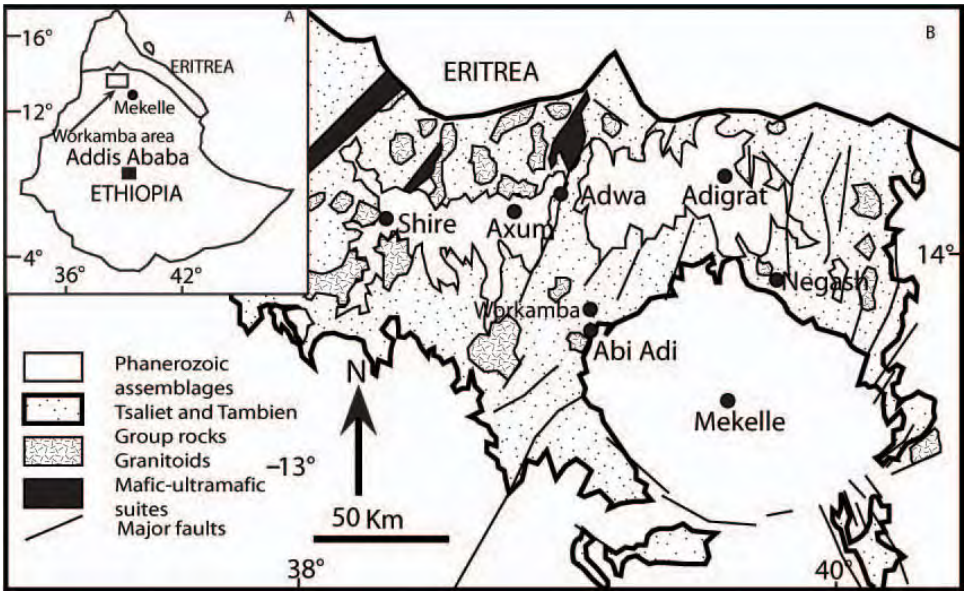

Figure1. a) Map of Ethiopia showing the location of the study area and b) regional map of Tigray province modified after Asrat (2002)

REGIONAL GEOLOGICAL SETTING

The Neoproterozoic basement of Tigray region is part of the Arabian-Nubian Shield (ANS) and comprises metavolcanic, metasedimentary, mafic-ultramafic rocks, carbonates, and granitoids (Fig. 1; Beyth, 1972; Tadesse et al., 1999; Alene et al., 2006). It is interpreted to represent east to west accreted intra-oceanic arc sequences (Tadesse et al., 1999) having variable lithological and geochemical characterstics. Beyth (1972) has subdivided the basement rocks in two units, the Tsaliet Group, and the overlying Tambien Group. The Tsaliet Group is composed of calc-alkaline island arc rocks (Alene et al., 2000, Tadesse et al., 1999) that include felsic to intermediate volcanic flows, volcanic greywacke, welded tuff, lappili tuff, and agglomerates, which are metamorphosed up to lower greenschist facies (Beyth, 1972; Beyth et al., 2003; Alene et al. 2000). The rocks of this unit are assumed to be the southern continuation of the metavolcanic rocks of Nakfa terrain of Eritrea (Tadesse et al., 1999; Alene et al., 2006), which are dated 854 ±3 Ma using the Pb/Pb single-zircon evaporation method (Teklay, 1997). The Tambien Group comprises highly deformed metasedimentary rocks including slate, phyllite, graphite schist, oolitic black limestone with detrital algal fragments, and limestone with well preserved stromatolites, greywacke, quartzite and dolomite (Beyth, 1972; Beyth et al., 2003). The rocks were deposited in a marine environment (Alene et al. 2006). Alene et al. (2006) estimate the age of the Tambien Group to be between 800 and 735 Ma based on $\delta^{13}C$ and $\delta\ ^{18}O$ and $^{87}Sr/^{86}Sr$ characteristics. Based on major, trace and rare earth element studies Sifeta (2003) concluded that the Tambien Group metasediments are derived from mafic source with some mixing from felsic sources. The

nature of the contact between the Tsaliet and Tambien groups is controversial. Beyth (1972) recognized an unconformable contact, whereas Alene et al. (1998) describe a conformable, gradational contact.
Syn- and post-tectonic I-type granitoids intruded both the Tsaliet and Tambien groups (Tadesse et al. 2000; Alene et al., 2000, 2006; Asrat, 2002). The deformation of the syn-tectonic granitoids is manifested by mylonitic fabrics. The ages of the syn-tectonic granitoids range from 800 to 750 Ma, whereas post-tectonic plutons were emplaced around 550 Ma (e.g. Tadesse et al., 2000, Asrat et al., 2001 and references therein). Two deformation phases (D1, D2) are recognized in the rocks of the Tsaliet and Tambien groups (Alene et al., 2006). They were caused by N-S or E-W compressional stress, respectively (Alene et al., 2006). D1 resulted in tight folds, lineation and pervasive foliations, while D2 formed long wave length, upright, open parallel folds. The ages of syn- and post-tectonic granitoids constrain the ages of these deformation phases to a range between 800 and 550 Ma.

Prospect geology

Both, the Tsaliet and Tambien group rocks crop out in the prospect study area (Fig.2). The Tsaliet group metavolcanic rocks are exposed in the northwestern part of the study area. They vary from basic to felsic pyroclastic flows having 1-5 cm size clasts. Local propylitic alteration affects these rocks especially towards the contact with the silicified rocks. Towards the north, malachite stains are observed on cleavage planes suggesting copper mineralization at depth. The silicified rocks are exposed in the central part of the area in the form of north to east trending belt. The Tambien Group rocks mainly occupy the southeastern portion of the study area and include talc-chlorite schist, slate, phyllite, and graphite-bearing schist. They are affected by local hydrothermal alteration such as silicification, sericitization, carbonatization, and/or chloritization. Both Tsaliet and Tambien groups exhibit D1 foliation with an average strike of N40°E and dip of 60° NW. An up to 100 m thick monzogranite dike intruded the Tambien Group in its lower part. Dike emplacement occurred along the strike of the foliation although cross-cutting relationships between the dike and the foliation are observed at some places. Aplitic dikes are observed within both, the Tsaliet and Tambien groups. These dikes are affected locally by propylitic alteration.

Drilling holes penetrated monzogranite and aplite dikes, sericite-rich rocks, talc-chlorite schist and carbonatized and silicified chlorite schist. Au and basemetal sulfides occur in highly altered and sheared metasedimentary rocks, which are cut by quartz and/or quartz-carbonate veins. Encountered sulfides include pyrite, chalcopyrite, sphalerite, and galena. Hematite is also present. They occur as veinlets and disseminations in host rocks as well as within quartz and/or quartz-carbonate veins.

Structure

Both brittle and ductile structures affect the rocks of the study area. Ductile deformation is represented by the occurrence of parasitic D1 folds occupied by 1 to 5 cm quartz veins. Ductile to brittle shear zones are recognized within the metavolcanic and at contact between the monzogranite and the mineralized metasedimentary rocks (Fig.2). Shear deformation is manifested by increased density of NE-trending foliation planes, intense crenulation cleavage, abundant NE to SW trending sinstral tension gashes, closely spaced fractures cutting foliation, and closely spaced second-generation quartz veins (Fig. 3 and 6). The brittle deformation includes north to west and north to south trending fractures. Some of the fractures are filled by 0.5 to 1 m thick undeformed second generation quartz and/or quartz-carbonate veins that occur parallel to and/or cut foliation at angles roughly between 30º and 60º. They also cut D1 folds.

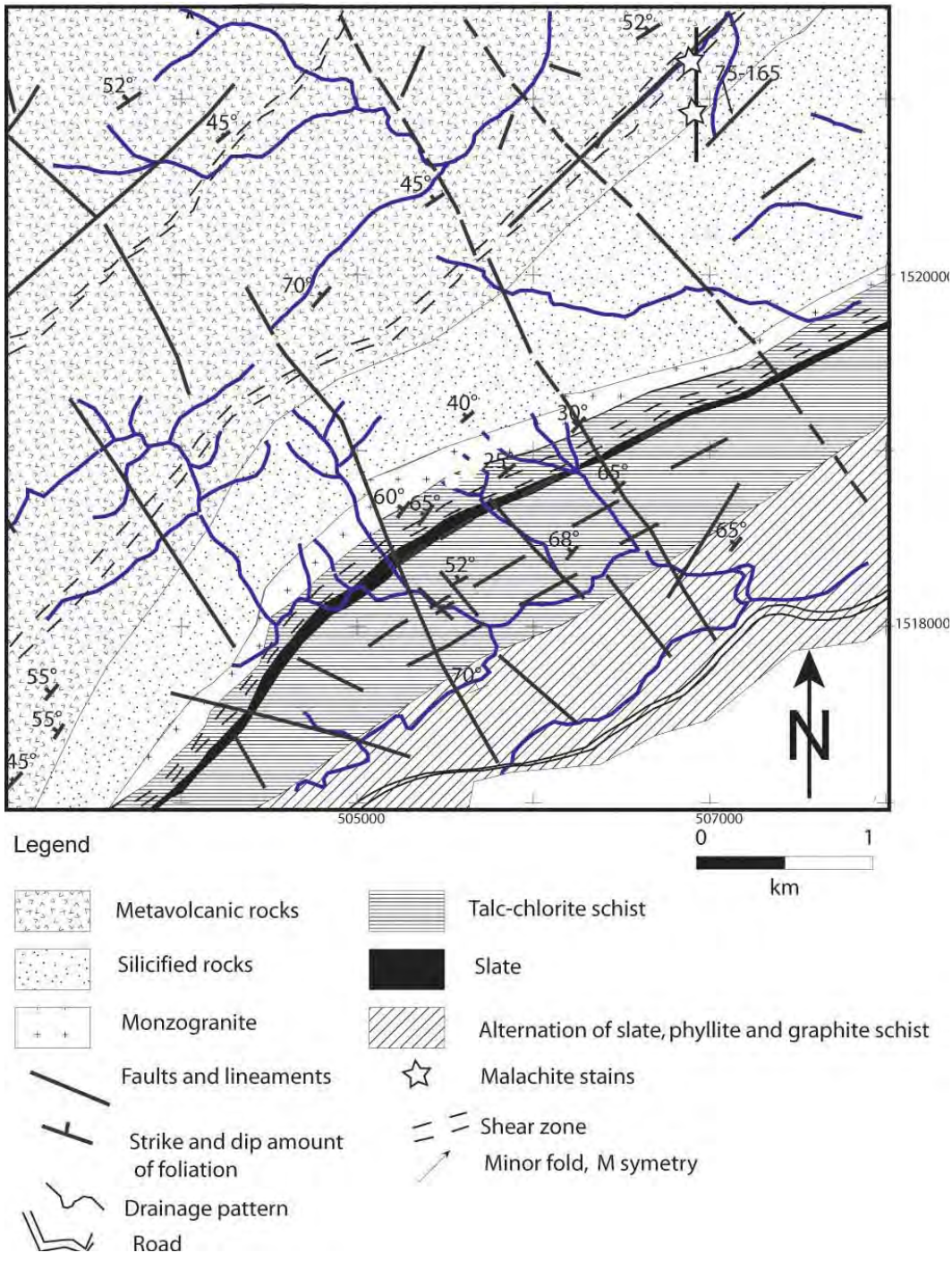

Figure 2: simplified geological map of the Workamba area. Circular dots represent the investigated boreholes

Geochemistry

Chondrite-normalized trace element patterns of the monzogranite and aplite dikes (Fig. 3a-b) show an enrichment in large ion lithophile elements (LILE; Ba, Rb and Th) relative to the high field strength elements (HFSE), and a negative Nb anomaly, which is characteristics of arc-related

magmas. The trace element distribution is similar to that in the Negash, Shire, and Mereb post- tectonic volcanic arc granites (VAG) in northern Ethiopia. Their average Rb/Sr and Rb/Ba values are ~ 0.14 and 0.06 respectively, which are lower as compared to those of I, A, and S-type granites (Whalen et al., 1987). Chondrite-normalized REE patterns show an enrichment of LREE over HREE (Fig. 3c, d). The dikes are highly fractionated with $(La/Yb)_N$ ranging from 17-18 for the granite and 13-30 for the aplite. These patterns may indicate derivation from a LREE-enriched or contaminated source. In a Rb vs. Y+Nb diagram of Pearce et al. (1984) (Fig. 4), the monzogranite and aplite plot within the VAG field along with Negash, Shire, and Mereb post-tectonic granites. Therefore, we suggest that the Workamba monozogranite and aplitic dikes are derived from the Pan-African arc related magmas.

Upper continental crust-normalized (UCC) trace element patterns of the Workamba metasedimentary rocks (WMS) indicate no significant enrichment or depletion with respect to the UCC (Fig. 5a-c). They are similar to the late Proterozoic felsic volcanic rocks of Condie (1993) and Tambien Group metasedimentary rocks of Sifeta (2003), which are included for comparison. All but one sample (J2-034, carbonatized rock) of the WMS are characterized by negative Sr anomalies and anomalous Pb values (up to 1130 ppm) for the samples J2-05, J2-023 and J2-034.

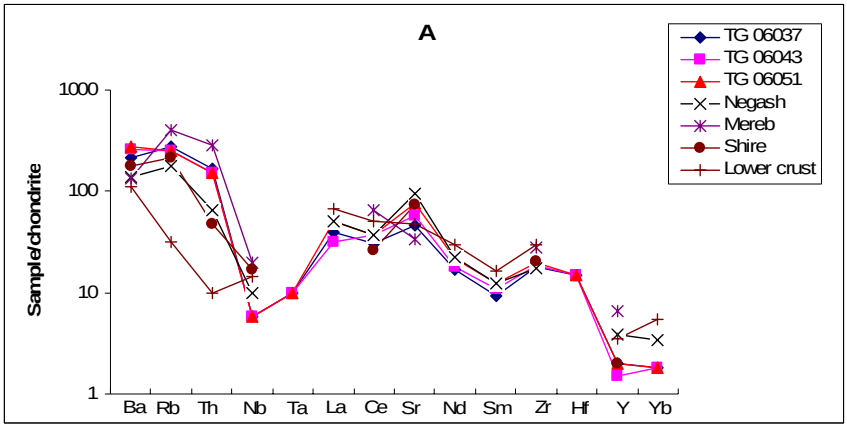

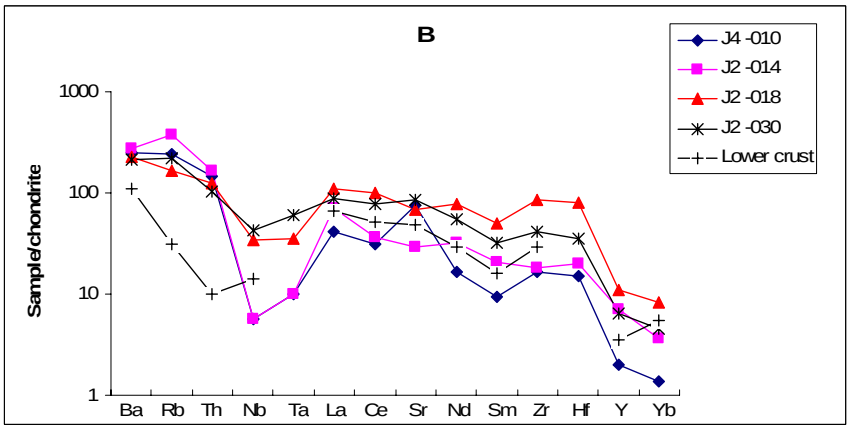

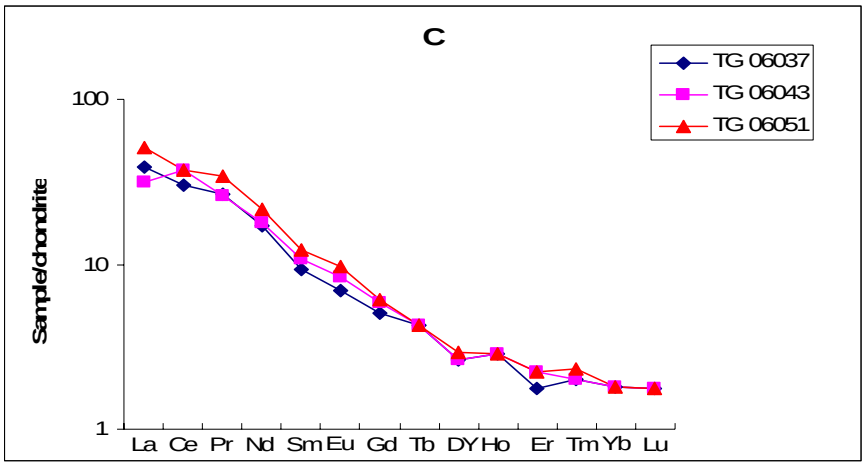

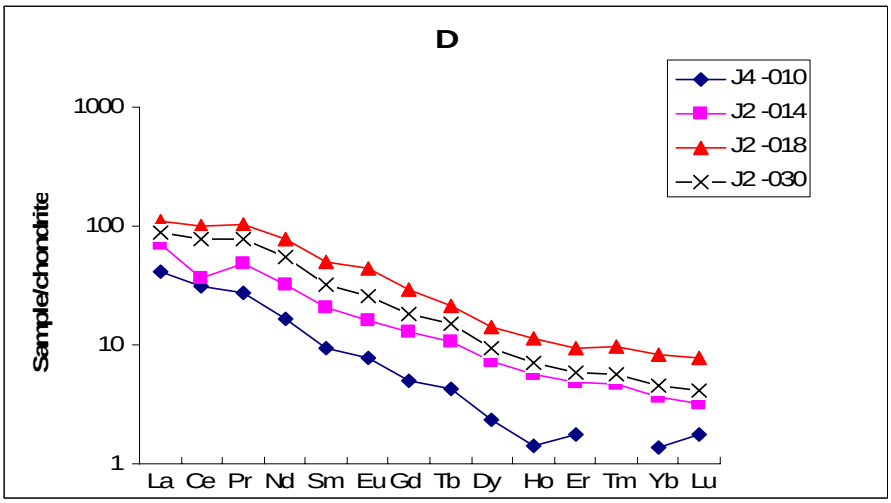

Figure 3. Trace and REE patterns: a) and c) monzogranite; b) and d) aplite.

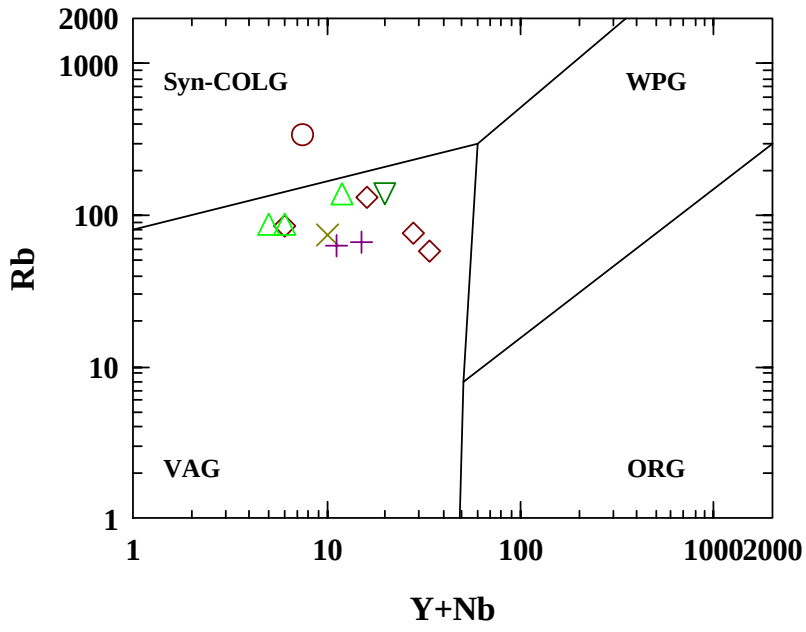

Figure 4: La vs. Y+Nb element discrimination diagram of the Workamba monzogranite and aplite dikes (Δ = monzogranites, ◊ = aplite, × = Shire granite, O = Negash aplite, + = Negash granite and inverted triangle represents Mereb granite).

The anomalous Pb values in some of the samples are due to presence of hydrothermal galena, which is part of the metallic minerlization. The reason for the comparably low Sr concentrations (7 to 24 ppm) is unknown. We did not find evidence for Sr-leaching by hydrothermal fluids that caused the mineralization though this possibility is not excluded.
The average La/Th for the WMS is 2.5 and therefore lower than that of the late Proterozoic felsic volcanic rocks (La/Th = 4.1) and late Proterozoic basalts and komatïtes (La/Th = 5; Condie, 1993). It is similar as that of felsic volcanic rocks (La/Th = 2-4; McLennan et al., 1980) and post Archean sedimentary rocks (La/Th = 2.7) derived from felsic source (McLennan et al., 1980). Other element ratios e.g. Ba/La, La/Sc, Ba/Nb, Zr/Nb, Cr/Th, Th/Sc are not comparable either with late Proterozoic felsic volcanic rocks or late Proterozoic basalts and komatïtes.

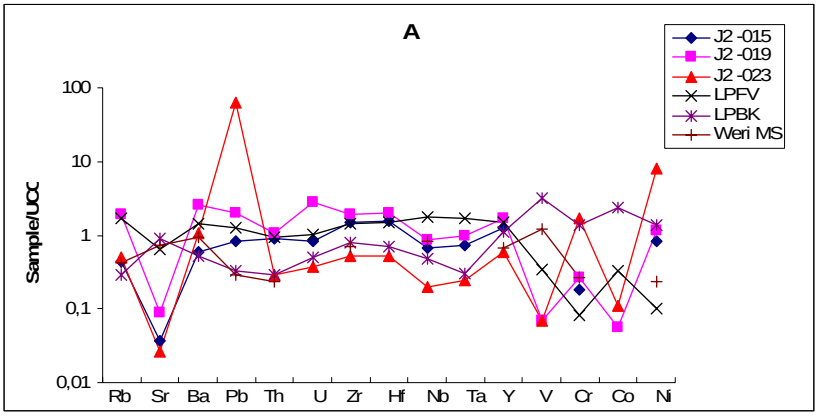
A
J2 -015
J2 -019
J2 -023
LPFV
LPBK
Weri MS
Sample/UCC
100
10
1
0,1
0,01
Rb Sr Ba Pb Th U Zr Hf Nb Ta Y V Cr Co Ni

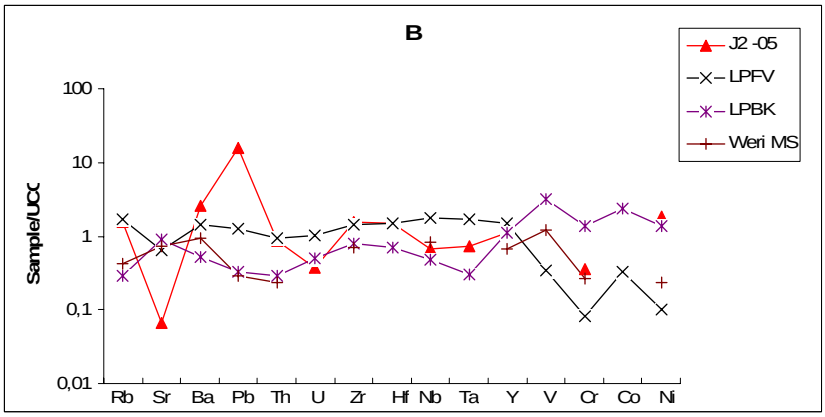
B
J2 -05
LPFV
LPBK
Weri MS
Sample/UCC
100
10
1
0,1
0,01
Rb Sr Ba Pb Th U Zr Hf Nb Ta Y V Cr Co Ni

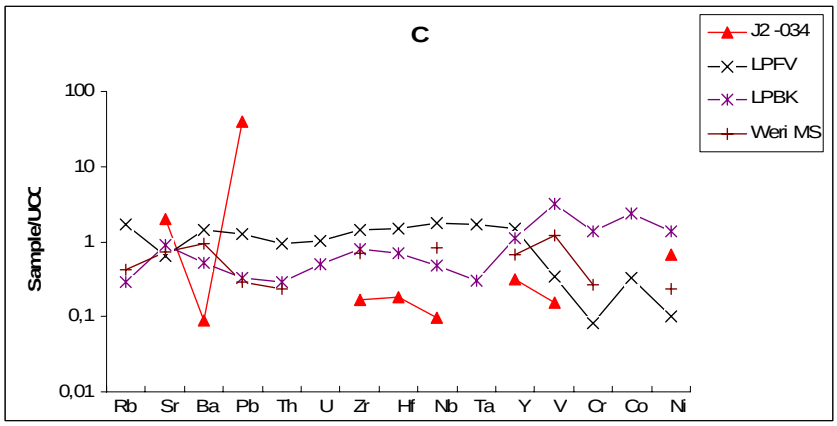
C
J2 -034
LPFV
LPBK
Weri MS
Sample/UCC
100
10
1
0,1
0,01
Rb Sr Ba Pb Th U Zr Hf Nb Ta Y V Cr Co Ni

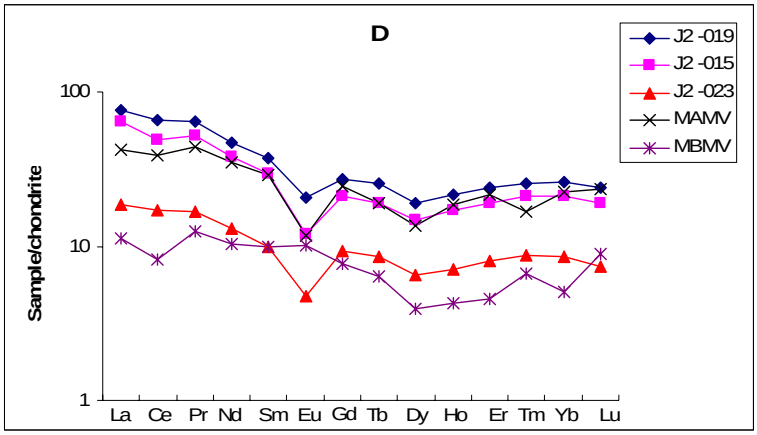

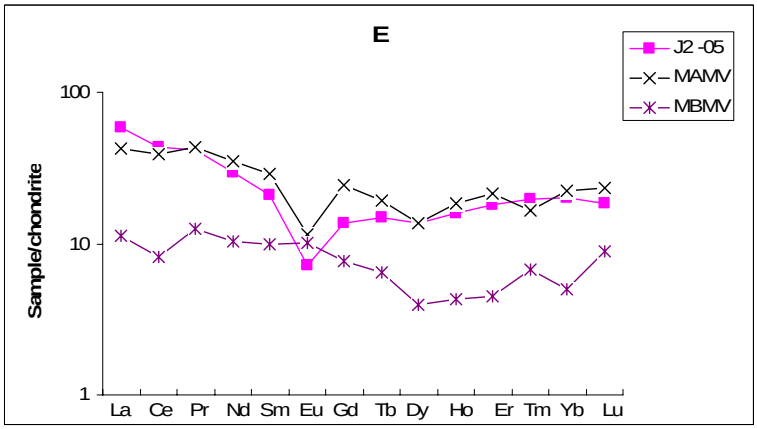

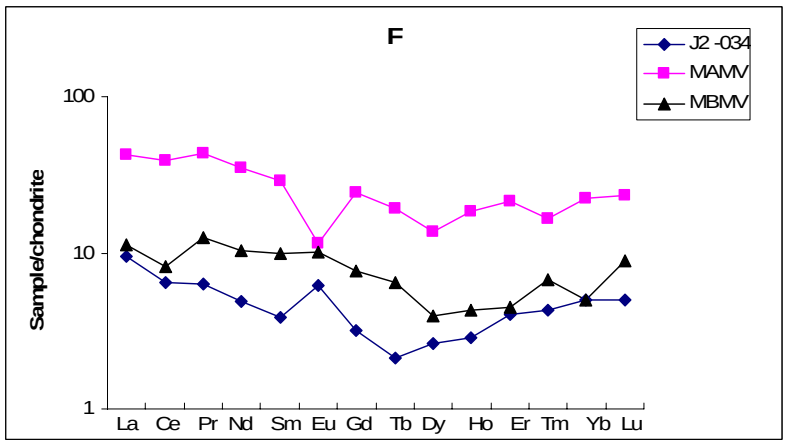

Figure 5: a-c and d-f showing trace and REE pattern of WMS respectively.

In chondrite-normalized REE pattern (Fig. 5d-f), all the WMS but one sample (J2-034) are characterized by enrichment of LREE over HREE and show negative Eu anomalies. These signatures are shared by post-Archean sedimentary rocks and acidic metavolcanic rocks exposed in the region (Alene et al., 2000). The $(La/Yb)_N$ of the WMS ranges from 1.8-2.9,

i.e. it is lower than that of late Proterozoic felsic volcanic rocks ($(La/Yb)_N$ = 6; Condie, 1993). The Eu/Eu* of the WMS ranges from 0.4 to 0.6, which is approximately similar to the value of the late Proterozoic felsic volcanic rocks that is, 0.68 (Condie, 1993). The carbonatized sample (J2-034) on the other hand is less enriched in LREE and have positive Eu anomaly and shows similar REE pattern as the basic Metavolcanics of the region (Alene et al., 2000). In general, however, the geochemical data on Workamba metasedimentary rocks support a derivation from felsic sources, and they may originate from the felsic volcanic flows of the underlying Tsaliet metavolcanic rocks.

CONCLUSION

Trace element, REE, and geochemical characteristics of the monzogranite and aplite dikes in the Workamba area are similar to those of volcanic arc Pan-African granitoids exposed in northern Ethiopia, which are resulted from subduction related magmatism involving melting of the subducted slab modified by mantle component. The geochemical data on Workamba metasedimentary rocks suggest that they originate from a felsic source.

ACKNOWLEDGMENT

The first Author would like to acknowledge DAAD (German Academic Exchange Service) for funding the project. The department of Applied Geology, Mekelle University, and National Mining Corporation (NMiC) are also thanked for providing a vehicle and logistics for the fieldwork. My special thanks go to Kibret Sifeta and Senbeto Chewaka (staff members of NMiC) for their guidance and help in the field.

REFERENCES

Alene, M., *et al.*, 2000. Geochemistry and geotectonic setting of Neoproterozoic rocks from northern Ethiopia (Arabian-Nubian Shield). *Gondwana Research*, 3, 3, 333-347.

Alene, M., *et al.*, 2006. The Tambien Group, Ethiopia: An early Cryogenian (ca. 800-735 Ma) Neoproterozoic sequence in the Arabian-Nubian Shield. *Precambrian Research,* 147, 79-99.

Asrat, A., *et al.*, 2001. *The Precambrian Geology of Ethiopia: a review*. *Africa Geosciences Review*, 8, 3, 271-288.

Asrat, A., 2002. Magma emplacement and mafic magma hybridization: structural evidence from the Pan-African Negash pluton, Northern Ethiopia. Ph. D Thesis, *CRPG-CNRS,15, Cedex,* France.

Berhe, S. M., (1990), Ophiolites in Northeast and East Africa: implications for Proterozoic crustal growth. *Journal of Geological Society of London*, v.147, p. 647-657.

Beyth, M., 1972. The Geology of Central-Western Tigre. Ph. D. Thesis, Rheinische Friedrich-Wilhems Universitaet, Bonn, Germany.

Beyth, M., *et al.*, 2003. Crustal exhumation and indications for Snowball Earth in the East African Orogen: north Ethiopia and east Eritrea. *Precambrian research*, 123, 187-201.

Condie, K.C., 1993. Chemical composition and evolution of the upper continental crust: contrasting results from surface samples and shales. *Chemical Geology* 104, 1-37.

McLennan, S. M., *et al.*, 1980. Rare earth element-thorium correlations in sedimentary rocks, and the composition of the continental crust. *Geochimica et Cosmochimica Acta,* Vol. 44, 1833-1839.

Sifeta, K., 2003. Geochemistry, tectonic setting, and provenance of Weri metavolcanic and sedimentary units, northern Ethiopia. Unpublished M.Sc. thesis, Shimane University, Japan.

Stern, R.J., 1994. Arc assembly and continental collision in the Neoproterozoic East African Orogen: implications for consolidation of Gondwana land. *Annual Reviews Earth Planetary Sciences*, 22, 319-351.

Tadesse, T., *et al.*, 2000. Sm-Nd, Rb-Sr, and Th-U-Pb zircon ages of syn- and post-tectonic granitoids from the Axum area of northern Ethiopia. *Journal of African Earth Sciences*, 30, 313-327.

Tadesse, T., *et al.*, 1999. Geochemistry of low-grade metavolcanic rocks from the Pan African of the Axum area, northern Ethiopia. *Precambrian Research*, 99, 101-124.

Teklay, M., 1997. Petrology, Geochemistry, and Geochronology of Neoproterozoic Magmatic Arc Rocks from Eritrea: Implications for Crustal Evolution in the southern Nubian Shield. vol. 1, *Eritrea Department of mines Memoir*, p.125.

Pearce, J.A., *et al.*, 1984. Trace element discrimination diagrams for the tectonic interpretation of granitic rocks. Journal Petrology 25, 956-985.

Whalen, J. B., *et al.*, 1987. A-type granites: geochemical characteristics, discrimination and petrogenesis. *Contributions to Mineralogy and Petrology*, 95, 407-419

The geothermal geochemistry of Western Turkey

Haklıdır Tut and Füsun Servin

TUBITAK-MRC Earth and Marine Sciences Institute,Gebze
Kocaeli-TURKEY
E-mail: Fusun.Tut@mam.gov.tr
Keywords: Geothermal, geochemistry, Western Anatolia

ABSTRACT

Turkey was strongly affected by the Alpine-Himalayan orogenic belt. The tectonically active areas are concentrated along high stress zones like North Anatolian strike-slip fault, East Anatolian transform fault and graben zones in Western Anatolia. Western Anatolian is such a tectonically active region in Turkey which has large grabens (such as Gediz and Menderes Grabens) association with extensional tectonic. The region also has been represented with young volcanics (such as Kula Volcanics). Because of thinning of the crust in this part of Anatolian, geothermal systems were occurred along grabens with high enthalpy. The high enthalpy are concluded largely variable in chemical composition of fluids. Geothermal reservoirs of the Aegean Region are generally composed of Permian limestones, Mesozoic limestones and marble levels of metamorphic Palaeozoic. With this reason geothermal water sources were affected by reservoir rock chemistry and the water types are generally dominated in terms of calcium and bicarbonate ions. The travertine deposits (such as Pamukkale; cotton castle, Urganlı) are observed around the hot sources.

INTRODUCTION

Western Turkey has so many geothermal areas and the geothermal fluid enthalpies are changed from 25 ºC to 240 ºC in this region. If the area is divided to three parts such as north, central and south, the central part will be the most high enthalpy region (Fig.1). The north part of the Western Turkey includes Bursa, Balıkesir, Çanakkale cities (Part I). This region is represented both low (20ºC -70ºC) and moderate (70ºC-150ºC) enthalpies. Second part, which is called central part of Western Anatolia, includes Manisa, İzmir, Aydın, Denizli, Kütahya and Uşak cities (Part II). This part is represented with from low to high enthalpy (over 200 ºC) fluids. The south part is represented with low enthalpy and includes Muğla city (Part III). Depend on changing enthalpies in these regions, the chemistry of fluids are also changed with dramatically.

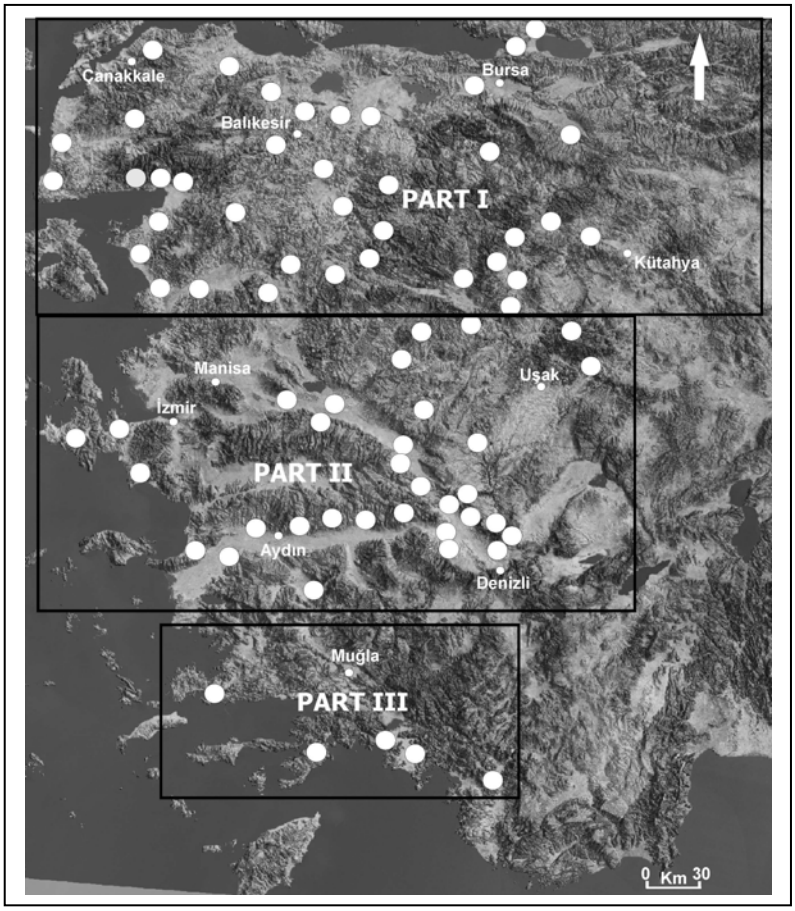

Figure.1. Important Geothermal Fields in Western Anatolia

GENERAL GEOLOGY OF WESTERN TURKEY

Turkey was strongly affected by the Alpine-Himalayan orogenic belt. The tectonically active areas are concentrated along high stress zones like North Anatolian strike-slip fault, East Anatolian transform fault and graben systems in Western Anatolia.

The Western part of Turkey is affected by The North Anatolian Fault Zone (NAF) and graben zones are. Especially Part I area is affected by south segment of NAFZ and Eskişehir Fault Zone (Fig.2). The segment is called Geyve-İznik Fault and runs north of Bursa (Herece, 1990). The Balıkesir geothermal area is represented by metamorphic rocks of the Menderes Massif which consists of from Palaeozoic to Early Mesozoic schist, gneiss, marble and melange units of Late Cretaceous and granitic plutons with Oligocene-Middle Miocene age (Delaloye&Bingöl, 2000). Çanakkale area is composed of Permian metamorphic rocks, granodiorite intrusive rocks, Miocene volcanics (rhyodacitic, ignimbrite, trachyte). Bursa city is consists of Palaeozoic metamorphic rocks (gneiss, schists, semi marbles and marbles), Early Permian marbles, Neogene sediments and Uludağ granodiorites (63 m.y. age, Delaloye&Bingöl, 2000).

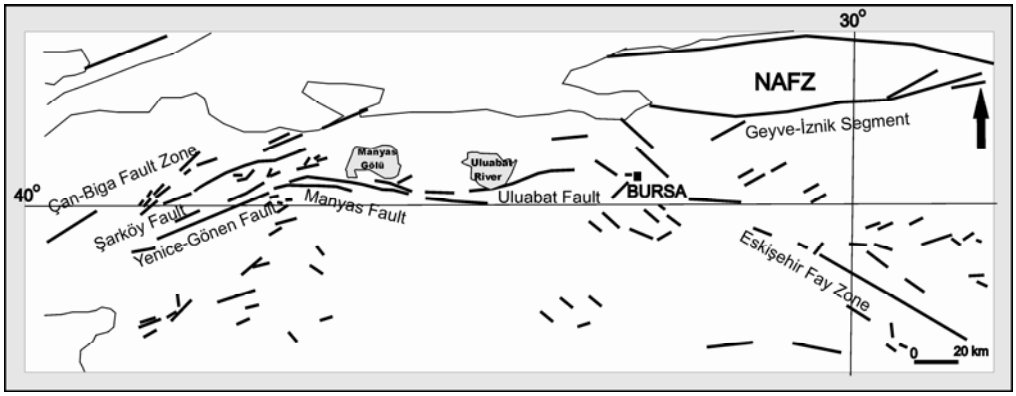

Figure.2 Effected tectonic lines of Part I region in Western Anatolian (modified Bozkurt, 2001)

Part II area is affected by Aegean graben systems. In this region, pre-Mesozoic aged metamorphics (marbles,quartzites,gneiss) of the Menderes and Kazdağ massives, Mesozoic limestones, Neogene volcano sedimentary units and restricted Quaternary volcanism (Kula volcanics) has been observed. As a result of graben systems, crustal thinning is shown in Part II.

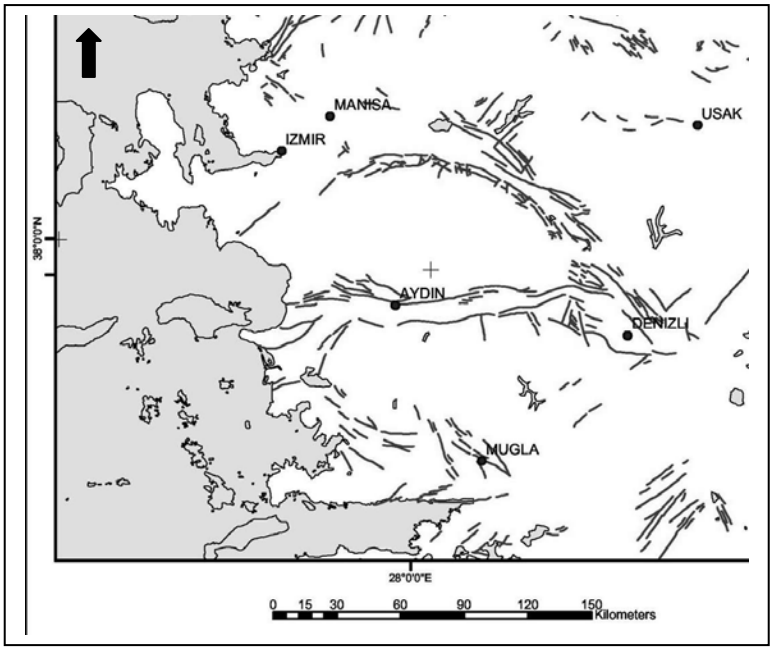

Figure.3 Tectonic lines in Part II and Part III regions (from MTA Active Fault Map)

In study area Part III is just represents with Muğla city that is affected Fethiye-Burdur Fault Zone.

HYDROGEOCHEMICAL EVALUATIONS

Geothermal Waters Chemistry of Part I region

Temperatures of the thermal waters are changed between 32 and 99 ºC in Balıkesir, 40-98 ºC in Çanakkale and 28-80 ºC in Bursa city. TDS (Total dissolved solids) content of thermal waters range from 300- 2580 mg/l in Balıkesir, 490-2310 mg/l (MTA, 2005) and 220-1759mg/l in Bursa. While the water types are shown Na-SO_4, Ca-HCO_3 in Balıkesir, Na-Ca-HCO3-SO_4 in Çekirge region, and Ca-Mg-Na-HCO_3 in Kaynarca region, Bursa. Çanakkale thermal waters are shown Na-SO_4 and Na-Cl type (Fig.4-Mutlu&Güleç,1998).

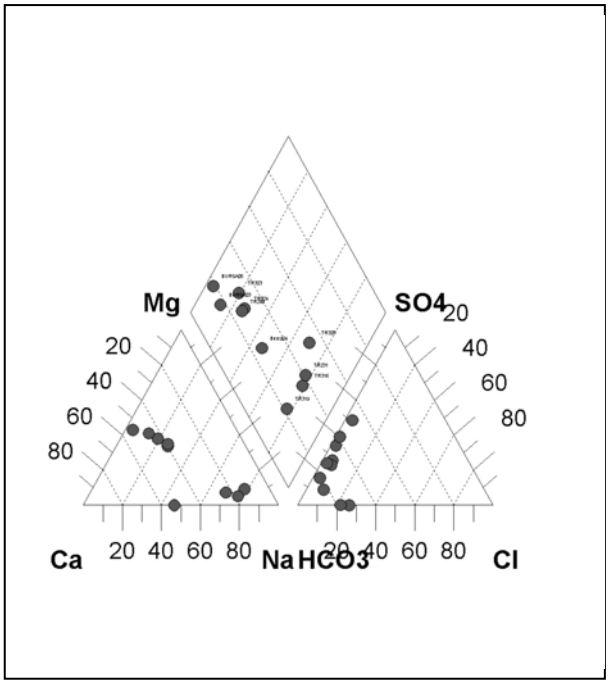

Figure.4 Bursa thermal and mineral waters types (Tut,2007)

Geothermal Waters Chemistry of Part II and III region

Gediz Graben geothermal waters have discharge temperatures between 25-95 ºC, and TDS 600-4500 mg/l. The waters are represented Na-HCO_3 and Ca-HCO_3 during the graben (Fig.5). There are some mineral water spring along graben which is so called Kurşunlu, Sarıkız and Kula mineral water.

Büyük Menderes Graben geothermal waters have discharge temperatures between 35-242 ºC. The graben has higher water temperature. Ömerbeyli-Germencik/Aydın thermal water temperature is 232 ºC and Kızıldere/Denizli thermal water temperature is 242 ºC and both of two have high Boron concentration (B_T 28 ppm Kızıldere thermal water, 63

ppm Ömerbeyli water, Mutlu&Güleç, 1998). The water type is Na- HCO_3 in Kızıldere and Na-Cl in Ömerbeyli.
Kütahya thermal waters temperatures change 38-75 ºC and they are represented as Na-SO_4 and Ca-HCO_3. Uşak thermal water temperatures are changed 39-60 ºC and TDS is changed between 4400-5160 mg/l (Barut et al., 2003)
In Part III region, Muğla thermal waters temperatures are changed 26-42 ºC. They include high Na and Cl ions because sea effect.

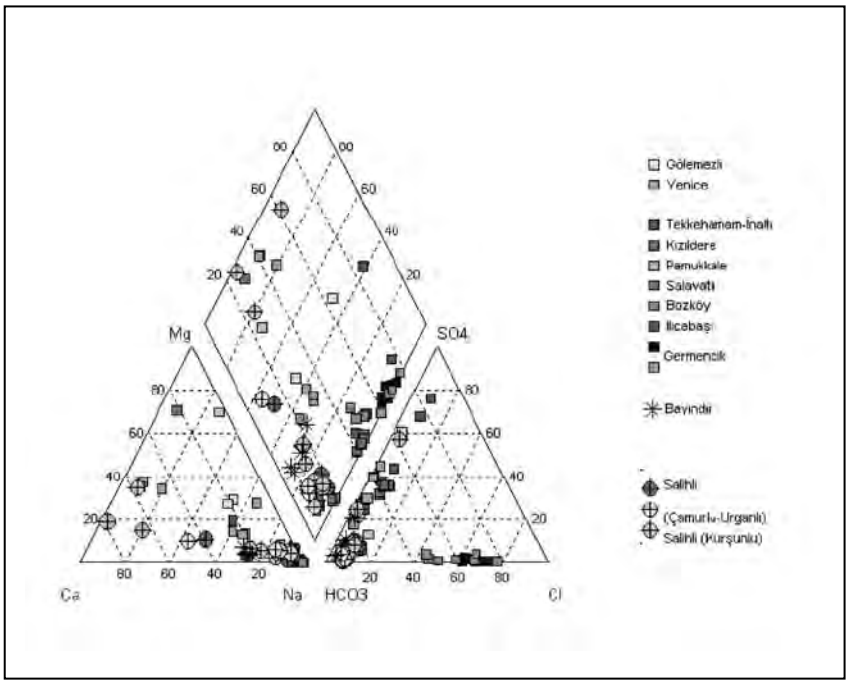

Figure.5 Part II thermal waters types

180-D Isotopic Compositions of Western Thermal Waters

Part I region thermal waters isotopic compositions are shown on Fig.6. Marmara Global Meteoric Water Line equation is represented $\delta D=8.\ \delta^{18}O+22$ and Global Meteoric Water Line equation is represented $\delta D=8.\ \delta^{18}O+10$. According the graphic Bursa-Uludağ mineral water (UMS) has been shown the most $\delta^{18}O$ enrichment in this area and Güre - Balıkesir thermal water has been shown the less $\delta^{18}O$ enrichment in the area. It means water-rock interaction is dominated in UMS location. Part II region thermal waters are also shown in Fig.7. According the graphic, the most $\delta^{18}O$ enrichment is observed in Bozköy (Alangüllü-Aydın) location.

ID	18O	D	City	Reference
Kaynarca	**-10.22**	**-70.3**	Bursa	Tut
U.MS.	**-8.38**	**-60.5**	Bursa	Tut
UMS	**-7.05**	**-48.1**	Bursa	Tut
Karamustafa	**-10.66**	**-68.4**	Bursa	Tut
Zeynine	**-9.96**	**-66.8**	Bursa	Tut
Küplüce	**-10.46**	**-68.3**	Bursa	Tut
BK1	**-10.97**	**-71.8**	Bursa	Tut
Vakıfbahçe	**-10.35**	**-68.2**	Bursa	Tut
G7	**-12.12**	**-76.83**	Balıkesir	Mutlu
G16	**-12.5**	**-77.39**	Balıkesir	Mutlu
EKS1	**-11.94**	**-60.91**	Balıkesir	Mutlu
MK1	**-9.91**	**-61.36**	Balıkesir	Mutlu
PMK	**-10.67**	**-63.81**	Balıkesir	Mutlu
BHS1	**-9.94**	**-71.1**	Balıkesir	Mutlu
SHS1	**-11.61**	**-68.49**	Balıkesir	Mutlu
EDR	**-10.05**	**-55.15**	Balıkesir	Mutlu
BLY	**-12.5**	**-76.8**	Balıkesir	Mutlu
SLK1	**-11.05**	**-63.16**	Balıkesir	Mutlu
Hıdırlar	**-8.37**	**-50.3**	Çanakkale	Yalçın
Çan	**-7.26**	**-59.55**	Çanakkale	Yalçın
Kırkgeçit	**-9.63**	**-61.76**	Çanakkale	Yalçın
Karaılıca	**-8.8**	**-59.1**	Çanakkale	Yalçın
Gölemezli	**-8.32**	**-57.8**	Denizli	Yaman
Bozköy	**-8.32**	**-60.4**	Aydın	Yaman
Kamara	**-8.28**	**-57.8**	Denizli	Yaman
Tekkehamam	**-8.28**	**-57.8**	Denizli	Yaman
Kızıldere KD13	**-5.31**	**-54.1**	Denizli	Yaman
Salavatlı	**-6.58**	**-60**	Aydın	Yaman
Pamukkale	**-9.14**	**-61**	Denizli	Yaman
Germencik	**-2.14**	**-38.9**	Aydın	Özgür
Turgutlu	**-7.72**	**-55.7**	Manisa	Özgür
Sart	**-6.72**	**-45.9**	Manisa	Özgür
Bayındır	**-6.57**	**-35.6**	İzmir	Özgür
Kurşunlu	**-5.16**	**-48.9**	Manisa	Özgür

Table. I Stable Isotope Values in Part I and Part II regions

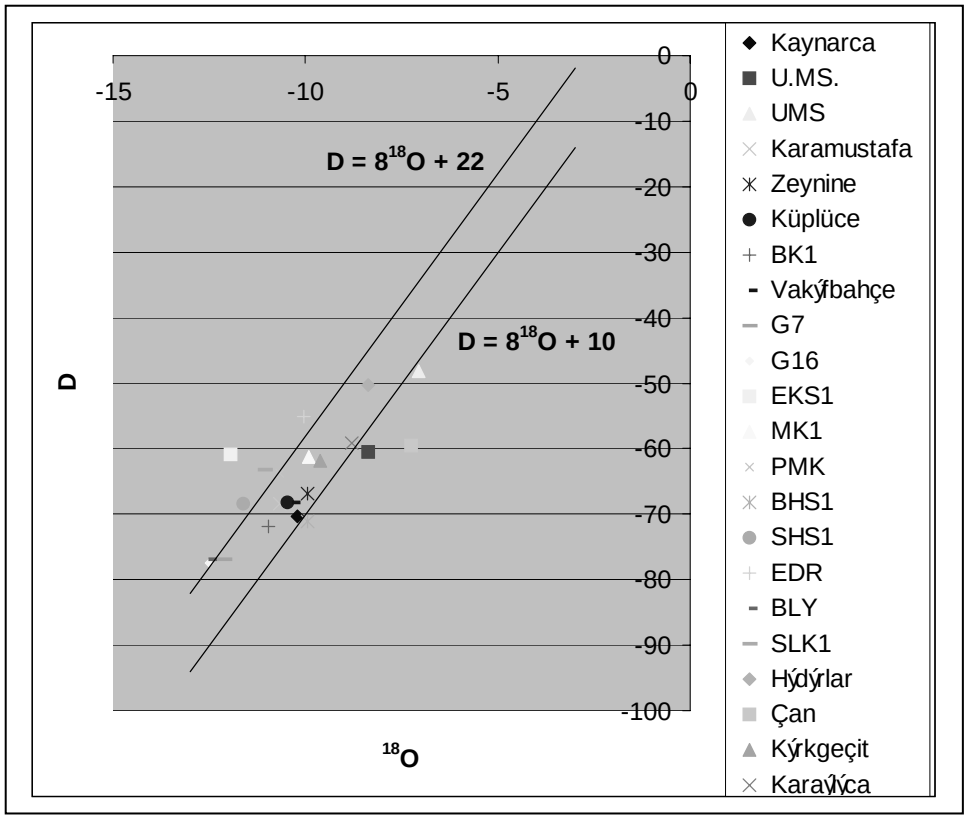

Figure. 6 $\delta^{18}O$- δD Isotopic Composition in Part I region

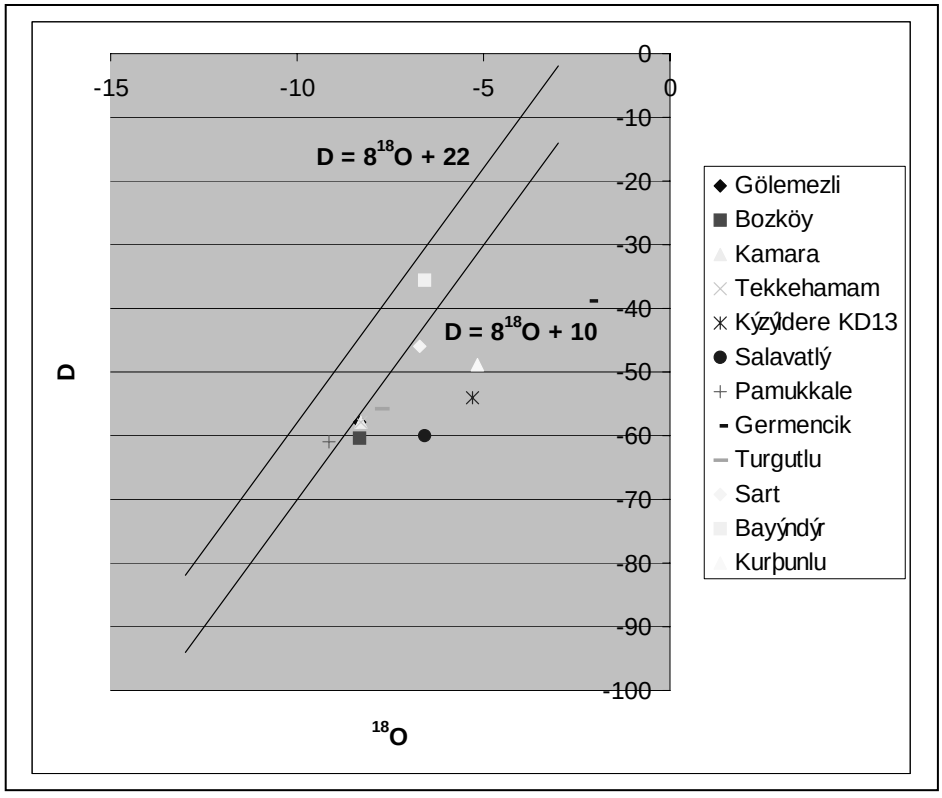

Figure. 7 $\delta^{18}O$- δD Isotopic Composition in Part II region

When the Part I and Part II regions are compared with each other, Part II regions shows the more water-rock interaction.

CONCLUSION

The thermal waters of Turkey are located along the tectonic active lines. These thermal waters are represented Na/Ca bicarbonate, NaCl and Na/Ca sulphate. The bicarbonate type waters may be occurred with large carbonate lithologies in Western Turkey. Sea intrusions are increased the chloride levels in waters. The calcite scaling is important problem in the region. Silica scaling is also observed in very hot reservoir like Kızıldere-Denizli. In addition $\delta^{18}O$ enrichment is more than Part I in Part II. So, water-rock interaction is more effective the Part II.
Although there are many high enthalpy geothermal fields around Aegean region, these hot sources don't use effectively at present. It is especially important to using new techniques on electricity production and house heating applications from geothermal energy around the world with energy saving around the world.

REFERENCES

Barut, F., Erdoğan, N., Başak, E. 2003. *Hydrogeochemical evaluation of Western Anatolian mineral.* Environmental Geology.V.45.P.494-503.

Bozkurt, E. (2001*)*. *Neotectonics of Turkey - a synthesis*, Geodinamica Acta, V. 14: (1-3) pp. 3-30.

Delaloye, M. Bingöl, E. 2000. *Granitoyids from Western and North western Anatolia: Geochemistry and modelling of geodynamic evolution*. International Geology Review. 42. 241-268.

Herece, E.1990. 1953 Yenice-Gönen Deprem Kırığı ve Kuzey Anadolu Fay Sisteminin Biga Yarımadasındaki Uzantıları. MTA Bulletin. 111. 47-59.
MTA.2005. *Geothermal Sources Inventory*. General Directorate of Mineral Research Exploration. 650 P.

Mutlu, H. & Güleç, N. 1998**.** *Geochemical characteristics of thermal waters from Anatolia (Turkey).* Journal of Volcanology and Geothermal Research*, 85, 495-515.*

Mutlu,H. 2007.*Constraints on the Origin of the Balikesir Thermal Waters (Turkey) from Stable Isotope ($\delta^{18}O$, δ D, $\delta^{13}C$, $\delta^{34}S$) and Major-Trace Element Compositions.* Turkish J. Earth Sci.V.16.pp13-32.

Özgür, N.1998. *Aktive und Fossile Geothermalsysteme in den kontinentalen Riftzonen des Menderes-Massives, W-Anatolien, Türkei: Habilitationsschrift*. FU Berlin, 171 p.

Tut, Haklıdır F.S. 2007. Geochemical monitoring thermal, mineral and ground waters in Bursa (continue).
Yalçın,T. 2006. *Geochemical characterization of the Biga Peninsula thermal waters (NW Turkey).*Aquat Geochem.DOI 10.1007/s10498-006-9008-2.

Yaman, D. 2005. *Menderes Masifi Kıtasal Rift Zonlarında Yer Alan Jeotermal Sulardaki Yüksek Bor Değerlerinin Kökeni*. Ph.D Thysis. Süleyman Demirel University -Isparta.180.p.

Coal Occurrences in Biga Peninsula, Northwestern Anatolia, Turkey

Maral Mehmet, Suner Fikret and Besbelli Berk

Department of Geology
Technical University of Istanbul,
Istanbul, Maslak 34469 Turkey
E-mail: maralm@itu.edu.tr
Keywords: coal formation, geochemistry, Biga Peninsula, Turkey

ABSTRACT

Turkey has important coal provinces. However, Turkish coals generally exhibit lignite or sub-bituminous (low rank) characters. The coal formed in various basin environments and geological periods. Also their chemical properties show dissimilarities each other. That differs even seen in local coal fields. Biga Peninsula is one of them.
In this study coal and clay formations, located in the central and eastern parts of Biga Peninsula, are evaluated and a formation model is postulated. Various types of Tertiary (Miocene) lignite occurrences had been formed and alternated with volcano-sedimentary Bigadic Formation in the field of study, which resides in the middle and eastern parts of Biga Peninsula. The focus of the study is to identify the geochemical properties of coal occurrences and the formation mechanism of the deposits.

INTRODUCTION

Turkey has an important lignite reserves and seventh largest reserve in the world with over 8 billion metric tons (Tuncali *et al.*, 2002; Lynch, 2003; Palmer *et al.* 2004). Lignite occurrences involve in different parts of Turkey. One of the recognizable is Biga Peninsula, NW Anatolia that is the study area.
The basement of the peninsula is belongs to Paleozoic Kazdag Massif and Karakaya Complex. The Kazdag Massif is mainly of gneisses, amphibolites, marbles and metaophiolites; and the Karakaya Complex are classified in four tectonic units (Okay, 1987; Okay, 1998; Okay *et al.* 1995, Okay & Goncuoglu, 2004). Jurassic Bayirkoy Formation overlies the former units and Bilecik Limestone overlies it. Eocene Ceylan Formation covers all of these formations (Siyako *et al.* 1989). Miocene is represented by Can Volcanits and Bigadic Formation where clay and coal deposits are observed.
The study area is tectonically very active and under the effect of North Anatolian Fault System (NAF). Numerous faults and crack systems had been developed under this mechanism, which had created favorable continental lake environments for coal and clay formation and deposition.

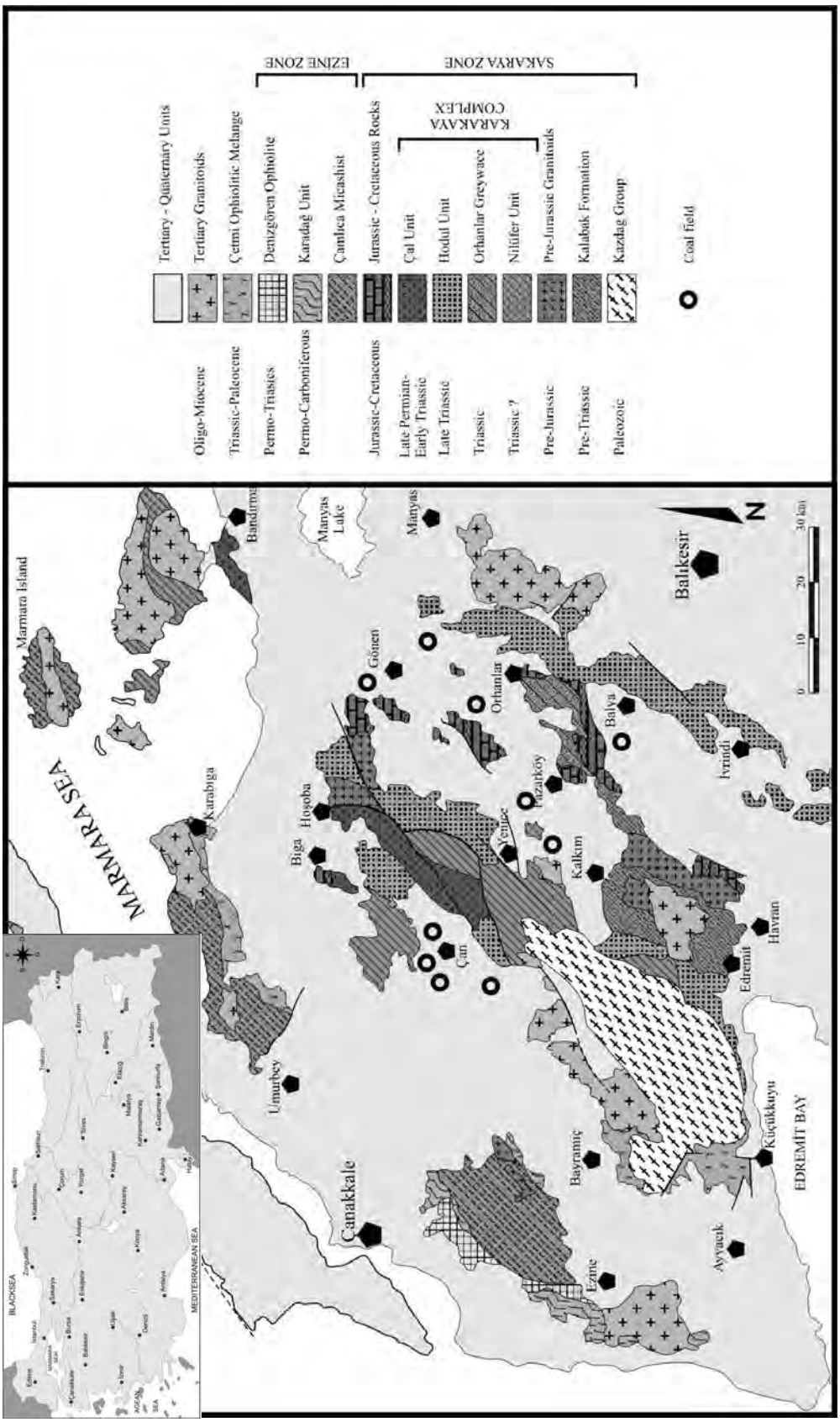

Figure 1: Geological map of study area (Okay *et al.* 1990)

In the peninsula, the earlier studies have revealed that many industrial raw materials and metallic ore depositions are available. Economic coal and clay depositions are of the principal occurrences.
Palmer *et al.* (2004) studied on trace elements in Turkish coals. Also Ayanoglu and Gunduz (1978 a, b, c) reported trace elements analyses using instrumental neutron activation analysis and recently, there has been more interest in trace elements in Turkish coal (Karayigit *et al.* 1999, 2000a, b, c; Querol *et al.*, 1997, 1999) (Palmer *et al.* 2004).
The peninsula is hosting various reserved and sized coal occurrences that are mainly located in three sub-areas that Can, Yenice and Gonen (Figure 1). Can district is then most noticeable one because of coal quality and reserve. Also different kinds of industry have been located in there so require large scale of energy. Thus most of lignite produced is used for generating electricity in the Can Power Plant. Rest of lignite is consumed in the industry and domestic heating.
Most tectonic effects were observed in Gonen among the main coal areas, particularly around Derekoy and Bengiler coal sub areas. In other two locations, tectonism had not been so effective.
In our study, the main aim is to investigate a geochemical relationship between clay and coal strata in terms of major and trace elements contents and behaviors, in order to postulate a reasonable geological explanation of coal formation steps and periods.
Channel coal samples were collected from working mines in the peninsula. All coal samples of each mine were combined as a composite sample thus one coal sample represented one coal field. Also clay strata, which located up and down side of coal seams, were sampled in that frame. Beside the samples were analyzed for major and trace elements, investigated by XRD and XRF.
Evaluations of all data it is geochemically postulated that coalification had been developed more than one period due to not only the presence different structural properties which had been determined in every single coal basin and also statistically determined geochemical data. Under the control of the tectonic feature, it is possible determine a series of folding, fracturing, faulting systems all of which had been responsible for coal and clay occurrences. In the studied area, the postulation is that tectonism had controlled the coalification with in a multi-periodical concept.

GEOLOGY

The base of the study area is represented by Paleozoic Kazdag Massif which is overlaid by tectonic units of Karakaya Complex. The complex was formed in Triassic period. In Tertiary, Ceylan Formation, which has turbiditic character, formed Eocene and covered previous units. Other Tertiary units are Miocene Can Volcanites and Bigadic Formation. The formation has clay and lignite bearings. A geological map of the study area is given Figure1.
Paleozoic base of the study area is formed by Kazdag Massif. That is made up gneisses, amphibolites, marble and also metaophiolites and

rarely granitoids. The gneisses are forming dominant rocks. There are fine or rough grain, thin layered, hard, grey – light grey and has occasionally homogenous texture. Marble is the other dominant unit. Generally, there is rough grain, hard, massif and white colored. Their strata thickness changes 1 to 20m.

Triassic Karakaya Complex, which was classified in four tectonic units, Nilufer Unit, Hodul Unit, Orhanlar Greywacke and Cal Unit, overlies Kazdag Massif (Okay, 1987; Okay, 1998; Okay *et al.* 1995, Okay & Goncuoglu, 2004). The Nilufer Unit, made up the lowest tectonic unit of the complex, is formed by fillate, micashist, calcshist, marble and metatuffite. Fillate and micashist have fine or medium grain and light or dark grey colored. The Hodul Unit is most common one in the complex. Light grey or white colored arkosic sandstone, dark grey or black, thin layered shale and siltstone are forming the unit. The Orhanlar Greywacke is distinguished with its yellowish green or brown, brown colored, non-significant layered. The Cal Unit is made up by spilite, Upper Permian limestone, olistostrom, sandstone, shale, radiolarite. The limestone includes fossils such as brachiopods, gastropods, ostracods and coral fragments (Okay & Goncuoglu, 2004; Okay & Altiner, 2004).

In Tertiary period, Eocene Ceylan Formation, this has turbiditic properties and includes tuff layers. Ceylan Formation is on all of these formations. The unit is occurred by light brown, yellowish brown, homogenous gravelstone, sandstone, siltstone and mudstone. Its 10 – 30 m thickness acidic tuff layer precipitated under the marine control.

Miocene is represented by Can Volcanits and Bigadic Formation where clay and coal deposits are being observed (Ercan *et al.* 1995; Ercan *et al.* 1998). Results of Oligocene Miocene volcanism, Can Volcanits were formed by andesitic, dasitic, riyodasitic volcanic materials. Miocene terrestrial precipitations, Bigadic Formation, are composed of shale, siltstone, sandstone, tuff and coal. The formation occurred in the far part of from the sea.

Biga Peninsula is tectonically very active and it had been controlled by North Anatolian Fault (NAF). Many crack systems and faults had been developed under this mechanism, which are responsible for coal and clay formation and deposition within continental lake environment.

COAL OCCURRENCES

The Biga Peninsula and around is a significant coal field with including lignite occurrences. These are various size and properties; on the other hand their coalifications were completed same age, in Miocene.

Different types of Miocene coal occurrences had been formed and alternated with volcano-sedimentary Bigadic Formation in the field of study, which resides in the middle and eastern parts of Biga Peninsula.

The peninsula could be divided three main areas that depend on locations of coal fields. There are Can, Yenice and Gonen districts from west to east.

Can district is used to strip mine and include Durali, Etili, Karlikoy, Yeniceri and Comakli coal fields. Various reserves have been investigated such as 87 mt in Durali, 56 mt in Karlikoy and 10 mt in Comakli (Tuncali *et al.*, 2002).
Presence of tectonic effects is invisible around Can district coal fields except Karlikoy. Generally, strata are almost horizontal or inclined several degrees. Coal zones made up one main coal seams and different thin layers. All layers exhibit parallelization each other. Also clastic sediments are seen in the coal zones. The thickness of coal seams show variety. While Durali and Comakli are around 16m thickness, Etili is 1.5m and Yeniceri is 3m (Tuncali *et al.*, 2002).
Yenice district is located east of Can and there has two significant coal fields. These are Cirpilar (39 mt) and Orencik (3 mt) (Tuncali *et al.*, 2002). Both of them are working as an open cast mine. Important tectonic signs invisible in Orencik but layers deviated from the horizontal. On the other hand, effects of tectonic activities are clearly recognizable in Cirpilar. Thickness of Cirpilar is around 10m, 1.6m in Orencik. Also oxidation was observed upper parts of coal seam in there.
Gonen district resides in the eastern part of the Biga Peninsula. Bengiler, Mancilik, Sebepli, Tutuncu and Derekoy are main coal fields and applied open cast mining procedures except Bengiler. The coal occurrences of Gonen were observed intensively tectonic effects so layers are extensively inclined. Local faults, cracks, fractures and folds were seen obviously in the field. The coal thicknesses are around 6m.

GEOCHEMISTRY

The collected samples from the study area were investigated by XRD, XRF, major and trace elementary analysis.
As a result of XRD analysis, the coal samples of Can District have 22% inorganic material. Most of them are quartz and kaolin, also pyrite, gypsum, plagioclase, K-feldspar and smectite group clays are detected. Inorganic material content is decreasing 18% in Yenice lignite occurrences. Quartz is dominant and it is fallowed by plagioclase, gypsum, pyrite, kaolin and other clay minerals. Gonen lignite occurrences involve 26% mineral matter that is made up firstly quartz like others, also kaolin, pyrite, gypsum.
Datum of major and trace element analysis are plotted the diagrams (Fig. 2, 3, 4) and interpreted. The main coal areas are displayed on the diagrams, although coal mines are not. There are represented by capital letters as C (Can district), G (Gonen district), Y (Yenice district).
When the correlation table is evaluated, a harmonious correlation is not completely recognized in even a similar element couple. Same element couples of coal and clay exhibit different manner according to each other besides similar behaviors are seen rarely.
Al_2O_3 – U diagrams are wavy. Generally, the trends are positive. However, behaviors of the couple are positive-negative and positive-negative-

positive. These similarities are seen in both of the basin progress (Figure2).
Figures of Zr – Ba exhibit different phase progresses. While coal is monophase, clay is multiphase.
In Zn – Sr couple, the coal trend is negative but the clay trend is wavy (+,-,+,-). Clay and coal presences do not exhibit parallelism to each other. When coal has monophase progress, clay has multiphase (Figure3).
Zr-U and V-Ba diagrams are seen various progress periods. Trends are a both parabolic and linear positive, linear negative.
The V– Cu couple exhibit similar behavior according to each other.
In Zn – Ba samples, monophase progress is seen. The coal sample shows a positive trend but clay is negative. Multiphase evolution could not be seen. In addition evaluation types show variation (Figure4).

In the couples of Al_2O_3 – Zr and Rb – Th, coal progress is seen as linear and monophase when clay occurrences are recognized as complex positive and negative attitude.

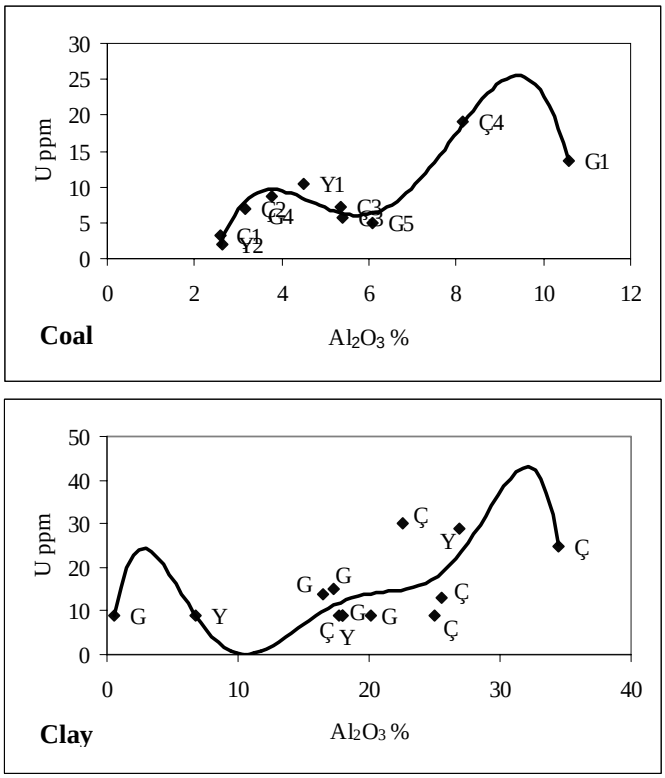

Figure 2: Al_2O_3 – U couple in coal and clay samples

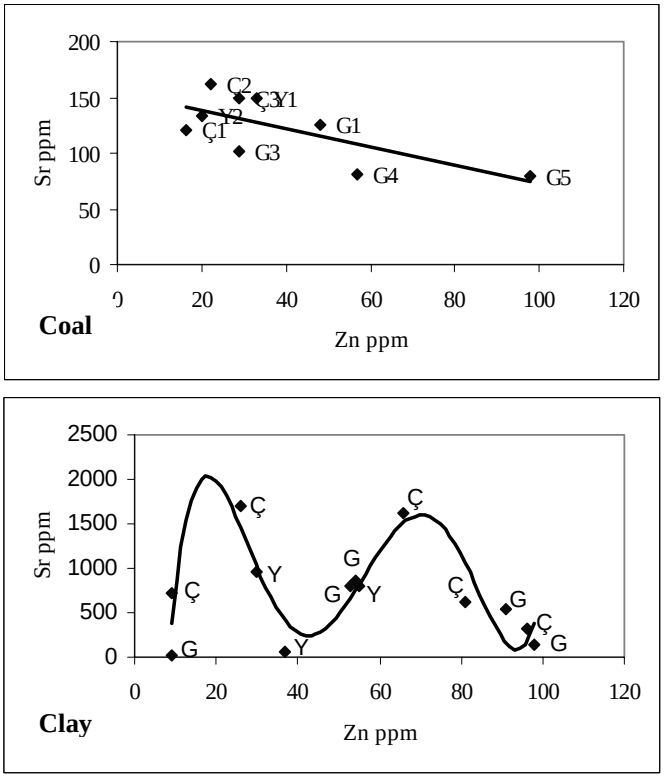

Figure 3: Zn – Sr couple in coal and clay samples

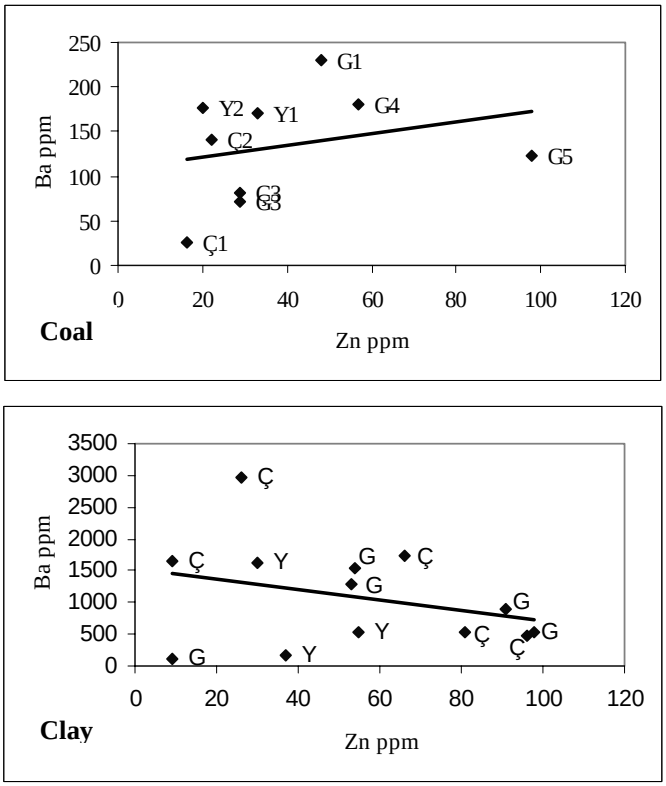

Figure 4: Zn – Ba couple in coal and clay samples

CONCLUSIONS

Even same couple of elements exhibited differences between types, progress and similarities of behaviors. Observed general tectonic effects were that some of the deposits were low sloped and low folded, some of them were influenced by semi-intensive tectonics, a single vein, multi-vein; others were affected by intensive tectonic events and had some folds, faults, crack systems and complex structures. Initial properties of coal were lost during the formation of coal due to tectonic activities. Coalification started at same time but tectonics developed in various frames in every basin, so lake environments which coalification evolution got presence had undergone secondary or multiphase or continental facies change.
Common behaviors of element couples were developed in neither clay nor coal. In other words, in terms of major, minor and trace elements typical element behaviors were not observed for the basin or sub-basin coal locations. A wide, single coalification area did not occur. But probably, three sub-basins formed as Can, Yenice and Gonen. Similar heterogeneous characters were observed in the basins. For this reason, tectonic effects had developed folds, cracks in further phase and sometimes slipped and cracked structure complexes in undiagenetic coal layers.

The coal progress model is trying to explain phase to phase and showed Figure 5, according to geological field observations, chemical analysis and geochemical interpretations.

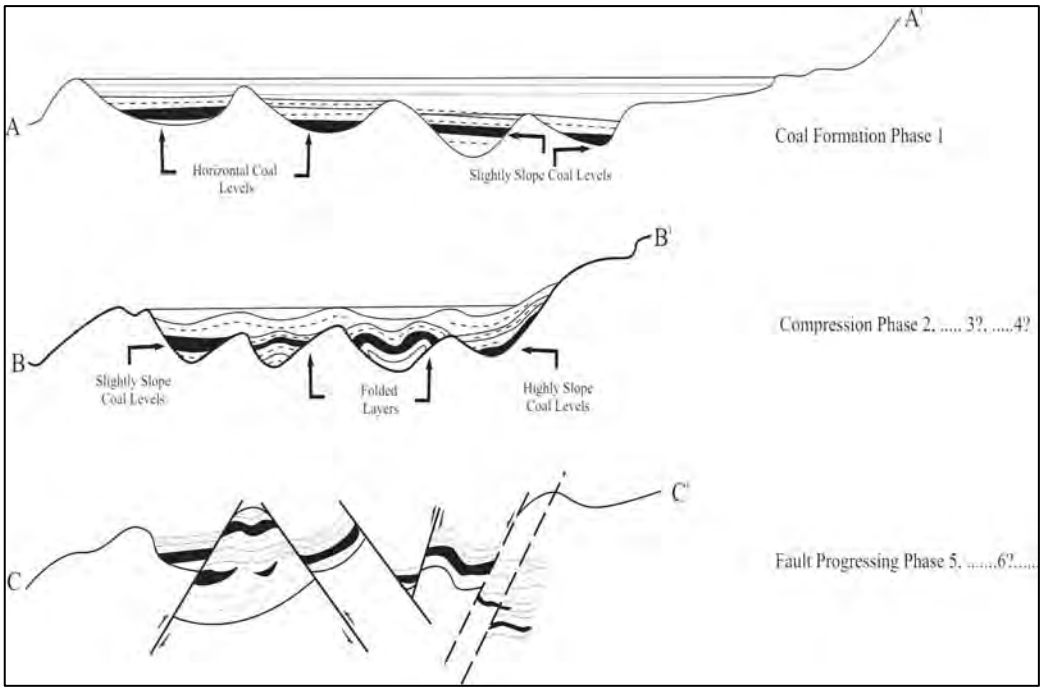

Figure 5: The coal progress model of the study area (Maral, 2004)

Phase 1:

It is supposed that a wide main basin, which was formed, by interconnected little basins existed in the beginning. Brought materials and organic substances accumulated to be horizontal or low sloped because of limited tectonic activity. The progress was valid for coal strata.

Phase 2:

After that, the region was affected by a compression regime. However, this effect was not homogenous in the district so to progressive coal properties started to change. Coal formed in that phase could be low sloped also folded and steep sloped. That phase was dominant on the extensive of coalification period.

Phase 5:

After the formation and compression phases, regional tectonic activities (faults) affected the coal progress, these effects are also important over the coal properties. Tectonism did not developed similarly in all parts of the region. Therefore, heterogenic characteristics were observed on the coal bed formed.

REFERENCES

Ayanoglu, S.F. & Gunduz, G. 1978a. Neutron activation analysis of Turkish coals; I. Elemental contents. *Journal of Radioanalytical Chemistry*, Vol. 43 (1), 155-157

Ayanoglu, S.F. & Gunduz, G. 1978b. Neutron activation analysis of Turkish coals; II. Analysis of ashes and the effects of burning condition on percent transference. *Journal of Radioanalytical Chemistry*, Vol. 43 (1), 159-164

Ayanoglu, S.F. & Gunduz, G. 1978c. Neutron activation analysis of Turkish coals; III. Relation between composition of coal and local earth crust. *Journal of Radioanalytical Chemistry*, Vol. 43 (1), 165-167

Ercan, T. *et al.*1995. Properties of Tertiary Volcanism in Biga Peninsula, Gokceada, Bozcaada and Tavsan Islands (NW Anatolia). *MTA Dergisi* Vol. 117, 55-86 (in Turkish)

Ercan, T. *et al.*1998. Properties of Tertiary Volcanism Around Marmara Sea (Dardanelle). *MTA Dergisi* Vol. 120, 199-221 (in Turkish)

Karayigit, A.I. *et al.* 1999. Qality, palynology, and paleoenvironmental interpretation of the Ilgin Lignite, Turkey. *International Journal of Coal Geology*, Vol. 38 (3-4), 219-236, Elsevier

Karayigit, A.I. *et al.* 2000a. Contents of major and trace elements in feed coals from Turkish coal-fired power plants. *International Journal of Coal Geology*, Vol. 44 (2), 169-184, Elsevier

Karayigit, A.I. *et al.* 2000b. Antimony and arsenic anomalies in the coal seams from the Gokler Coalfield, Gediz, Turkey. *International Journal of Coal Geology*, Vol. 44 (1), 1-17, Elsevier

Karayigit, A.I. *et al.* 2000c. Distribution of environmental sensitive trace elements in the Eocene Sorgun coals, Gediz, Turkey. *International Journal of Coal Geology*, Vol. 42 (4), 297-314, Elsevier

Lynch, R. 2003. An energy overview of the Republic of Turkey. U.S. Department of Energy. http://fe.doe.gov/international/turkover.html

Maral, M. 2004. *Coal Occurrences in Biga Peninsula (Can–Yenice–Gonen)*, M.Sc. Thesis, İ.TÜ. Fen Bilimleri Enstitüsü, Istanbul. (in Turkish)

Okay, A.I. 1987. Geology and Tectonics of the West Part of Biga Peninsula; İTÜ Yerbilimleri ve Yeraltı Kaynakları UYG-AR Merkezi; 5-57 (in Turkish)

Okay, A.I. 1988. Geology and Tectonics of Can – Yenice – Biga Region; İTÜ Yerbilimleri ve Yeraltı Kaynakları UYG-AR Merkezi; 4-44 (in Turkish)

Okay, A.I. *et al.* 1990, Geology and Tectonic Evolution of Biga Peninsula, *TPJD Bülteni,* Vol. 2/1, 83-121 (in Turkish)

Okay, A.I. *et al.* 1995. Paleo and Neo-Tethyan Events in Northwest Turkey. Geological and Geochronological Constraints, *Tectonics of Asia*, Cambridge University Press.

Okay, A.I. & Altiner, D. 2004. Uppermost Triassic limestone in the Karakaya Complex – stratigraphic and tectonic signicance. *Turkish Journal of Earth Sciences*, Vol. 13, 187-199, TUBITAK

Okay, A.I. & Goncuoglu, C. 2004. The Karakaya Complex: A review of data and concepts. *Turkish Journal of Earth Sciences*, Vol. 13, 77-95, TUBITAK

Palmer, C.A. *et al.* 2004. Characterization of Turkish coals: a nationwide perspective. *International Journal of Coal Geology*, Vol. 60, 85-115, Elsevier

Querol *et al.*, 1997. Geochemical controls on the mineralogy and geochemistry of the Beypazari lignite, central Anatolia, Turkey. *International Journal of Coal Geology*, Vol. 33 (3), 225-271, Elsevier

Querol *et al.*, 1999. Coal geology and coal quality of the Miocene Mugla basin, southwestern Anatolia, Turkey. *International Journal of Coal Geology*, Vol. 41, 311-332, Elsevier

Siyako, M. *et al.* 1989. Tertiary Geology and Hydrocarbon Potential of Biga and Gelibolu Peninsulas, *TPJD Bülteni,* Vol. 1/3, 183-199 (in Turkish)

Tuncali, E. *et al.*, 2002. *Chemical and technological properties of Turkish Tertiary coals*. MTA, Ankara, Turkey

Mass balance and geochemical anomalies related to the Mataralampi orogenic gold occurrence, Archaean Kuhmo Greenstone Belt, eastern Finland

[1]Eilu, Pasi and [2] Ojala, V. Juhani

[1] Geological Survey of Finland
PO Box 96. 02151 Espoo, Finland
E-mail: pasi.eilu@gtk.fi
[2] Geological Survey of Finland
PO Box 77. 96101 Rovaniemi, Finland
Keywords: Gold, alteration, mass balance, geochemical anomalies, Archaean, Finland

ABSTRACT

Mataralampi is an orogenic, quartz porphyry hosted gold occurrence in the Archaean Kuhmo greenstone belt in eastern Finland. Alteration related to mineralisation is characterised by sericitisation, carbonation and sulphidation. During mineralisation, Al, Cr, Ni, P, Ti, and Zr were immobile, Ba, Bi, CO_2, Cu, K, Rb, S, Sb, Te, and W enriched and Li, Na and Sr depleted throughout the alteration halo. In addition, Ag, Au, Cd, Pb, and Zn were enriched in the proximal alteration zone. Iron, Ga, La, Mg, and V were only enriched within the proximal zone. Mineralisation-related anomalies extending beyond the area drilled are defined by Bi, $[CO_2/Ca]_{mol}$, S, Sb, and Te. The most consistent local anomalies are defined by the threshold values for Au at 45 ppb, Bi at 0.10 ppm, Sb at 0.07 ppm, Te at 45 ppb, and W at 14 ppm. Also Ag, Cd, Cu, Pb, and Zn define anomalies at Mataralampi, but these only occur inside the gold anomalies. Within the geochemical anomaly, only Sb defines any consistent trend across strike towards the known high grade lode at Mataralampi.

INTRODUCTION

Mataralampi was one of the target areas in the gold exploration campaign of Polar Mining during 2000–2003 in the Archaean Kuhmo and Suomussalmi greenstone belts, eastern Finland (Fig. 1). At Mataralampi, an additional emphasis was put into evaluation of chemical changes and geochemical anomalies potentially related to gold mineralisation. The research methods used included surface mapping, drill core logging, investigation of polished thin sections, and mass balance and geochemical anomaly evaluation. For this purpose, 62 thin sections were prepared, and of these samples, 48 were analysed for SiO_2, TiO_2, Al_2O_3, FeO*, MnO, MgO, CaO, Na_2O, K_2O, P_2O_5, Ba, Ce, Cl, Co, Cr, Cs, Cu, Ga, La, Mo, Nb, Ni, Pb, Rb, Sn, Sr, Th, U, V, W, Y, Zn, and Zr by total digestion XRF, and for S and C by Leco. In addition, the full length of the core drilled (half core in one metre batches, total 450 samples) was analysed by aqua regia-

leach ICP-AES (Ag, Al, As, B, Be, Ba, Ca, Cd, Co, Cr, Cu, Fe, K, La, Li, Mg, Mn, Mo, Na, Ni, P, La, Pb, S, Sc, Si, Sr, Th, Ti, V, Y, and Zn) and GFAAS (Au, Bi, Sb, and Te). All the chemical analyses were performed in the laboratories of Geological Survey of Finland.

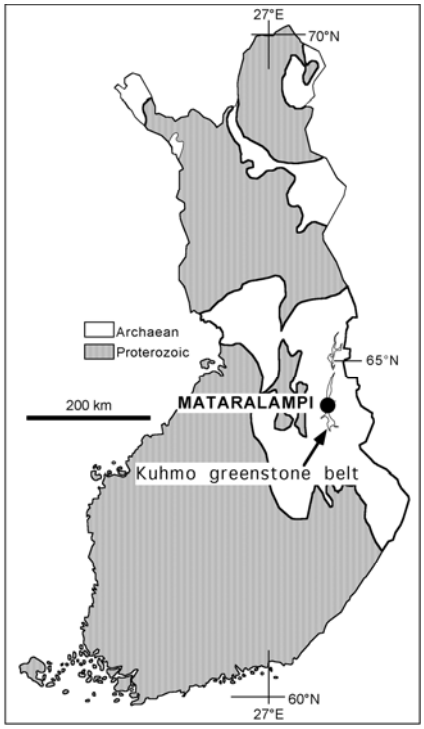

Fig. 1. Location of the Mataralampi gold occurrence in the Kuhmo greenstone belt, eastern Finland.

GEOLOGICAL SETTING

Regional geology

The Mataralampi gold occurrence is in the central part of the 120 km long, 10 km wide, N-S trending Kuhmo greenstone belt in eastern Finland (Fig 1). The Kuhmo belt is a typical Archaean greenstone belt surrounded by a Meso- to Neoarchaean granite-gneiss terrain. It is located in the western part of the Karelian domain of the Fennoscandian shield, and is similar to many of the greenstone belts in Western Australia, Canada, Brazil, and southern Africa. In its extent, shape, age, abundance of komatiitic and tholeiitic rocks, metamorphic grade, structure, deformation, and style of Au and Fe mineralisation, it greatly resembles the Southern Cross greenstone belt in the Yilgarn Block in Western Australia (Ho *et al.* 1990, Luukkonen 1992 and 2001).

The margins of the Kuhmo greenstone belt mostly comprise 3000–2800 Ma metavolcanic rocks dominated by mafic tholeiitic metabasalts, but the sequence also contains intermediate and felsic units. The central parts of the belt are chiefly formed by 2800–2750 Ma tholeiitic and komatiitic

metavolcanic rocks. Narrow banded iron formation (BIF) and mica schist units typically form interlayers between the tholeiitic metalavas. Also felsic to intermediate metavolcanic and volcaniclastic metasedimentary rocks are commonly present in the central parts. Swarms of E-W and NW-trending dolerites cut across the belt; these dykes were intruded at about 2450 Ma and 2200 Ma ago, respectively. (Luukkonen 1992, Sorjonen-Ward et al. 1997, Käpyaho et al. 2006)

Metamorphic grade in the area varies from upper-greenschist to mid-amphibolite facies. It typically increases from the inner parts towards the margins of the belt and towards the surrounding 2760–2690 Ma plutons (Luukkonen 1992).

Six deformation stages have been identified in the area (Luukkonen 1992). The stages D1 and D2 have only affected the oldest (>2.8 Ga) parts of the belt, and the D2 has been dated at 2850–2837 Ma (Luukkonen 2001). The D3 and D4 stages produced the dominant presently visible deformation features in the area. The D3 was predominantly plastic and D4 brittle in style, and both have affected all Archaean rocks in the belt. According to Luukkonen (2001), the D3 took place at 2701–2697 Ma, and the D4 peaked at 2657±32 Ma. The metamorphic peak was attained during the D3 (Luukkonen 1992). Our work suggests that the D3 and D4, which control gold mineralisation throughout the greenstone belt, possibly are substages of a single, long-lived, deformation stage during which the $_1$ of the stress field changed from E-W to N-S. The Archaean cratonisation was followed by Palaeoproterozoic reactivation with two or three weak deformation stages. These probably took place at 2450–2400, 2200–2100 and 1880–1800 Ma related to the two above-mentioned dolerite intrusion stages and (the last one) to the Svecofennian orogeny which was a major crust-forming event beyond the Karelian domain of the Fennoscandian Shield (Luukkonen 1992, Lahtinen *et al.* 2005).

Local geology

Mataralampi is close to the western margin of the Kuhmo greenstone belt. From west to east, there is a steeply west dipping sequence from granodiorite through quartz and feldspar porphyry units to mafic lava (Fig. 2). The granodiorite can be regarded as a part of the TTG granitoids bounding the greenstone belt. The granodiorite and the porphyries are calc-alkaline and the mafic lava Mg-tholeiitic in their primary composition (Fig. 3). The quartz porphyry has an U-Pb zircon age of 2734±2 Ma (Hyppönen 1983). The sequence is cut by NW-trending, apparently Proterozoic, dolerites and a younger N-trending alkalibasaltic dyke. Contacts between all lithological units are sharp. The presence of a metamorphic mineral assemblage in the dolerites indicates that the Mataralampi region was subject to reheating at greenschist-facies conditions during the Proterozoic.

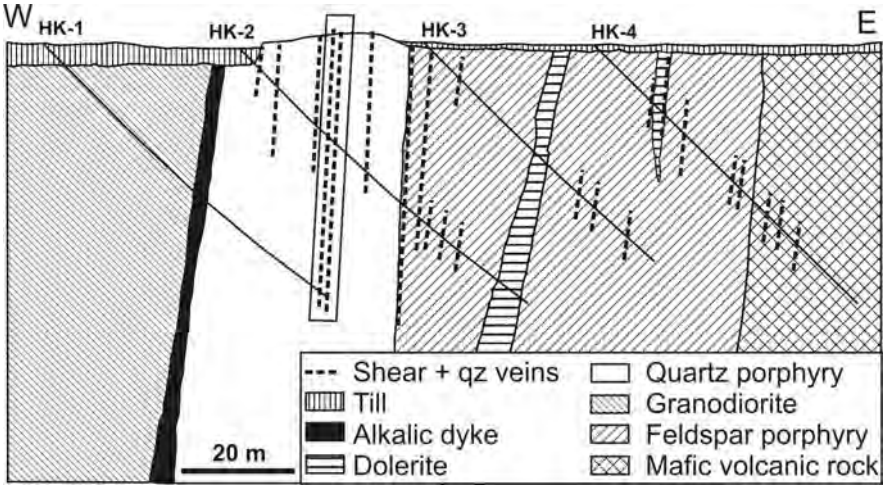

Figure 2. Schematic geological section across the Mataralampi gold occurrence, Kuhmo greenstone belt, eastern Finland. The main mineralised zone is indicated by the shear zones within the subvertical rectangle. HK-1 to HK-4 indicate diamond-drill holes sampled by us.

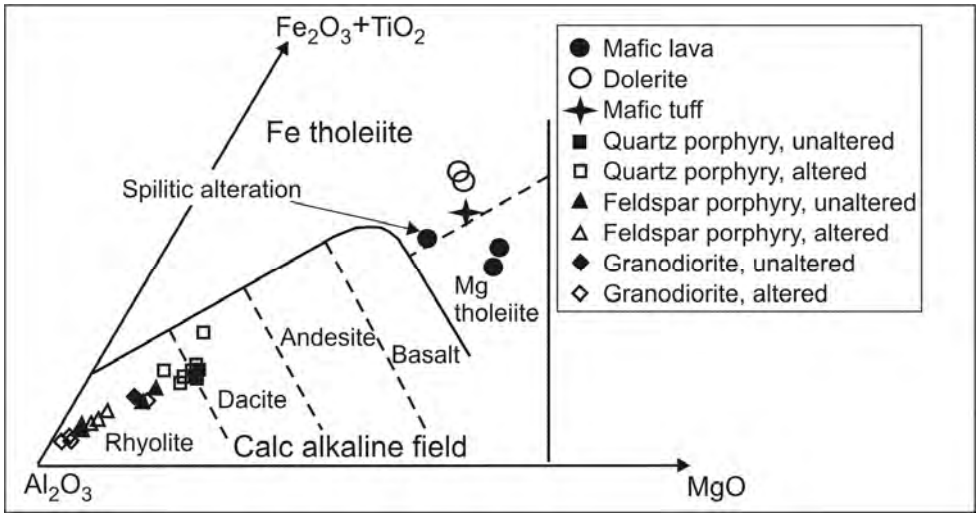

Figure 3. Jensen plot (Jensen 1976) for the Mataralampi rocks. XRF total-digestion data.

The gold occurrence at Mataralampi is related to subvertical, N- to NNW-trending, 0.5-5 m wide, shear zones containing quartz veins and intense alteration. The mineralised shear zones probably are local late-D3 or D4 structures whose age is somewhere between 2.70 Ga and 2.65 Ga (Luukkonen 1992, 2001), and the mineralisation hence took place under peak or slightly post-peak metamorphic conditions, close to the greenschist–amphibolite facies boundary PT conditions. The main host to gold is the quartz porphyry unit, but also the feldspar porphyry is weakly mineralised.

ROCK TYPES

Felsic to intermediate rocks

The granodiorite is heterogranular, deformed, and contains a small volume of plagioclase phenocrysts. Its composition varies from granodioritic to tonalitic in apparently irregular manner.
The quartz porphyry is characterised by pale-blue quartz phenocrysts which are 0.5–1 cm in diameter and form 20–35 vol.% of the rock. There also are distinct, reddish, K feldspar phenocrysts 1–3 cm in diameter, forming <5 vol.% of the rock. There is very little variation in primary composition, as shown by Figures 3 and 4.
The feldspar porphyry is heterogeneous, tonalitic to granodioritic, and with locally high contents of mafic minerals and high Cr, Fe, Mg, Mn, Ni (± Co), P, Ti and V contents. This probably reflects variation in primary composition, as the mass balance evaluation shows that the elements listed above were not significantly mobilised during alteration.
All felsic to intermediate rocks have as major minerals quartz, plagioclase, K feldspar, and biotite.

Mafic rocks

Massive to pillowed mafic lava forms the main part of the eastern mafic unit shown in Figure 2, but there also are minor, banded, interlayers of mafic tuff. Both are characterised by the mineral assemblage plagioclase - hornblende - epidote - titanite. The lava is Mg-tholeiitic whereas the tuff is transitional between Fe and Mg tholeiite (Fig. 3).
The cross-cutting dolerites have the same mineral assemblage as the mafic volcanic rocks. However in chemical composition, they are clearly different with the dolerites being distinctly Fe tholeiitic (Fig. 3), in defining trends in bivariate plots (Fig. 4), and having distinctly higher Fe, Mn, P, Ti, V and Zr and lower Cr contents than the mafic volcanic rocks.

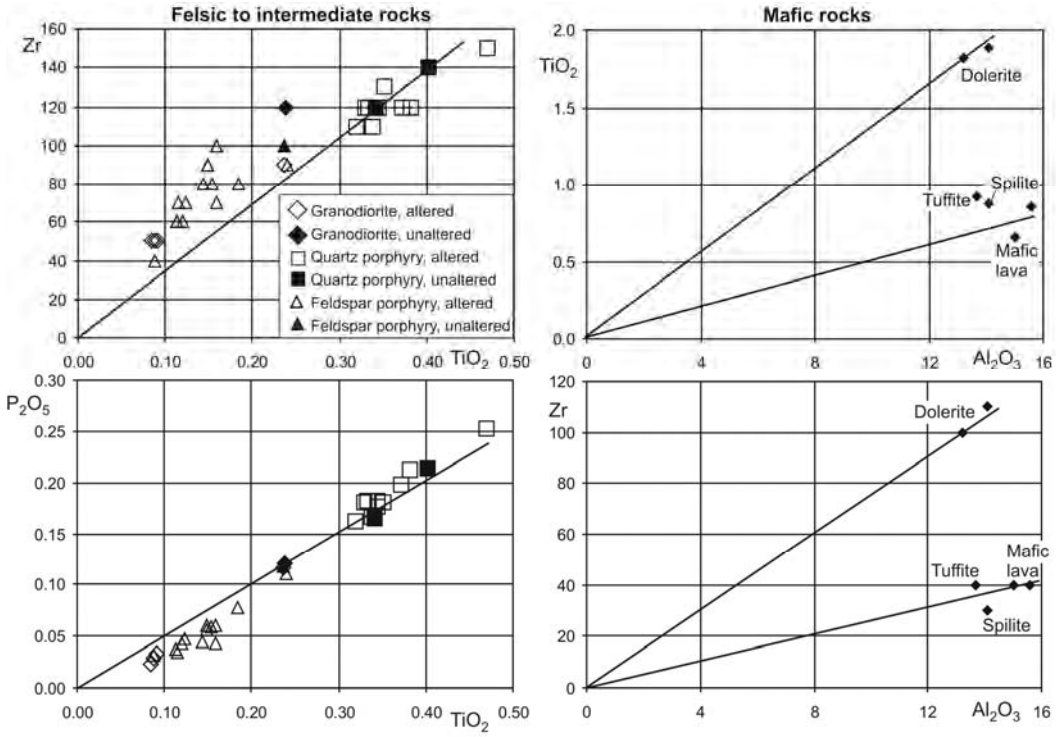

Figure 4. Bivariate plots for the Mataralampi rocks. The diagonal line in felsic to intermediate rock plots is drawn through the least altered quartz porphyry, and in the mafic rock plots through the mafic lava and dolerite samples. XRF total-digestion data.

ALTERATION STYLES

Pre-gold alteration

In mafic metavolcanic rocks, the locally abundant, paragenetically early, epidote-rich veins with epidote- and hornblende-rich selvages, and epidote- and hornblende-rich pillow selvages and inter-pillow matrices suggest that the rocks have been subject to synvolcanic spilitic alteration. In that stage, the mafic rocks may also have gained some iron sulphides and chalcopyrite, because pyrite, pyrrhotite and chalcopyrite are more abundant in the epidotised than in the unaltered parts of these rocks.

Gold-related alteration

Alteration related to gold mineralisation at Mataralampi is characterised by sericitisation (replacement of biotite and feldspars by muscovite), carbonation of feldspars and epidote, replacement of titanite by rutile, sulphidation, destruction of magmatic phenocrysts, and formation of quartz-calcite±sulphide veins. The intensity of all of these features, along with the degree of deformation, gradually increases towards the potential ore. As the change is gradual, definition of distinct zones within the alteration halo is difficult. The alteration zoning presented here is solely based on the degree of sericitisation which is easy to map in outcrop and drill core.

Distal alteration is characterised by incipient sericitisation of biotite, partial to total replacement of titanite by rutile and epidote by calcite, and the appearance of pyrite in the mineral assemblage. With increase in the degree of alteration and deformation, muscovite gradually becomes more abundant than biotite and forms continuous, 0.1–1 mm wide shear bands. In addition, calcite, quartz and rutile gradually replace all epidote and titanite, and feldspar phenocrysts start to disintegrate, whereas the quartz phenocrysts remain distinct by retaining their sharp boundaries.
Proximal alteration hosts the gold mineralisation. Here, the host rock is characterised by the mineral assemblage quartz-albite-muscovite-calcite-rutile-pyrite ± K feldspar and abundant quartz veins. The degree of deformation is intense: all feldspar phenocrysts disappear, are replaced by a fine-grained mass of albite + quartz + muscovite ± K feldspar. The quartz phenocrysts still are distinguishable with their sharp boundaries, although they can be so flattened that they resemble parts of boudinaged quartz veins. Pyrite occurs disseminated throughout the rock, but is concentrated in and near quartz veins. In the 'best ore', there also is sphalerite, galena, fahlore and traces of native silver in the pyritiferous quartz veins. So far, no gold has been identified in thin section.

CHEMICAL CHANGES RELATED TO ALTERATION

The Jensen plots (Fig. 3) and, especially, bivariate plots based on elements potentially immobile during hydrothermal processes (Fig. 4) were used at Mataralampi to check and classify the primary rock types and model the potential primary chemical variation within each rock type. After this was done, the isocon method (Grant 1986) was applied for the evaluation of chemical changes related to various styles of alteration in all major rock types. The isocons produced are exemplified here by the Figure 5. In the isocon evaluation, each rock type is treated separately by plotting data from the least altered sample(s) against data from altered samples. The regression lines (isocons) marked in these plots are fitted trough the elements shown by the bivariate plots (Fig. 4) to be immobile.
The mass balance evaluation indicates that during mineralisation:

- net mass and volume changes were minimal;
- Al, Cr, Ni, P, Ti, and Zr were consistently immobile;
- Fe, Ga, La, Mg and V were only mobilised in the areas of most intense alteration (in 'ore'), elsewhere these were immobile;
- the relative mass transfer for silica was minor; however, because the Si concentrations are significantly higher than those for any other element, even a relatively large absolute Si transfer is difficult to statistically detect;
- Ba, Bi, CO_2, Cu, K, Rb, S, Sb, Te, and W were enriched throughout the alteration halo;
- Ag, Au, Cd, Pb, and Zn were enriched chiefly in the most intensely altered rock;
- Li, Na and Sr were depleted throughout the alteration halo;

- there are no indications of As or B mobility, enrichment or depletion, and their concentrations remain on typical background levels.

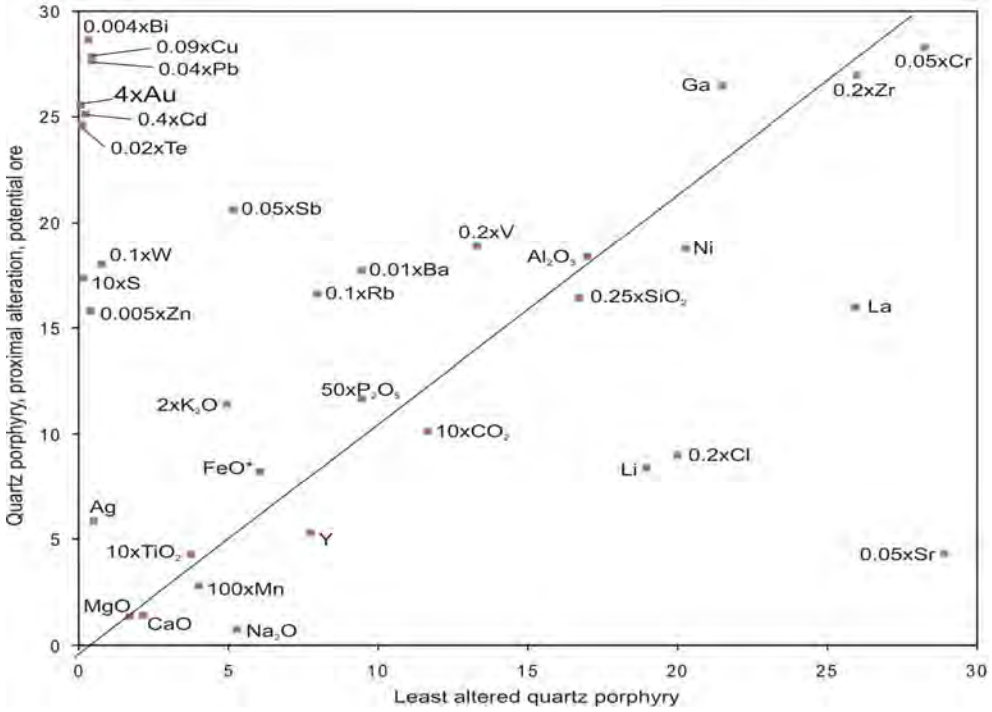

Figure 5. Isocon for the quartz porphyry. Chemical changes from the least altered to the most intensely altered rock and potential ore. Multiplied concentrations plotted as per cent for the major elements, S and CO_2, as ppb for Bi, Sb and Te, and as ppm for the rest of the trace elements. Some of the elements analysed are not plotted, because their concentrations consistently are below or only slightly above detection limit in the data available for this plot.

The unusual, albeit dominantly very local, enrichment of base metals in an orogenic gold mineralisation may be due to leaching Cd, Cu, Pb and Zn from the graphitic, sulphidic, black shale unit(s) located along strike about 800 m to the south of the area discussed here.

The effect of the syngenetic, pre-gold spilitisation in the mafic volcanic rocks is difficult to see, because all spilitised rocks also are potentially affected by gold-related alteration. However, comparison of various isocons (not shown here) indicates enrichment of Ca and Cl and depletion of Mg and Sr related to spilitisation. These changes also are relatively easy to explain by the spilitic epidotisation of plagioclase and primary mafic silicates.

GEOCHEMICAL ANOMALIES AND TRENDS

Background thresholds and ranges

Concentrations which define the boundaries between background and anomalous values for gold and potential pathfinder elements at Mataralampi are listed below. These thresholds are based on cumulative frequency plots of logarithmic values derived from the data populations (Sinclair 1976, 1991). For Bi, W and Zn, two threshold values are given. The lower value indicates the local background threshold and the higher a significant change in concentration within an anomaly. The latter value indicates a change from less intense to more intense enrichment.

Element	Local background threshold (ppm)
Au	0.045
Bi	0.10; 0.41
Cu	42
Pb	90
S	270
Sb	0.07
Te	0.065
W	14; 80
Zn	57; 160

Also the alteration indices describing sericitisation (enrichment in Ba, K and Rb), carbonation (enrichment in CO_2) and depletion of Na were investigated. These indices and their estimated background ranges are presented below. The background ranges are based on the values detected in unaltered or least altered samples. Indices with subscript *mol* are calculated on molar ratio basis.

Background range for:	Grano-diorite	Quartz porphyry	Feldspar porphyry	Mafic volc. rock
Sericitisation				
$[3K/Al]_{mol}$	0.60–0.75	≤0.50	≤0.40	≤0.10
Ba/Ti	≤0.14	≤0.16	≤0.20	≤0.10
Na depletion				
$[Na/Al]_{mol}$	0.40–0.50	≥0.50	0.40–0.70	≥0.30
Carbonation				
$[CO_2/Ca]_{mol}$	≤0.50	≤0.50	≤0.70	≤0.20

The alteration index table, the average values for alteration indices in various rock types and alteration zones (not shown here), and the

geochemical raw data indicate that the background Ba and K concentrations are so variable that the true extents of the sericitisation anomalies at Mataralampi remain unknown, except in the primarily most K- and Ba-poor, i.e., mafic rock types. Despite this, the sericitisation indices could be used to define locally significant anomalies. Their highest values indicate the locations of most intense sericitisation. They also show that the Ba and K enrichment (= sericitisation) extend beyond visible sericitisation, that is, beyond what can be detected during routine logging of the drill core.

The carbonation indices could be more useful than the sericitisation indices at Mataralampi, as all carbon in the host rocks is introduced by alteration. For example, the total extents of the anomalies due to carbonation could be defined. However, the early spilitisation-related and the post-gold dolerite-related carbonation stages complicate the situation.

Loss of Na is related to gold mineralisation-related alteration at Mataralampi. This is reflected by the decrease in the albitisation index values with increase in alteration intensity. It also means that the values *above* the background threshold for Na/Al form the range of the background. However, due to high primary variation in Na content within and between the rock types present, the Na/Al is of little use in defining the spatial extent of Na-depletion at Mataralampi.

Anomalies and trends within the section investigated

Geochemical anomalies and trends at Mataralampi were visually inspected within the vertical section drilled (Fig. 2). These are exemplified by Figure 6. In this section, many of the parameters investigated define extensive anomalies, and the main anomaly for some parameters extends across strike beyond the section drilled. The extents of the anomalies are variable but, at least, Ag, Bi, Cd, Pb, and Sb show a distinct positive spatial correlation with Au.

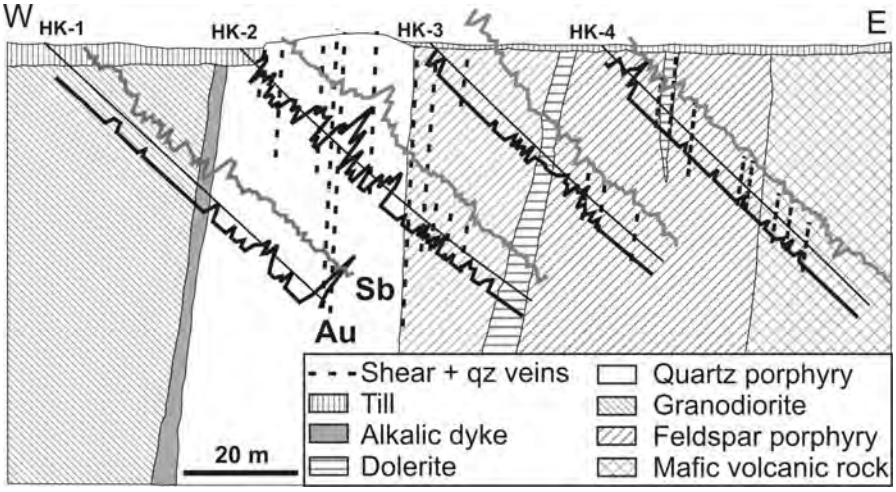

Figure 6. Gold and antimony profiles in the section 7149710N at Mataralampi. The log value of the Au concentration is plotted as a heavy black line siting (chiefly) below each of the drill hole traces.

For Sb (grey line), the zero-value line is the drill hole trace.

On the other hand, there are parameters that have only a partial positive spatial correlation with Au. This means that, despite defining an anomaly where there is distinct gold mineralisation, the following commonly also define anomalies with no obvious spatial relationship with Au enrichment: CO_2/Ca, Cu, 3K/Al, Na/Al, S, Te, and Zn. In addition, although showing mobility related to gold mineralisation, as indicated by mass balance evaluation, Ba, Cl and Sr seem to show very little, if any, spatial correlation with gold – these three elements probably are of no use in lithogeochemical exploration for orogenic gold at Mataralampi.

In the section investigated, the most extensive anomalies are those defined by Bi, CO_2/Ca, S, Sb, and Te (>10 ppb). Their main anomalies extend, across strike, beyond the drilled part of the section. Restricted (typically 1–3 m wide) anomalies only related to Au are defined by Ag, Cd and Pb. Copper and zinc define narrow anomalies both related and unrelated to Au. Potassic alteration and sodium depletion also seem to define extensive anomalies, but due to primary compositional variation of the host and wall rocks, their relationship and true extents were not possible to define. For W, there seems to be a positive spatial correlation with Au in the feldspar porphyry unit, but not elsewhere.

Despite the large number of elements analysed and a strong positive correlation between Au and a large number of other elements, only Sb seems to define extensive, consistent trends across strike towards potential gold ore at Mataralampi. This trend is most obvious where the hole HK-2 crosses the main mineralised zone, in the quartz porphyry (Fig. 6). There, the Sb anomaly, defined by values >0.5 ppm Sb, is about 30 m wide and extends for 10 m beyond the detectable Au anomaly.

Also the other geochemical parameters do define trends towards each peak or low in respective anomalies, but these trends typically do not extend beyond two or three consecutive samples. This feature reflects the deformation and alteration partitioning in a section across the mineralised structures. There may be more extensive trends along the strike of the mineralised shear zones, but there is not enough data to investigate this.

CONCLUSIONS

The Mataralampi orogenic gold occurrence is in the Archaean Kuhmo greenstone belt in eastern Finland. The main host to gold is a 2734±2 Ma, calc-alkaline, quartz porphyry unit in the western margin of the belt. Alteration related to mineralisation is characterised by the formation of the mineral assemblage quartz-albite-muscovite-calcite-rutile-pyrite and abundant quartz veins.

Mass balance evaluation shows that during mineralisation, Al, Cr, Ni, P, Ti, and Zr were immobile, Ba, Bi, CO_2, Cu, K, Rb, S, Sb, Te, and W enriched and Li, Na and Sr depleted throughout the alteration halo. In addition, Ag, Au, Cd, Pb, and Zn were enriched in the proximal alteration zone, whereas Fe, Ga, La, Mg, and V were only enriched within the proximal zone.

Concentrations which define the threshold values between background and anomalous values for gold and potential pathfinder elements include, in ppm, 0.045 Au, 0.10 Bi, 42 Cu, 90 Pb, 270 S, 0.07 Sb, 0.065 Te, 14 W and 57 Zn. The most consistent local anomalies are defined by Au, Bi, Sb, Te and W. The anomalies defined by Ag, Cd, Cu, Pb, and Zn only occur inside the gold anomalies. Copper and Zn define narrow anomalies both related and unrelated to Au. Mineralisation-related anomalies extending beyond the area drilled are defined by Bi, $[CO_2/Ca]_{mol}$, S, Sb, and Te.
All geochemical parameters define oscillating trends across the section investigated. Within an anomaly, only Sb defines any consistent trend across strike towards potential ore at Mataralampi.

ACKNOWLEDGEMENTS

Thanks to Polar Mining Oy for funding field work, thin section preparation and whole-rock geochemical analyses, and for the permission to publish the results.

REFERENCES

Grant, J.A. 1986. The isocon diagram – a simple solution to Gresens' equation for metasomatic alteration. *Economic Geology*, Vol. 81, 1976–1982.

Groves, D.I. *et al.* 1998. Orogenic gold deposits: A proposed classification in the context of their crustal distribution and relationship to other gold deposit types. *Ore Geology Reviews*, Vol. 13, 1–28.

Ho, S.E. *et al.* 1990. *Gold Deposits of the Archaean Yilgarn Block, Western Australia: Nature, Genesis and Exploration Guides.* Geology Department (Key Centre) & University Extension, The University of Western Australia, Publ. 20. 407 p.

Hyppönen, V. 1983. Explanation to the maps of Pre-Quaternary rocks, sheets 4411, 4412, 4413. *Geological map of Finland 1:100000.* Geological Survey of Finland, Espoo. 60 p.

Jensen, L.S. 1976. A new cation plot for classifying subalkalic volcanic rocks. *Ontario Division of Mines, Miscellaneous Paper*, Vol. 66. 22 p.

Käpyaho, A. *et al.* 2006. Growth of Archaean crust in the Kuhmo district, eastern Finland: U-Pb and Sm-Nd isotope constraints on plutonic rocks. *Precambrian Research*, Vol. 146, 95-119.

Lahtinen, R. *et al.* 2005. Paleoproterozoic tectonic evolution. In: *Precambrian Geology of Finland – Key to the Evolution of The Fennoscandian Shield.* Elsevier Science B.V., Amsterdam, 481–531.

Luukkonen, E. 1992. Late Archaean and Early Proterozoic structural evolution in the Kuhmo-Suomussalmi Terrain, eastern Finland. Annales Universitatis Turkuensis. Series A. II 78, 37 p.

Luukkonen, E. 2001. Pre-Quaternary rocks of the Lentiira map sheet area. Explanation to the bedrock maps 4414+4432 Lentiira. *Geological map of Finland 1:100000.* Geological Survey of Finland, Espoo. 68 p.

Sinclair, A.J. 1976. Probability graphs in mineral exploration. *Association of Exploration Geochemists Special Volume* 4. 95 p.

Sinclair, A.J. 1991. A fundamental approach to threshold estimation in exploration geochemistry: probability plots revisited. *Journal of Geochemical Exploration*, Vol. 41, 1–22.

Sorjonen-Ward. P. *et al.* 1997. Greenstone associations in Finland. In: *Greenstone Belts.* Clarendon Press, Oxford, 677-698.

The relationship between tectonics, granitoids and Mesozoic Au-Ag mineralization in the Hongseong Collision Belt, South Korea

Seon-Gyu Choi[1], V.J. Rajesh[1], Jieun Seo[1], Jung Woo Park[1], Chang-Whan Oh[2], Sung Won Kim[3], Sang Joon Pak[1]

[1]Dept. of Earth & Environmental Sciences, Korea University, Seoul, Korea
[2]Dept. of Earth & Environmental Sciences, Chonbuk National University, Jeonju, Korea
[3]Dept. of Earth Sciences, Chosun University, Gwangju, Korea
E-mail: seongyu@korea.ac.kr
Keywords: Hongseong Collision belt, Triassic high Ba-Sr granitoids, Au-Ag mineralization, Gyeonggi massif, South Korea

ABSTRACT

Extensive Mesozoic Au-Ag (160-130 Ma) mineralization in the Gyeonggi massif of the Korean Peninsula is closely related to deep-seated granitoids. The Haemi area in the Hongseong collision belt (eastern extension of the Dabie-Sulu collision zone in the China craton) within the Gyeonggi massif contains abundant post collisional granitoids with shoshonitic high Ba-Sr intermediate enclaves altogether intruded into the Precambrian metamorphic rocks. The granitoids are subdivided into high Ba-Sr and low Ba-Sr granitoids. They are high K- calc-alkaline, broadly peraluminous and broadly display I-type affinities. SHRIMP U-Pb dating of zircons from high Ba-Sr granitoids yielded 233 Ma age, slightly postdates the collision age. Combined field, petrographical, geochemical and stable O-isotope evidences suggest formation of high and intermediate Ba-Sr granitoids by the process of mingling/mixing of magmas derived from an enriched upper mantle and lower crust; and the low Ba-Sr granitoids are typical of highly fractionated granites by advance fractionation of granitic magma free of two-component mixing. Processes such as magma mingling/mixing, fractionation, remelting, remobilization and subsequent concentration of ore-forming fluids along with the regional tectonics play a significant role in metallogenesis. A four stage collision-metallogeny-fluid flow (CMF) model is widely documented for the geodynamic setting of significant Mesozoic gold deposits in the North China craton and also in the Dabie-Sulu collision zone in which the Triassic collision and subsequent extension tectonics along with change in P-T conditions have played a significant role. We envisage a similar genetic model for the Mesozoic Au-Ag mineralization in the Gyeonggi massif, South Korea.

INTRODUCTION

The East Asian continent is formed by collision and accretion of various microcontinents during the Late Permian to Triassic (e.g. Li et al.,1993; Sengor, 1985). It is widely accepted that the Triassic growth of the east

Eurasian landmass is primarily due to the continental collision of the North China Block and the South China Block (Yin and Nie, 1993; Chough et al., 2000). Phanerozoic subduction and collision along the southern and western borders of the North China block led to formation of the Qinling–Dabie–Sulu–Hongseong–Hida–Yanji belt connecting China, Korea and Japan (Oh and Kusky, 2007). The collision between the North and South China blocks began in the Korean peninsula during the Permian (290–260 Ma) and propagated westwards until the Late Triassic (230–210 Ma) (Oh et al., 2005). Syn- to post-collisional magmatism occurred along this continental collision zone. Along the margins of the North China Craton, profuse Au-Ag deposits are distributed proximal to Mesozoic granitoids (Yang et al., 2003). The widespread Mesozoic Au-Ag (160-130 Ma) mineralization in the Gyeonggi massif of the Korean peninsula is closely related to the deep-seated granitoids (Choi et al., 2005) The Haemi area in the Hongseong belt within the Gyeonggi Massif comprised of silica-rich granitoids including intermediate enclaves probably resulted from mixing and/or mingling processes between mafic and felsic magmas from mantle and lower crustal sources respectively. This study aims on elucidating the petrological, geochemical and chronological characteristics of the Haemi granitoids and the included enclaves, to establish a relationship between granitoid genesis, regional tectonics, and Mesozoic Au-Ag mineralization in the Hongseong Collision Belt, South Korea.

GEOLOGICAL SETTING, FIELD RELATIONS AND PETROGRAPHY

The Korean peninsula is tectonically positioned in the southeastern margin of the Sino-Korean platform and is composed of three Precambrian massifs (the Nangrim, the Gyeonggi and the Yeongnam massifs), two Phanerozoic mobile belts (the Imjingang belt situated at the northern fringe of the Gyeonggi massif and the Okcheon Belt flanked by Gyeonggi and Yeongnam massifs), volcano-sedimentary sequences and sedimentary basins (e.g. Cluzel et al., 1990). All the three massifs contain Precambrian basements rocks, mostly gneisses and schists, overlained by Paleozoic to Holocene sedimentary and volcanic rocks, which were extensively pierced by Mesozoic felsic to mafic plutons. The Honseong area is situated in the southwestern part of the Precambrian Gyeonggi Massif (Fig. 1). The area includes the Wolhyeonri Formation and Deokjeongri granitic gneiss to the west and the Yugu granitic gneiss to the east. The predominant lithological units of the Wolhyeonri Formation are closely allied biotite schists, metabasites and marbles. Amphibole- and biotite-bearing granitic gneiss

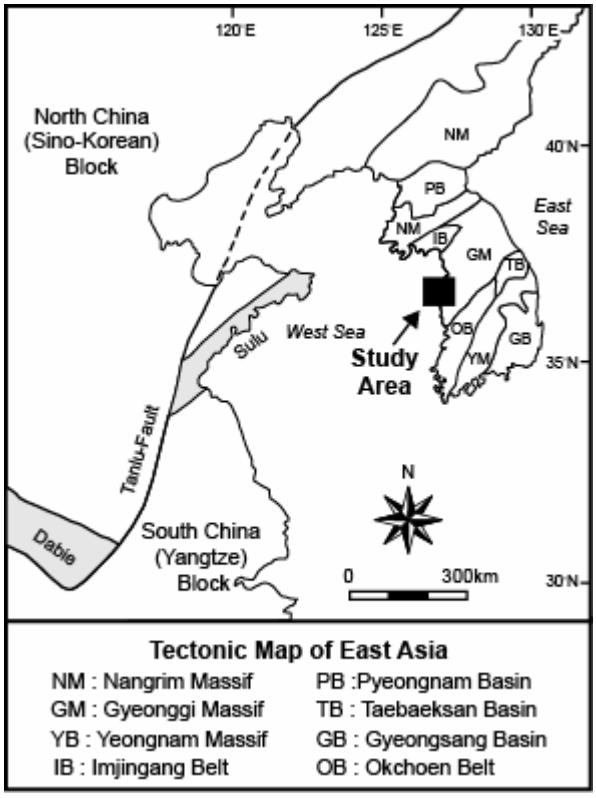

Figure 1: Generalized tectonic map of East Asia showing the position of the study area.

and leucogranites dominate the orthogneisses of the Deokjeongri granitic gneiss (Oh et al., 2004, 2005). Minor metabasites and marbles are also found in the Deokjeongri granitic gneiss. The Yugu granitic gneiss is believed to be paragneiss. Zircons from the Deokjeongri granitic gneiss yielded an intrusion age of 812 to 822 Ma and a metamorphic age of 223 to 235 Ma based on sensitive high-resolution ion micro-probe (SHRIMP) U–Pb zircon geochronology (Cho, 2001). Oh et al. (2005) obtained Sm–Nd internal isochron ages of 225 to 258 Ma for the metabasites of the Deokjeongri granitic gneiss and interpreted this age as eclogite facies metamorphism. The zircons from the metabasites also yielded inherited core ages of 887 $\pm$ 14 Ma with an overgrowth rim of 231 $\pm$ 3 Ma (SHRIMP U-Pb zircon ages; Guo et al., 2004).

The study area, Haemi is positioned in the western part of the Hongseong area. Many granitoids with abundant mafic enclaves are observed here. The rocks are medium- to coarse- grained with preserved igneous textures. The granitoids are categorized into high and low magnetic susceptibility granitoids based on insitu magnetic susceptibility (MS) measurements in the field. The nature of contact between the enclaves and the granites are mostly sharp, suggestive of similar/near similar temperatures of crystallization. The mineral assemblage of enclaves is K-feldspar + plagioclase +quartz ± biotite + ampbibole ± clinopyroxene + rutile + monazite + apatite+sphene + zircon ± magnetite ± chlorite,

whereas the mineral assemblage of the granitoids is K-feldspar + plagioclase + quartz + biotite ± amphibole ± muscovite + sphene + monazite + apatite + zircon ± magnetite ± chlorite. The enclaves and host granites display critical petrographical evidences for magma mixing and or mingling of mafic and felsic magmas in their genesis, which include plagioclase phenocrysts with complex zoning patterns, boxy and spongy cellular plagioclase grains, abundant mafic and felsic inclusions in plagioclase grains, mantling of quartz by mafic minerals such as hornblende and biotite, hornblende mantled by biotite and vice versa, presence of hornblende along the cleavage planes of biotite, mafic aggregates or blobs or clots noticed around the rim of felsic minerals, bladed and needle like mafic minerals such as hornblende and biotite, presence of acicular/needle shaped apatite, and so on.

GEOCHEMISTRY

The enclave samples have very narrow compositional variations with their SiO_2 contents ranging from ~ 58 to 59 wt. % and are least evolved; hence we group them as intermediate enclaves. They also have high MgO (~ 5 wt. %), K_2O (~ 6 wt. %), Cr (~ 200-250 ppm) and Ni (~100-150 ppm) contents than the granitoids. The granitoids are highly evolved in terms of their SiO_2 contents (69-74 wt. %). They have high Al_2O_3, very low MgO, Ni and Cr contents than those of the enclaves. The entire granite data plot within the granite field on a total alkali versus silica (TAS) diagram, where as the intermediate enclaves plot in syeno-diorite field. The granites fall within the calc-alkaline series on a SiO_2 versus K_2O (wt. %) diagram (Fig. 2a) while the enclaves plot in the shoshonitic field. The granites and enclaves samples fall in the calc-alkaline field on an AFM diagram (Fig. 2b). On an A/NK versus A/CNK plot the enclaves plot in the metaluminous field but the granitoids fall in the peraluminous field. Their ASI (molar Al_2O_3/Na_2O+K_2O+CaO) values are higher than 1 but significantly lower than 1.1. This categorizes them into I-type granites with A/CNK values < 1.1. Further, they have relatively high total alkali contents (Na_2O+K_2O) and low MgO/FeOt values (0.17-0.20). All these features are characteristic of I-type granites. The granitoids are further subdivided into high Ba-Sr and low Ba-Sr granitoids based on their Sr, Rb and Ba abundances (Fig. 3). The intermediate enclaves also have high Ba and Sr contents.

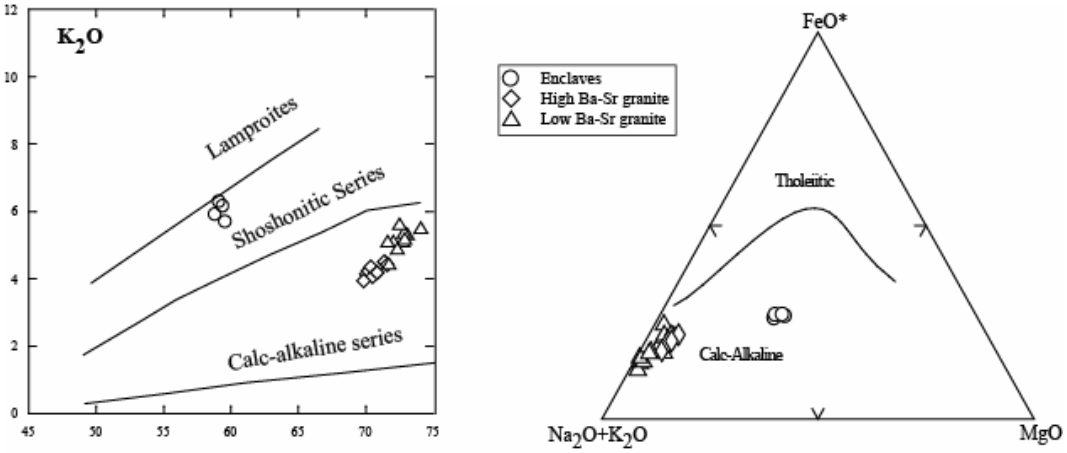

Figure 2: a; Total alkali versus silica diagram and b; the AFM plot illustrating the dominant calc-alkaline nature of the studied rocks.

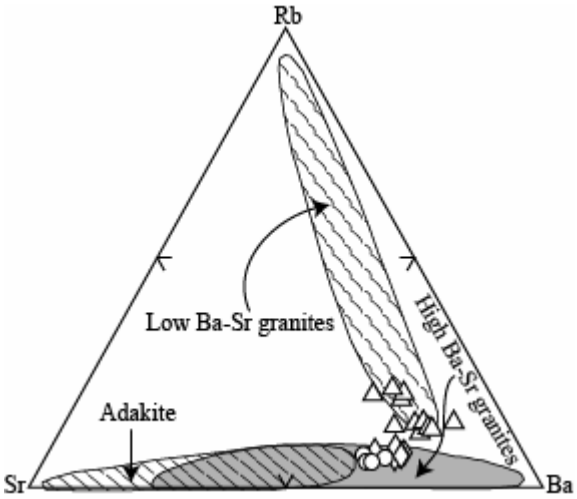

Figure 3: Sr-Rb-Ba plot (after Tarney and Jones, 1994). The symbols are same as those of Fig. 2.

A fractionated ($(La/Yb)_N$ ranging from 45-53) chondrite normalized rare earth element patterns with relative enrichment of LREEs over HREEs is with absence of significant Eu anomaly is common for enclaves and the high Ba-Sr granitoids on a chondrite normalized REE diagram (after Sun and McDonough, 1989; Fig. 4). However, fractionated and significant negative Eu anomaly (Eu/Eu* ratio varies from 0.42-0.59) is typical of low Ba-Sr granitoids (Fig. 4). A distinct negative Nb, P and Ti anomaly is common for all rock variations on a primitive mantle normalized trace element diagram (Fig. 4; after Sun and McDonough, 1989). This is typical of subduction-related magmatism and crustal-derived granites (e.g. Wang et al. 2006; Adams et al. 2006). The negative anomalies of P, Ti and Nb indicate fractionation of apatite, Ti-rich phases (rutile, anatase etc.) and amphibole from the source melt. However, they are enriched in Pb. A negative Ba anomaly is also observed for the low Ba-Sr granites on the same diagram. These features appeal to the role of crustally derived materials in the genesis of these rocks.

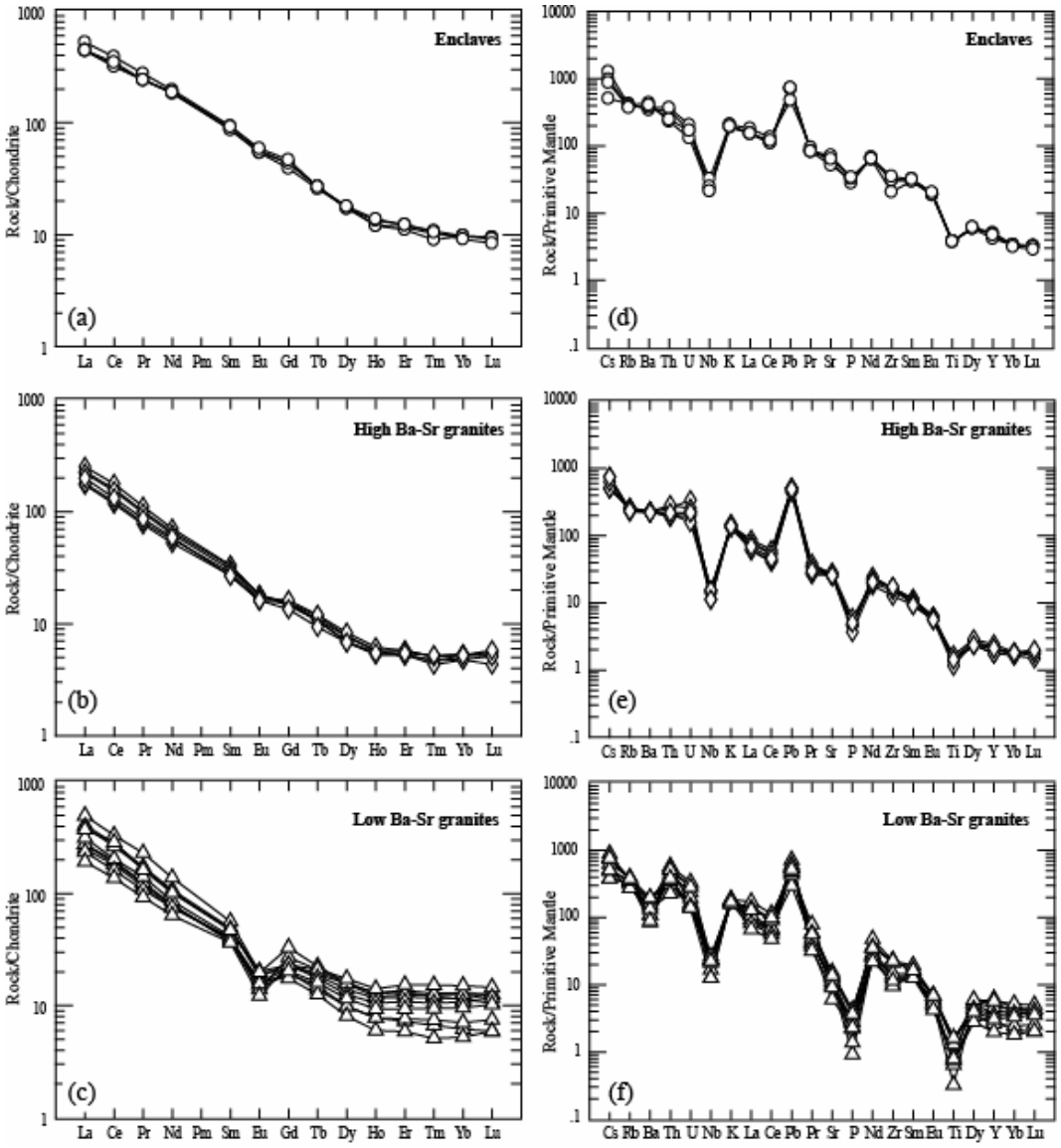

Figure 4: Chondrite- and primitive mantle- normalized trace element diagrams for the intursive rocks.

STABLE ISOTOPE GEOCHEMISTRY

The average $\delta^{18}O_{SMOW}$ values of high Ba-Sr granitoids are ~9 ‰. This value supports a mixed mantle and crustal origin for the high Ba-Sr granitoids (Fig. 5).

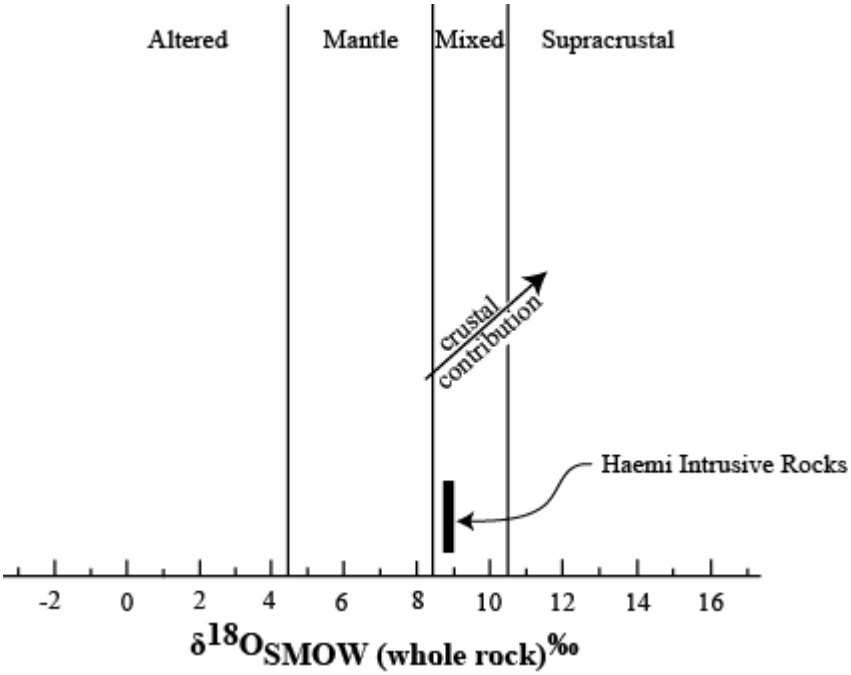

Figure 5: source ranges $\delta^{18}o_{smow}$ values for mantle, mixed, supracrustal and altered rocks, and the dark bar represents the range of values for the high ba-sr granitoids of the haemi area.

GEOCHRONOLOGY

Zircon grains from the high Ba-Sr granites were analyzed by SHRIMP and the results were plotted on a concordia diagram. The analytical spots yielded a weighted mean $^{207}Pb/^{206}Pb$ age of 233 ± 2 Ma (MSWD = 1.6). We interpreted this age as the crystallization age of the Haemi granites, and is slightly youger than that of the collision age.

PETROGENETIC CONSTRAINTS

Calc-alkaline and I-type granitoids of felsic compositions are commonly generated by low degree partial melting of crustal igneous rocks. They usually correspond to deeper levels of magma genesis. Again they were considered to be derived by advanced assimilation fractional crystallization of mantle derived basaltic magmas originated from a metasomatized mantle wedge above a subduction zone or from an enriched mantle source (enriched sub-continental lithosphere mantle or fluid modified mantle wedge). The mantle and the continental crust are the source regions that are widely involved in the formation of the continental igneous rocks.

The intermediate enclaves included in the Haemi granites have high MgO, Cr and Ni contents similar to upper mantle derived rocks such as potassic lamprophyres and lamproites. They are metaluminous, shoshonitic, and calc-alkaline with high Ba-Sr signatures. Fowler et al. (2001) and further Qian et al. (2003) considered the high Ba-Sr signatures of the granitoids

and associated mafic rocks as vital clue to the involvement of significant mantle components in their genesis. They interpreted the high Ba-Sr granitoids as products of crystal fractionation from associated mantle derived shoshonitic mafic magmas. The REE patterns are highly fractionated with LREE enrichment without a significant Eu anomaly. The amphiboles and biotites have higher Mg#s than those in granites. These features imply an upper mantle derivation for the intermediate enclaves. There existed some geochemical similarities for the intermediate enclaves and the high Ba-Sr granitoids. The intermediate and high Ba-Sr granites have no significant Eu anomaly. They have high Ba and Sr, LREE enriched patterns- and similar primitive mantle normalized patterns. This similarity can be attributed to the involvement of enriched mantle sources in the genesis of intermediate and high Ba-Sr granites. In Harker variation diagrams against SiO_2 contents (not shown in text), a good linear correlation can be observed between the enclaves, high Ba-Sr and low Ba-Sr granitoids. The good linear correlations in major oxide contents versus SiO_2 contents can be explained either by fractional crystallization or by mixing/mingling of granitic magma with a mafic magma. A compositional gap existed among the enclaves and the high Ba-Sr granitoids in the Harker diagrams against SiO_2 contents. The variations of elements among the granitoids are continuous. A petrogenetic model in which the felsic magmas were derived from the mafic magmas by the process of fractional crystallization is ruled out owing to less abundance of mafic enclaves when compared to the higher volumes of granitic rocks. The stable O-isotope compositions (~ 9 ‰) of high Ba-Sr granitoids advocates further the involvement of mantle and crustal components in their genesis. In the primitive mantle normalized diagrams, all the intrusive rocks display significant negative Nb and positive Pb anomalies. This is vital to interpret that minor amount of recycled crustal materials are involved in the genesis of intermediate enclaves and high Ba-Sr granitoids in the Haemi. The linear correlation between the enclaves and granites is possibly explained by two component mixing models. However, the geochemical characteristics of low Ba-Sr granitoids are typical of crustal derived granites. High Th/U ratios (> 3) are signatures of the input of recycled continental crustal sediments to the genesis of the felsic magma or melts. The Zr concentrations are also within the range of typical crustal rocks (100-200 ppm; Taylor and McLennan, 1985).

Hence, on the basis of field, petrographical, geochemical and stable O-isotope evidences we interpret here that the intermediate enclaves and high Ba-Sr granitoids were formed by the process of mingling/mixing of magmas derived from an enriched upper mantle and lower crust; and the low Ba-Sr granitoids are typical of highly fractionated granites by advance fractionation of granitic magma free of two-component mixing or with minor mixing. The chemistry of igneous rocks is widely used to deduce the tectonic environments of magma generation. Accordingly, on the diagram Y+Nb versus Rb all the data cluster in volcanic arc field but very close to the boundary between volcanic arc and syn-collision fields. The precise SHRIMP U–Pb zircon age of 233 Ma of the high Ba-Sr granitoids

represents a slightly younger than the the range of collisional ages already determined in the Hongseong area (235–290 Ma: Oh et al., 2004, 2005). These data, hence, indicate that the Hongseong area is an extension of the collision belt between the North and South China blocks within South Korea.

RELATIONSHIP BETWEEN TECTONICS, GRANITOIDS AND MINERALIZATION

It is widely acknowledged that the processes such as magma mingling/mixing, fractionation, remelting, remobilization and subsequent concentration of ore-forming fluids along with the regional tectonics play a significant role in metallogenesis. Many studies on Au-Ag mineralizations on the North China Craton and the Dabie Sulu Collision belt have aimed on the genetic relationship of mineralization to the collision tectonics and granitoids (e.g. Zhou and Lü, 2000; Qi et al., 2005). A collision-metallogeny-fluid flow (CMF) model is widely documented for the geodynamic setting of many significant gold deposits in North China craton (Qi et al., 2005). During Permian-Triassic continental collision, owing to the compressive forces and resultant crustal thickening along with increasing P-T conditions resulted in the generation of magmas with crustal affinities. The transition stage from compression to extension is marked by decompression melting (decreasing P and increasing T) which causes the influx of voluminous deep seated high K- calc-alkaline intermediate to highly felsic granites to the lower crust. In this stage structural features such as faults/shear zones can act as an opening for shallow-sourced fluid for circulation, and the mixing can lead to the formation of significant metals. Finally, the transition to extension stage marks a change in tectonics with decrease in T and P which resulted in the generation of highly evolved granites and flow of low-T meteoric fluids. We believe that Triassic collision and subsequent extension tectonics along with mixing and/or mingling of upper mantle and crustal magmas have an important influence on the later Jurassic to Early Cretaceous regional metallogeny in the Hongseong area. Similar tectonic scenario can be observed in the Haemi area, and hence we envisage a similar CMF model for the genesis of significant metals associated with Jurassic granites of the Hongseong area.

ACKNOWLEDGEMENTS

This work was supported by a grant (No.: R01-2006-000-10553-0 and Year: 2006) from the Basic Research Program of the Korea Science and Engineering Foundation (KOSEF).

REFERENCES

Adams A.J. *et al.* 2006. Contrasting silicic magma series in Miocene-Pliocene ash deposits in the San Miguel de Allende graben, Guanajuato, Mexico. *Journal of Geology*, Vol. 114, 247-266.

Cho, M. 2001. U-Pb zircon age of metamorphic rocks in the southwestern part of Gyeonggi Massif using ion microprobe; possible correlationship with the South China craton. Proceedings of Annual Joint Conference of Mineralogical Society of Korea and Petrological Society of Korea, Pusan, 141-142.

Choi, S-G. *et al.* 2005. Origin of Mesozoic gold mineralization in South Korea. *Island Arc*, Vol. 14, 102-114.

Fowler, M.B. *et al.* 2001. Petrogenesis of high Ba-Sr granites: the Rogart pluton, Sutherland. *Journal of Geological Society of London,* Vol. 158, 521-534.

Guo, J. *et al.* 2004. 230 Ma Eclogite from Bibong, Hongseong area, Gyeonggi Massif, South Korea: HP metamorphism, zircon SHRIMP U-Pb ages, and tectonic implication. In Abstract volume of International Association for Gondwana Res., South Korea Chapter, Miscellaneous Pbl., 2 Dec. 2004, Chonju, 11-12.

Li, S. *et al.* 1993. Collision of North China and Yangtze Blocks and formation of coesite-bearing eclogite: timing and processes. Chemical Geology, Vol. 109, 89-111.

Oh, C.W. & Kusky, T.M. 2007. The late Permian to Triassic Hongseong–Odesan collision belt in South Korea, and its tectonic correlation with China and Japan. *International Geology* Review*, in press*.

Oh, C.W. *et al.* 2004. Metamorphic evolution of the Baekdong metabasite in the Hongseong area, South Korea and its relationship with the Sulu collision belt of China. *Gondwana Research*, vol. 7, 809-816.

Oh, C.W. *et al.* 2005. First finding of eclogite facies metamorphic event in South Korea and its correlation with the Dabie-Sulu collision Belt in China. *Journal of Geology*, Vol. 113, 226-232.

Qi, J. *et al.* 2005. Tectonic setting of epithermal deposits in mainland China. In: Mineral Deposit Research:Meeting the Global Challenge, Springer,Berlin, 577-580.

Qian, Q. *et al.* 2003. Mesozoic high Ba-Sr granitoids from North China: geochemical characteristics and geological implications. *Terra Nova*, Vol. 15, 272-278.

Sengör, A.M.C. 1985. East Asian tectonic collage. *Nature*, Vol. 318, 16-17.

Sun S.-S. & McDonough, W.F. 1989. Chemical and isotopic systematics of oceanic basalts: implications for mantle compositions and processes. In: Magmatism in the Ocean Basins. Geological Society of London Special Publication 42, 313–345.
Tarney, J. & Jones, C.E. 1994. Trace element geochemistry of orogenic igneous rocks and crustal growth models. *Journal of Geological Society of London,* Vol. 151, 855-868.

Taylor SR, & McLennan SM (1985) The continental crust: its composition and evolution. Blackwell Scientific Publications, Oxford.

Wang, Y.C. *et al.* 2006. Geochemistry of the early Paleozoic Baiyin volcanic rocks (NW China): implications for the tectonic evolution of the North Qilian Orogenic Belt. *Journal of Geology*, Vol. 113, 83-94.

Yang, J-H. *et al.* 2003. A review of the geodynamic setting of large-scale late Mesozoic gold mineralization in the North China Craton: an association with lithospheric thinning. *Ore Geology Reviews*, Vol. 23, 125-152.

Yin, A. & Nie, S. 1993. An indentation model for the north and south China collision and the development of the Tan-Lu and Honam fault systems, eastern Asia. *Tectonics*, Vol. 12, 801-813.

Zhou, T. & Lü, G. 2000. Tectonics, granitoids and Mesozoic gold deposits in East Shangdong, China. *Ore Geology Reviews*, Vol. 16, 71-90.

Geochemistry of soils and waters close to W-Au-Sb old mines from Sarzedas, Castelo Branco, central Portugal

[1,2]Carvalho, P.C.S., [1,3]Neiva, A. M. R. and [1,4] Silva, M. M. V. G.

[1]Departamento de Ciências da Terra e Centro de Geociências, Universidade de Coimbra, Largo Marquês de Pombal, 3000-272 Coimbra
[2]paulacscarvalho@gmail.com [3]neiva@dct.uc.pt [4]mmvsilva@dct.uc.pt
Keywords: Soils, waters, contaminations, coatings, W-Au-Sb mineralizations, Sarzedas

ABSTRACT

In Sarzedas area, the Cambrian schist-metagraywacke complex predominates and is intersected by W-Au-Sb quartz veins and Sb-Au felsitic dikes which were exploited for W, Au, and Sb in Gatas-Santa and Pomar-Galdins. Soils and waters from Sarzedas area present contamination due to the past mining activities and host rock. Soils in Gatas-Santa and Pomar-Galdins must not be used for agriculture, human residence, commerce and industry due to their high Sb, Sn and As contents. Organic matter, clays and iron hydroxides and oxides in soils adsorbed metallic elements. Waters show high Fe and Mn contents and some of them also have high Sb contents due to mining activities. These waters must not be used for human consumption, but may be used for irrigation. Coatings on fragments from the waste heaps consist of goethite and symplesite. Goethite contains inclusions of arsenopyrite and stibnite and adsorbed As and Sb. Symplesite retains S and P. Therefore, coatings decreased contamination.

INTRODUCTION

Environmental pollution associated with mining activities has been studied by several authors (e.g., Armah et al., 2006; Kelepertsis et al. 2006). In general, old mine sites, where the rules of sustainable development were not applied, present environmental damage mainly due to waste heaps and mine tailings and their reactions with infiltrated water causing oxidation of sulphides, formation of sulphuric acid, which reduces the pH of the system that is responsible for dissolution of ore minerals and consequent release of metals. Therefore, water and soils will be polluted. If the rock contains carbonates, they neutralize the acidity and pH of water may be near neutral (e.g., Antunes et al., 2002) and consequently contamination will be less intense.
There are more than 100 abandoned mine workings in Portugal (Oliveira, et al., 2002) and the environmental impacts of some of them have been published (Antunes et al., 2002; Oliveira & Ávila, 1995; Oliveira et al., 2002; Pinto et al., 2004; Ávila et al; 2005; Gomes & Favas, 2006).
At Sarzedas, central Portugal (Fig. 1a), there are W-Au-Sb quartz veins and Sb-Au felsitic dikes containing stibnite (Fig. 1b), which were exploited

discontinuously from 1916 to 1951 for W, Au and Sb and produced 559 tons of stibnite concentrate containing W and Au. The tailings and rejected materials were deposited on the ground and are rarely covered by vegetation. Therefore, they are exposed to the water and air that may change the environmental geochemistry of the area.

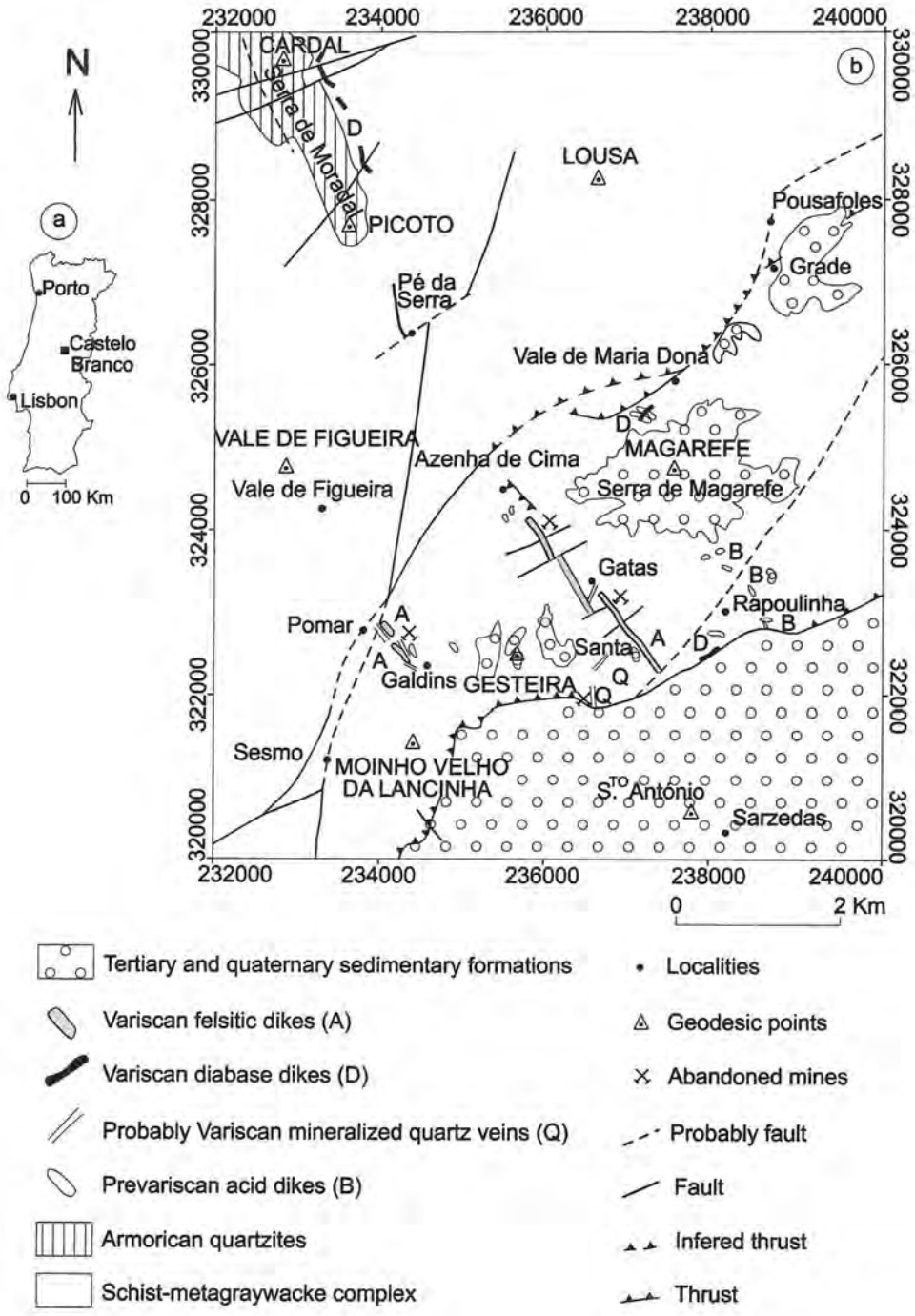

Fig.1 –a) Location of the Sarzedas area on the map of Portugal; b) Geological map of Sarzedas, central Portugal.

This paper evaluates the geochemical impact of W-Au-Sb quartz veins and Sb-Au felsitic dikes and of respective abandoned mine workings on soils and waters at Sarzedas.

GEOLOGICAL SETTING AND MINERAL PARAGENESIS OF MINERALIZED VEINS AND DIKES

The Sarzedas area lies about 19 km NW of Castelo Branco, central Portugal (Fig.1a). A Cambrian schist-metagraywacke complex predominates in the area (Fig. 1b), and consists of alternating muscovite schists, black schists and metagraywackes with rare metaconglomerate and marble intercalations (Sheperd, 1994). Armorican quartzites overlay this complex by angular unconformity and crop out at Serra do Moradal. N45-70ºW Pre-Variscan acid dykes deformed by the flux cleavage S1 intersect the schist-metagraywacke complex, are up to 5 m thick and crop out at Rapoulinha and Vale de Maria Dona.

Many breccia N25-50ºE W-Au-Sb quartz veins deformed by S1 are parallel to or at 45º of the fold axes (N25º-40ºE), probably Variscan, and intruded the schist-metagraywacke complex. They are discontinuously, up to 50 m long and 0.5-2 m thick at Gatas and contain 17 g/t Au. However, they are up to 150 m long at Santa and up to 200 m long and 2 m thick at Pomar-Galdins (Fig. 1b). N10º W Variscan diabase dikes intruded the same complex and crop out at W of Pé da Serra.

N20-30ºW subvertical Sb-Au felsitic dikes intruded the schist-metagraywacke complex. They are 3 km long and 5-10 m thick at Gatas and are 20 m long and 2-3 m thick at NE of Pomar. Mineralized veins are related to the intersection of N25-30ºW second Variscan deformation phase shear zone with the late-Variscan NE-SW faults (Sheperd, 1994).

The W-Au-Sb quartz veins consist of quartz, muscovite, apatite, ferberite, cobaltite, arsenopyrite, pyrite, sphalerite, chalcopyrite, tetrahedrite, glaucodot, semseyite, galena, stibnite and siderite. The felsitic dykes contain quartz, albite, potash feldspar, muscovite, zircon, rutile, montebrasite, apatite, lazulite, arsenopyrite, pyrite, sphalerite, tetrahedrite, stibnite and siderite. Stibnite is the most abundant ore mineral in quartz veins and felsitic dikes (Carvalho, 2004). The minerals were studied by transmitted and reflected-light microscopy and electron microprobe analyses.

METHODS

A total of 893 soil samples were collected in the Sarzedas area, corresponding to 609 and 284 at Gatas-Santa and Pomar-Galdins, respectively (Fig. 2) for mineral and geochemical prospections using a grid of 50×20 m, but close to the Pomar mine a grid of 25×20 m was used (Instituto Geológico e Mineiro, 1988). Antimony, Sn, W, As and Sb were

determined by ICP-AES at Instituto Geológico e Mineiro, S. Mamede de Infesta with a precision of 10%.
Eleven sampling points located close to the abandoned old mine workings (Fig.2) were chosen to collect water at each point four times (winter, February 2002; summer, August 2002; spring, March 2003; summer, July 2003) during a year obtaining a total of 36 water samples, because 8 points had no water due to the dry climate, particularly in summer. Temperature, pH, Eh, dissolved oxygen, specific conductance and alkalinity were determined in situ. The waters were acidified and kept at 4ºC. Alkalinity and Cl^- were determined by titrations. Nitrates, nitrites, phosphates and sulphates were determined by molecular absorption UV-visible Spectrometer Perkin Elmer Lambda 2 and Na, K, Ca, Mg, Fe, Mn, As, Sb, Pb, Zn, Cu were obtained using a Spectrometer Perkin Elmer 303 flame atomic absorption at the Department of Earth Sciences, University of Coimbra. W was not detected in waters from Sarzedas. All the analyses were obtained with a precision of ± 5%.

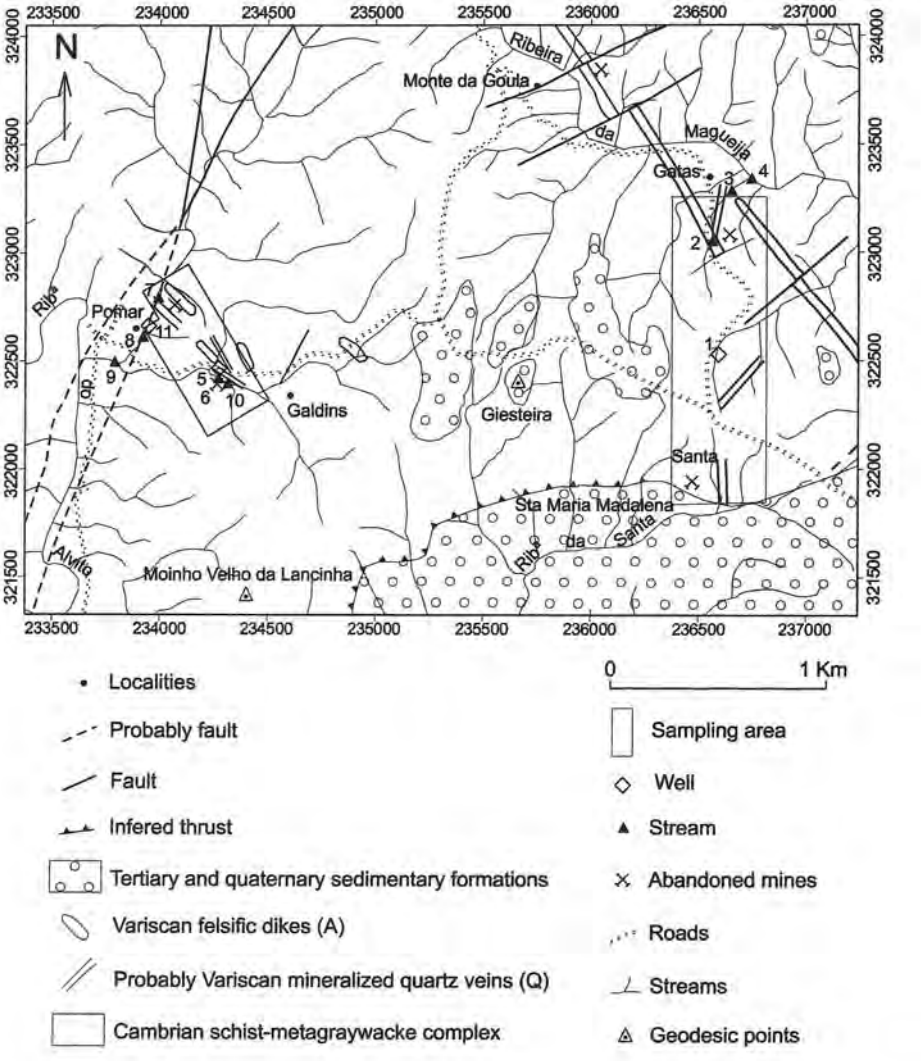

Fig. 2- Simplified geological map showing streams from Sarzedas, central Portugal with the two selected areas for soil prospection (Instituto Geológico e Mineiro, 1988) and location of water sampling points.

RESULTS AND DISCUSSION

Geochemistry of soils

At Gatas-Santa and Pomar-Galdins, soils have higher mean and maximum values of As and Sb than muscovite schist and black schist (Table 1). They also have higher maximum Sn, W, As and Sb contents than W-Au-Sb quartz veins. In schists, Sn and W are retained in micas, while As and Sb are concentrated in sulphides. In mineralized quartz veins, Sn is retained in muscovite, W, As and Sb are concentrated in ferberite, arsenopyrite and stibnite, respectively. In felsitic dikes, Sn is retained in muscovite and As and Sb are concentrated in sulphides. Wolframite and sulphides also concentrate metals in mine tailings and a small amount in waste heaps.

Table 1- Trace elements contents in ppm of soils from Sarzedas compared with recommended maximum concentrations

	Mus schists	Black schists	Miner. quartz veins	Gatas - Santa			Pomar - Galdins			Recommended maximum		
				Min.	Max.	Mean	Min.	Max.	Mean	1	2	3
Sn	2	2	2	0.5	2500	6	-	-	-	5	50	300
W	4	3	5	0.6	300	5	0	27	2	-	-	-
As	11	11	118	25	9300	63	25	170	34	20	30	50
Sb	11	12	454	2	11000	294	2	21600	293	20	20	40
N						609			284			

Contents of trace elements from schists and mineralized quartz veins (Oliveira et al. 1994). Mus-muscovite; Miner- mineralized. Min.-minimum; Max.- maximum; - not determined or not defined. 1-agricultural soil; 2- human residence soil; 3- commerce and industry soil (Canadian Council of Ministers of the Environment, 1991). N- number of samples. These data were supplied by Instituto Geológico e Mineiro.

The class distribution of analyzed elements in soils is given in Fig. 3. Tin, W, As and Sb contents of most soil samples are below the mean values. Anomalies of these trace elements in soils are mainly related to exploited W-Au-Sb quartz veins and Sb-Au felsitic dikes (Carvalho, 2004). Metals in soils depend mainly on the contents of these elements in mineralized veins and dikes and weathering processes. The minimum As value found in soils from Sarzedas is 25 ppm, which is higher than the recommended value for agriculture according to Canadian law (Table 1). Furthermore, about 40 % and 13 % soil samples from Gatas-Santa and Pomar-Galdins,

respectively have Sb contents higher than 20 ppm, which is the recommended value for Sb in soils for agriculture and human residence. Ore minerals have large exposed surfaces due to explotation, wich become weathered and metals are released from the abandoned exploited mineralized veins and dikes, mine tailings and waste heaps to soil, where they are absorved by clay minerals, Fe-oxides, Fe-hydroxides and organic matter. Chemical processes involving dissolution of ore minerals, transport of metals and their precipitations in soils are important. Soils are sinks of trace elements, where Sb dominates and As has 5 to 9 times lower content (Table 1). The highest Sb content occurs in soils from Pomar-Galdins. Soils from Gatas-Santa have higher maximum and mean As values. The mean value is about twice that in soils from Pomar-Galdins. However, mechanical transport of metals and ore minerals was also important as some stibnite fragments were found in soils. The soils have Sn, Sb and As contents showing that they must not be used for agriculture, human residence, commerce and industry (Table 1). Although

Gatas-Santa

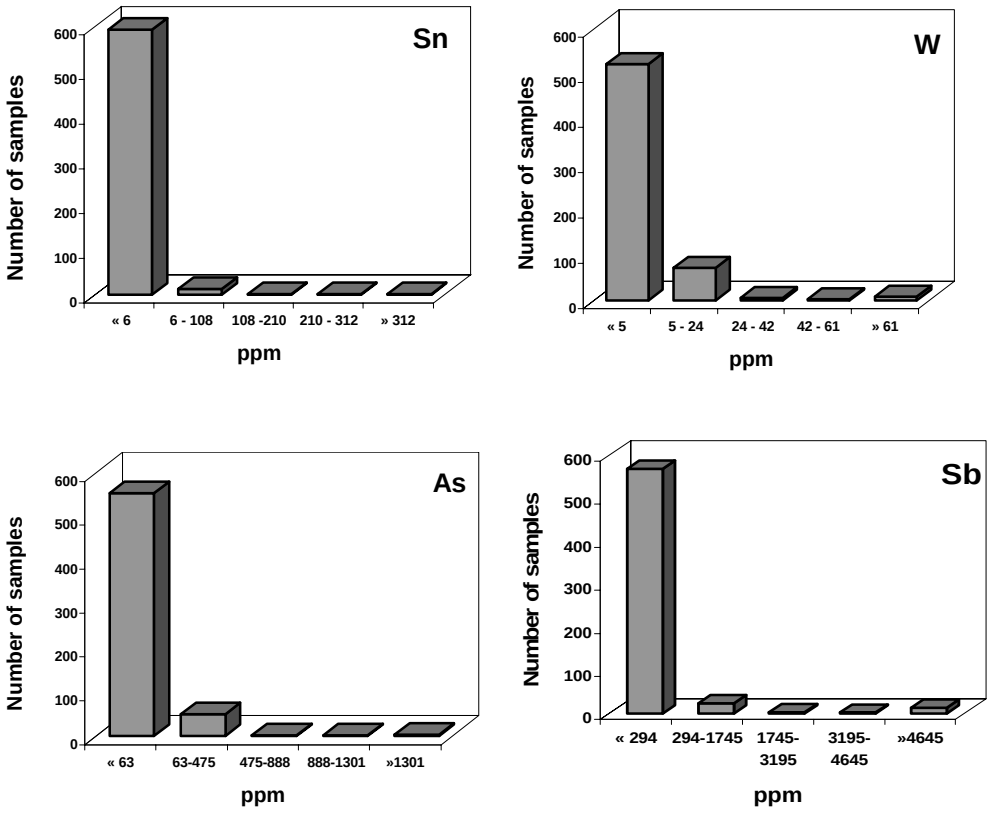

Pomar-Galdins

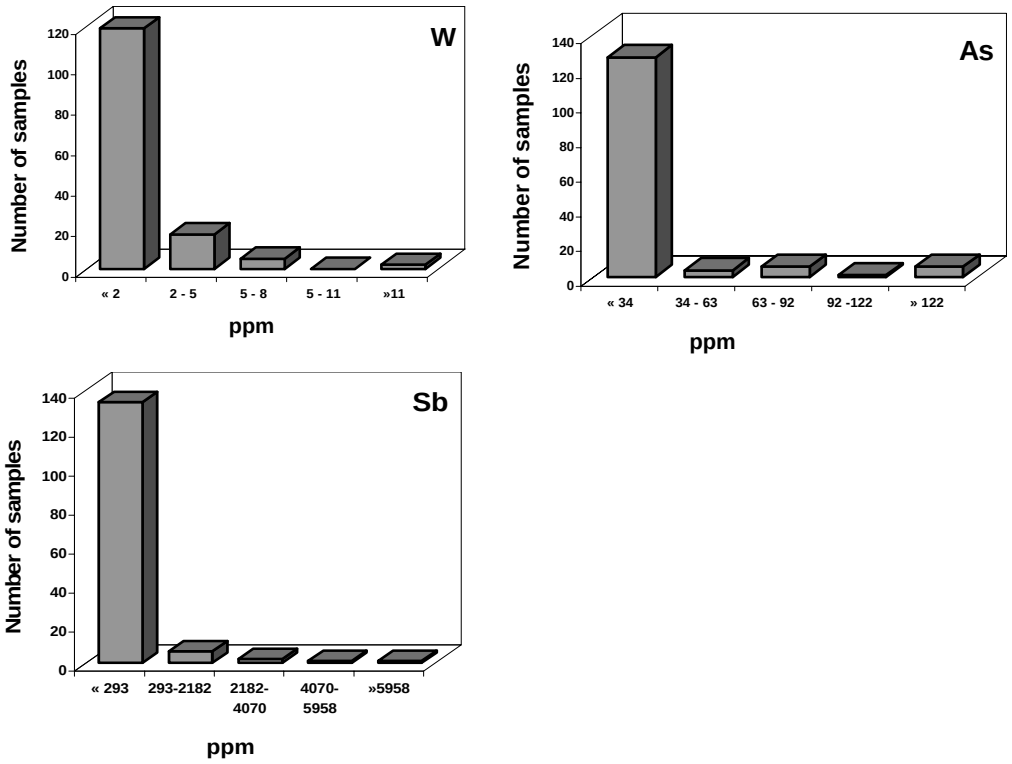

Fig. 3 – The class distribution of trace elements contents of soils from the two areas of Sarzedas marked in Fig. 2. The lower limits of the classes are the average, σ, 2σ and 3 σ.

Sb content is higher than As content in soils from Sarzedas area, the high toxicity of As makes the As content more problematic than Sb content. Therefore, contamination is more important at Gatas-Santa than Pomar-Galdins.

Oxides, hydroxides and arsenates occur in mine tailings and waste heaps and retain metals. Coatings on fragments of waste rock consist mainly of goethite that absorbed As and Sb and contains inclusions of arsenopyrite and stibnite. Goethite compositions obtained by electron microprobe have up to 8.10 wt% Sb_2O_5 and 2.26 wt% As_2O_5. Some symplesite $Fe_{3.02}{}^{2+}\left(As_{1.50}S_{0.26}P_{0.02}\right)_{\sum 1.98}O_8.7.90H_2O$ retains S and P and is associated with goethite. They retain metallic elements and prevent increase of contamination in soils. However, small particles of sulphides incorporated by mechanical processes in soils will be weathered and metallic elements will be released.

Geochemistry of waters

Chemical composition at water samples from Sarzedas are given in Table 2. The specific conductance shows low values ranging between 51.20 and 234.50 (µS/cm). pH ranges between 5.5 and 7.3 indicating absence of significant acid drainage, because W-Au-Sb quartz veins and Sb-Au dikes contain siderite and intersect a schist-metagraywacke complex containing marble intercalations. Carbonates, mainly siderite probably neutralize acid

waters by the reaction $FeCO_3 + H^+ \rightarrow Fe^{2+} + HCO_3^-$ (Seal & Hammarstrom, 2003) and consequently metal concentration and specific conductance are low (e.g., Rahn et al., 1996; Antunes et al., 2002). Only a value of 9.3 was found in the sample 6 at August 2002, which is attributed to a high phosphate content (0.472 mg/l) due to algae in water.

In general, waters from wells tend to have lower dissolved oxygen and higher specific conductance values than stream waters (Table 2) except in two points (up to 234.5 µS/cm) in summer, when there was no water flux in these two streams and temperature reached 40ºC. Temperature, specific conductance, Na, Ca, Zn, Cu, HCO_3^-, PO_4^{2-} and dry residue generally present higher values, while Eh and dissolved oxygen have lower values in summer than in winter, which is better shown in stream waters than in well waters, as expected (Carvalho, 2004).

Although most trace element contents of metals (As, Pb, Zn and Cu) in waters are low (Table 2) and well below the accepted values for human consumption (Portuguese law, 2001) and most Sb contents are below the detection limit, Sb values of 2.6 mg/l and 0.21 mg/l occur in stream waters from points 3 and 8, respectively, which are close to waste heaps. These two waters must not be used for human consumption. About 43 % of analysed water samples from wells and streams have Fe values exceeding 0.20 mg/l and most well waters present Mn values above 0.05 mg/l, which are the accepted values for human consumption (Table 2), but they may be used for agriculture. Antimony is concentrated in stibnite, Fe is mainly retained in pyrite, arsenopyrite and siderite and Mn in siderite from the mineralized veins and dikes and mine tailings.

Table 2- Concentration of constituents in waters from Sarzedas

Samples	Dates	T (ºC)	pH	Eh (mV)	D. ox. (mg/l)	Sp. Cond. (µS/cm)	Na (mg/l)	K (mg/l)	Ca (mg/l)	Mg (mg/l)	Fe (mg/l)
1w	February 2002	12.5	5.66	287	10.80	124.6	7.23	0.19	1.05	7.84	0.01
	August 2002	21.9	5.5	288	8.92	144.6	7.33	0.19	1.58	10.99	<0.050
	March 2003	13.7	5.82	285	8.49	155.3	8.06	0.25	1.85	11.74	0.028
	July 2003	19.5	5.5	221	5.35	142	7.63	0.3	1.54	9.92	0.119
5w	February 2002	12.1	6.31	219	6.25	148.4	8.35	1.04	4.38	11.46	1.16
	August 2002	19.8	6.66	44	5.82	140.9	9.07	0.78	4.61	9.98	0.558
	March 2003	12.7	6.16	198	4.31	120.1	6.58	0.78	3.73	9.7	2.03
	July 2003	18.1	6.03	107	6.10	96.7	8.16	0.49	1.92	4.3	0.73
11w	March 2003	13.9	6.31	209	5.85	100.5	9.78	0.32	3.44	8.48	1.88
	July 2003	18.4	6.31	*	5.50	175.0	11.38	1.12	5.05	11.21	5.55
2st	February 2002	11.7	5.98	268	5.52	81.8	7.6	0.42	0.66	4.82	0.1
	March 2003	12.9	6.38	174	9.32	56	5.67	<0.100	0.759	4.44	<0.050
3st	February 2002	9.7	6.19	271	12.65	164	7.79	0.93	3.05	11.46	0.1
	March 2003	12.5	6.23	229	10.40	136	6.34	0.36	2.79	11.16	0.049
4st	February 2002	12.3	6.51	218	14.72	71.7	6.86	0.7	1.72	3.62	0.21
	August 2002	21.9	7.25	204	10.32	125	11.02	1	3.37	7.12	0.454
	March 2003	13.6	6.54	169	11.43	54	5.06	0.36	1.02	2.46	0.079
	July 2003	23.1	6.6	153	6.15	85.1	7.68	0.83	2.21	4.34	0.421
6st	February 2002	12.0	6.64	268	14.42	64.4	7.79	0.63	1.14	2.71	0.07

	August 2002	27.8	9.32	197	14.70	234.5	22.76	3.25	8.15	14.4	2.2
	March 2003	14.4	6.6	191	11.25	56	5.93	0.61	1.23	2.34	0.058
	July 2003	19.8	6.3	221	7.95	83	8.66	0.76	1.52	3.04	0.142
7st	February 2002	14.1	6.55	235	12.73	58.8	6.31	0.22	0.67	2.71	0.04
	August 2002	23.2	6.83	137	6.42	112.7	10.96	0.72	2.2	6.66	1.35
	March 2003	16.4	6.61	228	11.00	54.1	5.64	0.55	0.767	2.91	0.053
	July 2003	22.8	6.63	*	8.20	78.5	7.27	0.27	1.21	4.03	0.218
8st	February 2002	13.4	6.65	208	12.60	64.8	6.68	0.37	0.76	3.32	0.05
	August 2002	28.2	7.17	202	8.91	229.4	16.24	2.05	5.72	16.72	0.063
	July 2003	20.2	7.22	164	8.60	108	8.65	0.52	1.72	6.15	0.345
9st	February 2002	12.7	6.53	206	13.20	66.4	6.68	0.41	0.91	3.32	0.12
	August 2002	26.7	6.81	230	10.38	113.8	11.6	2.71	2.76	4.87	0.124
	March 2003	16.0	6.69	195	10.64	54.8	5.61	0.34	0.831	2.68	0.042
	July 2003	24.6	6.13	156	9.95	122	9.61	2.29	3.62	5.65	0.215
10st	February 2002	12.0	6.51	272.4	12.10	63.94	7.05	0.53	1.05	2.56	0.07
	March 2003	14.8	6.53	221	10.00	56.9	6.05	0.6	1.41	2.32	<0.050
	July 2003	23.3	6.6	92	7.80	93.5	9.12	1.26	1.88	3.26	0.195
VMAh		25.0	9.5	**	**	400	150	12	100	50	0.20
VMRr		**	**	**	**	**	**	**	**	**	5.0

Mn (mg/l)	As (mg/l)	Sb (mg/l)	Pb (mg/l)	Zn (mg/l)	Cu (mg/l)	HCO_3^- (mg/l)	Cl^- (mg/l)	SO_4^{2-} (mg/l)	NO_3^- (mg/l)	NO_2^- (mg/l)	PO_4^{2-} (mg/l)	Dry residue (mg/l)
-	-	-	1.1	0.02	-	12.35	11.56	31	1.156	0.010	0.006	95
<0.005	<0.030	<0.050	<0.030	0.006	<0.005	11.21	8.79	56.1	0.81	0.030	0.072	89
0.011	<0.030	<0.050	<0.030	0.042	<0.005	9.24	18.41	50.91	1.62	-	0.015	98
0.007	<0.030	<0.050	0.031	0.086	0.011	10.56	13.15	32.29	1.08	0.001	0.010	97
0.23	0.006	-	-	0.03	-	40.5	9.56	20.48	0.031	-	0.054	108
0.112	<0.030	<0.050	<0.030	0.022	0.012	48.82	7.23	24.83	0.46	-	-	79
0.246	<0.030	<0.050	<0.030	<0.005	<0.005	43.21	5.26	12.44	-	0.004	0.056	70
0.067	<0.030	<0.050	<0.030	0.02	<0.005	25.07	13.15	5.57	0.19	-	-	58
0.166	<0.030	<0.050	<0.030	<0.005	<0.005	42.22	7.89	24.05	0.79	0.016	0.036	92
0.459	<0.030	<0.050	<0.030	0.052	0.008	65.97	9.21	19.12	0.29	0.002	0.304	108
-	**	0.095	**	0.02	-	*	9.56	7.93	0.977	0.020	0.067	93
<0.005	<0.030	0.124	<0.030	<0.005	<0.005	19.13	7.89	2.49	0.41	0.006	0.016	33
0.01	0.021	2.6	0.001	0.03	-	11.25	9.06	49.61	10.092	-	0.051	126
<0.005	<0.030	0.798	<0.030	0.011	<0.005	13.19	7.89	40.64	0.72	-	0.036	97
-	**	**	**	0.02	-	11.25	9.56	4.24	-	-	0.001	51
0.022	<0.030	<0.050	<0.030	0.006	<0.005	41.56	9.36	15.46	0.09	0.012	0.009	66
<0.005	<0.030	<0.050	<0.030	<0.005	<0.005	13.19	10.52	-	-	0.024	0.004	34
0.011	<0.030	<0.050	<0.030	0.008	<0.005	25.73	10.52	5.58	1.21	0.012	0.026	65
0.01	-	-	-	0.01	-	12.5	9.56	3.73	-	0.010	0.002	54
0.234	<0.030	<0.050	<0.030	<0.005	0.005	107.86	16.31	18.27	0.43	0.143	0.472	181
<0.005	<0.030	<0.050	<0.030	<0.005	<0.005	10.56	10.52	-	0.32	0.002	0.038	36

0.008	<0.030	<0.050	0.049	0.089	0.02	25.07	13.15	5.19	0.28	0.008	0.022	55
-	-	-	-	-	-	13	8.04	3.02	-	-	-	47
0.098	<0.030	<0.050	<0.030	<0.005	<0.005	36.94	7.09	15	0.52	0.002	0.018	60
<0.005	<0.030	<0.050	<0.030	<0.005	<0.005	14.51	7.89	4.98	0.34	0.006	0.018	51
0.012	<0.030	<0.050	<0.030		<0.005	21.77	10.52	4.9	0.48	-	-	58
-	-	0.028	**		-	13.25	9.06	2.64	0.757	-	0.014	67
0.014	<0.030	0.211	<0.030	<0.005	0.005	36.28	9.5	94.5	0.41	0.010	0.200	148
<0.005	<0.030	0.097	<0.030	0.287	<0.005	24.41	10.52	16.66	0.47	0.002	0.032	78
0.02	-	0.0068	-	0.01	-	13	9.06	4.48	-	-	-	53.33
0.012	<0.030	<0.050	<0.030	<0.005	<0.005	28.7	9.22	17.99	0.34	0.004	0.036	62
<0.005	<0.030	<0.050	<0.030	<0.005	<0.005	14.18	10.52	2.9	0.44	0.008	0.024	55
0.024	<0.030	<0.050	0.054	0.342	0.029	26.39	15.78	11.39	1.87	0.014	0.142	82
0.01	-	-	-	0.02	-	14.59	11.36	3.48	0.05	0.007	0.011	49.33
<0.005	<0.030	<0.050	<0.030	0.065	<0.005	14.18	7.89	1.66	1.08	-	0.012	47
0.006	<0.030	<0.050	<0.030	1.181	0.012	22.43	10.52	4.78	0.48	0.006	0.004	62
0.05	0.05	0.01	0.05	3.0	0.05	**	25.0	250.0	**	0.1	**	1500.0
0.20	0.10	**	5.0	2.0	0.20	**	70	575	50	-	-	**

T-temperature, D.ox.-dissolved oxygen, Sp. Cond- specific conductance. w- well; st- stream. (-): Not detected. (*): Not determined. (**): Not defined. 1,5 and 11- well; 2,3,4,6,7,8,9 and 10- streams. Analyst: Paula C. S. Carvalho. VMAh-Human accepted values; VMRr-agricultural recommended values (Portuguese law, 2001). Analyst: Paula Carvalho.

The Principal Component Analysis (PCA) is applied to hydrology (e. g., Simeonov et al., 2003) and the results for Sarzedas waters are shown in Table 3. Three significant components with eigenvalues >1 and accounting for 83% of the total variance were extracted (Table 3), following criteria of other authors (e.g., Davis, 2002). By taking only values of ±0.5, the first component is defined by the variables HCO_3^-, Cl^-, NO_2^-, PO_4^{3-}, Na, K, Ca, Mg, Fe and Mn. All are related to the schist-metagraywacke complex, but Fe and Mn may also be derived from the mineralized quartz veins and felsitic dikes. The second component is represented by the association of NO_3^-, SO_4^{2-} and Sb (Fig. 3) which is due to mineralization and mining activities, but also to agriculture. The third component consists only of Zn and is related to mineralization.

Table 3- Results of Principal Component Analysis on the water samples data(n=36)

	PCA 1	PCA 2	PCA1 3
HCO_3^-	0,9504	0,2103	-0,0735
Cl^-	0,6239	0,2873	0,4563
SO_4^{2-}	0,4121	-0,7527	-0,0851
NO_3^-	0,0621	-0,8152	0,2063
NO_2^-	0,8729	0,2717	-0,0640
PO_4^{3-}	0,9519	0,0111	-0,0120
Na	0,9569	0,0012	-0,0018
K	0,8275	-0,0227	0,2793
Ca	0,9469	-0,2097	0,0391
Mg	0,7464	-0,5711	-0,1355
Fe	0,8284	0,2559	-0,1720
Mn	0,8904	0,2242	-0,1670
Zn	-0,0028	0,1084	0,8840
Sb	0,0387	-0,9021	0,0789
Eigenvalues	7.67	2.74	1.21
Total variance (%)	54.78	19.60	8.65
Cumulative variance (%)	54.78	74.38	83.02

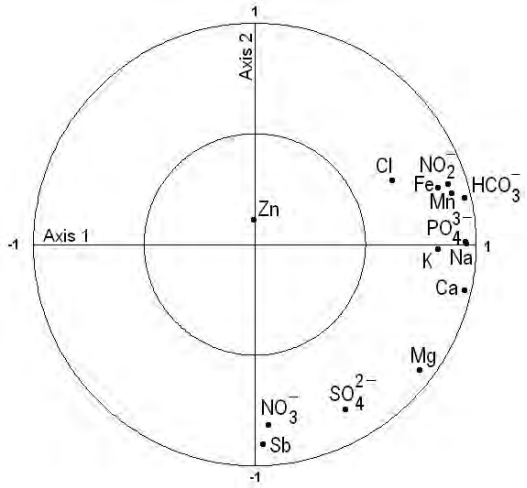

Fig. 3- Plot of the first factorial plan.

CONCLUSIONS

(1) At Sarzedas area, there are quartz veins containing ferberite, gold and stibnite and felsitic dikes with gold and stibnite cutting the Cambrian schist-metagraywacke complex. Veins and dikes also contain arsenopyrite, pyrite, sphalerite, stibnite and siderite, but quartz veins also have chalcopyrite, glaucodot, semseyite and galena.

(2) In schists, Sn and W occur in micas. As and Sb are concentrated in arsenopyrite and stibnite, respectively. In mineralized quartz veins, felsitic dikes, mine tailings and waste heaps, Sn is retained in micas, As and Sb are concentrated in sulphides, while W is concentrated in ferberite from quartz veins, mine tailings and waste heaps.

(3) At Sarzedas, the Sn, As and Sb anomalies in soils are related to mineralized quartz veins, felsitic dikes and old mining activities on them, and W anomaly in soils is associated with the W-Au-Sb quartz veins.

(4) Chemical transport was more important than mechanical transport for Sn, W, As and Sb in soils. The abandoned mining activities favoured weathering of micas and ore minerals and release of metals to soils and water.

(5) The high Sn, As and Sb contents of soils from Sarzedas are indicate that they must not be used for agriculture, human residence, commerce and industry. Soils from Gatas-Santa are more contaminated than those from Pomar-Galdins due to their higher As contents.

(6) Coatings on fragments from waste heaps are formed by goethite adsorbing As and Sb and symplesite retaining S and P and both contain inclusions of arsenopyrite and pyrite. Oxides, hydroxides and arsenates in mine tailings and waste heaps retain metals.

(7) The waters have lower W, As and Sb contents than the soils due to their relatively low mobility.

(8) In general, pH of waters associated with old mine workings at Sarzedas ranges between 5.5 and 7.3, showing that there is no significant acid drainage due to neutralization of acid waters (resulting from weathering of sulphides) with siderite from W-Au-Sb quartz veins and Sb-Au dikes and marbles from the schist-metagraywacke complex.

(9) At segura, waters associated with mineralized quartz veins and dikes and old mining activities must not be used for human consumption, but may be applied to agriculture.

ACKNOWLEDGEMENTS

We are grateful to INETI for the use of data on soils obtained by Instituto Geológico e Mineiro. This research work was carried out in the programme of Geosciences Centre, Coimbra University, Portugal.

REFERENCES

Antunes, I.M.H.R. *et al.* 2002. The mineralized veins and the impact of old mine workings on the environment at Segura, central Portugal. Chemical. Geology, Vol. 190, 417-431.

Armah, Y. S. et al. 2006. Levels of arsenic and antimony in water and sediment from Prestea, a gold mining town in Ghana and its environs. Water, Air, and Soil Pollution, Vol. 175, 181-192.

Ávila *et al*. 2005. Geochemical signatures and mechanism of trace elements dispersion in the area of the Vale the Gatas mine (Northern Portugal). Geochemical Exploration, Vol. 85, 17-29.

Canadian Council of Ministers of the Environment 1991: Interim Canadian Environmental Quality Criteria for Contaminated Sites. CCME EPC – CS34, Manitoba 1-20.

Carvalho, P. C. S. 2004. Impacte Ambiental de Antigas Explorações Mineiras na região de Sarzedas-Castelo Branco (central Portugal). MSc thesis. University of Coimbra, Portugal, 185 pp.

Davis, J. C. 2002. Statistic and Data Analysis in Geology, Second Edition. John Wiley & Sons, New York. 646 pp.

Direcção Geral de Geologia e Minas 1988. Relatório dos trabalhos realizados de 1 de Setembro a 31 de Dezembro de 1987 relativo à área de Sarzedas, Portugal, 18 pp.

Gomes, M. E. P & Favas, P. J. C. 2006. Mineralogical controls on mine drainage of the abandoned Ervedosa tin mine north-eastern Portugal. Applied Geochemistry, Vol. 21, 322-1334.

Kelepertsis, A. et al. 2006. Arsenic, antimony and other toxic elements in the drinking water of Eastern Thessaly in Greece and its possible effects on human health. Environmental Geology, Vol. 50, 76–84.

Oliveira, J.M.S & Ávila, P.F. 1995. Avaliação do Impacto Ambiental provocado por uma exploração mineira. Um caso de estudo no país. Estudos Notas e Trabalhos do Instituto Geológico e Mineiro, Portugal, Vol. 37, 25-50.

Oliveira, J. M. S. et al. 2002. Diagnóstico Ambiental das Principais Áreas Mineiras Abandonadas Degradadas do País. Boletim de Minas, Lisboa, Vol. 39, 67-85.

Pinto, M. M. S. C. et al. 2004. Pollution of water and stream sediments associated with the Vale de Abrutiga uranium mine, central Portugal. Mine Water and Environment, Vol. 23, 66-75.

Portuguese law 2001. Decree No 243/2001- Portuguese Legislation on Water Quality. I-A, 5754-5766.

Rahn, P. H. et al. 1996. Water quality impacts from mining in the Black Hills, South Dakota, USA. Environmental Geology, Vol. 27, 38-53.

Seal, R. R. & Hammarstrom, J. M. 2003. Geoenvironmental models of mineral deposits: examples from massive sulfide and gold deposits. In Environmental Aspects of Mine Wastes (J. L. Jambor & D. W. Blowes, eds.). Mineral. Assoc. Canadian Short Course, Vol. 31, 11-50.

Shepherd,T. J. 1994. Integrated Multidisciplinary Exploration Techniques for Gold and Precious Metals in the Western Iberian Peninsula, Final Report, Vol. I, 141 pp.

Simeonov, V. et al. 2003. Assessment of the surface water quality in Northern Greece. *Water Research,Vol.* 37, 4119-4124.

Hydrogeochemical characteristics of groundwater in Günyüzü Basin (Sivrihisar- Eskisehir) Western Turkey

Demiroğlu Muhterem [1], Yalçın Tolga [1], Örgün Yüksel [1], Yaltırak Cenk [1], Akdeniz Uğur [2]

[1]: Istanbul Technical University (ITU) 34462, Maslak-İstanbul Turkey
[2]: State Hydraulic Works (DSİ), Yücetepe-Ankara/ Turkey
e-mail: copuroglum@itu.edu.tr
Keywords: Günyüzü Basin, groundwater, hydrogeochemistry, aquifer, isotope

ABSTRACT

Groundwater is mostly the unique water source in semiarid regions of Turkey. The study area is located in the Sakarya Basin. The Günyüzü basin covers an area of 500 km^2 with an annual average precipitation of 393 mm. The study area comprises Mesozoic metamorphic rocks, Eocene granites, Neogene sedimentary rocks and recent alluvium. Marbles are main aquifers within the studied area, which take place at top of the impermeable metamorphic basement. Neogene limestones, conglomerates and alluvium are other important aquifers. 9 groundwater samples were taken from springs and wells in dry and wet seasons, chosen in order to represent aquifer characteristics. The groundwaters have Ph values ranging from 6.59 to7.56, and temperatures(T) changes 14 - 35^oC, The cation and anion permutation of the samples are mostly in rCa> rMg > rNa > rK and $rHCO_3$> rSO_4 > rCl form, respectively. These results indicate that most of these groundwaters are located within the marbles and limestones. $\delta^{18}O$ (‰ –11,2 - ‰-8,9) and δ^2H (‰ -79 - ‰ -60) isotope values show that all waters (thermal and cold) are meteoric origin. The EC-tritium relationship indicates the existence of water with different origins. These groups that have high EC and low ^3H (0 – 4 TU) values represent the deep circulating water. Low EC and high ^3H (4-10 TU) values represent the shallow circulating waters where these waters mix in various proportions

INTROUDUCTION

The aim of this study, in the Günyüzü basin located in the upper Sakarya main basin (Fig.1 a,b), in semiarid regions of Turkey with an annual average precipitation of 393 mm., is to define aquifer characteristics. The study area comprises different hydrogeological properties such as unconfined-confined-semi confined karstic, fractured and granular aquifers together with elevated temperatures higher than cold waters. Marbles are main karstic aquifers within the studied area; karstic systems are characterized by heterogeneous permeability distribution. This heterogeneity induces a wide spectrum of water origin, transfer mechanism and residence times. Hydrological and hydrogeological data were supported by hydrochemical and isotopic tools. Monitoring of

chemical composition of karstic systems allows the origin of the water flowing from the karstic spring to be determined, since the different reservoirs will have characteristic chemical signature (Aquilina et al., 2005).
Water discharging from a karst spring carries imprints of upstream in the aquifer.

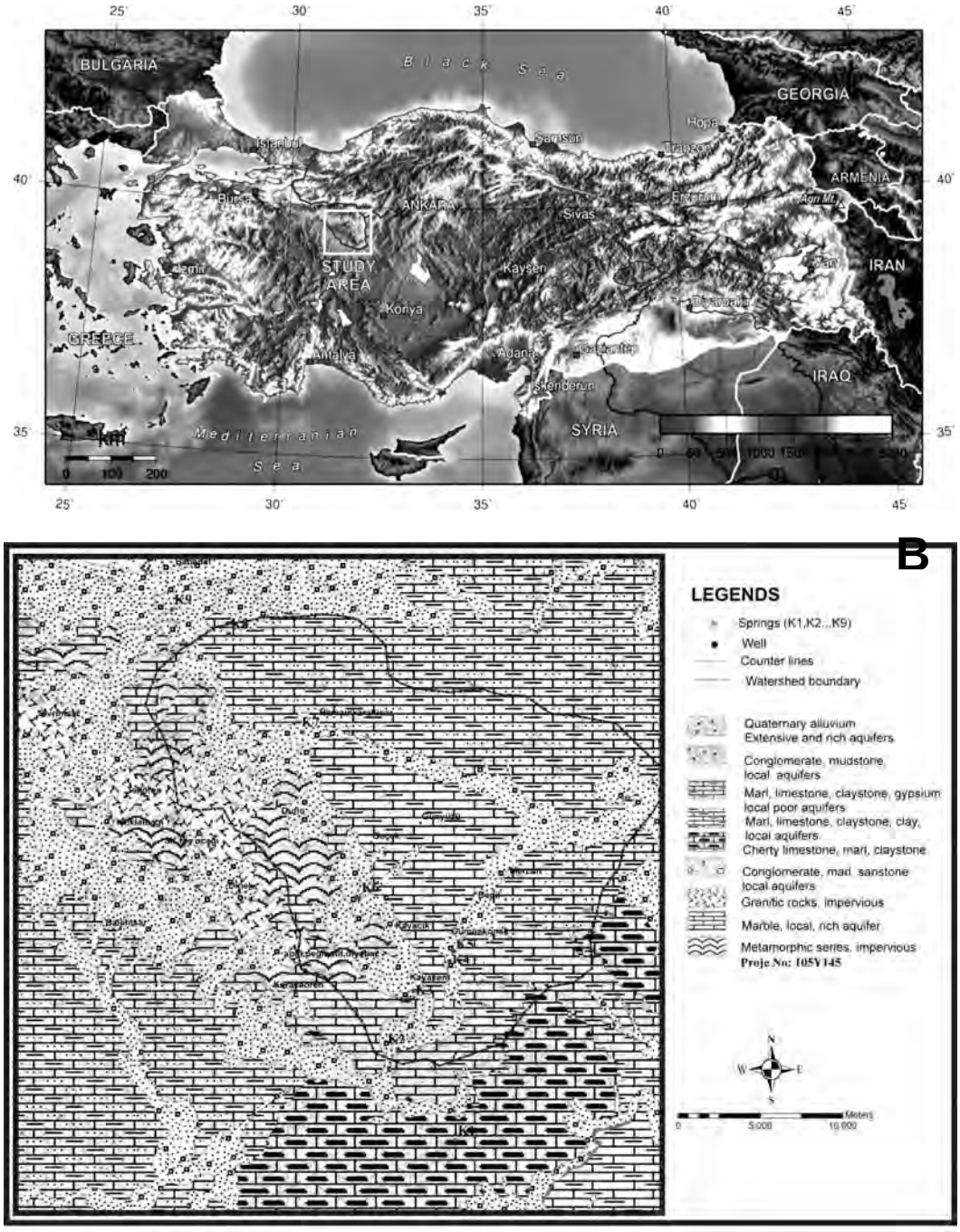

Figure 1: A) Location of the study area in Turkey B) Simplified hydrogeological map of the study area

GEOLOGICAL AND HYDROGEOLOGICAL OUTLINES

The study area comprises Paleozoic-Mesozoic metamorphic rocks, Eocene granite, Neogene sedimentary rocks and recent alluvium. The metamorphic basement begins with radiolarite, serpantinite, splitic basalt and diabases which are overlain by micaschist, quartzite, calcschist and marble, where the thickness of brown, beige, light gray marble is more than 100 meters and seen at the top of metamorphic series. This series is cut by granitic and volcanic rocks, where the main marble aquifer is bordered by these impermeable intrusions at sides and by impermeable schists at the bottom within the studied area. Neogene units cover all of the older units in the study area by disconformity. The youngest unit in the region is alluvium of Quaternary age

The geological units in the study area are classified hydrogeologically as permeable, local permeable and impermeable (Fig.1b).

Paleozoic marbles have been fragmented and faulted as evaluated as permeable units. They contain and conduct significant amount of groundwater. According to data obtained from pumping tests at wells drilled in the marbles, the hydraulic conductivity is 1,19 and 98.9 m/day and specific capacity is between 0.64 and 75 l/sec/m. Although these measurements do not represent the whole aquifer, however they provide an idea of the heterogeneity of the system. Most of the spring discharge from this aquifer. Marbles also play an important role on recharge of the basin, because the thickness of marbles are more than 100 meters and seen at the top of metamorphic series at higher altitudes of basin. Short and heavy rainfalls and snowmelts directly affect the recharge in this karstic area where reflections of these on spring discharge rates have been observed in the study area. Quaternary alluvium and Neogene conglomerates and limestones are secondary important aquifers. According to data obtained from the pumping experiments carried out at the wells drilled in the basin, the hydraulic conductivity of the Neogene limestones varies between 1.39 and 4.1 m/day and specific capacity varies between 1.8 and 2.9 l/sec/m. the hydraulic conductivity of the Neogene conglomerates is 0.39 and 1.75 m/day and specific capacity is between 0.5 and 3.4 l/sec/m. The impermeable units in the study area are ophiolite, schists of the metamorphic complex, which are the oldest units in the area. Eocene granites, Neogene marl, clays and diabases are other impermeable levels in basin.

SAMPLING AND ANALYSES

The hydrogeochemical studies were carried out under varying meteorological conditions to determine the hydrodynamics and chemical response of the system. Samples obtained from springs and wells within the researched area from 9 locations (K1,…K9), (fig 3.) chosen in order to represent the aquifer characteristics. Water samples were collected and

analyzed for physical and isotopic parameters in August, September 2005, representing dry period and March, April 2006, representing wet period.
The physical and chemical data used in this study were obtained using in situ measurements and laboratory analyses. Field measurements of pH, electrical conductivity (EC µS/cm), dissolved oxygen (DO-mg/lt), redox potential (Eh mV), total dissolved solids (TDS-g/l), salinity (ppt), acidity and alkalinity were measured at sampling sites. For the remaining analyses, major ions (Ca^{+2}, Mg^{+2}, Na^{+} K^{+}, HCO_3^{-}, CO_3^{-2}, Cl^{-}, SO_4^{-}), samples were collected and treated before being sent to the laboratory to prevent changes before analyses. Samples for cation analysis were acidified to pH<2 with 2 ml 65 % HNO_3. All analyses were performed in the Water Chemistry Laboratory of the International Research and Application Center for Karst Water Resources at Hacettepe University in Ankara. The results of the hydrochemical analyses for major constituents of thermal and cold water in meq/l have accuracy better than 5 %. Stable isotope compositions of the water are expressed using δ notation denoted as $‰_0$ relative to SMOW. The oxygen-18, deuterium contents of the sample were measured at the Nevada stable isotope laboratories in USA, tritium contents were measured in the Water Chemistry Laboratory of the International Research and Application Center for Karst Water Resources at the Hacettepe University in Ankara.

RESULTS

The water recharged into karst aquifers moves down–gradient through using highly anisotropic pathways. Karst aquifers are usually discussed in terms of triple porosity model or triple permeability model.
a) Matrix permeability: The intergranular permeability of the unfractured bedrock.
b) Fracture permeability: Mechanical joints, joint swarms and bedding plane partings, all of these possible enlarged by solution.
c) Conduit permeability: Pipe-like openings with apertures ranging from 1 cm to a few tens of meters where groundwater flows in conduits in a turbulent regime (White 2002).
High discharges rates (Qmax/Qmin) and rapidly changing chemical composition reveals turbulence flow conditions. Low discharges rates, and nearly constant chemical composition characterize fractured system, long residence time and diffuse infiltration (Aydın, 2005). The conduit type reveals significant temperature variations, whereas a spring with the diffuse type of flow reveals steady temperatures. Temperature is the best and most reliable tool to establish the depth of groundwater circulation (Mazor, 1991).
Springs in Günyüzü basin mostly displayed nearly constant temperature, low variation chemical composition and low variation of the measurements (coefficient of variation = S.D./mean) both dry and wet season (Table 1, 2)

Spring Nr.	Spring name	Q_{max} (lt/sec)	Q_{min} .(lt/sec)	Q_{max}/Q_{min}	CV_Q	CV_{ec}	CVca	Obsevation Date
K1	Yeniçıktı spring	108	49	2.2	36.4	10.3	8.04	1986-2006
K2	Musluk çeşmesi	0,5	0	∞				2004-2006
K5	Subaşı sprins (total)	181	112	1.61	50.6	11.,9	8.9	2000-2006
K6	Atlas spring	91	50	1.82	19.65	19.07	0.21	1998-2006
K7	Çardak hamamı	140	39	3.58	29.39	26.6	4.2	1991-2006
K8	Nasrettin hoca	219	152	1.44	13.48	3.96	6.63	1994-2006
K9	Babadat spring	100	68	1.47	22.6	4.95	6.01	1979-2006

Table 1 springs Qmax/Qmin and variation of the measurements

Spring Nr.	Spring name	August 2005 (T ^oC)	September 2005 (T ^oC)	March 2006 (T ^oC)	April 2006 (T ^oC)	May 2006 (T ^oC)
K1	Yeniçıktı spring	22.82			22.91	
K2	Musluk çeşmesi	24.88		5.35	10.39	12.31
K3	Çukurçeşme	13.95	14.09	13.44	13.36	13.56
K5	Subaşı springs	29.9	29.76	31.07	31.06	31.06
K6	Atlas spring	18.96	19.02	18.8	18.94	18.97
K7	Çardak hamamı	35	34.5	33.7	34.82	34.81
K8	Nasrettin hoca	22.7	22.8	22.07	22.25	22.21
K9	Babadat spring	20.5	20.5	20.46	20.46	20.46

Table 2. Springs temperatures (T ^oC)

Temperatures measured in wells and mines reveal a general increase with depth, or a geothermal gradient. The geothermal gradient varies from one location to another. Ex; the geothermal gradient was determined 9-10^{o}C/100 m. in Ontario (Canada) and Transvaal (South Africa) (Ketin, 1977). Average value is 3^{o}C /100 m. Groundwater is commonly temperature-equilibrated with the aquifer rocks. Thus, measured in spring or wells reflect the temperature attained at depth, and therefore provide information on the depth of circulation (Mazor, 1991).
The calculation is straightforward:
Depth (m) = (T measured- T surface)/ ΔT/100
T measured: The measured temperature of springs in the study area.
T surface: Local average annual surface temperature
ΔT : 3 ^{o}C /100 m. is applied.
The depth of groundwater circulation for sampling springs within the basin were calculated and given in Table 3.

Spring Num	Name	X (K) m.	Y (D) m.	Elv.(m.)	Depth (m.)	T (°C)
K1	Yeniçıktı spring	4341980	399353	887	382	22.8
K2	Musluk çeşmesi	4347658	395851	1068	12	13.2
K3	Çukurçeşme	4351171	396769	1011	88	14.0
K5	Subaşı springs	4353611	399217	961	622	30.0
K6	Atlas spring	4356938	393466	1055	255	19.0
K7	Çardak hamamı	4366839	390127	925	788	35.0
K8	Nasrettin hoca	4373481	385292	943	378	22.7
K9	Babadat spring	4374508	320558	917	305	20.5

Table 3. The depth of groundwater circulation for sampling points

The cation and anion permutation of the samples are mostly in rCa> rMg > rNa > rK and $rHCO_3$> rSO_4 > rCl form, respectively. These results indicate that most of these groundwaters are located within the marbles and limestones. Piper diagram provides a tool to classify waters into facies for cations and anions (Piper, 1944). The data of all water samples were plotted on Piper diagrams. Piper and Schoeller semilogaritmic diagrams are both used in order to specify the dominant lithology in the formation of chemical composition, and to classify water samples with respect to their chemical composition (figs 2 and 3).

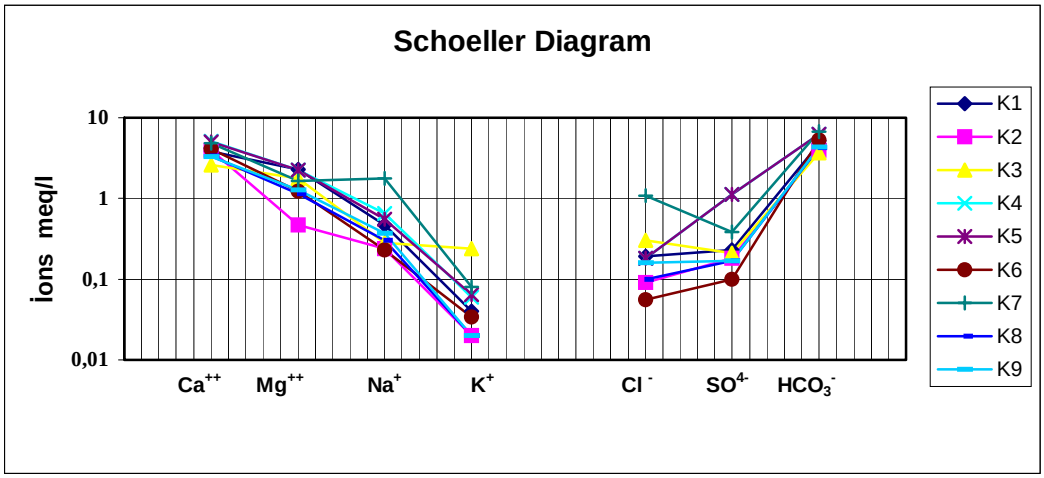

Figure 2: Schoeller diagram of the sampling points

Results indicate that they generally have Ca^{++}>Mg^{++}>Na^{+}>K^{+} and HCO_3^{-} >SO_4^{-2}>Cl^{-} anions and cations which show that carbonate rocks dominate in the formation. The chemical composition of water samples is in the harmony with the lithological properties of the researched area. Only Hamamkarahisar spring (K7) is characterized by located in has Ca^{++}>Na^{+}>Mg^{++}>K^{+} and HCO_3^{-}>Cl^{-}>SO_4^{-2}.

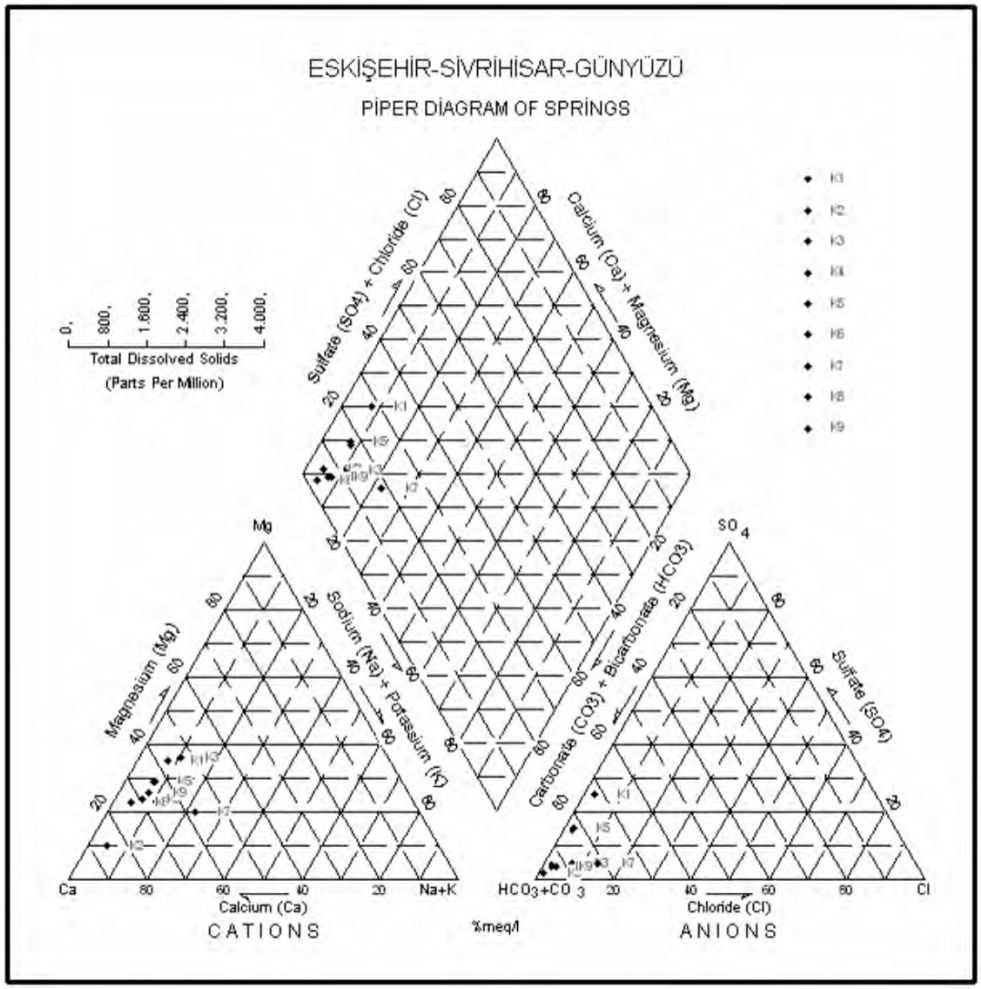

Figure 3: Piper diagram of the sampling points

By using the isotope data obtained from Ankara Meteorology station, which collaborates with the International Atomic Energy Agency (IAEA) observation network since 1963, the Ankara Meteoric Line was drawn. The equation for the line is $\delta^2H = 8.\delta^{18}O + 14.5$. All waters samples in study area except for Çukurçeşme spring are located in between the Ankara meteoric line ($\delta^2H = 8.\delta^{18}O + 14,5$) and Global meteoric line ($\delta^2H = 8.\delta^{18}O + 10$). This shows that all waters (thermal and cold) are of meteoric origin (fig.4).

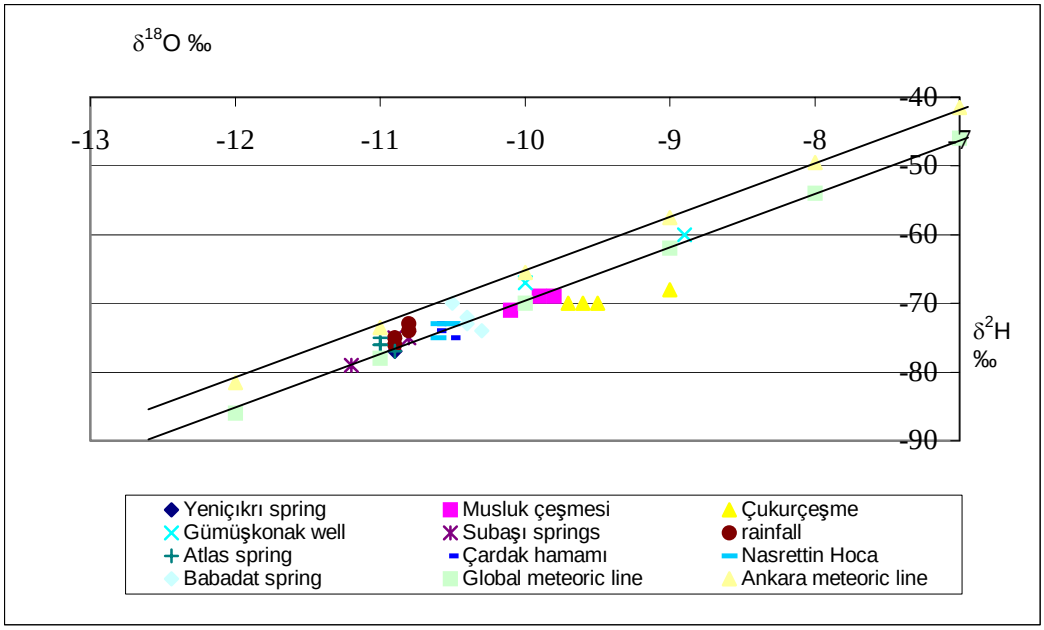

Figure 4: $\delta^{18}O$- $\delta^{2}H$ relationship of the waters from the study area

Isotope hydrology studies showed that elevation is the major parameter that determines the isotopic values of precipitation together with other parameters such as temperature, continental effect, amount effect etc The elevation effect in weighted mean precipitation is seen between ‰o-0,15 and ‰o –0,50/100 m. $\delta^{18}O$ (Clark & Fritz., 1997). $\delta^{18}O$ values in weighted mean precipitation (Günay, 2006) in Sakarya basin and $\delta^{18}O$ values in Muslukçeşmesi spring chosen to represent precipitation, from different altitudes revealed an average altitude of –0,32 ‰o / 100 m (fig. 5). The elevation- oxygen-18 relationship in Günyüzü basin is found to be –0,32 ‰o / 100 m.

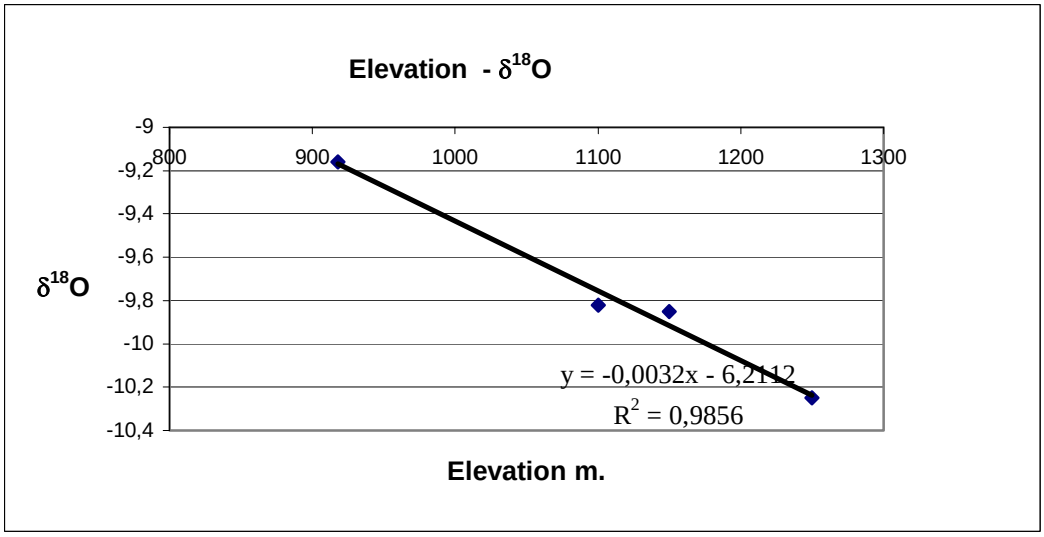

Figure 5: $\delta^{18}O$- Elevation relationship of the water samples from the study area

The recharge elevation of the springs was found by using $\delta^{18}O$-elevation relationship (Table 4).

Num.	Sample Name	$\delta^{18}O$	Discharge Elevation.(m)	Recharge Elevation. (m)
K1	Yeniçıkrı spring	-10.9	887	1465
K3	Çukurçeşme spring	-9.4	991	996
K4	55886/A well	-10.95	910	1480
K5	Subaşı spring	-10.85	951	1450
K6	Atlas spring	-11	1065	1497
K7	Çardak hamamı spring	-10.55	919	1356
K8	Nasrettin Hoca spring	-10.55	934	1356
K9	Babadat spring	-10.4	904	1309

Table 4. Averages recharge elevations of the water samples as defined by their oxygen- 18 isotope contents

The EC-Tritium relationship indicates the existence of groups with different origins. These groups that have high EC and low tritium values represent the deep circulating waters (K4, K5, K7), low EC and high tritium values represent the shallow circulating waters (K2, K3, K6, K8, K9) where these waters mix in various proportions

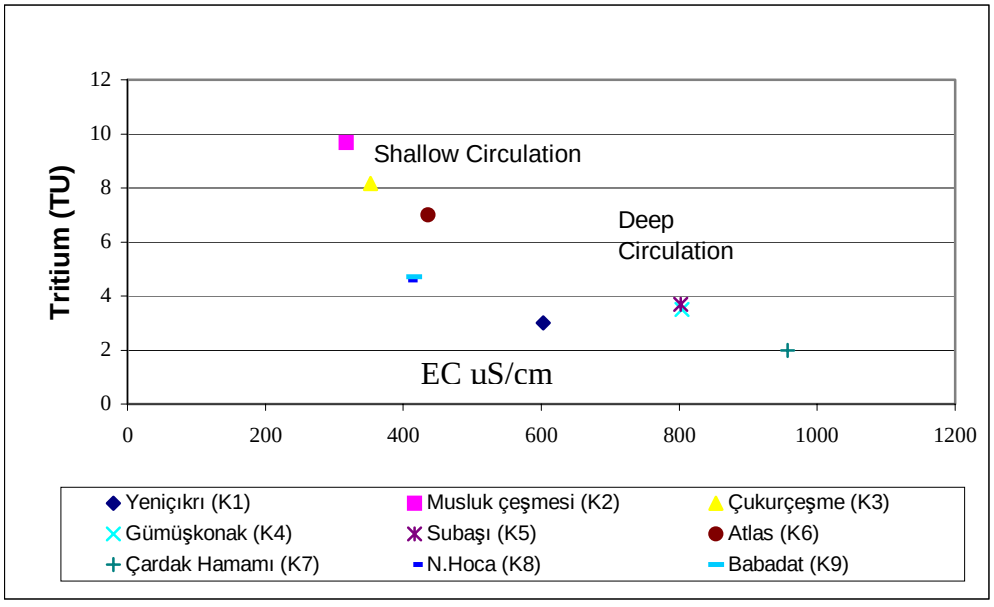

Fig 6: Tritium-EC relationship of the water samples from the study area

CONCLUSIONS

The hydrological, hydrochemical and isotope characteristics of waters showed the existence of two main groups of groundwater systems. The deep circulating of meteoric water (622m.-788m.) where fracture permeability and diffuse infiltration (laminar flow conditions) controls groundwater flow. But partly developed conduit permeability and point infiltration from nearly vertical bedding planes and joints of marbles reveals turbulent regime in this karstic area where reflections of these on discharge rates of Subaşı spring has been observed. The shallow circulation of meteoric water (12-378 m.) has with laminar flow conditions. Variations of chemical and isotopic composition of waters result from their mixing with cool groundwater in a shallow aquifer during their ascent to the surface or mixing with surface water during storm events.
Tritium values shows (0 - 4 TU) the existence of old static water in these aquifer systems. Carbonate rocks are dominating in the formation of chemical composition of water samples which is similar for the winter and summer periods.

REFERENCES

Aquilina, L., *et al.* 2005. Recharge processes in karstik systems investigated through the correlation of chemical and isotopic composition of rain and spring waters. Applied Geochemistry, vol. 20, issue 12, p. 2189-2206

White, W. B., 2002. Karst hydrology; recent developments and open questions. Engineering Geology, vol. 65 (2-3), pp. 85-105.

Mazor E., 1991. Applied chemical and isotopic groundwater hydrology, Open University Pres, Celtic Court 22, Ballmoor Buckingham

Aydın H., 2005. Investigation of morphology- hydrogeology relations in Harmanköy- Belyayla (Bilecik) karst system. Hacettepe University, PhD thesis.pp.,114-123, Ankara.

Ketin İ., 1977. General Geology, Istanbul Technical University Pres, Gümüşsuyu, İstanbul. vol 1, p. 520-525

Piper, A. M., 1944. A graphic procedure in the geochemical interpretation of water analyses. Trans. Amer. Geophys. Union, v. 25, p. 914-923.

Clark, D. & Fritz, P., 1997**.** Environmental Isotopes in Hydrogeology, USA

Günay G., 2006. Hydrology and hydrogeology of Sakaryabaşı karstic springs, Çifteler, Turkey, Environmental Geology, vol. 51, pp.229-232.

Historical trends in the chemical composition of river bed sediments of an Atlantic Basin

[1]Devesa, R., [1]Ruiz, M., [1]Ruiz, B., [1]Iglesias, L., [2]Jouanneau, J.-M., Díaz-[1]Fierros, F., [1]Barral, M.T.

[1]Dpto. de Edafología y Química Agrícola. Facultad de Farmacia, 15782. Universidad de Santiago de Compostela.
[2]DGO, UMR – 5805 EPOC Université Bordeaux Av. des Facultés, 33405. Talence, France.
Corresponding author: rosadrey@usc.es
Keywords: heavy metal, cores, Pb^{210}

ABSTRACT

During recent years, several studies have been dedicated to the geochemistry of metals in the Anllóns basin (NW Spain). In such studies, evidences of anthropogenic contamination were found. So, As levels higher than 260 $mg \cdot kg^{-1}$ were found in the superficial layers, as well as Cu (>60 $mg \cdot kg^{-1}$) and Zn (>280 $mg \cdot kg^{-1}$), exceeding highly the values expected for the crust. To investigate the historical trend of the total metal content, four cores were taken along the watercourse and the following elements were determined: Pb, Cr, Mn, Co, Cd, Cu, Ni, Fe, Al, Zn and As. The core 4, located at the mouth of the river, was submitted to dating by using Pb^{210}, as it is the end point of the basin and accumulates the whole erosive processes and, in consequence, may reflect the pollution phenomena of the basin. The concentration of most of the metals remained unchanged in time, except for Pb and As, which showed a decrease after the closing of the gold mine that was formerly operating in the area.

INTRODUCTION

The main problems regarding water contamination arouse approximately 200 years ago, with the Industrial Revolution and the fast growing of human settlements. Before that, the rivers were able to support the contaminant wastes due to their self-purification character. However, with the notable increase in population and the creation of higher human settlements, high amounts of wastes were released to the environment, which have severely polluted the rivers, lagoons and coasts.

In the aquatic environment, many pollutants, especially metals, are easily adsorbed on suspended particles. A fraction of these particles will be deposited and fixed onto bed sediments. In some circumstances, these adsorption processes can be positive, as the potentially dangerous materials can be inactivated in sediments. On the other side, the sedimentation of a pollutant can suppose long-term problems, as it can drastically alter the benthic population. Due to the low solubility of the metallic salts, they tend to bind to the organic matter and to different inorganic materials, and thereby they store in sediments (Establier, 1977). However, it has been verified that the metals do not stay permanently fixed to sediments and, in fact, the upper layers can release until 75% of some metals (Reimers et al., 1974).

In sediments, the metals can be present in different chemical forms, and they generally exhibit different physical and chemical behaviours in terms of chemical interaction, mobility, biologic availability and potential toxicity. In particular, the mobility and bioavailability of the heavy metals in sediments depends on the total content and the chemical forms of these metals (Kabata-Pendias & Pendias, 1984). With little differences between authors, it is considered that the trace elements can exist in sediments in several forms: soluble, exchangeable, bound to organic matter, occluded in Mn and/or Fe oxides, as mineral phases such as carbonates, phosphates, sulphurs,... or bound to silicates. Exchangeable metals are bound to low energy adsorption sites and, therefore, it should be the most bioavailable fraction. However, only 1% of the metals in sediments are in this form (Luoma and Bryan, 1981). Organic matter can be an important sink for metals. Luoma & Bryan (1981) found that the affinity of Cu, Pb and Zn for the humic fraction had a great importance in sediments with low levels of Fe oxides. The Fe and Mn oxides are considered as a sink for heavy metals (Jenne, 1977), and it is considered that this fraction can be responsible for the adsorption of the 10-15% of the total metal content. Carbonates appear in high concentrations in areas with marine influence. Results of Tessier et al. (1982) showed that concentrations of Cu, Pb, Zn and Fe in this fraction are relatively low, being of importance only for Mn. For this reason, carbonate would act as diluting agents, excepting for Mn (Luoma & Bryan, 1981). Finally, the metal concentration of metals in the residual fraction vary as a function of the lithology, the physical properties (grain size, density, transport, deposition,...), the mineral stability and the intensity of the weathering.

Once the elements are incorporated to sediments, they can be recycled by chemical or biological agents, returning to the water column (Ward, 1984). Sediments act, therefore, as important suppliers of nutrients and metals to the pore water, influencing the composition of the superficial waters by processes of diffusion, consolidation, erosion and bioturbation (Salomons et al., 1985). In this work, five cores of the Anllóns River were taken and submitted to a physico-chemical characterization in order to: i) examine the geochemical distribution with depth, ii) identify anomalous enrichments and iii) date the cores to evaluate the patterns of anthropogenic emissions to the environment in the last one hundred years.

MATERIALS AND METHODS

Site description and sampling

The Anllóns River is located in the NW of Spain. The basin drains a rural catchment of 516 km^2 with a history of agricultural, forestry and cattle raising activities (Fig.1). Two main human settlements are located in the basin: Carballo, with a population of over 25000 and a sea food canning industry, and Ponteceso, with a population of about 7000. The climate is wet (1200 mm on average), with a mean temperature of 9ºC in winter, and a mean summer temperature of 20ºC. The river runs over schists in the upper area, turning into a smooth profile in the middle area of the river, characterized by basic rocks (gabbros and amphibolites). Finally, the

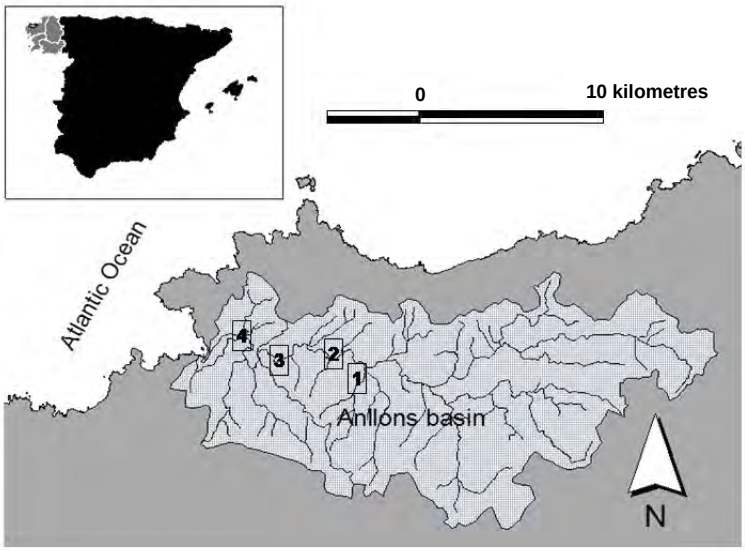

Fig. 1. Location of the Anllóns basin and location of the 4 sampling sites.

lower stretch of the river runs over granite of two micas, followed by biotitic gneiss at the mouth. The land use of the area is a mixed forest of *Eucalyptus globulus*, *Eucalyptus alba* and *Pinus pinaster* (60% of the total cover), cultivated lands (18%), pastures (12%), scrublands (9%) and urban uses (1%).

To investigate the sedimentological processes, colour aerial photographs taken in 1956 and 1995 were compared, as a guide to select the sampling points. The lengthwise profile of the river showed three low slope areas, which are favourable for the sediment deposition (Fig. 2). In these depositional areas, 4 sites were selected, between the locality of Carballo and the river mouth, covering a distance of approximately 30 km (Table 1). The sampling areas were completely shaded by trees, except at point 5, which were located at the river mouth. The riparian vegetation is characterized by *Alnus glutinosa* and *Fraxinus excelsior* (*Alnon-padion*, *Alnon incanae* and *Salicion albae* associations). Each deposition site was

sampled at two points, except the site 4 where only one core was taken. The sediment samples were collected with a Livingstone probe and taken to the laboratory in hermetic cylindrical plastic containers (prewashed and rinsed with deionised water MilliQ). Once in the laboratory they were split in 2cm sections, described, freeze-dried and sieved by 2 mm.

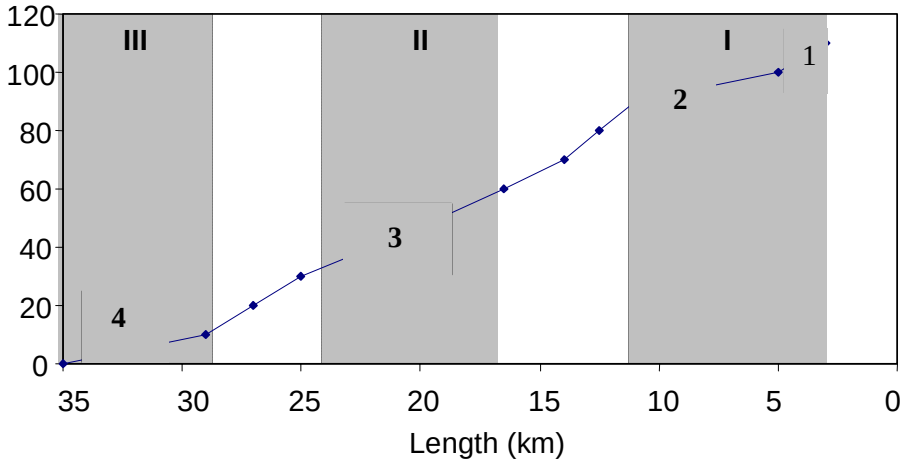

Fig. 2 Lengthwise profile of the Anllóns River which shows the three low slope areas (I, II and III) and the sampling points.

Methods

The methodology followed in this work was:

- Grain size distribution was determined by sieveng. According to this, particles were classified as coarse fraction (>50 µm) and fine fraction (<50 µm).
- The C, N and S concentration were determined in an element analyzer (LECO-SC32), based on an infrared detection after combustion of the samples at 1100ºC.
- The metal concentration was determined by microwave digestion with a mixture of acids (HNO_3, HCl and HF). In the extracts Cu, Fe, Zn, Mn, Ni, Pb, Cr, Co, Cd were determined by atomic absorption spectrometry (Varian Spectra 220-FS). As was determined by the hydride generation technique (Perkin Elmer M2100 eqquiped with a MSH-10 hydride generation unit).
- Sedimentation rate of the sediments was realized by using the activity of the ^{210}Pb. The activity of the ^{210}Pb in excess is a function of the age of the sediment.
- In order to examine the degree of contamination, an Enrichment Factor (EF) was calculated by using the following equation proposed by Hakanson (1980):

$$EF = (M / M_{reference})_{sample} / (M / M_{reference})_{crust}$$

Where $(M/M_{reference})_{sample}$ is the analyzed metal to reference metal ratio in the sample and $(M/M_{reference})_{crust}$ is the analyzed metal to reference metal ratio in the crust. The element concentrations in the crust were taken from Wedepohl (1995).

RESULTS AND DISCUSSION

Morphological description

Cores taken at sampling points 2 and 3 have two well differenced portions: the upper portion with black-greyish colour, containing vegetal debris and a sandy texture; the lower portion has a poor structure, is less compacted, with coarser texture (gravel) and brown-greyish colour. The cores taken at sampling point 1 show similar patterns than the 2 and 3, but with higher concentrations in organic matter in different states of decomposition in the upper layers, causing a blackish colour with a strong putrefaction odour, whereas, the deeper layers have a sandy texture and brown-redish colours. The core 1.1 has a coarser texture in the upper layers than the core 1.2. The core taken at sampling point 4 is the deepest and its morphological description differs from the rest. It is highly compacted from the surface to the deeper layers, although the grain size decreases with depth. The upper layers have blackish shades because of the high content of organic matter. The blackish shade turns into brownish-red shades with depth and, finally, it converts into green-greyish shades, attributed to the presence of sulphurs.

Physico-chemical characterization

The grain size distribution showed a clear predominance of the sandy fraction in the cores taken from points 1 to 3 (Table 2). The cores 1.1 and 1.2 differ in their grain size distribution. So the core 1.1 shows coarser particles in the upper layers (up to 35%), whereas the core 1.2 shows a percentage of fine fractions always lower than 6%. The cores 2.1 and 2.2 showed low values of fine fraction, ranging between 6 and– 27%.

The cores 3.1 and 3.2 had a predominance of the fine fraction [1 – 11%], with highest percentage of the coarse fraction in the upper layers. The core 4, located in the mouth of the river, showed the finest feature, with an average value of the <50 µm fraction of 30% [7 – 59%].

Cores	*>50 µm (%)*	*<50 µm (%)*	*C (%)*	*N (%)*	*C/N*	S (%)
1.1a	74	26	5.62	0.44	13	0.10
1.1b	88	12	3.75	0.23	16	-0.04
1.1c	65	35	9.29	0.53	18	0.21
1.1d	85	15	2.28	0.20	12	0.03
1.1e	97	3	0.34	0.05	7	0.03
1.1f	98	2	0.32	0.04	7	0.01
1.1g	55	45	2.98	0.28	11	0.06
1.1h	97	3	3.82	0.29	13	0.12
1.2a	94	6	1.11	0.12	9	0.00

Cores	>50 µm (%)	<50 µm (%)	C (%)	N (%)	C/N	S (%)
1.2b	97	3	0.57	0.09	6	0.03
1.2c	97	3	0.53	0.08	6	0.03
1.2d	99	1	0.31	0.04	7	0.03
1.2e	99	1	0.32	0.06	5	0.03
1.2f	99	1	0.17	0.03	7	0.00
1.2g	95	5	0.71	0.09	8	0.03
2.1a	94	6	0.58	0.07	8	0.04
2.1b	92	8	0.64	0.08	8	0.01
2.1c	85	15	0.93	0.10	9	0.02
2.1d	75	25	1.20	0.13	10	0.04
2.1e	82	18	0.96	0.10	10	0.02
2.1f	85	15	0.72	0.09	8	0.02
2.1g	77	23	0.91	0.11	8	0.02
2.1h	73	27	1.07	0.12	9	0.02
2.1i	93	7	0.64	0.09	7	0.04
2.2a	94	6	0.92	0.10	10	0.02
2.2b	89	11	0.79	0.08	10	0.01
2.2c	91	9	0.63	0.08	8	0.01
2.2d	92	8	0.99	0.11	9	0.02
2.2e	83	17	0.83	0.10	9	0.02
2.2f	76	24	1.73	0.17	10	0.03
2.2g	84	16	0.90	0.11	8	0.01
2.2h	78	22	0.90	0.10	9	0.02
2.2i	91	9	0.63	0.07	9	0.01
3.1a	90	10	12.76	0.69	19	0.19
3.1b	95	5	9.81	0.57	17	0.12
3.1c	94	6	17.37	0.96	18	0.22
3.1d	98	2	0.92	0.07	13	0.03
3.1e	99	1	0.34	0.06	6	0.01
3.1f	98	2	0.25	0.03	8	0.01
3.1g	99	1	0.26	0.02	11	0.01
3.1h	98	2	0.32	0.03	10	0.02
3.2a	89	11	5.73	0.37	16	0.08
3.2b	94	6	8.29	0.50	17	0.10
3.2c	93	7	9.86	0.61	16	0.15
3.2d	91	9	4.22	0.30	14	0.05
3.2e	99	1	0.48	0.06	8	0.01
3.2f	99	1	0.26	0.02	11	0.00
3.2g	99	1	0.24	0.03	8	0.00
3.2h	99	1	0.55	0.05	10	0.01
3.2i	98	2	0.31	0.03	12	0.00
4.1a	89	11	1.25	0.13	9	0.13
4.1b	89	11	1.59	0.16	10	0.33
4.1c	79	21	2.30	0.21	11	0.61
4.1d	81	19	2.21	0.19	12	0.41

Cores	*>50 µm (%)*	*<50 µm (%)*	*C (%)*	*N (%)*	*C/N*	S (%)
4.1e	87	13	1.40	0.13	11	0.52
4.1f	83	17	1.89	0.16	12	0.17
4.1g	42	58	4.89	0.48	10	0.54
4.1h	92	8	0.63	0.07	9	0.17
4.1i	93	7	-	-		-
4.1j	83	17	1.66	0.15	11	0.64
4.1k	71	29	3.77	0.37	10	1.76
4.1l	42	58	5.15	0.47	11	2.24
4.1m	41	59	4.77	0.46	10	1.48
4.1n	47	53	4.46	0.46	10	1.30
4.1ñ	57	43	3.74	0.35	11	1.23
4.1o	46	54	3.91	0.35	11	1.29

Table 1. Grain size distribution, C, N, C/N ratio and S percentages

The C, N and S concentrations are shown in Table 2. The cores 1.1 and 1.2 show different patterns. The values observed for C and N are higher in the core 1.1 than in the core 1.2. This can be related with the highest content in the fine fraction of the core 1.1. The cores 2.1 and 2.2 show similar values for the entire profile for C, N and S. The values are, in general, very low as well as the C/N ratio, with an average value of 9, indicative of the high evolution of the organic matter. The cores 3.1 and 3.2 show low values of C, N and S. Regarding to the %C, there are a clear difference among the 8 upper cm, with high values, and the deeper layers, whose %C content do not reach the 1%. In the upper layers high values of the C/N ratio, as well as high values of %S, can also be observed. S can be related with the presence of sulphurs coming from the mineralization of the arsenopirite of the area. The core 4 shows also low values of C, N and S. In this case, %C increases with depth, particularly from 20 cm. The %N varies in parallel with %C, so the C/N ratio does not show significant variations along the core, showing an average value of 11. %S follows the same pattern than C and N, with the highest values in the deeper layers.

The C/N ratio is used to describe the organic matter status. The wide range of C/N ratio indicates the extent to which OM has been degraded (Müller, 1977). Also, the C/N ratio can also be used to distinguish sources of organic matter in river sediments: a C/N ratio between 4 and 10 suggests OM without cellulosic structure, coming from algae and phytoplankton, whereas a C/N ratio ≥20 suggests OM with cellulosic structure, coming from terrestrial plants. In this study, the cores have low values of the C/N ratio, suggesting that there are no significant allocthonous contributions to the OM. In several studies (Mead et al., 2004; Ishiwatari et al., 2005) it was found that the allochthonous/terrestrial component seems to have a low contribution to the total OM content in aquatic systems, whereas the authocthonous component (aquatic macrophytes and macroalgae) has a major contribution.

Cores	Fe	Al	Pb	Cr	Mn	Co	Cd	Cu	Ni	Zn	As
1.1a	0.2	204	247	90.0	898	57.3	15.3	52.4	72.2	170	16.11
1.1b	32.9	191	277	48.5	483	29.2	0.0	16.3	36.1	115	12.23
1.1c	61.2	191	140	27.0	525	53.0	8.0	38.0	50.5	56	21.1
1.1d	49.1	224	214	61.1	990	32.4	10.5	183.4	68.9	157	15.6
1.1e	36.8	208	306	49.5	843	73.3	0.5	14.1	25.2	45	12.62
1.1f	51.7	172	195	75.3	568	43.4	15.0	21.9	44.9	110	1.94
1.1g	170.4	119	267	74.7	564	43.0	14.8	21.8	44.5	109	16.77
1.1h	84.1	149	205	92.0	524	55.3	15.7	106.3	55.8	93	17.55
1.2a	38.8	101	211	47.2	856	5.9	6.4	48.2	48.7	141	15.2
1.2b	62.3	119	235	67.5	560	26.6	0.0	46.8	48.8	166	10.4
1.2c	56.6	124	53	92.7	519	46.8	13.9	42.1	56.9	122	1.5
1.2d	40.1	109	214	69.1	765	19.4	0.0	98.4	51.7	124	11.6
1.2e	32.0	231	184	36.3	524	18.4	9.0	89.3	58.3	79	11.3
1.2f	33.5	185	184	58.5	482	39.6	12.6	70.0	32.4	150	7.1
1.2g	38.5	169	307	55.0	825	76.8	6.9	21.3	48.6	61	12.6
2.1a	224	123	170	124.3	1011	49.9	13.5	196.7	52.9	123	10.58
2.1b	145	23	117	154.5	603	27.7	4.4	16.5	25.8	23	10.93
2.1c	105	136	216	107.1	803	25.1	0.0	23.6	58.5	136	9.78
2.1d	249	42	298	88.8	980	39.8	5.3	26.4	57.1	42	14.5
2.1e	110	92	274	68.3	974	20.2	12.5	31.8	52.5	92	9.43
2.1f	140	125	224	106.0	1028	98.5	6.5	66.7	64.2	125	11.04
2.1g	150	103	204	116.1	1076	25.0	0.0	20.4	69.4	103	14.62
2.1h	203	86	274	106.6	1162	81.2	0.0	5.8	70.1	86	20.08
2.1i	163	76	307	150.7	1175	56.1	13.2	25.9	69.8	76	16.98
2.2a	36.5	43.6	187	67.3	936	23.4	2.8	31.8	52.4	85.6	8.88
2.2b	46.0	137.2	147	107.4	760	40.7	10.3	5.9	57.8	89.2	10.25
2.2c	46.6	142.2	139	96.1	728	43.1	8.4	4.5	52.0	76.8	10.8
2.2d	97.2	260.1	191	89.2	769	26.4	16.4	49.1	81.9	36.9	9.78
2.2e	90.9	234.2	199	89.0	1042	27.7	13.6	29.7	74.4	67.6	11.81
2.2f	48.4	240.3	207	123.5	1047	34.6	14.9	34.6	60.1	86.0	13.84
2.2g	38.3	192.5	243	110.2	951	20.9	0.0	38.4	55.9	87.9	11.95
2.2h	52.4	224.2	282	103.2	977	50.6	0.0	18.6	65.9	70.2	15.09
2.2i	54.8	135.7	199	155.3	1095	54.8	8.7	84.9	44.6	76.2	28.72
3.1a	40.1	82.4	199	83	755	26.3	3.0	28.8	55.1	135	201.54
3.1b	35.6	169.0	226	130	697	37.1	0.5	103.8	166.1	86	90.9
3.1c	31.1	145.0	194	131	711	58.5	22.8	211.8	64.0	217	57.34
3.1d	78.5	248.5	226	145	990	16.4	13.0	34.6	67.4	69	235.18
3.1e	68.0	118.7	196	122	829	12.3	0.0	254.5	57.4	184	54.83
3.1f	98.9	117.7	178	155	942	66.1	2.7	36.9	67.5	140	58.25
3.1g	51.0	79.8	188	106	722	12.4	0.0	34.7	53.0	82	74.88
3.1h	80.0	233.2	312	123	1077	125.4	1.5	54.0	60.0	59	74.88
3.2a	60.0	252	204	102	692	35.9	16.5	43.2	84.9	154	157
3.2b	85.1	183	153	76	729	43.4	8.4	52.8	64.6	67	78
3.2c	40.2	181	166	146	726	22.9	15.6	80.1	74.2	174	100

Cores	*Fe*	*Al*	*Pb*	*Cr*	*Mn*	*Co*	*Cd*	*Cu*	*Ni*	*Zn*	As
3.2d	57.2	176	219	132	869	45.2	12.2	85.6	64.7	193	48
3.2e	105.3	239	237	128	823	25.7	12.1	78.0	72.2	138	70
3.2f	72.1	193	195	144	734	30.0	13.5	13.0	57.5	44	92
3.2g	93.6	70	220	137	699	25.4	5.0	28.9	50.9	117	61
3.2h	62.6	168	202	123	747	50.2	0.0	20.7	62.0	72	75
3.2i	66.1	109	208	94	733	25.6	4.4	22.7	43.5	179	68
4.1a	47.1	92	278	89.7	463	43.9	11.7	38.0	45.8	48	31
4.1b	23.4	121	239	71.3	379	17.6	0.0	31.7	48.8	97	35
4.1c	37.6	464	235	75.9	315	40.4	11.5	22.5	52.4	29	42
4.1d	23.4	75	214	57.4	339	19.0	0.0	12.2	44.8	129	35
4.1e	22.7	194	245	49.4	306	44.4	12.0	63.4	44.4	99	29
4.1f	19.1	131	215	55.6	380	12.7	0.0	23.4	42.5	118	34
4.1g	37.9	264	277	84.7	405	14.4	0.0	119.4	74.3	130	55
4.1h	38.1	175	277	62.3	506	28.7	5.4	10.9	45.0	96	43
4.1i	25.6	49	138	111.0	593	65.5	8.8	34.5	46.2	110	53
4.1j	24.9	105	231	47.7	422	22.6	0.0	37.4	44.3	94	140
4.1k	37.8	253	252	44.8	361	29.0	16.2	89.5	75.2	85	220
4.1l	67.5	212	240	94.0	390	526.0	12.0	16.5	69.5	113	198
4.1m	83.2	78	244	55.1	426	11.7	5.4	67.3	67.8	149	146
4.1n	48.2	166	228	96.7	350	49.6	6.4	21.3	69.9	89	159
4.1ñ	34.3	223	320	47.8	393	87.1	3.4	63.5	54.7	53	219
4.1o	90.0	56	194	54.8	388	28.4	0.0	45.3	57.8	107	235

Table 2. Element units are given in mg·kg^{-1}. Fe and Al are given in g·kg^{-1}

The concentration of the metals (including As) is shown in Table 3. The degree of contamination was estimated by calculating the EF. Aluminium was chosen as the reference element as it is the second most abundant metal in the earth´s crust, the proportions of metal to aluminium are relatively constant in the crust and the Al concentrations are not likely to be significantly affected by anthropogenic aluminium sources (Schropp et al., 1990). According to Szefer et al. (1999), EF values around 1.0 suggest that the element comes from geogenic sources, whereas EF much higher than 1.0 suggest anthropogenic sources. According to the results, no significant enrichments can be observed for most of the elements with depth. However, three elements must be remarked. On the one side, Pb shows significant EF at core 1, attributed to the nearest of the town of Carballo. On the other side, the EF for As can be attributed to the mineralizations of arsenopirite in the area, which accumulate in sediments, favoured by the past extractive activities of a gold mine located upstream of the core 3.

Another question altogether is the case of Mn, which showed high EF from points 1 to 3. This is attributed to the lithology, developed over basic rocks, which contributes with significant Mn concentrations to the bed sediments.

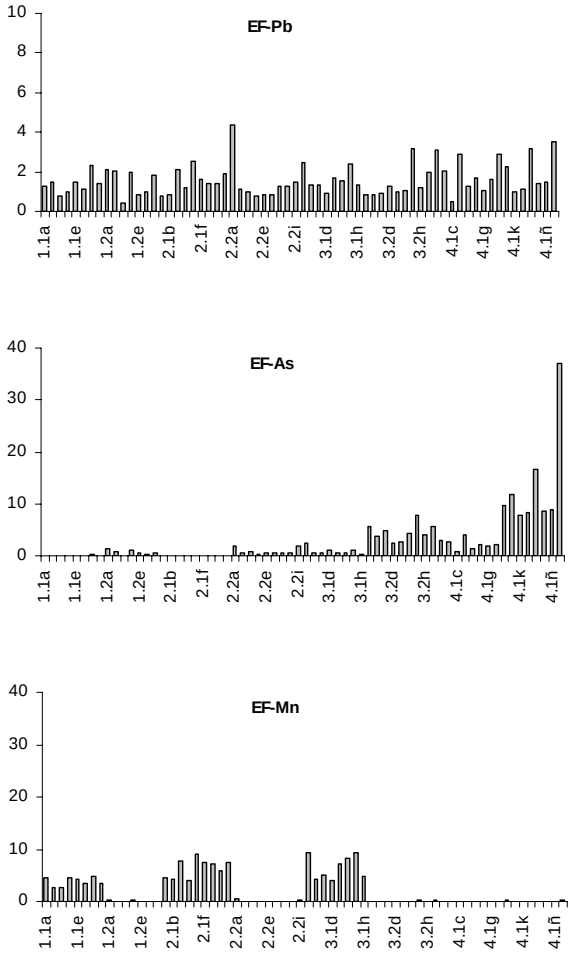

Fig. 3EF calculated for Pb, As and Mn

The sedimentation rate of the core 4 was realized by using ^{210}Pb (Table 4). Although a high uncertainty can be observed in the superficial layers, it is observed clearly a decrease in the ^{210}Pb values with depth. The level corresponding to 30-32 cm does not show excess of ^{210}Pb, therefore this level corresponds to an age older than 100 years. As an approximation, a mass accumulation rate of 30 cm/100 years can be stated at this point.

Depth (cm)	^{210}Pb excess (Bq·kg^{-1})
0 – 2	95 ± 38
2 – 4	48 ± 28
12 – 14	27 ± 14
22 – 24	23 ± 15
30 – 32	9 ± 11

Table 3. ^{210}Pb levels in core 4

So, the highest levels of As, obtained for the level 30-32 cm, correspond to an age older than 100 years. In fact, the gold mine, which had been formerly exploited during the Roman Empire, was again exploited from 1895 to 1910, with intermittent extractions after this period. As a consequence, bed river sediments show an enrichment in As, which has decrease downstream the mineralized area since the decline in the activities of the gold mine.

CONCLUSIONS

In this work, four cores of the Anllóns River were submitted to a physico-chemical characterization and the following results were obtained:

- C/N ratios minor than 15 were obtained in all cases, thus suggesting that there are no significant terrestrial sources of OM in sediments.
- No significant enrichments were observed for Fe, Cr, Mn, Co, Cd, Ni and Zn. Pb showed a little enrichment in sediments in the core located downstream of Carballo, whereas As showed higher EF (up to 36), related to the mineralizations of arsenopirite of the area, which accumulates in sediments through the extractive activities of a gold mine. Mn also showed significant EF, attributed to the lithology.
- According to the results obtained with ^{210}Pb, the As accumulation in sediments has decreased since the closing of the mining activities. To this respect, the licence to exploit the gold mine was renewed in 2003 and after the preliminary studies, new extractive activities are beginning in a little while. So, special careful must be taken with the dragging activities to avoid sediment contamination.

ACKNOWLEDGMENTS

The present study was financed by the Science and Education Ministry of Spain (MEC, REN 2003-08673/BES-2004-5894). Rosa Devesa was granted with a FPI grant.

REFERENCES

Establier, R., 1977. Estudio de la contaminación marina por metales pesados y sus efectos biológicos. Instituto de Investigaciones Pesqueras (Ed.) Barcelona, 36 pp.

Hakanson, L., 1980. An ecological risk index for aquatic pollution control. A sedimentological approach. Water Research, 14(8), 975-1001.

Ishiwatari, R. *et al*. 2005. Lipid and lignin/cutis compounds in Lake Baikal sediments over the last 37 kyr: implications for glacial-interglacial palaeoenvironmental change. Organic Geochemistry 36(3), 327-347.
Jenne, E.A., 1977. Chemical modelling in aqueous systems: speciation, sorption, solubility and kinetics. In: ACS Symposium series. American Chemical Society (Eds.) Washington, 914 pp.

Kabata-Pendias, A. & Pendias, H., 1984. Trace elements in soils and plants. CRC Press. Boca Raton, Florida, 315 pp.

Luoma, S.N. & Bryan, G.W., 1981. A statistical assessment of the form of trace metals in oxidized estuarine sediments employing chemical extractants. Science of the total environment 17(2), 165-196.

Mead, R. *et al*. 2005. Sediment and soil organic matter source assessment as revealed by the molecular distribution and carbon isotopic composition of n-alkanes. Organic Geochemistry 36(3), 363-370.

Müller, P.J., 1977. C/N ratios in Pacific deep sea sediment: Effect of inorganic ammonium and organic nitrogen compound sorbed by clays. Geochimica et Cosmochimica Acta 41(6), 765-776.

Murphy, J. & Riley, J.P., 1962. A modified single solution method for the determination of phosphate in natural waters. Analytica Chimica Acta 27, 31-36.

Salomons, W. & Förstner, U., 1984. Metals in the hydrocycle. Springer-Verlag (Ed.) Berlín, 349 pp.

Schropp, S.J. *et al*. 1990. Interpretation of metal concentrations in estuarine sediments of Florida using aluminium as reference element. Estuaries 13(3), 227-235.
Szefer, P. *et al*. 1999. Distribution of selected heavy metals and rare earth elements in surficial sediments from the polish sector of the Vistula Lagoon. Chemosphere, 39 (15), 2785-2798.

Tessier, A. *et al*. 1982. Particulate trace metal speciation in stream sediments and relationships with grain size: implications for geochemical exploration (Quebec, Canada). Journal of geochemical exploration 16(2), 77-104.

Ward, G.S., 1983. Manual de métodos de investigación del medioambiente acuático. Parte 6, ensayos de toxicidad. FAO documentos técnicos de pesca (Ed.) Roma, 25 pp.

Wedepohl, K., 1995. The composition of the continental crust. Geochim. Cosmochim. Ac., 59 (7), 1217-1232.

Gold uptake in Australian plants - a preliminary experimental study

[1] Lintern, M.J., [2]Verall, M.R. and [3]Belton, D.X.

[1]CRC LEME, CSIRO Division of Exploration and Mining, Kensington 6151, Australia. (email Mel.lintern@csiro.au)
[2]CSIRO Division of Exploration and Mining, Kensington, WA 6151, Australia.
[3]CSIRO, School of Geosciences, Monash University, Clayton, VIC 3168, Australia.
Keywords: biogeochemistry, Acacia, Eucalyptus, vegetation.

INTRODUCTION

Phytogeochemical methods have been used to explore for mineralisation in the United States, Canada and Russia, but less extensively elsewhere. In Australia, only a few published examples of phytogeochemistry have been reported for regional scale exploration surveys (e.g., Rattigan et al., 1977; Marshall and Lintern, 1995; Cohen et al., 1999), partly because sampling of other surficial media (e.g. soil, calcrete and lateritic residuum) has been very successful (Butt et al., 2000). However, as Australian exploration companies broaden their search outside areas of outcrop and shallow transported cover to areas of deeper cover, these sample media are becoming less sucessful. Phytogeochemistry will gain importance if it can be demonstrated that roots of widespread Australian plant species can penetrate deep cover, adsorb and translocate metals and reflect buried mineralisation in their accessible aerial parts.
One of the reasons for the success of Biogeochemistry in the Northern Hemisphere is the presence of vast boreal forests consisting of monocultures or of a few species (Dunn, 1995). Australia, on the other hand, has an extremely diverse flora dominated, in the arid interior, by spinifex, acacia and eucalypts. With many species occurring in a variety of regolith settings across Australia it can be difficult to find a consistent plant sample medium. How should we compare the geochemical contents of different plants? Plant growth under controlled conditions provides an opportunity to make comparisons between inherent metal uptake rates of different plants (Schaefer et al., 2005). Metal uptake estimates may be used to investigate adsorption rates, different metal interactions, salinity and variable nutrient effects, micro-organism effects, and metal speciation differences. A preliminary experiment was designed to look at similarities and differences in metal uptake between two species of Australian plants that appear to adsorb Au in the natural environment.

METHODS

Approximately twenty replicates of two species of plant (*Eucalyptus incrassata* and *Acacia aneura*) were grown in individual plant pots containing potting mix and slow release fertiliser over three months.

Specific volumes of waters containing different concentrations of soluble Au (0, 10, 100 and 1000 µg/L) were applied to the pots on a daily or twice daily basis. A control set of twenty replicates that was not exposed to Au was also established at the same time. All plants flourished equally and were exposed to identical natural variations in temperature, rainfall and naturally-occurring bacteria growing in the soil medium during the period of the experiment. For the last two weeks of growth, Au was not added to the plants with the exception of two plants of each species where additional, high concentrations of Au (1000 mg/L) were applied.

RESULTS

After twelve weeks, the plants were dissected into individual plant organs (roots, branches, leaves and phyllodes). After drying, samples were analysed for Au by ICP-MS following an aqua regia digest. Gold concentration in each plant organ and Au concentration in the applied treatment solution showed a linear trend over several orders of magnitude. The differences between plant organs and between the two species have sampling implications for mineral exploration e.g. acacia foliage had at least twice as much contained Au as eucalyptus foliage.
Addition of supplementary Au (1000 mg/L) to two of the plants from each species resulted in rapid health decline followed by death. This concentration is unlikely to be encountered in the natural environment. These plant parts were examined by SEM and PIXE (proton induced X-ray emission) for Au and other elements, and the images showed the specific location (e.g. xylem tissue) and the particulate form of metals within the plant. Several hundred ppm (mg/kg, dry weight) of Au was found when a separate portion of the plant parts were digested in acid and analysed by ICP MS.

FUTURE WORK

More hydroponic investigations have commenced as part of AMIRA Project P778. A variety of experiments involving plant metal uptake have commenced using a hydroponic environment. The results of these experiments will be crucial to investigate controls on metal uptake and to further improve confidence in the use of phytogeochemical exploration in Australia.

ACKNOWLEDGEMENTS

CRC LEME and CSIRO EM are thanked for their financial support during this project. R.R.P. Noble, I.D.M. Robertson and R.R. Anand are thanked for earlier comments on this manuscript.

REFERENCES

Butt, C.R.M., Lintern, M.J. & Anand, R.R., 2000. Evolution of regoliths and landscapes in deeply weathered terrain - implications for geochemical exploration. Ore Geology Reviews **16**, 167-183.

Cohen, D.R., Silva-Santisteban, C.M., Rutherford, N.F., Garnett, D.L. & Waldron, H.M., 1999. Comparison of Vegetation and Stream Sediment Geochemical Patterns in Northeastern New South Wales. Journal of Geochemical Exploration, **69,** 469-489.

Dunn, C.E., 1995. Biogeochemical prospecting for metals. In: R.R. Brooks, C.E. Dunn and G.E.M. Hall, (editors), *Biological systems in Mineral Exploration and Processing*. Ellis Horwood Limited: Hemel Hempstead, England. p 371-425

Marshall, A.E. & Lintern, M.J., 1995. Biogeochemical investigations in the Murchison and Telfer Regions of arid Western Australia. In Applied Biogeochemistry in Mineral Exploration and Environmental Studies. Notes to accompany course held on 13–14th May, 1995, in conjunction with the 17th IGES, Townsville, Australia, 1995. **Workshop Volume**, 29 pp.

Rattigan, J.H., Gersteling, R.W., & Tonkin, D.G., 1977. Exploration geochemistry of the Stuart Shelf, South Australia. *Journal of Geochemical Exploration*, **8,** 203-217.

Schaefer, R.M., Stanley, C.R., Evans, R.C. & Bell, C.R., 2005. Gold and arsenic uptake and sequestration by *Eucalyptus salmonophloia*: Two possible phytotransportation mechanisms of metals to the surface. 22nd IGES Perth, Australia. Abstracts Volume, p 159-160.

Chemical, mineralogical and ceramic properties of rhyolitic tuff from Arabaalan – Elmalı (Biga) district (Biga Peninsula – Turkey)

Ayten Çalık[1] – Yasemin Erçetin Akyar[2]

[1]Çanakkale Onsekiz Mart University, Faculty of Engineering and Architecture, Department of Geological Engineering, TR-17100, Çanakkale, Turkey
[2] Kalemaden A.Ş. Semedeli Köyü, 17403, Çan – Çanakkale, Turkey
E-mail: aytencalik@comu.edu.tr
Keywords: Rhyolitic tuff, ceramic properties, floor tiles, the Biga Peninsula.

ABSTRACT

Rhyolitic tuff is an important preferential raw material because it is used as alkaline and silica containing materials. Additional to that, It is easy to exploite, and is cheaper than many other raw materials. Rhyolitic tuffs crop out in the Arabaalan – Elmali district (Southeast of Biga village, the Biga Peninsula) were investigated in order to asses their potential in the ceramic industry. The Parent rock types of this raw material are Early - Middle Miocene aged, calcalkalen Biga volcanics are composed of mainly rhyolite – rhyodacite lava, tuff, ignimbrite and perlite at the base and andesite lavas above.
Chemical and mineralogical analyses were performed on representative samples by XRD and XRF methodologies. The chemical analyses generally show high silica, low alumina and low iron contents. Total alkali content of the Arabaalan rhyolitic tuff is about 4.96 – 8.02 %. The main mineralogical association consists of quartz, sanidine, albite and biotite with kaolinite, montmorillonite, illite and opaque mineral. Sericite and calcite excite as secondary mineral.
Colour measurement, viscosity, firing shrinkage, water absorption was tested by mineralogical and the thermal analysis techniques (TG – DTA) and their firing behaviour were investigated. From these studies it was understood that the Arabaalan – Elmali rhyolitic tuff could be used for ceramic industry, floor tile

INTRODUCTION

The study area is located at southeast of Biga Town of Çanakkale between Elmali village and Arabaalan village, Northwest Turkey (Figure 1).

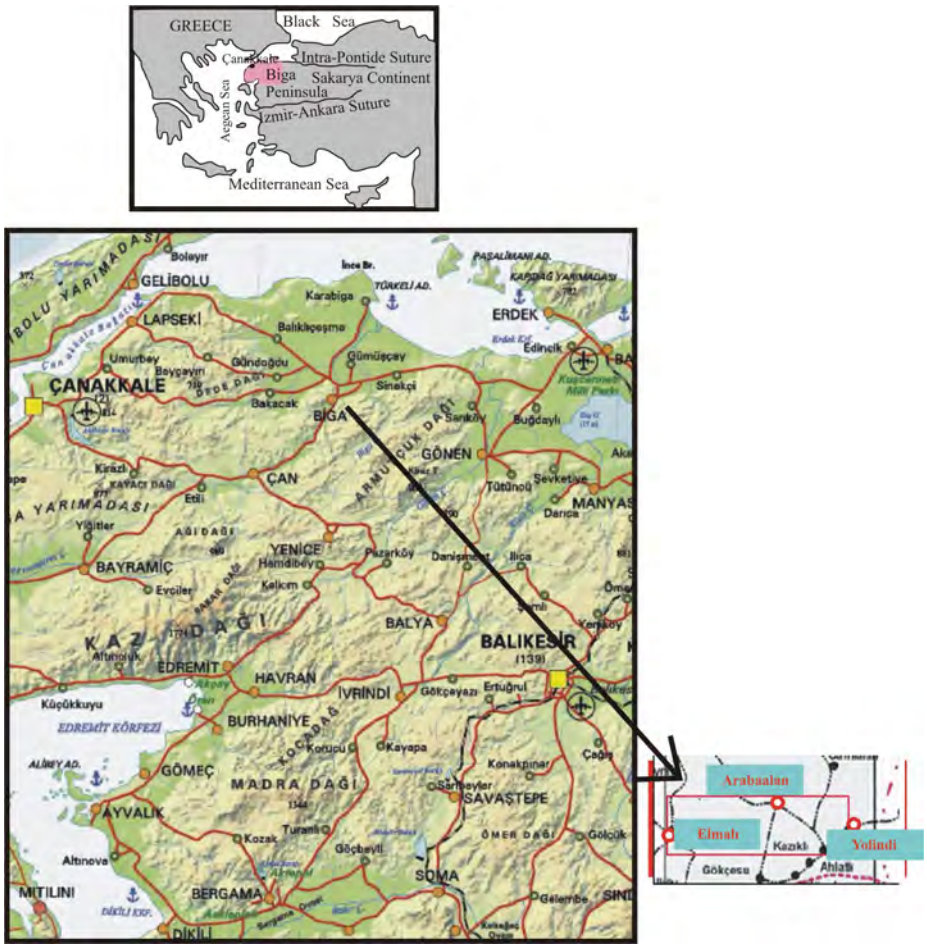

Figure 1 Location map of studied area

A widespread magmatic activity began during Oligocene – Middle Miocene in northwestern Anatolia, following the continental collision between the Sakarya and the Tauride – Anatolide platform (Yılmaz et. al 2001). This magmatic activity produced intrusive as well as extrusive rocks as exemplified from the Biga volcanics.

The majority of the most the Biga Peninsula Industrial mineral deposit - types derive from Cenozoic volcanic rocks. Rhyolitic tuffs crop out in the Arabaalan – Elmalı district belong to Early – Middle Miocene aged calcalkalen Biga volcanics.

Because of alkaline and silica containing, rhyolite tuff is an important raw material in ceramic industry. Rhyolite tuff does not require large – scale investment both in exploitation and beneficiation processes. So, small and medium sized enterprises also operate more frequently in the Industrial Mineral sector. This point makes rhyolitic tuff to be an important preferential raw material.

The attempt of ceramic industry to achieve higher profitability, led to the focusing on local raw material deposits. The investigated area in this study

is the concession area the biggest production of Kalemaden Ceramic Factory in Çan – Turkey.
This work aims to investigate chemical, mineralogical and ceramic properties of rhyolitic tuff from Arabaalan – Elmali district as used new potential local raw material in ceramic industry.

MATERIAL & METHODS

The representative samples of the rhyolitic tuff were assessed for ceramic industries. 193 samples were collected from the rhyolitic tuff. Chemical and mineralogical composition of the rhyolitic tuff investigated using XRF, XRD, DTA and TG methods. Petrography was studied of thin sections by polarized – light microscopy. Mineralogical analyses were performed by X – ray diffraction analysis, utilizing a Philips PW 3710 difractometer, operating with Cu tube at 30 kv and 30 mA.
Chemical analyses were carried out by a ARL 9400 XRF spectrometer, operating with Rh tube at 30 kv and 80 mA (samples are fused with…. Gram of $Li_2B_4O_7$ or / and $Li_2B_4O_7$ + LiF) at 1300°C in the Pt – Au alloy jar.
The ceramic properties were studied on a laboratory scale using the same processing procedures as that of the ceramic industry. For this purpose, the samples were ground with grinder. Powder of ground materials were characterized by particle size analysis, humidified and pressed in bars (31 MPa, 50x7 mm). These bars were then dried in oven (110 °C) and fired in the SACMI oven (1185 °C; 45 min.)

GEOLOGICAL SETTING

The geology of the area is shown in fig. 2. The older rocks outcropping in the region belong to Yolindi metagranite. The Yolindi metagranite is highly altered and foliated granite. The unit's contact with all other units is tectonic and no age analysis is available, complicates the process of explanation of the stratigraphic position of the unit. As a result of its comparison with other granites of Sakarya zone. Yolindi metagranite is accepted as Upper – Palaeozoic aged (Aysal, 2005).
The Çal unit, which is an upper structural unit of the Karakaya Complex. The Karakaya Complex is general tectonostratigraphic term for the strongly deformed and locally metamorphosed Permo – Triassic orogenic series in the Pondides. The Karakaya Complex have been described as the Lower Karakaya Complex, and the overlying clastic and volcanoclastic series under the Upper Karakaya Complex (Okay & Göncüoglu 2004).

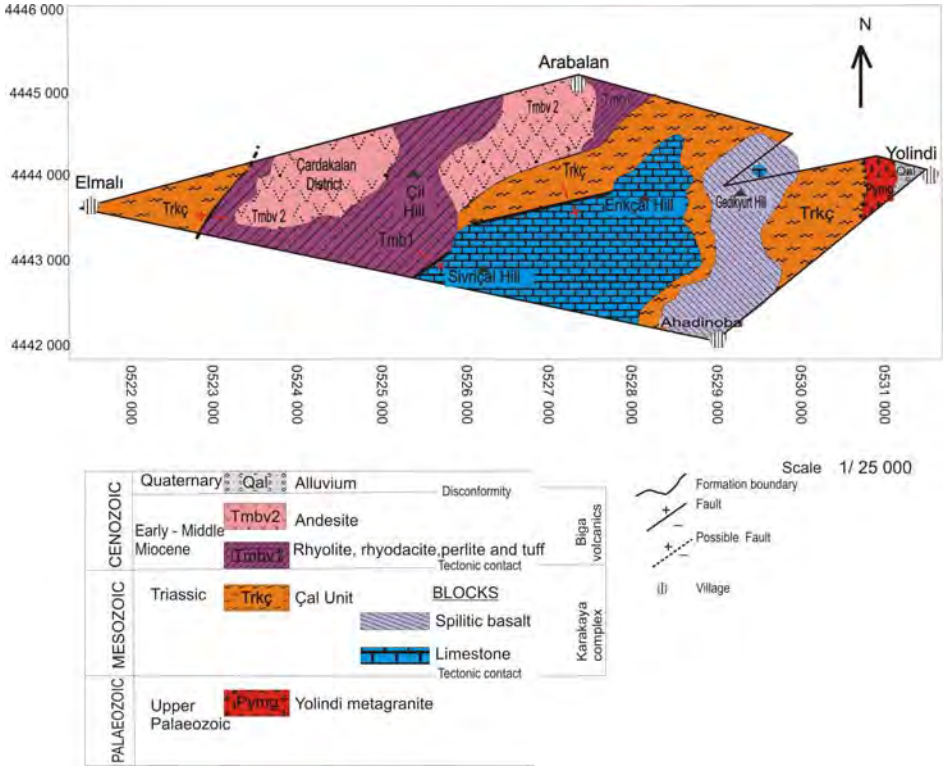

Figure 2 : Geological map of Arabaalan – Elmalı – Yolindi region

The upper structural unit of the Upper Karakaya Complex is represented by basalt, limestone, grain flows and Olistostrome series. This series have been mapped as the Çal Unit in the Biga Peninsula (Okay et. al. 1991). Çal unit is represented by the limestone and spilitic basalt blocks outcropping Erikçaltepe, Sivriçaltepe, Gedikyurttepe, and Elmalı village and around in the study area.

Biga volcanics, which are Early – Middle Miocene aged are composed of rhyolite, rhyodacite lava, tuff, ignimbrite and perlits at the at the base, andesite lavas above. Biga volcanics was identified by Ercan et. al 1995 in the name of Behram volcanics in the Biga Peninsula.

PETROGRAPHY, MİNERALOGY AND CHEMİCAL COMPOSİTİON

In the area lying between Arabaalan and Elmalı, the volcanic rocks display the following stratigrapy; the sequence begins with the rhyolitic, the rhyodacite lava and tuff, and the associated agglomera rocks. Toward the top the andesite dominate the succesion. These volcanic rocks belong to Early – Middle Miocene aged, calcalkalen Biga volcanics widely crop out the Biga Peninsula.

The rhyolitic tuff is white - coloured and is highly altered. It consists of the perlite and the rhyolitic lava layers. The phenocrst of quartz and sanidine visible in hand specimen in the fine grained groundmass.

The main mineralogical association consists of quartz, sanidine, lesser amount of plagioclase (albite), and biotite with opaque mineral. Sericite

and calcite excite as secondary minerals. Matrix (% 67 – 75) is composed of lithic fragments, crystal, and vitric ash. Kaolin and montmorillonite widely occur as alteration of the rhyolitic tuff. Perlite is also occur as alteration of the rhyolitic lavas.
Chemical data on fresh volcanic rock samples are ploted in the classification diagram of Le maitre, 1989 in the figure 3.

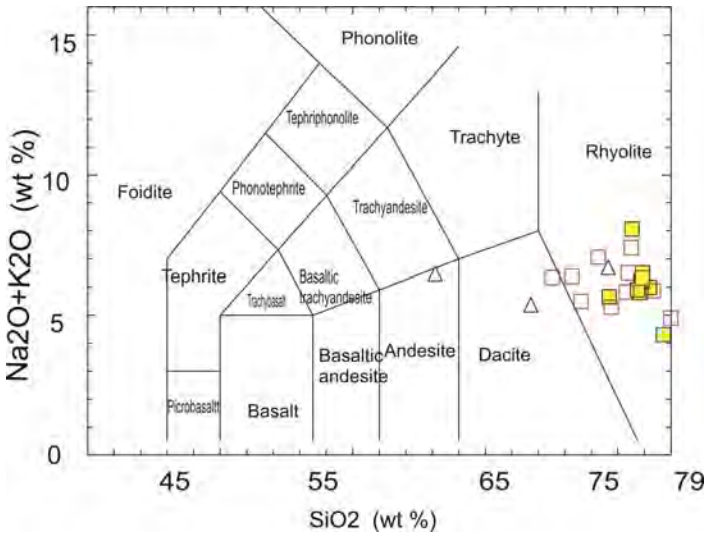

Figure 3. Total alkali ($Na_2O + K_2O$) versus silica (SiO_2) diagram (Le Maitre 1989) of the rhyolitic tuff.

The twenty five samples of the rhyolitic tuff were identified by XRD Powder technique. The four selected patterns of the rhyolitic tuff are shown in Fig. 4. They contained quartz, kristobalite, sanidine, albite, montmorillonite, kaolinite, palygorskite, illite. Some of the samples have mordenite as sample 1464.

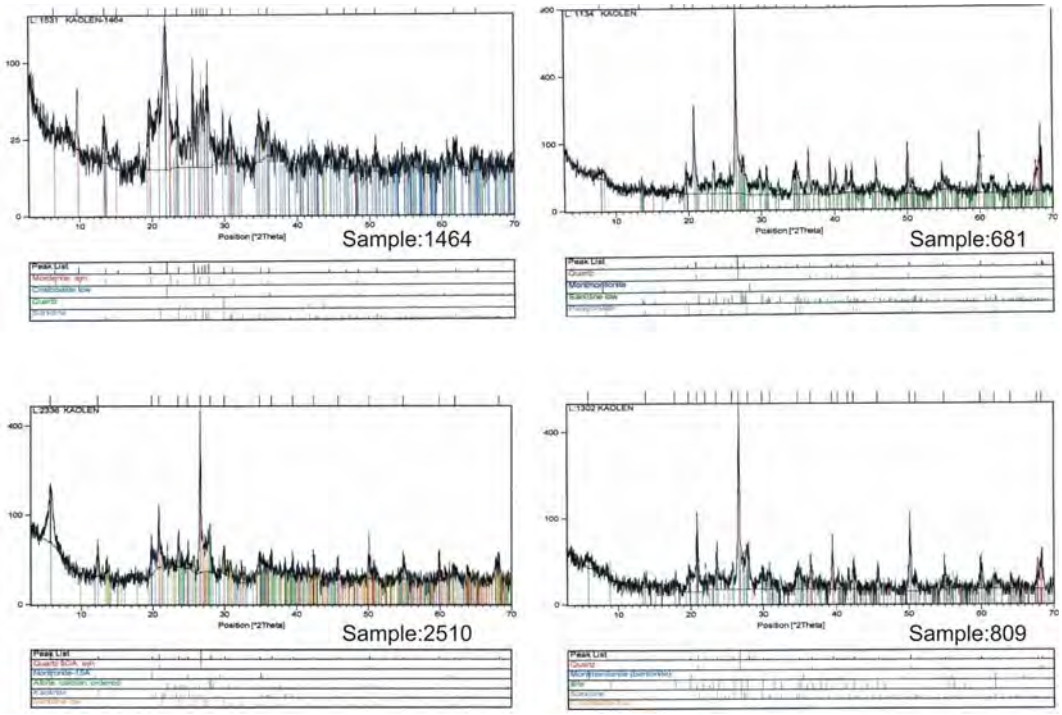

Figure 4: X – ray diffraction patterns of the rhyolitic tuff

The 190 samples of the rhyolitic tuff were identified by XRF Powder technique. The selected samples of the rhyolitic tuff are shown in Fig. 5 The chemical analyses generally show high silica (SiO_2; 65, 18 - 77, 21), low alumina and low iron (0.53 – 1.88) contents. Total alkali content of the Arabaalan rhyolitic tuff is about 4.96 – 8.02 %.

Sample No	LOI %	SiO_2 %	Al_2O_3 %	TiO_2 %	Fe_2O_3 %	CaO %	MgO %	Na_2O %	K_2O %	Total Alkali %
1459	2,12	74,15	14,81	0,15	0,53	0,63	0,08	2,63	4,58	7,21
1464	5,38	68,16	18,31	0,18	1,54	0,78	0,21	0,77	4,42	5,19
1561	5,96	69,86	15,89	0,14	1,23	1,52	0,18	1,21	3,75	4,96
1562	4,68	69,84	16,12	0,14	1,11	0,92	0,15	0,55	6,16	6,71
1563	5,28	71,34	14,94	0,13	0,99	1,28	0,14	1,03	4,47	5,50
1603	6,12	66,93	18,1	0,16	1,31	0,81	0,3	1,4	4,57	5,97
1604	6,67	65,18	18,89	0,18	1,57	0,78	0,54	1,65	4,25	5,90
681	2,25	75,91	14,19	0,17	1,38	0,1	0,24	0,63	5,11	5,74
682	2,21	74,08	15,03	0,2	1,69	0,08	0,33	0,57	5,79	6,36
683	2,23	77,21	14,48	0,12	0,95	0,13	0,06	0,01	4,78	4,79
684	2,32	74,96	15,53	0,15	1,16	0,19	0,01	0,46	5,22	5,68
685	2,22	75,11	15,05	0,13	0,9	0,13	0,24	0,74	5,44	6,18
688	2,4	74,63	15,45	0,14	1,12	0,18	0,28	0,78	4,99	5,77
799	2,26	75,13	14,9	0,14	0,89	0,12	0,2	0,57	5,78	6,35

801	2,31	75,01	15,11	0,13	1,01	0,1	0,21	0,5	5,59	6,09
802	2,3	74,94	15,15	0,12	1,01	0,1	0,27	0,6	5,47	6,07
986	2,75	72,16	16,78	0,22	1,88	0,07	0,47	0,39	5,1	5,49
987	2,36	74,72	15,42	0,15	1,14	0,1	0,32	0,6	5,07	5,67
989	2,93	76,07	15,19	0,12	1,05	0,1	0,28	0,41	3,77	4,18
1399	1,45	74,65	14,82	0,13	0,66	0,12	0,06	1,1	6,92	8,02

Figure 5: Chemical analyses of samples of the rhyolite tuff

TECHNOLOGİCAL PROPERTİES

Thermal analysis

The eighteen samples of the rhyolitic tuff were identified by DTA – Thermal analysis methodology. The ten patterns of them are shown in Fig. 6.

The calculated thermal chracteristics of the samples of the rhyolitic tuff generally resemble each other except the samples consists of mordenite. Kaolinite presented two endothermic peaks and an exothermic peak as the common characteristics feature of kaolinite. The first endothermic peak around 100°C . Between 500 – 600°C, the second, much larger endothermic peak correspond to the loos of structural hydroxyl groups and transformation of kaolinite to metakaolinite; $Al_2Si_2O_5(OH)_4 \rightarrow Al_2Si_2O_7 + 2\ H_2O$.

Lastly, the intense exothermic peak observed 980°C and 1050 - 1100°C, correspond to the reorganization the products of decomposition to give mullite. Montmorillonite presented the peaks as the first endothermic peak around 150°C, second is at 680°C. Mica also presented the endothermic peak around 850°C as sample 682 showed.

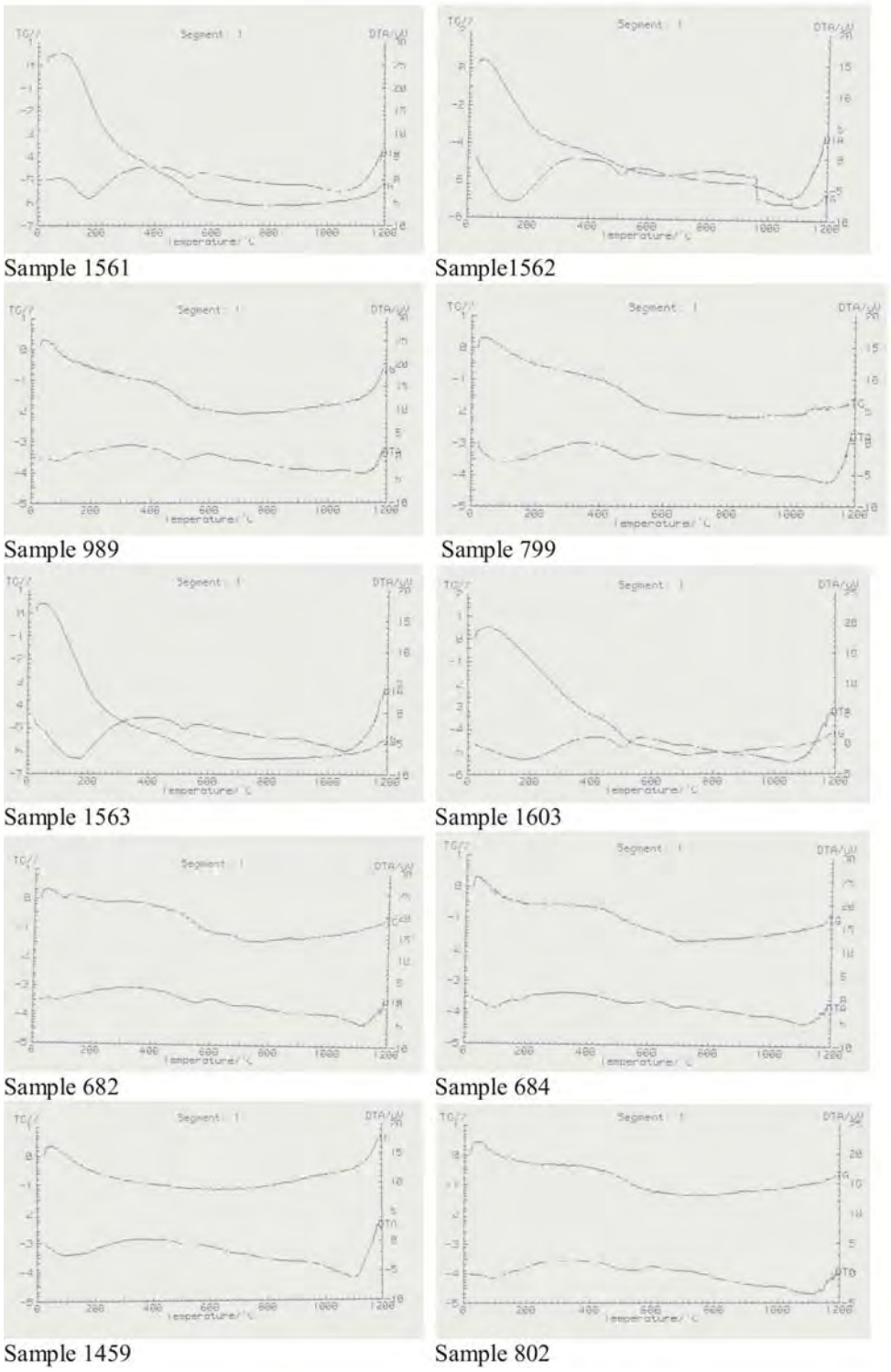

Figure 6: The DTA / TGA graphs of the rhyolitic tuff

Viscosite

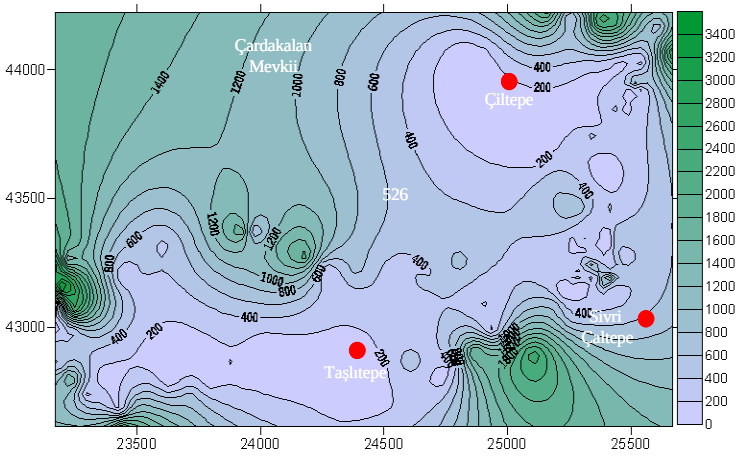

Figure 7: The map of viscosity values of the rhyolitic tuff

Figure 7 shows the viscosity value distributions of the rhyolitic tuff. The expected values are between 200 -500 cps. The values from northwest of Çiltepe, Taşlıtepe, and Sivriçaltepe are compatible with the expected values. The high values are from the areas consist of the alteration of kaolinitic and montmorillonitic alterations.

Water absorption

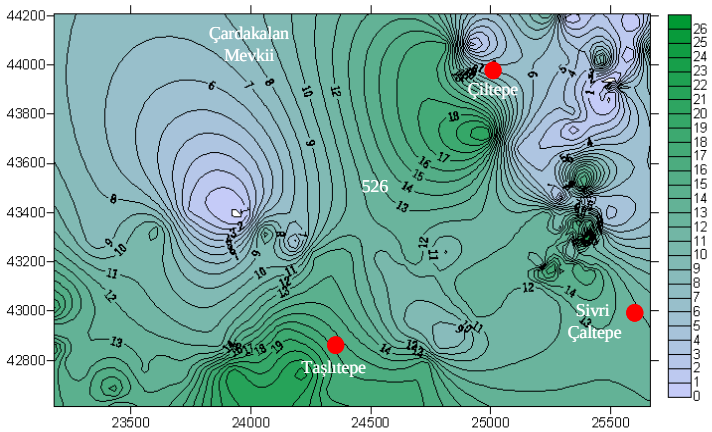

Figure 8: Water absorbtion values (%) of the rhyolitic tuff

According to the Turkish standardization (TS –EN 176), the water absorption should be lower than 3 % for the floor tiles. The water absorption values the samples from south of Çardakalan, and east of Çiltepe are lower than 3 % as seen in figure 8.

Firing Shrinkage

Figure 9 shows the firing shrinkage value distributions of the rhyolitic tuff. The recommended values are between 9.5 - 11 in the floor tile industries.

The value of the samples from southeast of çiltepe are compatible with the recommended values.

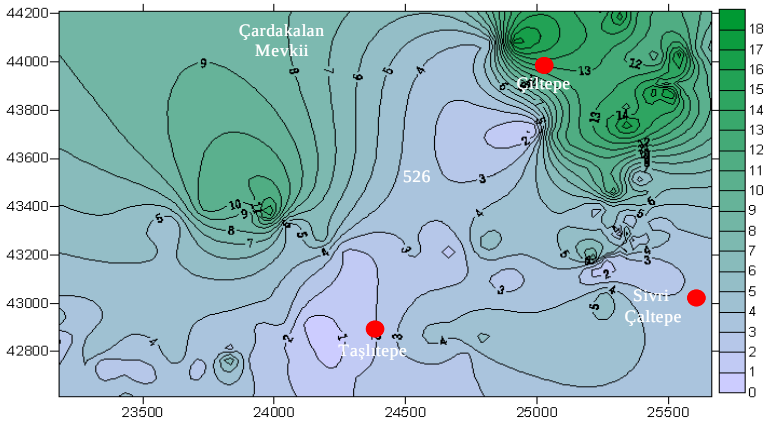

Figure 9: Firing shrinkage values (%) of the rhyolitic tuff

Colour Measurement

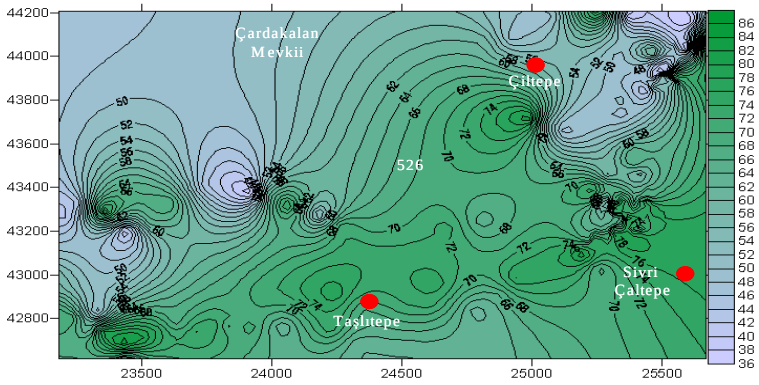

Figure 10: Colour measurement values of the rhyolitic tuff

Figure 10 shows the colour measurement value distributions of the rhyolitic tuff. The expected value is minimum 44 L. The value of samples are compatible with the expected value.

CONCLUSİON

The chemical, mineralogical and ceramic properties of rhyolitic tuff crops out in Arabaalan – Elmali district studied. Based on the microscopic study, the main mineralogical composition is as follows; quartz, sanidine, the lesser amount of plagioclase, biotite, and opaque mineral. Matrix is composed of lithic fragments, crystal and vitric ash. Sericite and calcite excite as secondary mineral.

Chemical analysis was performed on represantative samples of the rhyolitic tuff by XRF methodology. The chemical analysis show high silica, low alumina, and iron contents. Total alkali content of the rhyolitic tuff is about 4.96 – 8.02 %. In the industrial processing of ceramic bodies such

as floor tiles require some signifant chemical and physical properties. The one of them is the iron content that the expected value is 1.5 % in the samples. The iron contents of the rhyolitic tuff are between 0.53 – 1.69. The total alkali content is also compatible with the recommended values.
The result of XRD analysis show that the rhyolitic tuff consist of mainly kaolin, albite, sanidine, quartz, cristobalite, mica, montmorillionite, palygorskite and mordenite. The DTA curves show the prence of kaolinite, montmorillionite, mica and mordenite. The result of the X- ray diffraction analysis are agreement with the thermal analysis.
Firing shrinkage, viscosity , colour measurement and water absorption were tested for the rhyolitic tuff. The values from the area of around Çiltepe do reach the level recommended by the floor tile industries.
These results show that the rhyolitic tuff crops out in Arabaalan – Elmali district could have potential as raw materials for ceramic uses.

REFERENCES

Aysal, N. 2005, Biga (Çanakkale) doğusunun Mesozoik – Tersiyer Magmatizması ve Metamorfizmasının Petrolojisi (Petrology of the Mesozoic – Tertiary magmatism and metamorphism in northern Biga (Çanakkale). *Doktora tezi, İstanbul Üniversitesi, Fen Bilimleri Enstitüsü,* (*in Turkish with English abstract*).

Bingöl, E., Akyürek, B., & Korkmazer B. 1975. Biga Yarımadsının Jeolojisi ve Karakaya Formasyonunun bazı özellikleri (The geology of the Biga Peninsula and same features of the Karakaya Formation). *Cumhuriyetin 50.Yılı Yerbilimleri Kongresi. Madern Tetkik araştırma Enstitüsü (MTA) Publication, 70 – 77 (in Turkish with English abstract).*

Ercan, T., et. al. 1995, Biga Yarımadası Ile Gökçeada, Bozçaada Ve Tavşanlı Adalarındaki (KB Anadolu) Tersiyer Volkanizmasının Özellikleri. *MTA Dergisi, Cilt 117, S. 55–86 (in Turkish with English abstract)*.

Le Maitre, R. W. 1989. A classification of Igneous Rocks and Glossary of Terms. *Blackwell, Oxford,193 pp.*

Okay A. & Göncüoglu C. 2004. The Karakaya Complex: A review of Data and Concepts. *Turkish Journal of Earth Sciences (Turkish J. Earth Sci.). Vol 13, 2004, pp 77 – 95. Copyright © TÜBİTAK.*

Okay A. et. al. 1991. Geology and tectonic evolution of the Biga Peninsula, northwest Turkey. *Bulletin of the Technical University of İstanbul 44, 191 – 256.*

Şengör, A. M. C. et. al. 1984. Tectonics of the Mediterranean Cimmerides: nature and evolution of the western termination of Paleo – Tethys. *In: Dixon, J. E. & Robertson, A. H. F, (eds).The Geological Evolutionof the*

Eastern Mediterranean. Geological Society, London, Special Publications 17, 77 – 112.
Yılmaz, Y. et. al. 2001. Two contrasting magmatic associations of NW Anatolia and their tectonic significance. *Journal of Geodynamics 31 (2001) 243 – 271.*

Early Cretaceous productive and barren granitoids in the Gunbuk-Jindong area in the Gyeongsang basin, South Korea: petrogenesis, geochronology and implications for Cu (-Au) mineralization

[1]Soo-meen Wee, [2]Jung Woo Park, [2]Seon-gyu Choi, [1]Yun-ji Kim, [3]In-chang Ryu and [2]V.J. Rajesh

[1] Dept. of Earth Sciences, Korea National Univ. Education, Cheongwon, 636 – 791
[2] Dept. of Earth & Environmental Sciences, Korea Univ., Seoul, 136 – 713
[3] Dept. of Geology, Kyeongbuk National Univ., Daegu, 702 – 701
E-mail: weesm@cc.knue.ac.kr
Keywords: adakite, Cretaceous granite, Gyeongsang basin, Gunbuk granitoids, Cu(-Au) mineralization.

ABSTRACT

The Gunbuk-Jindong area in the southwestern part of the Gyeongsang Basin in South Korea consists of spatially related gabbro, quartz diorite, granodiorite and granite that are intruded into Cretaceous sedimentary rocks of the Jindong formation. Majority of Cu (-Au) deposits are located in the region of the Gunbuk granitoids (northern part) whereas the region around the Jindong granitoids (southern part) is almost barren. Gunbuk granitoids have geochemical features similar to slab-derived adakites such as high Al_2O_3, and Sr contents, high Sr/Y and La/Yb, but low Y and Yb contents. The Rb-Sr isotopic age of 97.0±8.4 Ma with an initial Sr ratio of 0.7046 recommend that the magma has mantle signature and intruded during Early Cretaceous. In contrast, the Jindong granitoids have low Sr and high Y contents and are typical of calc-alkaline I-type granitoids. The geochemical and tectonic features reveal that adakite-like signatures of the Gunbuk granitoids were generated by the interaction of subducted slab-derived adakitic melts (caused by the thermal effect of ridge subduction) and calc-alkaline magmas. Numerous vein-type Cu (-Au) ore deposits are associated with the Gunbuk granitoids and have features (geochemistry, alteration patterns, vein mineralogy and stable isotope characteristics) similar to the parental magmas of Cu (-Au) deposits associated with adakites. Hence a close genetic relationship existed between the adakitic magmas and associated Cu (-Au) mineralization. The Gunbuk granitoids are considered as the associated pluton of the proximal-type Cu (-Au) Gunbuk ore deposits.

INTRODUCTION

The eastern extension of the Cordilleran-type orogenic belt continues from southeastern China to the Chukot Peninsula through the Korean Peninsula. The Gyeongsang Basin, located in the southeastern part of the Korean Peninsula and the Inner Zone of southwest Japan are

characterized by extensive distribution of Cretaceous to Tertiary I-type calc-alkaline series of intrusive rocks. These intrusive rocks are possibly the result of intensive magmatism which occurred in response to the subduction of the Izanagi Plate beneath the northeastern part of the Eurasian Plate. The lithofacies, geochronology and geochemical characteristics of the Cretaceous Gunbuk granitoids in the Gyeongsang Basin are quite consistent with the granitoids in southwest Japan (Cheong *et al*., 1998). The Shiraishino granodiorites of Kyushu Island (Kamei, 2004) and the Tamba granitoids of San'yo belt (Kiji *et al*., 2000), located on the southwest Japan, display paleogeographical locations, and paleotectonic environments, intrusion ages similar to those of Gunbuk granitoids and are reported to be adakite, whose signatures are high SiO_2, Al_2O_3, Sr, Sr/Y, La/Yb and low Y, Yb contents.

The purposes of this study are : a) to present the geochemical characteristics of the Gunbuk granitoids in order to constrain the conditions of their genesis, and b) to compare the Gunbuk granitoids with the Cretaceous adakites in southwest Japan in order to discuss the environment in which it could have formed. c) to examine the relation between the Gunbuk Cu (-Au) mineralization and its associated granitoids.

GEOLOGICAL SETTING

Tectonostratigraphic units in the South Korea include the Gyeonggi massif (Precambrian), the Ogcheon-Taebaek belt (late-Precambrian to Paleozoic), the Youngnam massif (Precambrian), and the Gyeongsang Basin (Mesozoic) from north-west to south-east (Fig. 1). The Gyeongsang Basin mainly consists of siliciclastic sedimentary and calc-alkaline volcanic rocks, deposited in a continental arc setting (Choi *et al*., 2005). During the Cretaceous to early Tertiary periods, the Gyeongsang Basin was formed by transtension during the oblique subduction of the Izanagi Plate beneath the Eurasian Plate. Orthogonal subduction following oblique subduction of the Izanagi Plate along the Pacific continental margin during the Cretaceous caused intensive magmatism in the Gyeongsang Basin (Ryu *et al*.., 2006). The basin is bounded on the west and north by the Precambrian metamorphic rocks (Youngnam Massif) as well as the Jurassic granitoids, and overlapped on the east by Early Tertiary calc-alkaline volcanic succession intercalated with minor amounts of sedimentary rocks.

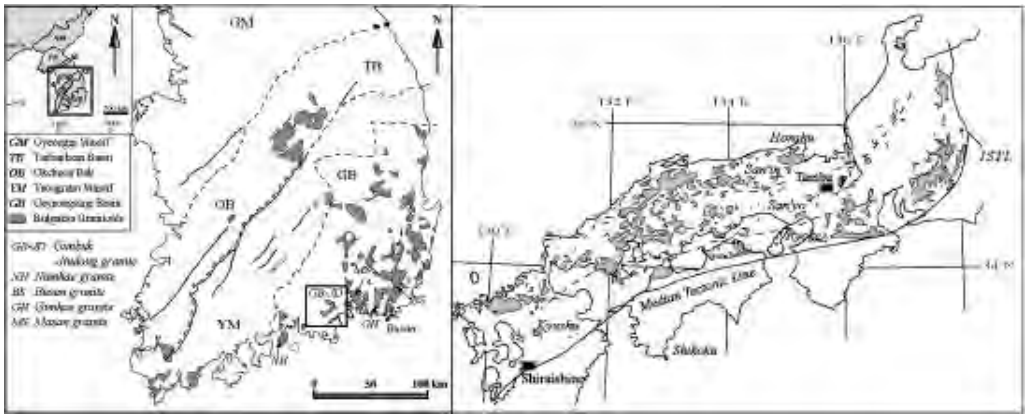

Figure 1: Cretaceous granitic provinces of South Korea and southwest Japan. Left figure shows tectonic provinces of southern part of the Korean peninsula and location of study area.

The granitoids, which show typical porphyritic, micrographic and miarolitic cavity textures, are closely associated with coeval volcanic rocks and ring dikes. They have petrographical and geochemical features indicating shallow-depth emplacement (<2.0 kbar), and are calc-alkaline, I-type and magnetite series intrusives that occurred in a subduction related igneous suite. Sedimentation in this basin was initiated in the Hauterivian and continued into the Albian, whereas much of the volcanism is constrained sporadically to a period of 110 – 50 Ma, with a major population between ca. 90 and 70 Ma (Choi *et al*., 2005). The Late Cretaceous granitoids are correlated with the granitoids in the southwestern Japan that have similar intrusion age (Ishihara, 1998). The intrusive ages of granitoids in both areas cluster between about 100 and 50 Ma.

The Cretaceous granitoids in the Gyeongsang Basin are often associated with mineral deposits of various types (Choi *et al.*, 2006). Vein type Cu (-Au) ore deposits lie in the Gunbuk-Jindong area, which have close relationships with subvolcanic graniotids. They have characteristics of porphyry-related ore deposits based on their alteration zone, vein mineralogy, and the temperature, salinity and isotopic study of ore forming fluids, (Lee et al., 2003)

GEOCHEMISTRY

Major elements

The granitoids in the Gunbuk-Jindong area show a wide range of composition, with SiO_2 varying continuously from 44.3 to 68.1 wt.%. The Gunbuk granitoids exhibit relatively low $Fe_2O_3^{(T)}$/MgO (1.6-3.5) ratios and K_2O and relatively high Al_2O_3 (16.3-21.7, ave.=17.3), MgO (1.7-6.7, ave.= 2.7) and Na_2O (1.6-5.1) contents compared with the other Cretaceous granitic rocks in the Gyeongsang Basin. On a (Na_2O+ K_2O) vs. SiO_2 diagram, they plot in the calc-alkaline field. However, because of high Na_2O and low K_2O contents, their K_2O/Na_2O ratios are low (0.04-0.92, except JD-1). The variation trends of the major element oxides of Gunbuk

granitoids are similar to those of the Kyushu and San'yo Belt adakites, and are consistent with the average range of adakites determined by Xiong *et al*. (2006) (Fig. 2). Molar $Al_2O_3/(CaO+ Na_2O+ K_2O)$ ratio of the granitoids have values between 0.82 and 1.06 which represent I-type signature.

Trace elements and Rb-Sr isotopes

The LILE (Ba, Rb, Th, Sr), which are relatively soluble in aqueous fluids, is enriched while HFSE (Nb, Ta, Ti, Y) shows depleted pattern (Fig. 2a), exhibiting typical patterns of granitoids generated in a volcanic arc environment. Trace elements allow a better and indisputable distinction between adakitic and typical arc calc-alkaline magmas. Ni (4-20 ppm) and Cr (19-56 ppm) contents of the Gunbuk granitoids are higher than in typical arc calc-alkaline granites. Furthermore, trace elements characteristics such as high Sr, Sr/Y, La/Yb and low Y, Yb contents of the pluton are similar to those of adakites. Rb and Nb contents are especially low compared to other Cretaceous granitic rocks in the Gyeongsang Basin. The REE patterns (LREE enriched and depleted HREE with no Eu anomalies) are typical of adakites (Fig. 2b). They are strongly fractionated with La, and the HREE contents are low (Yb<3.1 ppm). In comparison, the typical calc-alkaline granitic rocks are rich in HREE ($HREE_N$ >10; Yb>2.5 ppm); which will result in lower REE fractionation ($(La/Yb)_N$ <10) (Martin, 1999).

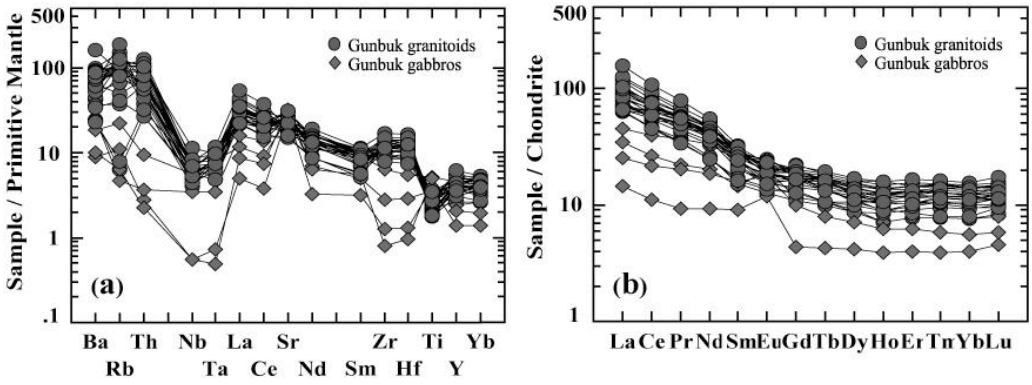

Figure 2: (a) Primitive mantle-normalized trace element patterns and (b) Chondrite-normalized REE patterns of Gunbuk granitoids. Normalizing factors after Sun and McDonough (1989).

The whole rock Rb-Sr isochron of the Gunbuk granitoids, and calculated whole rock age represents 97.0±8.4 Ma. This age suggested that the intrusion took place in the early Cretaceous. The Rb-Sr whole rock age of the adakites found in Kyushu and the Inner Zone of Southwest Japan is 121±14Ma and the $^{87}Sr/^{86}Sr$ initial ratio is 0.70493±7 (Kamei, 2004). The K-Ar age of the adakites found in San'yo belt is 101~107Ma (Kiji *et al*., 2000), indicating that they have similar intrusion age. $^{87}Sr/^{86}Sr$ initial ratio of the granitoids is 0.70457±6(2σ), which is consistent with the range of initial ratios of the Cretaceous granitoids in South Korea (between 0.704 and 0.707; Jin, 1980). This indicates that the magma source which created

Gunbuk granitoids is closely related to the upper mantle.

DISCUSSION

Adakitic signatures of the Gunbuk granitoids

After Kay(1978) discovered volcanic rocks with unique composition caused by melting of subducting slab in Adak Island of the Aleutian Islands, Defant and Drummond(1990) defined adakites as either volcanic or intrusive rocks that are created in an arc environment in association with melting of subducting slab. Defant and Kepezhinskas (2001) defined chemical characteristics of adakite as SiO_2 (>56 wt.%), Al_2O_3 (>15 wt.%), Na_2O (>3.5 wt.%), Sr (>400 ppm), Y (<18 ppm), Sr/Y (>40), Yb (<1.9 ppm), La/Yb (>20). Rollinson and Martin (2005) defined it as SiO_2 (>56 wt.%) and average values of Mg-number (0.51), Ni (24 ppm), Cr (36 ppm), strongly fractionated REE, Sr (>400 ppm), Y (<18 ppm), Sr/Y (>40), Yb (<1.9 ppm), $(La/Yb)_n$ (>40) to distinguish it from TTGs and Sanukitoids.

Adakite	Gunbuk granitoids (average)
high SiO_2 (>56wt%)	SiO_2 = 44.26 ~ 68.05 (60.00)
high Al_2O_3 (>15wt%)	Al_2O_3 = 14.93 ~ 21.72 (17.30)
low MgO (<3wt%)	MgO = 1.13 ~ 6.73 (2.65)
high Sr (>300ppm)	Sr = 320 ~ 674 (483)
low Y (<15ppm)	Y = 6.3 ~ 28.5 (18.2)
high Sr/Y (>20)	Sr/Y = 14.60 ~ 91.75 (29.90)
no Eu anomaly	no Eu anomaly
low HFSE's : Nb, Ta	low HFSE's : Nb, Ta, Ti, Y
low $^{87}Sr/^{86}Sr$ (<0.704)	$^{87}Sr/^{86}Sr$ = 0.704545 ~ 0.705949

Table 1: Geochemical characteristics of adakite and Gunbuk granitoids.Adakite data from Castillo(2006)

As the main differences between adakites and calc-alkaline granitic rocks are recorded by REE, Y and Sr behaviors, the diagram discriminating between these two types of magmas are based on Sr/Y vs. Y variation diagram (Defant and Drummond, 1990) due to its chemical characteristics of having high Sr content and low Y content.

Gunbuk granitoids fall well within the adakite range (Fig. 3) along with Kyushu and San'yo belt adakites in the Inner Zone of Southwest Japan (Kamei, 2004; Kiji *et al*., 2000). Geochemical characteristics of the Gunbuk granitoids have overall consistency with the adakite series (Table 1).

In the spider and REE diagrams, the Gunbuk granitoids along with the adakites from Kyushu and San'yo belt (Kamei, 2004; Kiji *et al*.., 2000), Sulu belt and Dexing (Guo *et al*., 2006; Wang *et a*l., 2006) and the average adakite (Condie, 2005) show similar trace element pattern corresponding with previously reported adakites and a signature of notable

Nb deficiency (Fig. 4).

Haman-Gunbuk Cu (-Au) Mineralization and Gunbuk granitoids

Porphyry Cu (-Au) deposits are preferably generated by the S-enriched magma with high fO_2. Adakitic magmas, derived from subducting slab melts, are one of the fertile magmas responsible for the production of Porphyry Cu (-Au) deposits (Mungall, 2002). Haman-Gunbuk Cu(-Au) ore deposit is vein type, but has similar characteristics in metal ratio, alteration zonation and vein mineralogy. Furthermore, ore-forming fluids in the early mineralization have the high temperature (300-500°C), high salinity (30-55 eq. wt% NaCl) and isotopic values of dominant magmatic source (average $\delta^{18}O$=11.8‰, average δD=-78‰). These signatures represent that Haman-Gunbuk Cu (-Au) ore deposit is a proximal type ore deposit which has close relationship with associated granitoids in time and space (Lee *et al*, 2003).

In Gunbuk-Jingdong area most mines are located around the Gunbuk granitoids than the Jindong granitoids. The Gunbuk granitoids have features of magmatism in a moderately oxidized environment and are geochemically similar to the granitoids which are associated with Cu (-Au) mineralization. In addition, adakitic signatures shown in the Gunbuk granitoids are known for preferable formation of Cu (-Au) porphyry deposits. Based on the aforementioned facts, the Gunbuk granitoids are thought to be as the related pluton of the proximal-type Cu (-Au) Gunbuk ore deposits.

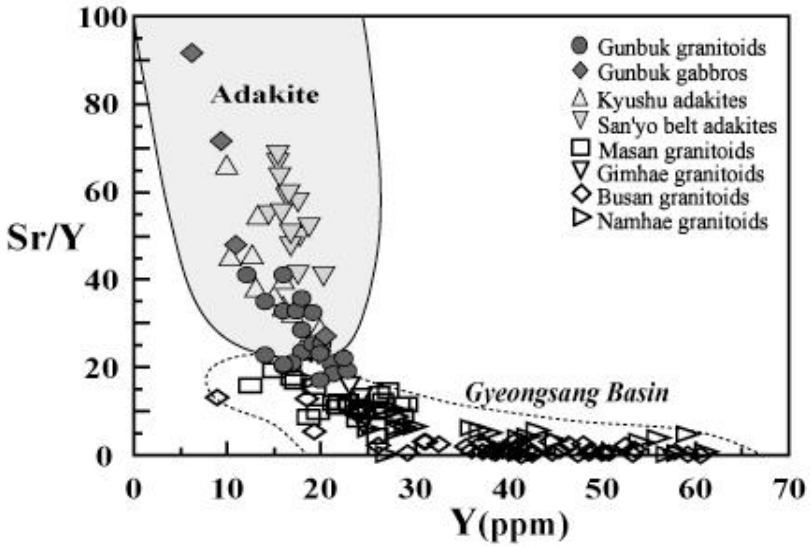

Figure 3: Sr/Y vs. Y discrimination diagram for the adakite (Castillo, 2006). Shaded areas represent adakite range (light gray) and composition of other Cretaceous granites (dashed line) in the Gyeongsang Basin(Lee, 1991; Lee, 1991, 1997; Kim and Park, 1995; Jwa and Park, 1996).

Petrogenetic model of the Gunbuk granitoids

Defant and Drummond (1990) who defined adakites for the first time,

suggested that they are created in modern convergent margins where young (<25Ma) and thus still hot oceanic lithosphere is being subducted. Afterwards, the involvement of slab-derived melts was suggested as an alternative petrogenetic model (Yogodzinski *et al*., 1995). Other petrogenetic models proposed by various workers include subduction initiation of old (>25Ma) oceanic crusts (Sajona *et al*., 1993), subduction collision (Sajona et al., 2000), shallowing of subduction angle (Gutscher *et al*.., 2000) and tearing of the slab, which led to the opening of an asthenospheric window (Yogodzinski *et al*., 2001). Researches on petrogenetic processes other than slab melting models have revealed that adakaitic rocks can also be generated due to partial melting, which led to the interaction between thickened lower crusts with mantle peridotites (Atherton and Petford, 1993), a metasomatized mantle wedge through differentiation of parental basaltic magma (Castillo *et al*., 1999), a mafic lower crust that is consistent with the results of basalt melting at high pressure where garnet is a stable and residual phase (Xu *et al*., 2002), and a high pressure crystal fractionation of the original arc basalts derived from the metasomatized mantle wedge (Macpherson *et al*., 2006).

The geochemical data of adakitic Gunbuk granitoids were compared with the aforementioned previous models to examine their petrogenetic models. It was found that Gunbuk granitoid data are well matching to the slab melting model that include an young oceanic lithosphere in a subduction environment. Gunbuk granitoids is genetically related to melting of an eclogite or a garnet restite based on MORB (Fig. 5a). When Gunbuk granitoids is applied to the Zr/Sm vs. La/Sm variation diagram (Drummond *et a*l., 1996), it can be assumed that adakites are generated from magma whose restite of eclogite or garnet melting stands between 30 and 50 % (Fig. 5b). In addition, because it is difficult for the primary slab melting, which contributes to the creation of adakites, to persist as it undergoes changes in the mantle wedge, an additional discussion on the possibility of metasomatism or hybrid magma at the mantle wedge after slab melting is necessary. The Gunbuk granitoids's trace element tendency expressed in the Sr initial ratio and Nb deficiency indicates upper mantle activities at the mantle wedge.

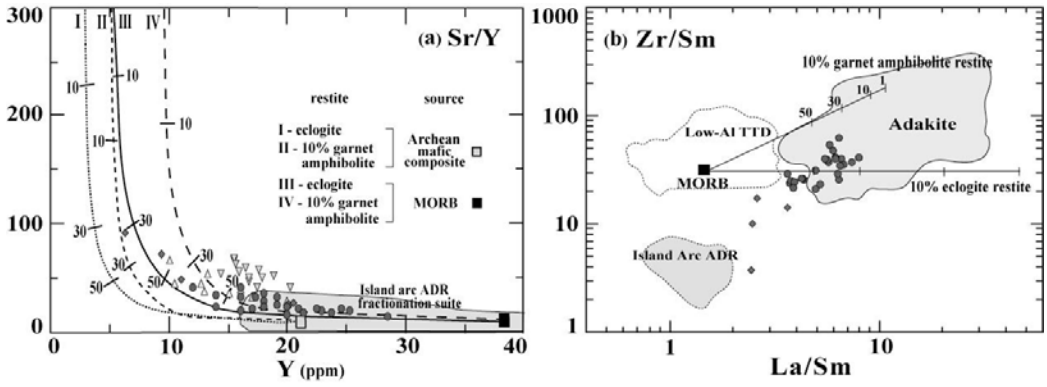

Figure 4: (a) Sr/Y vs. Y diagram for the adakite relative to partial melt curves of MORB and Archean mafic composite sources leaving

either eclogite (curves I and III) or 10% garnet amphibolite (curves II and IV) restite, (b) Zr/Sm vs. La/Sm diagram for the adakite, Island arc ADR and low-al TTD relative to partial melt curves of MORB leaving either a 10% garnet amphibolite (upper curve) or eclogite (lower curve) restite. Symbols are the same as in Fig. 3.

CONCLUSION

1. The granitoids in the Gunbuk-Jindong area are calc-alkaline, I-type and magnetite series intrusives that occurred in a subduction related igneous suite. They have petrographical and geochemical features indicating shallow-depth emplacement (<2.0 kbar),
2. Rb-Sr isotope data of the Gunbuk granitoids show that the whole rock age and Sr initial ratio are 97.0±8.4 Ma and 0.7046, respectively. The Sr initial ratio is very similar to those of the Creataceous granites in the Gyeongsang Basin ($^{87}Sr/^{86}Sr$ = 0.7049-0.707). These results suggest that the magma have the mantle signature and intruded into the area during the early Cretaceous age. On the A/NK vs. A/CNK and tectonic discrimination diagrams, parental magma type of the granites corresponds to I-type, VAG granite. Interpretations of the geochemical characteristics of the granitic rocks favor their emplacement at continental margin during the subduction of Izanagi plate.
3. Major and trace element contents of the Gunbuk granitoids fall well within the adakitic range, and show similar geochemical features to the those of adakites from Kyushu and San'yo belt in the Inner Zone of Southwest Japan, and Sulu belt and Dexing in southern China. But geochemical signatures are different from other Cretaceous granitoids in the Gyeongsang Basin which have low Sr and high Y contents and are typical of calc-alkaline affinities.
4. The proximal type, porphyry-like Haman-Gunbuk Cu (-Au) ore deposits lie in the region of the Gunbuk granitoids, not the Jindong granitoids, and thought to be resulted from the Gunbuk adakitic magmatism.
5. The geochemical and tectonic features reveal that adakite-like signatures of the Gunbuk granitoids were generated by the interaction of subducted slab-derived adakitic melts (caused by the thermal effect of ridge subduction) and calc-alkaline magmas.

REFERENCES

Atherton, M. P. & Petford, N. 1993. Generation of sodium-rich magmas from newly underplated basaltic crust*.. Nature*, Vol. 362, 144-146.

Castillo, P. *et al.* 1999. Petrology and geochemistry of Camiguin Island, southern Philippines: insights to the source of adakites and other lavas in a complex arc setting. *Contributions to Mineralogy and Petrology*, Vol. 134, 33-51.

Castillo, P. R. 2006. An overview of adakite petrogenesis. *Chinese Science Bulletin*, Vol. 51, 257-268.

Cheong, C. S. *et al*. 1998. Isotopic and geochemical compositions of Onjeongri granites in the Northern Gyeongsang Basin. *Journal of Petrological Society of Korea*, Vol. 7, 77-97.

Choi, S. G. *et al.* 2005. Cretaceous epithermal gold-silver mineralization and geodynamic environment, Korea*. Ore Geology Reviews*, Vol. 26, 115-135.

Choi, S. G*. et al*. 2006. The origin and evolution of mineralizing fluids in the Cretaceous Gyeongsang Basin, Southeastern Korea. *Journal of Geochemical Exploration,* Vol. 89, 61-64.

Condie, K. C. 2005. TTGs and adakites: are they both slab melts?. *Lithos*, Vol. 80, 33-44.

Defant, M. J. & Drummond, M. S. 1990. Derivation of some modern arc magmas by melting of young subducted lithosphere. *Nature*, Vol. 347, 662-665.

Defant, M. J. & Kepezhinskas, P. K. 2001. Evidence suggests slab melting in arc magmas. *EOS Transactions*, Vol. 82, 65-69.
Drummond, M. S. *et al*. 1996. Petrogenesis of slab-derived trondhjemite – tonalite -dacite / adakite magmas. *Transactions of the Royal Society Edinburgh: Earth Sciences*, Vol. 87, 205-215.

Gutscher, M. A. *et al*. 2000. Can slab melting be caused by flat subduction?. *Geological Society of America*, Vol. 28, 535-538.

Guo, F*. et al.* 2006. Geochemistry of late Mesozoic adakites from the Sulu belt, eastern China: magma genesis and implications for crustal recycling beneath continental collisional orogens. *Geological Magazine*, Vol. 143, 1-13.

Ishihara, S. 1998, Granitoids series and mineralization in the circum-Pacific Phanerzoic granitic belts*. Resource Geology*, Vol. 48, 219-224.

Jin, M. S. 1980. Geology and Isotopic Contrasts of the Jurassic and the Cretaceous Granites in South Korea. *Journal of the Geological Society of Korea*, Vol. 16, 205-215.

Jwa, Y. J. & Park, J. M. 1996. Petrology of the igneous rocks in the Goseong area, Gyeongsang Basin. Major element geochemistry and K-Ar radiometric age*. Economic and Environmental Geology*, Vol. 29, 561-573.

Kamei, A. 2004. An adakitic pluton on Kyushu Island, southwest Japan

arc. *Journal of Asian Earth Sciences*, Vol. 24, 43-58.

Kay, R. W. 1978. Aleutian magnesian andesites; melts from subducted Pacific Ocean crust. *Journal of Volcanology and Geothermal Research*, Vol. 4, 117-132.

Kiji, M. *et al*. 2000. Cretaceous adakitic Tamba granitoids in northern Kyoto, San'yo belt, southwest Japan. *Japanese Magazine of Mineralogical and Petrological Sciences,* Vol. 29, 136-149.

Kim, H. N. & Park, C. Y. 1995. Lithogeochemical and mineral chemistry features of granitoids and their relation to mineralization in the Namhae area. *Journal of Korean Earth Science Society*, Vol. 16, 522-535.

Lee, J. D. 1991. Petrological study on granitoids in Chindong-Masan area, Gyeongsangnam-do. *Journal of Korean Earth Science Society*, Vol. 12, 230-247.

Lee, J. I. 1991. Petrology, Mineralogy and Isotopic Study of the Shallow - depth Emplaced Granitic Rocks, Southern Part of the Kyeongsang Basin, Korea -Origin of Micrographic Granite-. The Tokyo University, 231p.

Lee, J. I. 1997. Trace and rare earth element geochemistry of granitic rocks, southern part of the Kyongsang Basin, Korea. *Geoscience Journal*, Vol. 1, 167-178.

Lee, S. Y.*et al.* 2003. Base-metal mineralization in the Cretaceous Gyeongsan Basin and its genetic implications, Korea: the Haman-Gunbuk-Goseong(-Changwon) and the Euiseong metallogenic Provinces. *Economic and Environmental Geology,* Vol. 36, 257-268.

Macpherson, C. G. *et al.* 2006. Adakites without slab melting: High pressure differentiation of island arc magma, Mindanao, the Philippines*.. Earth and Planetary Science Letters*, Vol. 243, 581-593.

Martin, H. 1999. Adakitic magmas: modern analogues of Archean granitoids, *Lithos*, Vol. 46, 411-429.

Mungall, J. E. (2002) Roasting the mantle: Slab melting and the genesis of major Au and Au-rich Cu deposits. *Geology*, Vol. 10, 915-918.

Rollinson, H. & Martin, H. 2005. Geodynamic controls on adakite, TTG and sanukitoid genesis: implications for models of crust formation - Introduction to the Special Issue*. Lithos*, Vol. 79, 9-12.

Ryu, I. C*. et al.* 2006. An inquiry into the formation and deformation of the Cretaceous Gyeongsang Basin, Southeastern Korea. *Economic and Environmental Geology,* Vol. 39, 129-149.

Sajona, F. G. *et al*. 1993. Initiation of subduction and the generation of slab melts in western and eastern Mindanao, Philippines. *Geology*, Vol. 21, 1007-1010.

Sajona, F. G. *et al*. 2000. Magmatic source enrichment by slab-derived melts in a young post-collision setting, central Mindanao (Philippines). *Lithos*, Vol. 54, 173-206.

Sun, S. S. & McDonough, W. F. 1989. Chemical and isotopic systematics of oceanic basalt: implications for mantle composition and processes. In: *Magmatism in the ocean basins. Geological Society Special Publication*, Vol. 42, 313-345.

Wang, Q. *et al*. 2006. Petrogenesis of Adakitic Porphyries in an Extensional Tectonic Setting, Dexing, South China: Implications for the Genesis of Porphyry Copper Mineralization. *Journal of Petrology*, Vol. 47, 119-144.

Xiong, X. L. *et al*. 2006. Na depletion in modern adakites via melt/rock reaction within the sub-arc mantle. *Chemical Geology*, Vol. 229, 273-292.

Xu, J. F. *et a*l. 2002. Origin of Mesozoic adakitic intrusive rocks in the Ningzhen area of east China: Partial melting of delaminated lower continental crust?. *Geological Society of America*, Vol. 30, 1111-1114.
Yogodzinski, G. M. *et al*. 1995. Magnesium andesite in the western Aleutian Komandorsky region. Implications for slab melting and processes in the mantle wedge. *Geological Society of America Bulletin*, Vol. 107, 505-519.

Yogodzinski, G. M. *et al*. 2001. Geochemical evidence for the melting of subducting oceanic lithosphere at plate edges. *Nature*, Vol. 409, 500-504.

Assessment of reactivity of sulphidic tailings and river sludges

Komnitsas, K., Manousaki, K. and Zaharaki D.
Department of Mineral Resources Engineering
Technical University Crete
E-mail: komni@mred.tuc.gr
Keywords: tailings reactivity, contamination risk

ABSTRACT

The present paper aims to assess the long term reactivity of sulphidic wastes disposed of in a tailings dam at Bor, Serbia, as well as of the sludges from a stream receiving acidic effluents and estimate the risk for the wider ecosystem. The laboratory assessment was carried out according to the slightly modified AMIRA protocol, using conventional free draining leach columns. Deionised water and simulated acid rain were used as leaching agents. The experimental results over a period of 80 weeks show increased solubilisation for a number of heavy metals and subsequently high risk for contamination of surface- and groundwater. Finally, feasible and effective remediation measures are proposed.

INTRODUCTION

The oxidation of sulphide minerals present in mixed sulphide and coal waste dumps through a complex series of direct, indirect and bacterial reactions, results often in acid generation, dissolution and mobilisation of heavy metals and subsequent contamination of surface- and groundwater (Ritcey 1989; Kontopoulos *et al*. 1995; Bhattacharya *et al.* 2006). The overall oxidation reaction of pyrite (FeS_2), which is the main mineral phase responsible for Acid Mine Drainage (AMD), is expressed as follows:

$$2FeS_2\ (s) + 7O_2\ (aq) + 2H_2O \rightarrow 2Fe^{2+}\ (aq) + 4H^+\ (aq) + 4SO_4^{2-}\ (aq) \quad (1)$$

The rate of this reaction can be accelerated by several orders of magnitude through the action of *Thiobacillus ferooxidans* according to reaction (2):

$$4Fe^{2+} + O_2\ (aq) + 4H^+ \rightarrow 4Fe^{3+} + 2H_2O \quad (2)$$

Fe^{3+} generated from reaction (2) oxidizes FeS_2 by the indirect reaction (3). The produced Fe^{2+} ions are again oxidized to Fe^{3+}, according to reaction (2), and participate again in the oxidation of additional quantities of pyrite (autocatalysis).

$$FeS_2\ (s) + 14Fe^{3+} + 8H_2O \rightarrow 15Fe^{2+} + 2SO_4^{2-} + 16H^+\ (aq)$$

Preventing the formation and/or the migration of AMD from its source is

considered in general as the most preferable option, even though this is not possible in most cases (Peppas *et al.* 2000; Pérez-López *et al*. 2007); it is therefore necessary to collect and treat the generated effluents (Johnson & Hallberg 2005). AMD is traditionally treated by active technologies, involving addition of chemical-neutralising agents, such as hydrated lime, limestone, soda ash, caustic soda, ammonia, calcium peroxide, kiln dust or fly ash. The major disadvantages of these methods include the need for continuous addition of reactive agents, the relatively slow reaction rates and the production of huge volumes of toxic sludge that has to be stabilized and safely disposed. Passive systems such as bioreactors and constructed wetlands may prove feasible alternatives; their efficiency is limited though by high AMD flow and toxic load (Goebes & Younger 2004; Batty & Younger 2004 and 2007; Hallberg & Johnson 2005; Younger *et al*. 2005; Neculita *et al.* 2007). Prevention of groundwater contamination in wider mining and waste disposal sites, caused by the migration of leachates, or clean up of contaminated groundwater may be enabled by the application of permeable reactive barriers (Amos & Younger 2003; Komnitsas *et al*. 2004 and 2006a; Doerr *et al.* 2005).

The ability to identify in advance mineral phases that can potentially produce AMD is essential for timely implementation of mine waste management strategies (Pagnanelli *et al*. 2004; Pinetown *et al.* 2007; Adams *et al.* 2007). A number of experimental static and kinetic procedures have been developed to determine the acid forming potential of mine wastes and sludges. The most widely used static tests are the Acid-Base Accounting (ABA) (Sobek *et al.* 1978) and the Net Acid Generation (NAG) (Miller *et al*. 1997) confirmation test. These tests may also define the boundary between non-acid forming and potentially acid forming phases present in a waste mass. The fact that organic or sulphate sulphur do not take part in acid generating reactions should not be neglected in such calculations. Kinetic tests are more reliable, involve a number of measurements over time and are used to assess the long term behaviour of potentially hazardous wastes. Kinetic NAG and free draining leach column tests are examples of kinetic procedures. Other tests can be used to assess the toxicity as well as to determine the bioavailable fractions and speciation of heavy metals (US EPA 1986 and 1990; Tessier *et al.* 1979).

The accurate prediction of leachability of hazardous elements is a difficult task because it depends on waste mineralogy, factors such as grain size and compaction degree, climatic conditions, understanding and simulation of specific geochemical issues in each area under study. Several studies were carried out over the last ten years to harmonize the various leaching/extraction tests that have been developed (Sahuquillo *et al*. 2003; van Der Sloot et al. 1997; van Der Sloot 2003). Long term evaluation studies are often required to accurately predict the volume and intensity of the potentially generated AMD and assess the contamination risk for surface- and groundwater (Sand *et al*. 2007; Trois *et al.* 2007). Leach columns which in most cases run under the assumption that oxygen is freely available throughout the sample provide in most cases reliable long

term results. Leachate analysis provides therefore a measure of the relative reactivity of a given sample under atmospheric oxygen concentration. If a column sample is too wet, then the assumption that oxygen is freely available is not valid. If a sample is too dry, secondary mineral solubility is triggered, so that the leachate collected significantly underestimates sulphide reaction rates. The required leach column test period varies and depends on waste characteristics and investigation needs; the results are usually reviewed on a 6 monthly basis.
In the present experimental study the reactivity of sulphidic wastes disposed of in a tailings dam at Bor, Serbia, as well as of the sludges from a stream receiving acidic leachates is assessed using the modified AMIRA protocol (ARD Test Handbook 2002).

STUDY AREA - MATERIALS – METHODS

Bor is a town of eastern Serbia with 40,000 inhabitants. The intensive mining and metallurgical activities over the past years resulted in the production of huge quantities of hazardous wastes that have been improperly disposed of in the vicinity of the town, causing thus widespread contamination of soil, surface- and groundwater. Flotation tailings have been disposed of in three tailing dams; the samples used in this study were collected from the walls (20 cm depth) of the operating Veliki Krivelj Dam 3A, which contains more than 50,000,000 t of tailings (Figure 1).

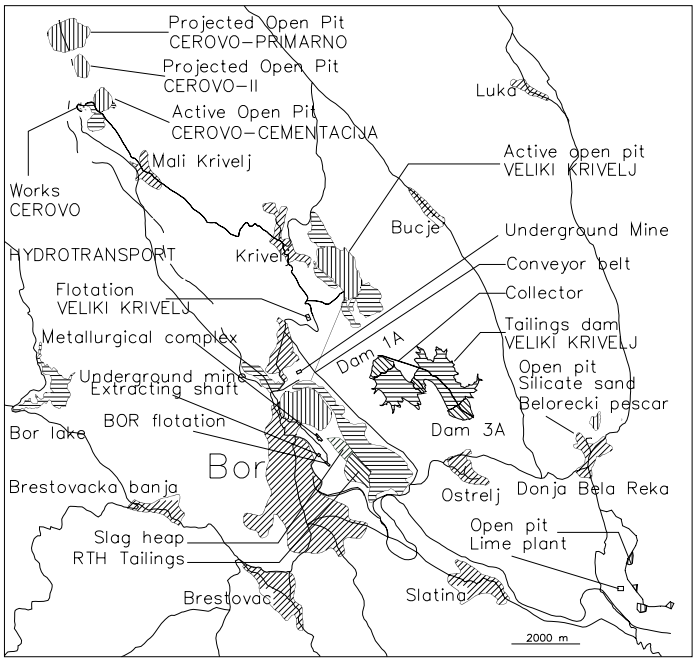

Figure 1: Map of the wider Bor area, showing the location of mining and metallurgical activities and dam 3A

Sludge samples were collected over a distance of 1 km from a stream receiving acidic leachates generated from the oxidation of the tailings at dam 3A. Composite samples were prepared in both cases using 4 waste

and 3 sludge samples.
The chemical analysis of the wastes averages SiO_2: 58.6 %, Al_2O_3: 17 %, CaO 4.8%, MgO 2.5%, K_2O: 2.4%, Na_2O: 3%, V_2O_5: 230 ppm, TiO_2: 250 ppm, Fe: 5.8%, Cu: 300-1000 mg/kg, Zn: 90 mg/kg, Pb: 17 mg/kg. The sulphur content of the sulphidic tailings and sludges was 1.9 % and 3.6 % respectively.
XRD analysis, carried out by a Siemens D500 diffractometer using Cu tube, scanning range between 3° and 70° 2-theta, step 0.03° and measuring time 4 sec/step indicates that the main mineralogical phases present in the sulphidic tailings are quartz (SiO_2), albite ($Na(AlSi_3O_8)$), gypsum ($CaSO_4$ $2H_2O$), kaolinite ($Al_4(OH)_8(Si_4O_{10})$), vermiculite ($Mg_3Si_4O_{10}(OH)_2$), illite ($K(AlFe)_2AlSi_3O_{10}$), clinochlore ($Mg_6Si_4O_{10}(OH)_8$), talc ($Mg_3(Si_2O_5)_2(OH)_2$) and jarosite ($K(Fe_3(SO_4)_2(OH)_6$). The main mineralogical phases identified in sludges are quartz, albite, kaolinite, calcite and illite.
For the assessment of the reactivity of the wastes and rivers sludges and therefore the estimation of the risk for surface- and groundwater the slightly modified AMIRA protocol was used. A conventional laboratory free draining leach column system was set-up to achieve a weekly wet-dry cycle and a monthly flushing cycle. Leach columns, having 13.5 cm internal diameter and 6 cm height, were filled with 500g of tailings (code A) or 500g of river sludges (code B) homogenously mixed with silica sand (ratio 1:1) to ensure adequate porosity. The samples were subjected to weekly wet-dry cycles. Samples A1 and B1 were wetted by applying 250 mL of deionised water, while samples A2 and B2 by applying 250 mL of simulated acid rain solution (H_2SO_4:HNO_3, 60:40 w%, pH 3 ± 0.2), that account for 1000 mm annual rainfall, which is typical for the area under study. Acid rain solution was used to simulate conditions prevailing in industrial areas. 40 W heat lamps were used to ensure drying of the samples between applications of solutions. The laboratory test conditions are summarised in Table 1.
Leachates were collected every week and analysed for volume, pH, oxidation-reduction potential (using a Hanna 211 pH/Eh meter), electrical conductivity (using a Hanna EC215 conductivity meter), SO_4^{2-} concentration (using a visible spectrophotometer Hach 3450, λ=450nm) and metals concentration, i.e. Fe, Al, Cu, Mn, Zn, Ni and Pb (using a Perkin-Elmer Analyst 100 atomic absorption spectrophotometer). Solid samples were collected after an experimental period of 60 weeks and analyzed to detect the formation of any new mineralogical phases. All experiments as well as analyses were carried out in duplicate.

RESULTS AND DISCUSSION

Experimental results are seen in the following Figures. Figure 2 shows pH, and Eh (mV) variation in the leachates over time. Figures 3-6 show the cumulative Fe, Al, Cu and Mn dissolution (in μg/g waste or sludge) over time. Figure 7 shows the cumulative SO_4^{2-} dissolution (in mg/g waste) over

time (A denotes Bor sulphidic wastes, B denotes Bor river sludges; 1 denotes use of water while 2 denotes use of simulated acidic rain as leaching agent).

Funnels	*Code*	*Tailings weight (g)*	*Sludge weight (g)*	*Silica sand weight (g)*	*Deionised water addition (mL)*	*Acid rain addition (mL)*
Homogenous mixture of suphidic tailings and silica sand (1:1)	A1	500	-	500	250	-
	A2	500	-	500	-	250
Homogenous mixture of sludges and silica sand (1:1)	B1	-	500	500	250	-
	B2	-	500	500	-	250

Table 1: Test conditions

The experimental results over a period of 70 weeks show that:
pH of leachates generated from tailings and river sludges drops gradually over a period of 30 weeks and then increases slightly until week 70, ranging between 2.7 and 3.8. It is seen that while the initial pH of the leached river sludges varies between 6 and 7, pH of the sulphidic tailings is just above 4, indicating thus continuous generation of acidity. The limited presence of acid consuming minerals both in wastes and sludges causes this fast drop of pH. It is clearly seen from the following figures that higher dissolution of heavy metal and sulphates is seen after almost 20 weeks, when pH drops to values below 4; this may also cause, especially for river sludges, secondary dissolution of initially precipitated phases. Manganese, due to its increased mobility over a large pH range, is solubilised much more easily; its concentration though in the leachates is limited.
Eh of leachates ranged the first 30 weeks between 200 and 280 mV, indicating the development of mild oxidation conditions in the systems studied. Then it started to gradually drop and after 80 weeks ranged between 170 and 240 mV.
Conductivity values (data not seen) are in line with pH and Eh measurements, increase gradually the first 30 weeks and then start to drop and range between 0.9 and 2.7 mS/cm.
Al and Cu are the elements exhibiting the highest solubility for sulphidic tailings; relatively high solubility is seen for Mn until week 30, while Zn, Ni, Pb (data not seen) exhibit limited solubility. The dissolution of iron from the tailings is limited and does not exceed 100 µg/g over a period of 70 weeks

even when simulated acid rain is used as leaching agent; this is probably due to previous solubilisation of iron present in the surface tailings and its subsequent deposition in deeper horizons. Iron dissolution from the sludges is initiated after 20-30 weeks and slows down after 50 weeks, reaching 3.8 and 11 mg/g when deionised water and simulated acid rain is used, respectively.

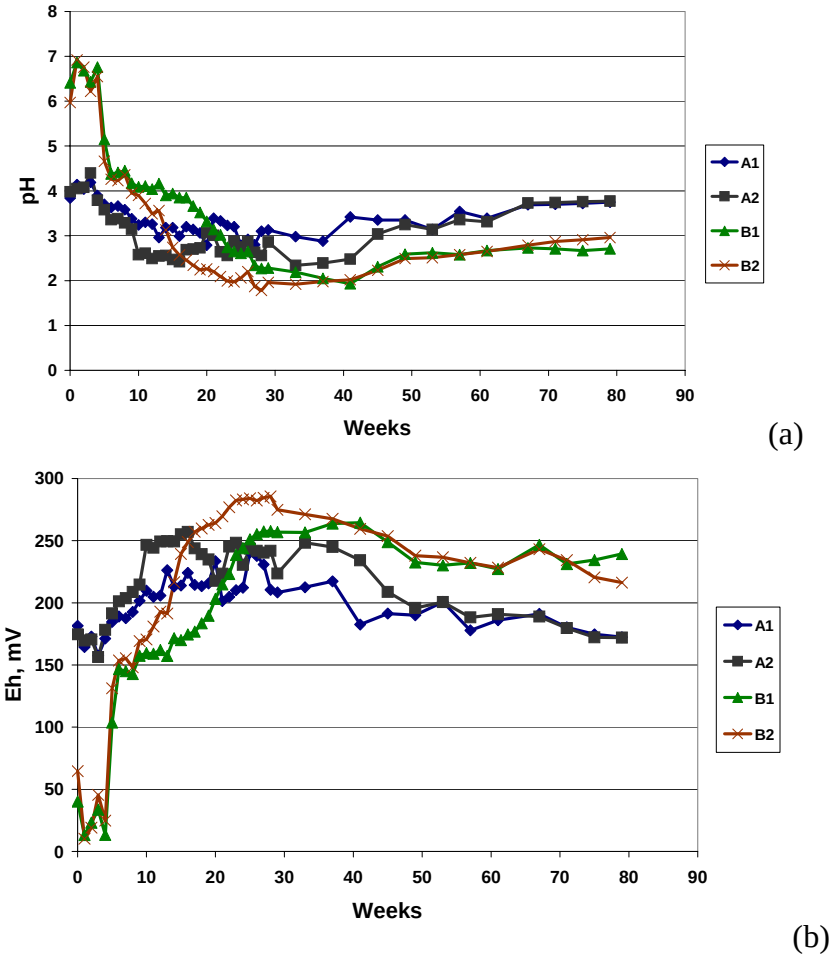

Figure 2: (a) pH and (b) Eh variation vs. time

Dissolution of aluminium from the tailings is continuous and reaches 350 and 700 µg/g when deionised water and simulated acid rain is used respectively. Dissolution of aluminium from the river sludges is initiated after 10-20 weeks and varies between 480 and 850 µg/g when deionised water and simulated acid rain is used respectively. This is due to gradual solubilisation of previously precipitated aluminium compounds. Dissolution of copper from the tailings is almost identical for both leaching media and after 70 weeks reaches 190 µg/g. Dissolution of copper from river sludges shows a similar trend with aluminium and after 70 weeks reaches 210 and 300 µg/g respectively. The reduced solubility of copper may be due to sorption/co-precipitation on/with Fe and Al hydroxides and hydroxyl-sulphates. Manganese solubility is continuous but limited in all cases and varies between 50 and 80 µg/g.

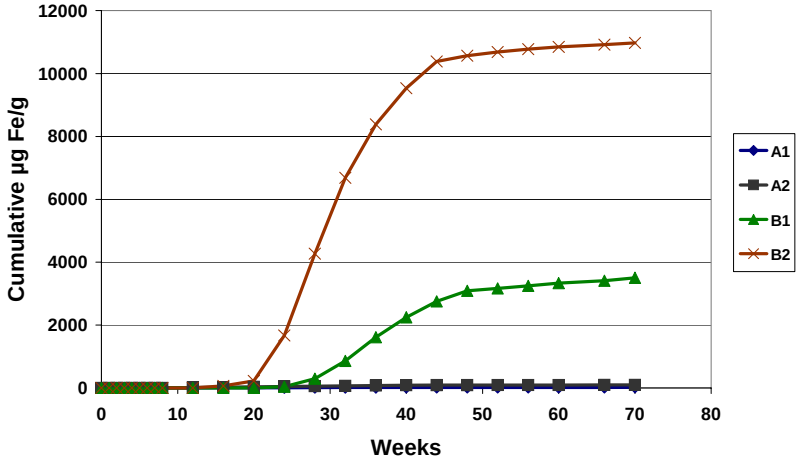

Figure 3: Cumulative dissolution of Fe over time

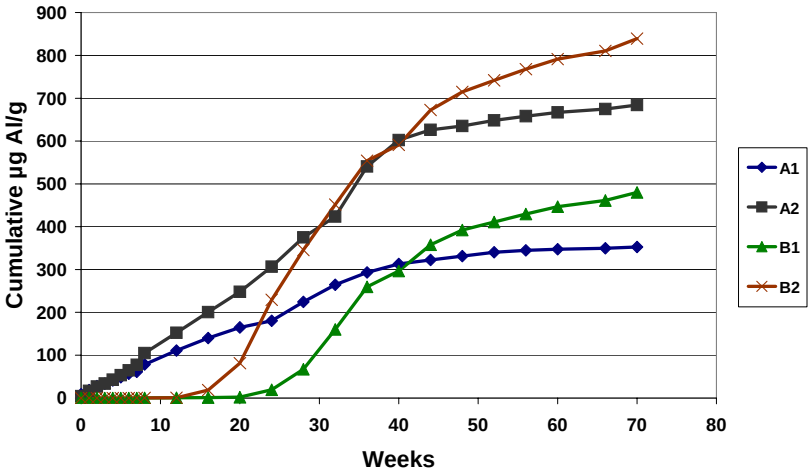

Figure 4: Cumulative dissolution of Al over time

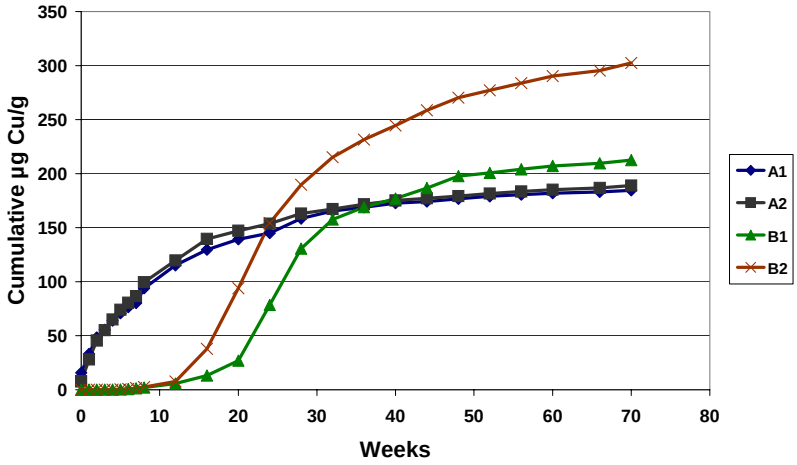

Figure 5: Cumulative dissolution of Cu over time

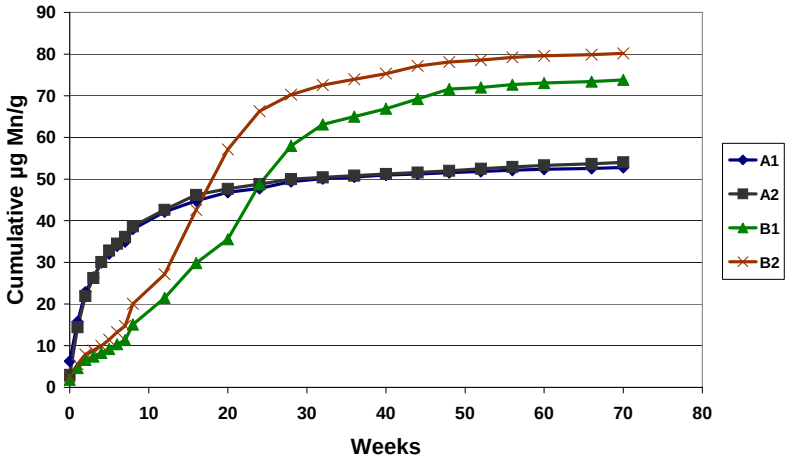

Figure 6: Cumulative dissolution of Mn over time

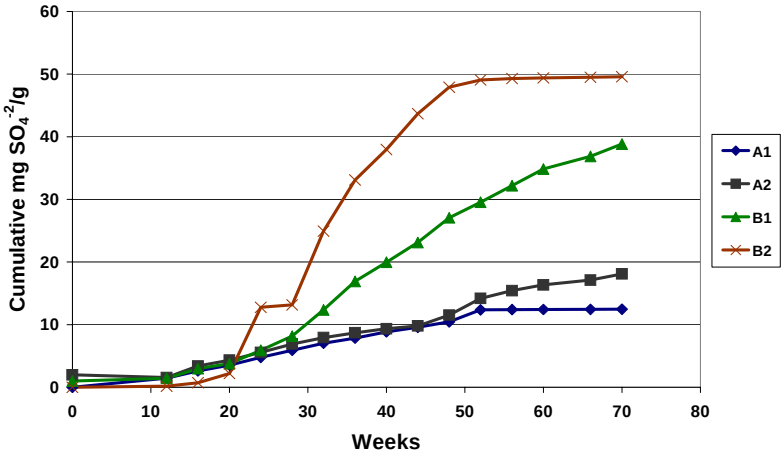

Figure 7: Cumulative dissolution of SO_4^{-2} over time

SO_4^{2-} dissolution is quite high, exceeding 10 and 40 mg/g after 70 weeks for tailings and river sludges respectively when deionised water is used. Higher values are seen when simulated acid rain is used as leaching agent. The reduced sulphate concentration seen in the leachates at early stages, when pH values are higher than 4.7, is probably due to dissolution of CaO and subsequent precipitation of gypsum (Komnitsas *et al.* 2006b).
The experimental results show that the reactivity of sulphidic tailings and river sludges over the period studied is noticeable, therefore the risk for regional water contamination is high and immediate action should be taken. The absolute cumulative values for the heavy metals studied may be small, but if the total volume of the disposed tailings is taken into account then the toxic flux that is generated from dam 3A and enters the receiving stream is very high. If for example is considered that only the upper 10% of the wastes contained in the dam (5,000,000 t) is subjected to oxidation, then 900 t of copper are solubilised over a period of 70 weeks and enter the receiving stream. Part of this quantity reaches Danube which flows a few kilometres downstream.

It is known that the acidity generated from sulphide oxidation depletes carbonate and Al-silicate minerals present in the tailings up to a certain depth that may vary between 1-6 meters. In some cases a hardpan layer consisting of secondary minerals may be formed resulting thus in inhibition of leachates migration to deeper tailing horizons and in reduced reactivity of dam base wastes due to limited infiltration of oxygen (Moncur et al, 2005). This effect was not considered though in the present study.
While it was somehow anticipated that the reactivity of the tailings, although they have been disposed of over a long period, could be still high, the noticeable reactivity of the river sludges, which are continuously washed by water, was not expected. It is therefore confirmed that the receiving stream bed, due to continuous precipitation and re-solubilisation of secondary mineral phases, can hardly sustain any form of aquatic life; similar impacts have been reported elsewhere (Kuma *et al.* 2004; Olías *et al.* 2006; Lin *et al.* 2007).
Heterotrophic microorganisms present in wastes and especially river sludges accelerate solubilisation of hazardous elements and therefore enhanced migration to longer distances is expected (Willscher *et al.* 2007; INTREAT 2007); this factor though was not considered in the present experimental study.
It is clearly seen from the experimental data that the release of hazardous ions from the tailing dam at Bor, despite the fact that the flux of dissolved ions exhibits seasonal variations and depends on precipitation in the area under study, affects the water chemistry and the ecotoxicity of the stream sediments and contributes to the contamination of Danube.
In order to reduce the risk for contamination of surface- and groundwater in the wider area remedial technologies such as isolation of the tailings by the application of a (vegetative) cover or amendment of the upper part of the tailings with alkalinity producing materials should be immediately considered. The application of a vegetative cover requires addition of nutrients and organic matter. These actions will minimize erosion and water infiltration into the tailings mass eliminating thus the generation of acidity. In addition they will result in stabilization of the dam walls and prevention of potential future leakage that may endanger bank stability. Such geotechnical issues should be considered by taking into account a flood event scenario with a return period of even 100 years to avoid environmental disasters, similar to those happened in Wheal Jane, UK, in 1992 (Neal *et al.* 2005), Aznalcollar, Spain, in 1998 (Morillo *et al.* 2005) and Baia Mare, Romania in 2000 (Kraft *et al*. 2006).

CONCLUSIONS

Laboratory experiments carried out using the modified AMIRA protocol to assess the reactivity for sulphidic wastes and river sludges at Bor, Serbia, show increased long term solubilisation and migration of heavy metals and sulphates, affecting thus severely the water chemistry and the ecotoxicity of the stream sediments and ultimately contributing to the contamination of Danube.

River sludges exhibit increased heavy metal and sulphate solubility when either deionised water or simulated acid rain is used; this indicates that the stability of the previously formed precipitates is rather limited and gradual solubilisation occurs when fresh acidic leachates, generated from the oxidation of the dam tailings, enter the receiving stream.
It is therefore concluded that in order to mitigate environmental impacts immediate action should be taken so that the surface of the tailings is maintained permanently unexposed. Such measures may include the application of a (vegetative) cover or mixing the upper layer of the tailings with acid consuming materials (e.g limestone or fly ash), which will also result in stabilization of the dam walls and minimization of geotechnical risk.

ACKNOWLEDGEMENTS

The financial support of the European Commission in the framework of the FP6 STREP project entitled “Integrated treatment of industrial wastes towards prevention of regional water resources contamination” (INTREAT), (FP6-2002-INCO-WBC-1, Contract No: INCO-CT-2003-509167) is greatly acknowledged.

REFERENCES

Adams, R. *et al*. 2007. Investigating the potential for ongoing pollution from an abandoned pyrite mine. *Mine Water and the Environment*, Vol. 26 (1), 2-13.

Amos, P.W. & Younger, P.L. 2003. Substrate characterisation for a subsurface reactive barrier to treat colliery spoil leachate. *Water Research*, Vol. 37 (1), 108-120.

ARD Test Handbook, 2002. Prediction and Kinetic Control of Acid Mine Drainage, Ian Wark Research Institute. Environmental Geochemistry International Pty Ltd, Australia.

Batty, L.C. & Younger, P.L. 2004. The use of waste materials in the passive remediation of mine water pollution. *Surveys in Geophysics*, Vol. 25 (1), 55-67.

Batty, L.C. & Younger, P.L. 2007. The effect of pH on plant litter decomposition and metal recycling in wetland mesocosmos supplied with mine drainage. *Chemosphere*, Vol. 66 (1), 158-164.

Bhattacharya, A. *et al*. 2006. Environmental assessment of abandoned mine tailings in Adak, Västerbotten district (northern Sweden). *Applied*

Geochemistry, Vol. 21 (10), 1760-1780.

Doerr, N.A. *et al*. 2005. Effects of a reactive barrier and aquifer geology on metal distribution and mobility in a mine drainage impacted aquifer. *Journal of Contaminant Hydrology*, Vol. 78 (1-2), 1-25.

INTREAT Annual Project Report 2005. Contract No INCO-CT-2003-509167, Technical University Crete.

Goebes, M.D. & Younger, P.L. 2004. A simple analytical model for interpretation of tracer tests in two domain subsurface flow systems. *Mine Water and the Environment*, Vol. 23 (3), 138-143.

Hallberg, K.B. & Johnson, D.B. 2005. Microbiology of a wetland ecosystem constructed to remediate mine drainage from a heavy metal mine. *Science of the Total Environment*, Vol. 338 (1-2), 53-66.

Johnson, D.B. & Hallberg, K.B. 2005. Acid mine drainage remediation options. A review. *Science of the Total Environment*, Vol. 38 (1-2), 3-14.

Kontopoulos, A. *et al.* 1995. Environmental characterisation of the sulphidic tailings in Lavrion. *Minerals Engineering*, Vol. 8 (10), 1209-1219.

Komnitsas, K. *et al*. 2004. Efficiency of limestone and red mud barriers: laboratory column studies. *Minerals Engineering*, Vol. 17, 183-194.

Komnitsas, K. *et al*, 2006a. Inorganic contaminant fate assessment in zero-valent iron treatment walls. *Environmental Forensics*, Vol. 7, 207-217.

Komnitsas, K. *et al*. 2006b. Modeling of reaction front progress in fly ash permeable reactive barriers. *Environmental Forensics*, Vol. 7, 219-231.

Kraft, C. *et al.* 2006. The effects of mining in Northern Romania on the heavy metal distribution in sediments of the rivers Szamos and Tisza (Hungary). *Acta Hydrochimica et Hydrobiologica*, Vol. 34 (3), 257-264.

Kuma, J.S. *et al*. 2004. Water quality trends in the Tarkwa gold-mining district, China. *Bulletin of the Engineering Geology and the Environment*, Vol. 63 (2), 119-132.

Lin, C. *et al*. 2007. Water chemistry and ecotoxicity of an acid mine

drainage affected stream in subtropical China during a major flood event. *Journal of Hazardous Materials*, Vol. 142 (1-2), 199-207.

Miller, S. *et al*. 1997. Advances in Acid Drainage Prediction Using the Net Acid Generation (NAG) Test. *4th International Conference on Acid Rock Drainage*, Vancouver, May 31-June 6, II, 535-549.

Moncur, M.C. *et al*. 2005. Release, transport and attenuation of metals from an old tailings impoundment. *Applied Geochemistry*, Vol. 20 (3), 639-659.

Morillo, J. *et al.* 2005. Study of fractionation and potential mobility of metal from the Guadalquivir estuary: Changes in mobility with time and influence of the Aznalcollar mining spill. *Environmental Management*, Vol. 36 (1), 162-173.

Neal, C. *et al.* 2005. The water quality of the River Carnon, west Cornwall, November 1992 to March 1994: The impacts of Wheal Jane discharges. *Science of the Total Environment*, Vol. 338 (1-2), 23-39.

Neculita, C.M. *et al*. 2007. Passive treatment of acid mine drainage in bioreactors using sulphate reducing bacteria: Critical review and research needs. *Journal of Environmental Quality*, Vol. 36 (1), 1-16.

Olías, M. *et al*. 2006. Evaluation of the dissolved contaminant load transported by the Rio Tinto and Odiel rivers (South West Spain). *Applied Geochemistry*, Vol. 21 (10), 1733-1749.

Pagnanelli, F. *et al*. 2004. Sequential extraction of heavy metals in river sediments of an abandoned pyrite mining area: pollution detection and affinity series. *Environmental Pollution,* Vol. 132 (2), 189–201.

Peppas, A. *et al*. 2000. Use of organic covers for acid mine drainage control. *Minerals Engineering*, Vol. 13 (5), 563-574.

Pérez-López, R. *et al*. 2007. Utilization of fly ash to improve the quality of the acid mine drainage generated by oxidation of a sulphide rich mining waste : Column experiments. *Chemosphere*, Vol. 67 (8), 1637-1646.

Pinetown, K.L. *et al*. 2007. Quantitative evaluation of minerals in coal deposits in Witbank and Highveld coalfields and the potential impact on acid mine drainage. *International Journal of Coal Geology*, Vol. 70 (1-3), 166-183.

Ritcey, G.M. 1989. Tailings management: problems and solutions in the mining industry. New York: Elsevier.

Sahuquillo, A. *et al*. 2003. Overview of the use of leaching/extraction tests for risk assessment of trace metals in contaminated soils and sediments. *Trends in Analytical Chemistry*, Vol. 22 (3), 152-159.

Sand, W. *et al*. 2007. Long-term evaluation of acid rock drainage mitigation measures in large lysimeters. *Journal of Geochemical Exploration*, Vol. 92 (2-3), 205-211.

Sobek, A.A. *et al*. 1978. Field and Laboratory Methods Applicable to Overburden and Minesoils. Cincinnati, Ohio: U.S EPA.

US EPA, 1986. Toxicity characteristic leaching procedure, Appendix 1, Federal Register 51(216).

US EPA, 1990. Characteristics of EP Toxicity. Paragraph 261.24, Federal Register 45(98.

Tessier, A. *et al.* 1979. Sequential extraction procedure for the speciation of particulate trace metals. *Analytical Chemistry*, Vol. 51 (7), 844-851.

Trois, C. et al. 2007. The environmental risk posed by small dumps of complex arsenic, antimony, nickel and cobalt sulphides. Journal of Geochemical Exploration, Vol. 92 (1), 83-95.

van Der Sloot, H.A. *et al*. 1997. Harmonisation of leaching/extractions tests. Studies in environmental science 70. Amsterdam, Elsevier Science.

van Der Sloot, H.A. 2003. Horizontal standardisation of test methods for waste, secondary raw materials, construction materials, sludge, biowaste and (contaminated) soil. *Waste Management*, Vol. 23 (9), v.

Willscher, S. *et al*. 2007. Solubilisation of heavy metals from a fluvial AMD generating tailings sediment by heterotrophic microorganisms. Part I: Influence of pH and solid content. *Journal of Geochemical Exploration*, Vol. 92 (2-3), 177-185.

Younger, P.L. *et al.* 2005. The contribution of science to risk based decision making: Lessons from the development of full scale treatment measures for acidic mine waters at Wheal Jane, UK. *Science of the Total Environment*, Vol. 338 (1-2), 137-154.

Quaternary geological and till geochemical studies in verifying GIS-based prospectivity mapping in the Central Lapland Greenstone Belt, northern Finland

Sarala P., Nykänen V., Sarapää O., Peltoniemi A. and Ojala V. J.

Geological Survey of Finland
P.O. Box 77, FIN-96101 Rovaniemi, FINLAND.
E-mail: pertti.sarala@gtk.fi
Keywords: Glacial geology, till geochemistry, gold, exploration, prospectivity mapping, Finland

ABSTRACT

The Geological Survey of Finland has explored for gold since early 1980's in the Central Lapland Greenstone Belt in northern Finland. The whole area is proven to have potential for Au mineralization, in addition to three gold mines over 30 drilling indicated occurrences have been located. New methods have been used to define the most prospective areas for gold exploration in this district. GIS-based prospectivity analysis is one of them and four target areas (Vuomanperänmaa, Nuttiot, Petäjäselkä and Lauttaselkä) have been selected for detailed exploration. The aim has been to use surficial geological methods to test the GIS generated target areas and also to focus exploration. In the target areas, up to six metres deep pits and trenches have been dug to study the till stratigraphy, and to get samples for geochemical and heavy mineral studies. These methods proved to be effective and fast to get information of the till deposits and to estimate the glacial transport distance of mineralized material. The results of this study strengthen the decision to continue gold exploration in all the selected target areas.

INTRODUCTION

Since joining the European Union in 1994, gold exploration has increased steadily in Finland. Particularly the Palaeoproterozoic Central Lapland Greenstone Belt (CLGB) has been in the centre of investigations of international exploration companies and the Geological Survey of Finland (GTK). The whole area is proven to have potential for Au mineralization and many Au deposits have been already found including three Au mines, Saattopora (1988-1995), Pahtavaara (in operation) and Suurikuusikko (under construction). Of those deposits, Pahtavaara and Suurikuusikko were located by the GTK by using till geochemical methods.
Large amounts of data have been collected from the CLGB during several geological, geophysical and geochemical mapping projects and numerous exploration programs, and with the use of GIS software, the data can be effectively handled and used in prospectivity analysis. Also, traditional exploration methods, e.g., till stratigraphy, till geochemistry and heavy mineral studies (Hirvas *et al.* 1977; Hirvas 1989, 1991; Hirvas & Nenonen 1990) can still powerful tools due to increased knowledge of glacial dynamics and deposition processes in the central areas of large Scandinavian continental glacier (Sarala 2005).

Prospectivity mapping

GIS based prospectivity analysis can be used to define target areas inside a large exploration area. The aim is to integrate spatially referenced data from various sources to generate a single response theme, a mineral potential or a prospectivity map (Bonham-Carter 1994). The software used in this study is a freely downloadable add-on called ArcSDM (Sawatzky *et al.* 2004) to a commercial ArcGIS 9.1. High-resolution airborne multi-element geophysical survey data, radiometric, magnetic and electromagnetic ground survey datasets and a nationwide till geochemical dataset in resolution with 1 sample per 4 km^2 are used in the analysis. For several exploration target areas within the CLGB also datasets derived from more detailed surveys are available. Bedrock mapping and Quaternary geology mapping programs have generated vast databases of field observations and geological maps that, as fully attributed digital versions are also suitable for spatial data analysis. The known examples of the Au mineralized targets are being used as training sites in the empirical prospectivity modelling.

Study area and methods

The prospectivity mapping defines many target areas potential for Au exploration (Nykänen & Salmirinne 2007; Nykänen *et al.* in press). Four target areas (Vuomanperänmaa, Nuttiot, Petäjäselkä and Lauttaselkä) have been selected for detailed studies (Fig. 1). These targets situate between the presently active gold mine Pahtavaara (in situ resource estimate of 15 t gold) and Kittilä mine (Suurikuusikko deposit; in situ resource estimate of 110 t gold), which is planned to start production in 2008 (FINGOLD Database). The aim has been to field test the high prospectivity targets defined by the prospectivity mapping. In the field, the structure and composition of the glacial overburden have been analyzed using up to 6 m deep test pits and trenches. Till samples were collected for geochemical (200-300 g/sample) and heavy mineral studies (12 litre/sample; concentrated by mechanical spiral separator), and counting the proportion of different rock types in the pebble size fraction (50 pieces/sample). In addition, weathered bedrock and fresh bedrock were sampled where the bedrock was reached. Systematic percussion till sampling with a 200x200 m grid was also done as well as complementary bedrock and erratic boulder mappings. Chemical analyses of till size fraction <0.06 mm have been done in GTK's laboratory using GAAS and ICP-AES instruments after partial dissolving. Furthermore, earlier exploration data (till geochemistry, geophysics, bedrock and boulder observations) have been integrated into the new datasets.

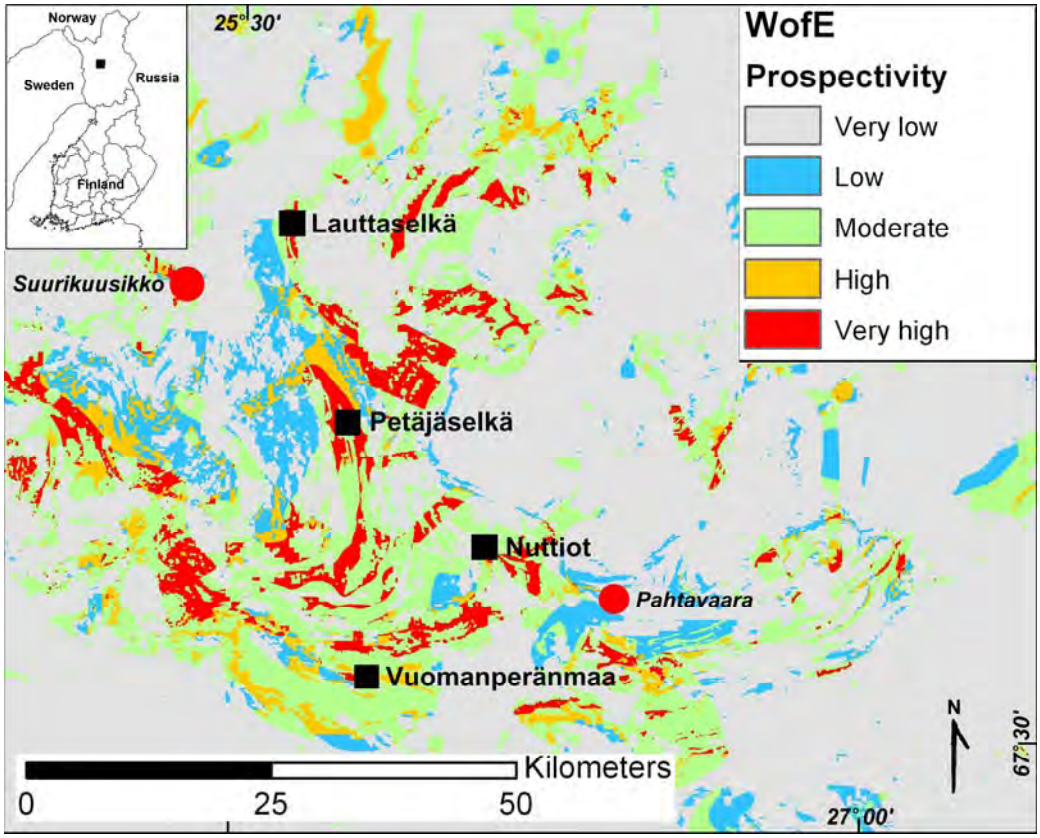

Fig. 1. A location of the four target areas in Central Lapland Greenstone Belt in northern Finland.

RESULTS

Preliminary results of the till geochemistry and heavy mineral analyses indicate that the GIS-based prospectivity modelling is an effective method generating viable targets for Au exploration. Glacial overburden is 2-6 m thick and it consists of 1-2 sandy till units. The angular shape of pebbles indicates quite short glacial transportation in the lower till unit. The proportion of long-distance rocks (> 15 km), like granite and gneiss, which are not seen in local outcrops, is low in all sampled sites. Bedrock is commonly covered by few centimetres to 3 metres thick weathering crust. The mixture of material from the weathering crust into till is problematic in places due to different element rations in weathered material compared to till derived from fresh bedrock. Heavy mineral studies indicate that background gold nugget counts are from zero to two per 12 l sample.

Till geochemistry and heavy mineral studies show that all target areas have anomalous Au concentrations in till. In the Vuomanperänmaa and Nuttiot areas the highest Au contents (10-35 ppb) indicate Au enrichment at the contact zones between different lithological units. The bedrock of the targets is composed of mafic volcanic and sedimentary rocks (mica schists and black schists; Fig. 2), metamorphosed at upper greenschist facies conditions. Deformed zones with carbonatization and occasional quartz mark hydrothermal alteration in the bedrock.

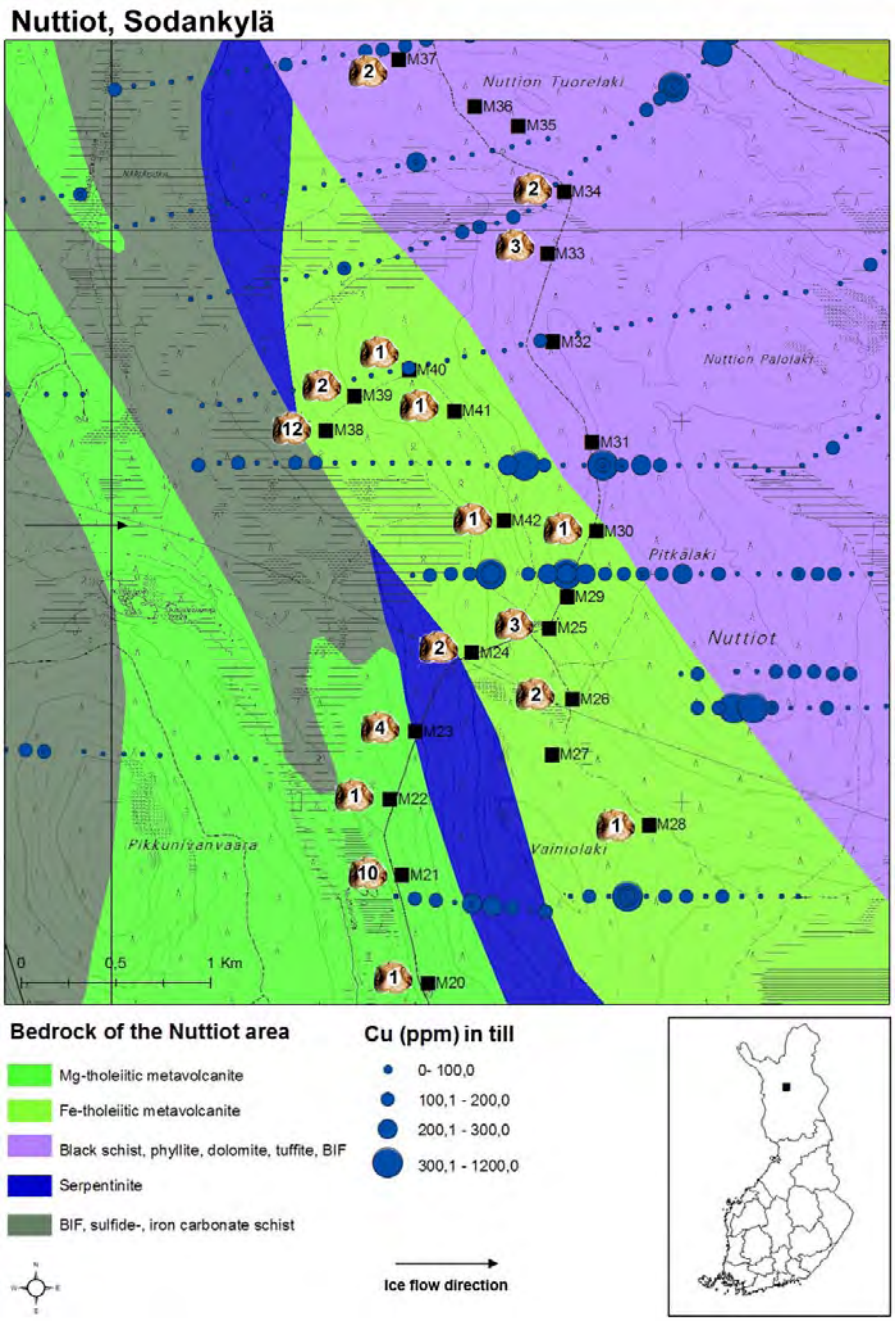

Fig. 2. Till geochemical (AAS) and heavy mineral sampling site on the geological map of the Nuttiot area. Bold numbers indicate the total number of Au nuggets in heavy mineral samples (ca. 12 l) of the test pits (1-2 samples/test pit) marked as M20-M42.

Furthermore, banded iron formation (BIF) black schists and serpentinite units in the Nuttiot ophiolite area are clearly seen in pebble and boulder composition of till. In the Nuttiot target 2-4 gold nuggets per heavy mineral sample were found on the distal side of the Au-mineralized shear zone at the contact zone between serpentinites and volcanic rocks (Fig. 2).

In the Petäjäselkä target area the gold anomalous zone follows a hetero-geneous and deformed NNW trending zone of graphic tuffs, cherts and intermediate volcanic rocks within a mafic volcanic rock dominated domain. In addition to deformation zones subparallel the main trend, the area is cut by NE-SW shear zones. Gold contents in till are strongly anomalous (ranging 10 ppb to 900 ppb) at the several sampling sites. The highest contents (from 200 ppb to 900 ppb) were in till in the 100 m long, west-east oriented test trench (2006 AMPE-000009), in which the shear zone hosted Au mineralization was exposed (Fig. 3). Glacial transport distance (or dilution distance of till material) is short: the distal tail at the anomalous Au contents is only about 50 m from the bedrock source. In heavy mineral sampling, 21 Au nuggets were found in till above the Au-mineralized shear zone.

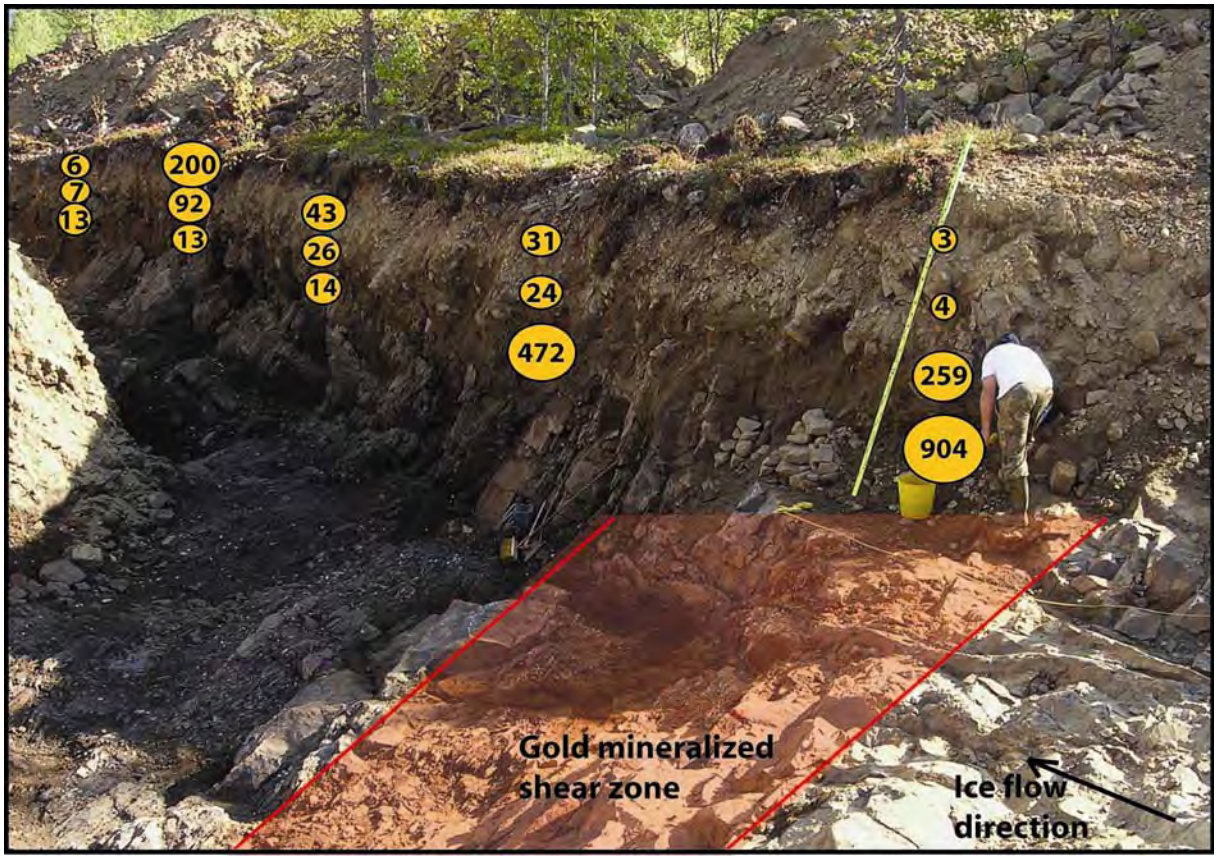

Fig. 3. Gold contents (ppb) in <0.06 mm size fraction in till on the test trench M9 in Petäjäselkä. Samples were analyzed by GAAS. Photo P. Sarala.

Lauttaselkä is the latest target under testing. Test pit excavations have been done during the late autumn 2006 and till geochemical sampling by percussion drilling will be finished before summer 2007. The bedrock in the target is composed of mafic volcanic rock, black schist and serpentinite, which have been strongly altered (carbonatized with quartz and graphite veins) in places. Till geochemical analyses are not ready at the time of writing this paper but the heavy mineral study indicates gold mineralization in the local bedrock. Gold nugget counts (12 l samples) indicate Au mineralization related to the alteration zones. The highest amount is 18 nuggets

in the weathered bedrock sample and the nugget counts in till are 2-5 in the down-ice direction (eastern side of the alteration zone).

CONCLUSIONS

Till geochemical and heavy mineral analyses in the CLGB, northern Finland indicate that GIS-based prospectivity analysis is a practical tool to define new gold target areas. Detailed surficial geological studies including geomorphological and till stratigraphical investigations, geochemical and heavy mineral sampling are effective methods in focusing exploration in the target areas. All field tested sites have shown signs of anomalous gold geochemistry, elevated nugget counts and sericite-carbonate-sulphide alteration in the bedrock typical to the other gold occurrences in the region. In the near future drilling programs will be carried out in our target areas to get more information and samples from the most promising structures and alteration zones in bedrock.

REFERENCES

Bonham-Carter, G.F. 1994. Geographic Information Systems for Geoscientists – Modelling with GIS. Computer Methods in the Geosciences 13. Pergamon Press, New York, 398 p.

FINGOLD Database. Gold deposits in Finland, Geological Survey of Finland, 02/05/2007, http://en.gtk.fi/ExplorationFinland/Commodities/Gold/gtk_gold_map.html.

Hirvas, H. 1989. Application of glacial geological studies in prospecting in Finland. In: DiLabio, R.N.W., Coker, W.B. (Eds.), Drift Prospecting. Geol. Surv. Canada, Pap. 89 - 20, 1-6.

Hirvas, H. 1991. Pleistocene stratigraphy of Finnish Lapland. Geological Survey of Finland, Bulletin 354, 123 p.

Hirvas, H., Alftan, A., Pulkkinen, R., Purnanen, R. & Tynni, R. 1977. Raportti malminetsintää palvelevasta maaperätutkimuksesta Pohjois-Suomessa vuosina 1972-1976. Summary: A report on glacial drift investigations for ore prospecting purposes in northern Finland 1972-1976. Geological Survey of Finland, Report of Investigation 19, 54 p.

Hirvas, H. & Nenonen, K. 1990. Field methods for glacial indicator tracing. In: Kujansuu, R., Saarnisto, M. (Eds.), Glacial indicator tracing. Balkema, Rotterdam, pp. 217-247.

Nykänen, V. 2006. Spatial analysis as prospectivity mapping tool. Geological Survey of Finland 1/12/2006. http://en.gtk.fi/Research/CR/Spatial_analysis.html; e-mail: *vesa.nykanen@gtk.fi*

Nykänen, V.M., Groves, D.I., Ojala, V.J. & Gardoll, S. (in press). Combined conceptual/empirical prospectivity mapping for orogenic gold in the Northern

Fennoscandian Shield, Finland. Australian Journal of Earth Sciences, Thematic Issue on Conceptual Targeting.

Nykänen, V.M. & Salmirinne, H. 2007. Prospectivity analysis of gold using regional geophysical and geochemical data from the Central Lapland Greenstone Belt, Finland In: Ojala VJ (ed.) Gold in the Central Lapland Greenstone Belt. Geological Survey of Finland, Special Paper 44, 235-253.

Sarala, P. 2005. Glacial morphology and dynamics with till geochemical exploration in the ribbed moraine area of Peräpohjola, Finnish Lapland. PhD thesis, Geological Survey of Finland, Espoo, 17 p + 6 original articles.

Lithogeochemistry of the volcanic sequence hosting the río tinto ore deposit (Iberian pyrite belt, Spain).

Conde, C., Tornos, F., González-Clavijo E., Mellado, D. and Martín Rubí, J. A

Instituto Geológico y Minero de España. Of. de Proyectos de Salamanca. Azafranal, 48, 1ºA. 37001. Salamanca, España. E-mail: c.conde@igme.es Saloro, S.L. Avd. Italia, 8. 37006. Salamanca, España
Laboratorios Generales del Instituto Geológico y Minero de España. Caldera, 1. 28760. Tres Cantos, Madrid. España
Keywords: Río Tinto, lithogeochemistry, volcanic rocks, immobile-element, massive sulphides, IPB, Spain

ABSTRACT

The complex geological setting of the Rio Tinto mine makes difficult to define its general stratigraphic sequence and the nature of the ore hosting rocks. Based on geological data and immobile-element ratios, two main volcanic units have been identified. The lower Mafic-Siliciclastic Unit consists of basaltic-andesite and high Ti-Zr basalt that show a tholeiitic affinity. The overlying Felsic Unit hosts the massive sulphides and is volumetrically dominant. It is formed by massive and volcaniclastic rocks with dacitic to rhyodacitic composition. HREE, Al, Y, Zr, Ti and Yb contents of all the felsic rocks are similar, suggesting that they derived from a single magmatic pulse. Thus, the geochemical data support that the volcaniclastic rocks interbedded with the massive ones are not exotic distal aprons but product of the synvolcanic erosion of the coetaneous sills and domes. All these rocks have been affected by a widespread hydrothermal alteration related with the formation of the massive sulphides. The TiO_2 vs. Zr plot suggests that both the mafic and felsic rocks have had an analogous alteration, dominated by chloritic and sericitic assemblages.

INTRODUCTION

The Río Tinto district is probably the largest concentration of volcanic-hosted massive sulphides in the earth's crust, with more than 2,500 Mt of pyrite-rich massive sulphides and an underlying Cu-bearing stockwork (Leistel *et al.* 1998; Tornos, 2006). It is located in the eastern Iberian Pyrite Belt (IPB) and, in detail, it includes six lenses of massive sulphides (Filón Norte, Filón Sur, San Dionisio, Salomón, Lago and Planes-San Antonio) as well as a large zone of hydrothermal alteration with irregular stockwork ore. The complex deformation and pervasive hydrothermal alteration have been major obstacles when trying to map the area and correctly identify the lithostratigraphic sequence.
Lithogeochemical studies are a powerful technique for correlating volcanic sequences in highly deformed, hydrothermally altered or metamorphosed volcanic sequences. Thus, they have been actively used for the understanding and mineral exploration in several volcanogenic massive sulphide (VMS) districts such as the Bathurst camp, Tasmania, or the Skellefte district (Lentz, 1999; Gemmell & Fulton, 2001; Barret *et al.* 2005; Montelius, 2005). In this contribution, we present a geochemical study of the volcanic rocks of the Rio Tinto district using the

geochemistry of the major and immobile elements with the main objective of identifying their original composition, characterize the different units and for assisting in the geological reconstruction of the lithostratigraphic sequence in this complex mining area.

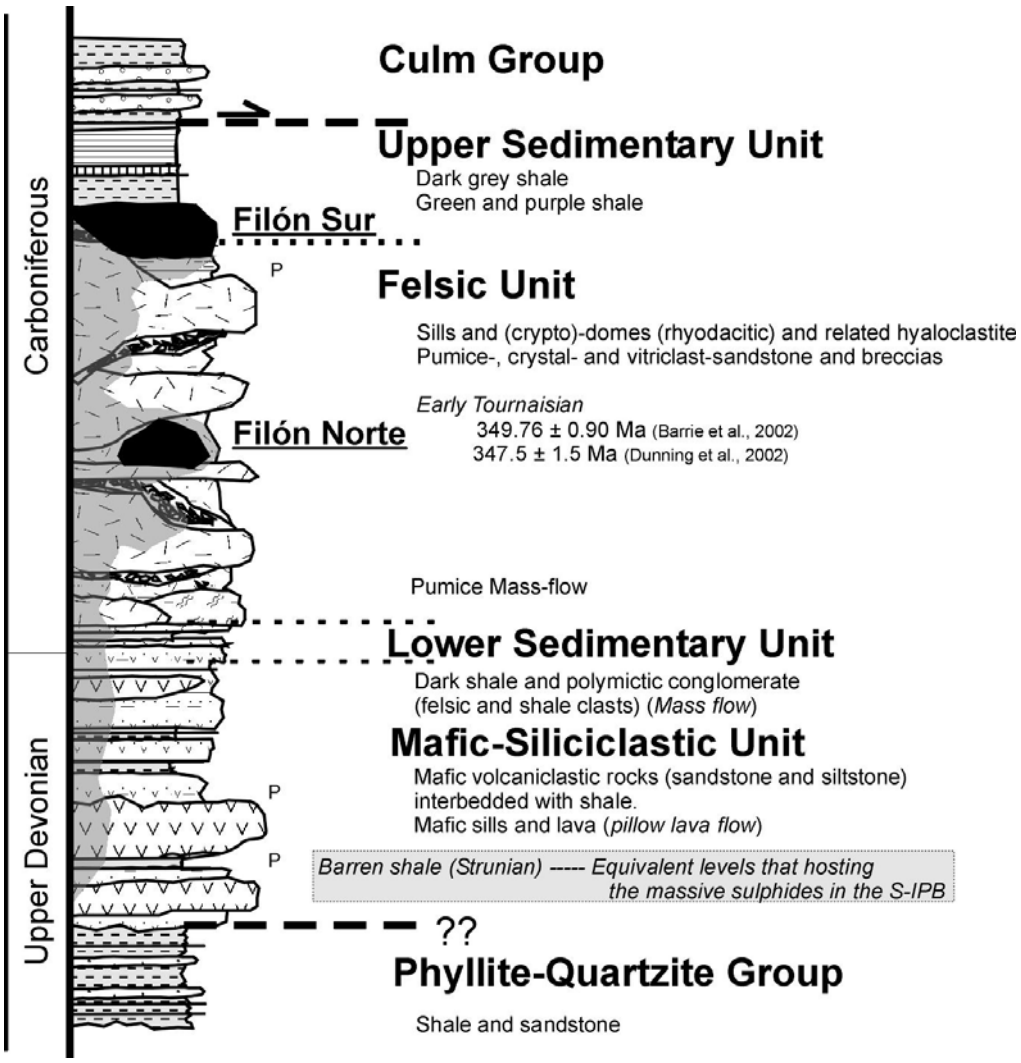

Figure 1: Summarized stratigraphic column of Río Tinto area (modified from Mellado *et al.* 2006)

GEOLOGY OF THE ORE-BEARING SEQUENCE

The Río Tinto district is located in the core of a major E-W trending subvertical synclinal structure that folds an earlier northwards dipping thrust and fold sequence (Mellado *et al.* 2006). The lithological succession in Río Tinto is similar to that in other areas of the Iberian Pyrite Belt, but characterized by the presence of an unusually thick unit of mafic volcanic rocks overlain by felsic rocks. The three main lithostratigraphic units of the IPB, the Phyllite-Quartzite (PQ) Group, the Volcanic-Sedimentary Complex (VS Complex) and the Culm Group, crop out in the area. The

sequence is late Devonian to early Carboniferous in age and has been affected by a synorogenic low grade regional metamorphism of Variscan age.

The PQ Group is the oldest unit and it is formed by a monotonous sequence of shale with interbedded sandstone. It does not crop out in the mined area but it can be found in the adjacent areas on the north and the south of the Río Tinto synclinal. Conformable above it, the thick VS Complex has been divided in four well differentiated units (Fig. 1). The lowermost unit, the Mafic-Siliciclastic Unit, comprises mafic sills and lava (pillow lava flows, Fig. 2-f) interbedded and intruding a sequence dominated by dark shale intercalated with mafic volcaniclastic rocks (sandstone and siltstone). The sills show common peperitic textures, suggesting that these rocks intruded in unconsolidated sediments (Boulter, 1993). This volcanic unit is conformably overlain by the Lower Sedimentary Unit which is made up of dark shale and a characteristic layer of polymictic conglomerate. This heterogeneous conglomerate is shale-supported and includes fragments of shale, felsic rocks and locally, there are some pyrite rich nodules of likely hydrothermal replacive origin. The thick Felsic Unit forms the bulk of the outcrops of the Río Tinto area. It is a complex volcanic sequence that includes quartz-feldspar porphyritic dacite to rhyodacite domes (see Fig 2-a and 3-a) and sills with associated hyaloclastite and autobreccias, that are intrusive and interbedded with pumice-, crystal- and vitriclast-rich sandstone (Fig 3-b) and breccias with only some minor shale. Peperites such as those shown in the Figure 2-d have been described in the margin of the intrusive bodies (Boulter, 1993; Tornos, 2006). The massive rocks have been dated between 349.76 ± 0.9 Ma (Barrie *et al*.2002) and 347.5 ± 1.5 Ma (Dunning *et al.* 2002). Capping the Felsic Unit there is a second sedimentary unit (Upper Sedimentary Unit). It is formed by dark shale, chemical sediments (chert) and laterally grade into volcanic sandstone. Locally, the shale package is hydrothermally altered near thrusts causing a colour change to green and purple shale. This sedimentary level has been dated as Early Tournaisian (Rodríguez *et al*. 2002). The Culm Group, made up of turbiditic shale and sandstone, is thrusted above the VS Complex (Mellado *et al.* 2006).
The massive sulphide orebodies occur in two different positions within the VS Complex. The uppermost lenses are hosted by dark shale in the Upper Sedimentary Unit (Filón Sur, San Dionisio). They are similar to other shale hosted deposits located on the southern domain of the IPB (Aznalcóllar-Los Frailes, Tharsis and Neves Corvo). However, they are significantly younger, middle Tournaisian in compared with the upper Fammenian age of the other massive sulphides (Tornos, 2006). A second group of deposits is hosted by the dacite of the Felsic Unit (Filón Norte, Salomón and Lago).

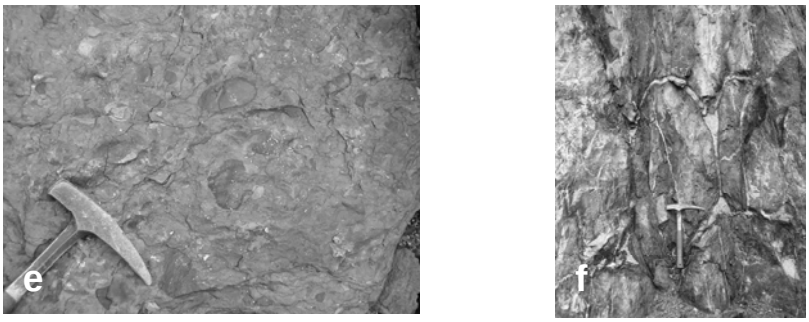

Figure 2: Photographs of the some aspects of the main volcanic facies of Río Tinto district. (a) Coherent rhyolitic crypto-dome intruding a thick pumice-rich volcaniclastic unit (Atalaya open pit). (b) View of the Mafic-Siliciclastic Unit with volcaniclastic sandstone and siltstone interbedded with shale (Cerro Colorado open pit). (c) Sulphide stringer zone: pyrite-quartz veins crosscutting massive dacite of the Felsic Unit affected by pervasive chloritic alteration (Atalaya open pit). (d) Peperite formed by interaction of dacitic sills with shale of the Felsic Unit. (e) Polymictic conglomerate level characteristic of the Lower Sedimentary Unit (Atalaya open pit). (f) Multiple-rind structure in mafic pillow lavas of the Mafic-Siliciclastic Unit (Cerro Colorado).

These massive sulphides, located in the northern part of the district, have been interpreted as formed by selective replacement of the felsic volcanic rocks.
An irregular and broad aureole of hydrothermal alteration affects most of the outcropping VS Complex. The Felsic Unit is pervasively sericitized and only locally, near major faults or close to the massive sulphides, the sericitic alteration is replaced by a chlorite + quartz assemblage. By contrast, both the Lower Sedimentary Unit and the Mafic-Siliciclastic Unit have a pervasive chloritic alteration (Fig 3–c and d) that is enriched in quartz in the more altered zones. The sulphide-bearing stockwork consists

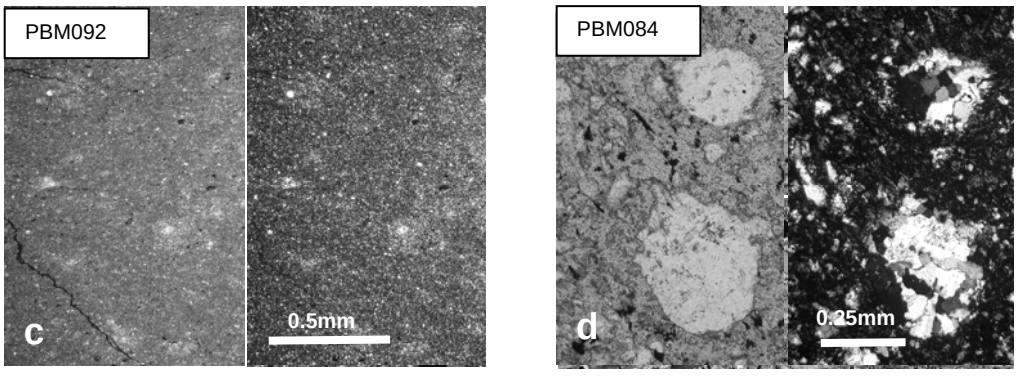

Figure 3: Photomicrographs of selected samples showing the mineralogy and textures of primary and altered volcanic rocks. All photos were taken under reflected and plane-poralized transmitted light. (a) Coherent porphyritic rhyolite composed by quartz and feldspar phenocrysts that have been selectively

altered. The groundmass comprises a microporphyritic matrix of qtz + fd (plag and fd-k) + ser ± chl. (b) Dacitic volcaniclastic rock formed by quartz grains and sulphides which have been rotated parallel to the intensive cleavage. The micro-grained matrix shows penetrative foliation and pervasive sericite+chlorite assemblages. (c) Cryptocrystalline texture (aphanitic) of mafic volcaniclastic rock. (d) Intensely chlorite-altered mafic rock that it shows subrounded vesicles filled with polycrystalline quartz.

of an anastomased network of quartz-sulphide or sulphide veins that crosscut rocks affected by both sericitic and chloritic alteration with disseminated sulphides (see Fig. 2-c). The distribution of the alteration and stockwork seems to be controlled by the reactivity and porosity of the host rocks and determined by E-W and NW-SE trending faults that probably correspond to inverted synsedimentary extensional structures.

Lithogeochemistry of volcanic rocks

43 samples from outcrops within the major open pits were analyzed out in the General Laboratory of the Instituto Geológico y Minero de España (IGME), using X-ray flourescence (XRF) for major elements, and ICP-MS for REE and trace elements. The study includes 10 analyses from the previous study of Costa (1996) and 15 previous analyses from internal reports of the IGME. Of these samples, 18 are from Mafic-Siliciclastic Unit, and 50 are from the Felsic Unit.

More of the half of the analyzed mafic and felsic rocks show a major hydrothermal alteration, having alteration indexes higher than 50 (see below). They are characterized by an almost complete replacement of the original mineralogy by quartz, sericite, chlorite and sulphides. For this reason, interpretation the geochemistry of the mobile components has been only performed in the least altered samples. The ratios between immobile elements have been used in all the samples, as essential parameters for the lithogeochemical classification, determination of the magmatic affinity and the quantification of the intensity of the hydrothermal alteration.

In the fresh and least altered rocks, the magmatic affinity has been determinate using major elements. The samples were plotted in the AFM diagram (Irvine & Baragar, 1971) (see Fig 4-c). Porphyritic coherent felsic rocks and volcaniclastic rocks plot in the field of the calc-alkaline series, whereas mafic rocks fall on the transitional to tholeiitic fields. In the highly altered samples, the incompatible trace-element ratios such as Zr/Y, La/Yb and Th/Yb should record the original geochemical characteristics (MacLean & Barret, 1999). The felsic samples have values of Th/Yb >0.65, confirming that they are calc-alkaline, while the mafic rocks are also classified as transitional to tholeiitic (Th/Yb rates between 0.1 and 0.65) (see Fig 4-d).

The samples from Río Tinto can be clearly discriminated in the TAS diagram (Fig. 3-a). The rocks from Felsic Unit have compositions of dacite to rhyolite but while the massive rocks forming the sills and domes have an ample SiO_2 content (dacite-rhyolite), the volcaniclastic ones show compositions restricted to the dacitic field. When these volcanic samples are plotted in the immobile-element diagrams, such as Zr/TiO_2 vs. Yb, both coherent and volcaniclastic rocks are identified as rhyodacite, more according to the characteristics observed in the petrologic study. The projection of samples in the binary diagrams involving ratios of immobile elements (Zr/Al_2O_3 vs. Al_2O_3/TiO_2, Fig 3-e) indicates that the rocks belonging to the Felsic Unit probably form a unique magmatic unit that

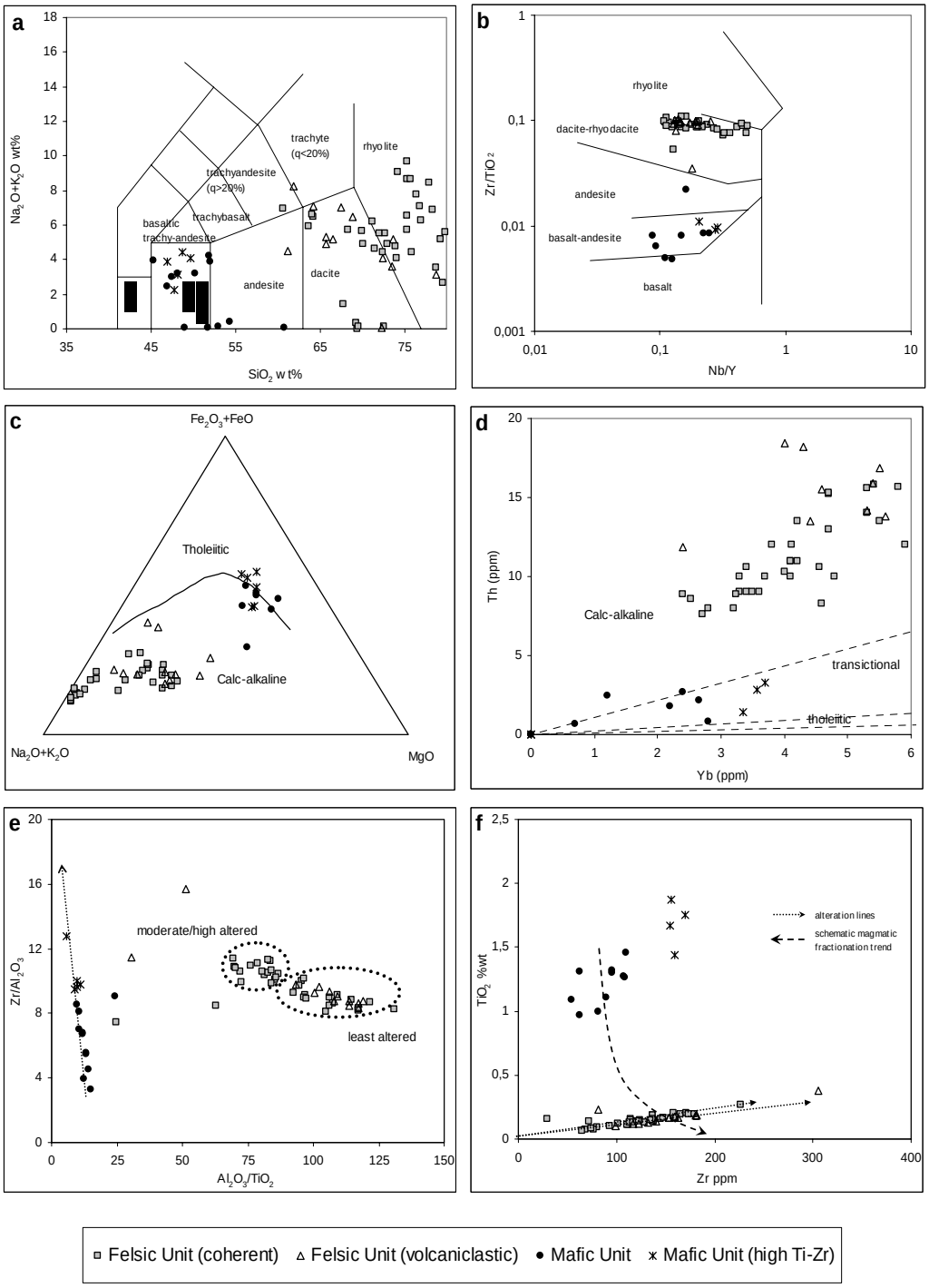

Figure 4: Summary of geochemical diagrams for the different type rocks from Río Tinto district. Discrimination plots for least altered samples: (a) Na_2O+K_2O vs. SiO_2 (Le Bas *et al.*1986); (b) Nb/Y vs. Zr/TiO_2 (Winchester & Floyd, 1977). Magmatic affinity of volcanic rocks based on: (c) AFM diagram (Irvine & Baragar 1971) and (d) Yb/Th ratio (Barret & MacLean, 1999). (e) Immobile-element ratio versus ratio plot. (f) Zr vs. TiO_2 diagram, displaying the main lithological groups and the alteration trends.

Probably formed in a magma chamber within a single magmatic pulse. The pumice and glass-rich sandstone and breccia plot above the massive samples, and are displayed along an alteration line that suggests a common origin. This strongly suggests that the coherent facies are accompanied by their volcaniclastic aprons that fill the valleys between independent domes. An interesting feature of these rocks is the wide variation in the Al_2O_3, TiO_2 and Zr contents, which result from mass changes during the alteration processes (see Fig. 4-f).

The coherent rocks belonging to the Mafic-Siliciclastic Unit have a composition close to that of basaltic-andesite, as has been shown in previous studies (Boulter *et al.* 2004). However, the contents in Al_2O_3, TiO_2, and Zr suggest that there are two different types of mafic rocks, a basaltic-andesite and a high Ti-Zr basalt (Fig. 4-f). The Zr/Al_2O_3 vs. Al_2O_3/TiO_2 binary plot shows that both groups spread along a unique trend (see Fig 4-e) suggesting that they are probably related by crystal fractionation processes.

The REE chondrite-normalized patterns (McDonough & Sun, 1995) of the felsic rocks are characterized by a steep slope with enrichment of LREE vs. HREE ($[La/Yb]_N$= 4.67), being the profiles similar in both massive and volcaniclastic rocks (not shown). The spider diagram of the rhyodacitic rocks shows an strong enrichment in LREE, but a relatively flat HREE pattern as well as a clearly defined negative Eu anomaly. These patterns are typical of the calc-alkaline rocks, and they are consistent with an evolutionary process dominated by the fractionation of plagioclase. Minor vertical shifts in the REE patterns could be caused by alteration process. Basalt and basaltic-andesite show almost flat patterns with $[La/Yb]_N$ values between 1.6 and 2.75. This is consistent with their tholeiitic affinity, characteristic of the most basaltic rocks from the IPB (Mitjavila *et al.* 1997).

The degree of hydrothermal alteration can be quantified in the alteration box plot proposed by Large *et al.* (2001) that is able to discriminate between different trends of alteration (Fig.5). Within this diagram, the samples from Río Tinto plot define at least three different alteration trends and two sets of unaltered rocks that correspond to the least altered rhyolite and basalt. The most altered samples plot towards the upper-right corner (AI>90 and CCPI>95) and correspond to the mafic and felsic rocks located immediately beneath the massive sulphide orebodies and affected by the chloritic alteration. While the mafic rocks seem to be directly replaced by the chloritite, the evolution of the felsic volcanics is more complex and there seems to be a gradation from rocks with negligible alteration towards a sericitic alteration and a later chloritic one. The vectors 1 and 2 identify different hydrothermal trends. Weak to strong sericite-chlorite alteration is defined by the vector 1, that corresponds to a depletion in Na and Ca, whereas the CCPI index is kept constant. The array becomes vertical (trend 2), defining an increase in the CCPI index due to the enrichment in Fe and Mg associated to the intense sericite-chlorite ± pyrite alteration in these rocks. In general, the felsic volcaniclastic rocks are more easily altered than the massive ones. The trend 3 defines a trend of albitization which has also been observed in the petrographic studies. This trend defines a type of alteration that is common in felsic volcanic rocks within the hanging wall of VMS deposits, as recorded in previous studies have described (Gemmell & Fulton, 2001).

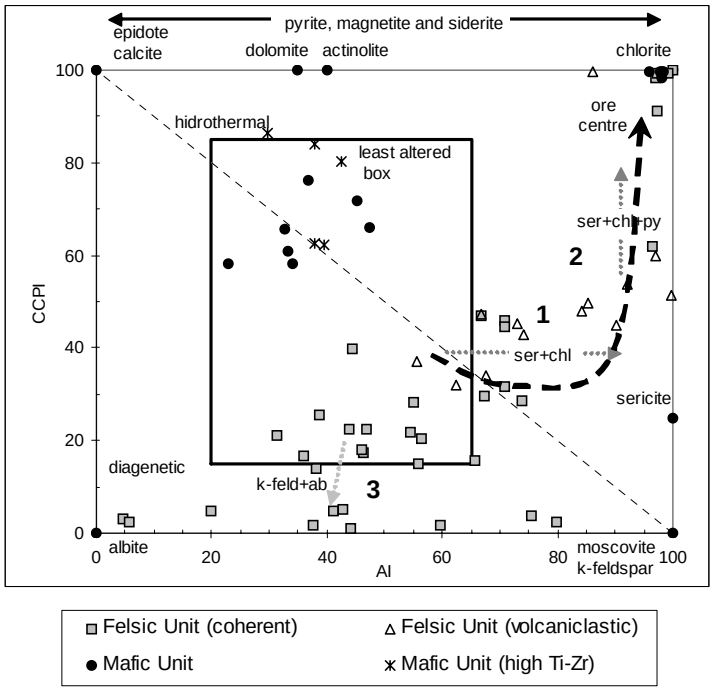

Figure 5: Alteration box plot for volcanic-hosted rocks from the Río Tinto area (Large *et al.* 2001), showing the vector alteration trends. Al=100(K_2O+MgO)/(K_2O+MgO+Na_2O+CaO) and CCPI=100(Mg+FeO)/(MgO+FeO+Na_2O+K_2O)

CONCLUSIONS

Two main volcanic units overlain by sedimentary sequences can be distinguished in the Río Tinto mining district on the basis of lithostratigraphic and lithogeochemical data. They are described as the Mafic-Siliciclastic Unit, being local of the Río Tinto area, and the dominant upper Felsic Unit. Despite major hydrothermal alteration, both units keep some of their primary geochemical features allowing their mapping all along the district. The geochemical data also show that these volcanic rocks are equivalent to those found in all the IPB and very similar to those found nearby, but affected by a pervasive hydrothermal alteration. The felsic rocks have a rhyodacitic composition and a calc-alkaline affinity while the mafic ones are basaltic andesite to andesite of tholeiitic to transitional geochemistry. The geochemistry of the immobile and incompatible elements show that the rocks of the Felsic Unit, both coherent and volcaniclastic, have equivalent Zr/TiO_2 and $[La/Yb]_N$ ratios and display similar alteration trends, supporting that the volcaniclastic rocks derive from erosion of the adjacent coherent rocks (domes and sills). The data show that all the felsic rocks evolved from an unique parental magma. Regarding the hydrothermal alteration, the geochemistry shows that while the mafic rocks are directly affected by a chloritization, the felsic rocks grade into chloritites via the formation of an intermediate chlorite-sericite-pyrite assemblage. Above the massive sulphides and distal to them there is an irregular albitization.

ACKNOWLEDGEMENTS

We thank MANTESUR Company and especially J. Robledo for providing the access for mapping and sampling of the Río Tinto area. This study has been funded by the DGI–FEDER project 2003-0209.

REFERENCES

-Barret T.J. & MacLean W.H. 1999. Volcanic sequence, lithogeochemistry and hydrothermal alteration in some bimodal volcanic-associated massive sulphide systems. In: *Volcanic-associated massive sulphide deposits: processes and examples in modern and ancient settings. Reviews in Economic geology,* Vol. 8, 101-131.

-Barrie, C.T. *et al.* 2002. U-Pb geochronology of VMS mineralization in the Iberian Pyrite Belt. *Mineralium Deposita,* Vol. 37, 684-703.

-Barret *et al.* 2005. The Palaeoproterozoic Kristineberg VMS deposit, Skellefte district, northern Sweden. Part II: Chemostratigraphy and alteration. *Mineralium Deposita*, Vol. 40, 351-367.

-Boulter, C.A. 1993. High level peperitic sills at Rio Tinto, Spain: implications for stratigraphy and mineralization. *Institution of Mining and Metallurgy. Transactions*, Vol. B102, 30-38.

-Boulter, C.A. *et al.* 2004. Provenance and geochemistry of sedimentary components in the Volcano-Sedimentary Complex, Iberian Pyrite Belt: discrimination between the sill-sediment-complex and volcanic-pile models. *Journal of the Geological Society*, Vol. 161, 103-115.

-Costa, I.M.S.R., 1996. Efeitos mineralogicos e geochimicos de alteraçao mineralizante en rochas vulcanicas felsicas de Rio Tinto (Faixa Piritosa Iberica, Espanha). Unplublished MSc Thesis, Universidad de Lisboa, 2002.

-Dunning, G.R. *et al.* 2002. Geocronologia U/Pb del volcanismo ácido y granitoides de la Faja Pirítica Ibérica, Zona Surportuguesa. *Geogaceta,* Vol. 32, 127-130.

-Gemmell J.B. & Fulton, R. 2001. Geology, genesis and exploration implications of the footwall and hanging-wall alteration associated with the Hellyer volcanic-hosted massive sulphide deposits, Tasmania, Australia. *Economic Geology,* Vol. 96, 1003-1035.

-Irvine, T.N. & Baragar, W.R.A. 1971. A guide to chemical classification of the common volcanic rocks. *Canadian Journal of Earth Sciences,* Vol. 8, 523-548.

-Large, R. *et al.* 2001. The alteration box plot: a simple approach to understanding the relationship between alteration mineralogy and lithogeochemistry associated with volcanic-hosted massive sulphide deposit. *Economic Geology,* Vol. 96, 957-971.

-Le Bas, M.J. *et al*.1986. Chemical classification of volcanic rocks based on the total alkali-silica diagram. *Journal of Petrology*, Vol. 27, 745-750.

-Leistel, J.M. *et al.* 1998. The volcanic-hosted massive sulphide deposits of the Iberian Pyrite Belt. *Mineralium Deposita,* Vol. 33, 2-30.

-Lentz D.P. 1999. Petrology, geochemistry, and oxygen isotope interpretation of felsic volcanic and related rocks hosting the Brunswick 6 and 12 massive sulfide deposits (Brunswick Belt), Bathurts minig camp, New Brunswick, Canada. *Economic Geology*, Vol. 94, 57-86.

-McDonough, W.F. & Sun, S.S. 1995. The composition of the Earth: *Chemical Geology*, Vol. 120, 223-253.

-Mellado, D. *et al.* 2006. Geología y estructura de la Mina de Río Tinto (Faja Pirítica Ibérica, España). *Geogaceta,* Vol. 40, 231-234.
-Mitjavila *et al*. 1997. Magmatic Evolution and Tectonic Setting of the Iberian Pyrite Belt Volcanism. *Journal of Petrology*, Vol. 38, 727-755.

-Montelius, C. 2005. The genetic relationship between rhyolitic volcanism and Zn-Cu-Au deposits in Maurliden volcanic centre, Skellefteå district, Sweden: Volcanic facies, lithogeochemistry and geochronology. PhD. Thesis, Luleå University of Technology, Sweden, ISSN: 1402-1544.

-Rodríguez, R.M. *et al.* 2002. Datación palinoestartigráfica del volcanismo en la sección de la Ribera del Jarama (Faja Pirítica Ibérica, Zona Surportuguesa). *Geogaceta,* Vol.32, 247-250.

-Tornos, F. 2006. Environment of formation and styles of volcanogenic massive sulfides: The Iberian Pyrite Belt. *Ore Geology Reviews*, Vol. 28, 259-307.

-Winchester J.A. & Floyd P.A. 1977. Geochemical discrimination of different magma series and their differentiation products using immobile elements. *Chemical Geology,* Vol. 20, 325–343.

Metal element distribution in two river basins of contrasting lithology

Iglesias, M.L.; Devesa, R.; Pérez, R.; Barral, M.T. & Díaz-Fierros, F.

Departamento de Edafología y Química Agrícola.
Universidad de Santiago
Facultad de Farmacia. Campus Sur. 15782. Santiago de Compostela. España.
E-mail: edbarral@usc.es
Keywords: Geochemical exploration, soil use, discriminant analysis, watersheds

ABSTRACT

122 surface soil samples (0-2 cm) were taken from two sub-basins of the Anllóns river (NW Spain), a half from schist (the Anllóns upstream watershed), and the other half from gabbros (the river Grande basin). In each basin samples were distributed between culture soils (23%), forested soils (29%), pasture (20 %), road talus (14 %) and river banks (14 %). The total element concentrations were determined by Energy Dispersion XR Fluorescence Spectrometry. The river Anllóns basin has a more complex geochemical composition than the river Grande basin. After a complete statistical study, we can conclude that lithology is the main factor that differentiates the distribution of the metallic elements in soils, whereas the soil use does not affect the element distribution. Discriminant analysis shows that the main elements that differentiate the basins are Rb, Cr, Mn, Cu, Zn, Nb, Zr and Ni. Also, corrrelation analysis indicates that, in the two basins, the elements Al, Cr, Ni, Cu, Ga are positively related to Fe. Additionally, Y or Ti are related to Fe in the the Grande basin and the Anllóns basin, respectively.

INTRODUCTION

The heavy metal content in soils is a critical factor which can impede the growth of many plants. So, “critical concentrations” for soil and plant health in the mineral soil layers have been provided by Kabata-Pendias and Pendias (1984) as, for example, Cr: 75-100 mg/kg, Ni: 95 mg/kg, Mn: 1500-3000 mg/kg, Zn: 170 mg/kg, Cu: 60 mg/kg and Pb: 100-400 mg/kg.
The concentrations of heavy metals in undisturbed soils depend mainly on bedrock lithology, and this imprints on soil geochemistry changes with age because of pedogenetic processes, moreover, the main factors affecting the heavy metal distribution in soils are the lithology and the land use. So,

Sultan (2006) found in his study in Central Victoria (Australia) that soils derived from Ordovician bedrock were characterized by coarse texture, low CEC, and low content of heavy elements caused by a high degree of weathering compared with metal-rich soils from basalt bedrock areas. In the same way, Migaszewski et al. (2005) found that the variability of S and trace metals in soils and plant bioindicators of Wigierski National Park is primarily governed by bedrock lithology and to a lesser extent by anthropogenic factors. Nava & Machín (2002) also found that soil types and parent materials have an effect on the variations of most elements, although parent materials appear to have greater effect on such variations.

In addition to indirect industrial emision, factors asociated to land use, such a deforestation and liming are considered by Kempter & Frenzel (1999) and Reimann et al. (2007), as the most important factors governing the distribution of heavy metals in soils. Some land uses can yield specific element enrichments as, for example, the land application of phosphate fertilizers, copper-based fungicides or lead-rich vehicle exhaust (Luo et al., 2007). Almeida et al. (2005) found differences in the Hg content under different land uses. These differences were significant at the topsoil, being non-significant below 60 cm of depth.

In this study, two sub-basins characterized by different geology and land uses were compared in order to: i) examine the metal concentration and distribution across the two sub-basins, ii) evaluate the differences in the metal concentrations as a function of lithology and land use and iii) identify anomalous enrichments in the sub-basins.

MATERIALS AND METHODS

Site description

The Anllóns River is located in the NW of Spain. The basin drains a rural catchment of 516 km^2 with a history of agricultural, forestry and cattle raising activities. It is characterized by soft winters, fresh summers, wet air, extensive cloud cover and frequent rainfall all over the year. The pluviometric regime is oceanic with a seasonal concentration of 1.72, which means that the maximum rainfall is in winter, but there is significant rainfall the rest of the year (Rial, 2002). There are several vegetation units which denote the anthropogenic influence, in terms of environmental modifiers and land uses. So, it can be found reforestations of *Pinus pinaster* and *Eucaliptus globulus*. As regards the cultivation, it is dedicated to potatoes and maize in spring, whereas it is dedicated to wheat and turnip in winter. In this study two sub-basins were characterized (Figure 1), the Upper Anllóns sub-basin and the river Grande sub-basin.

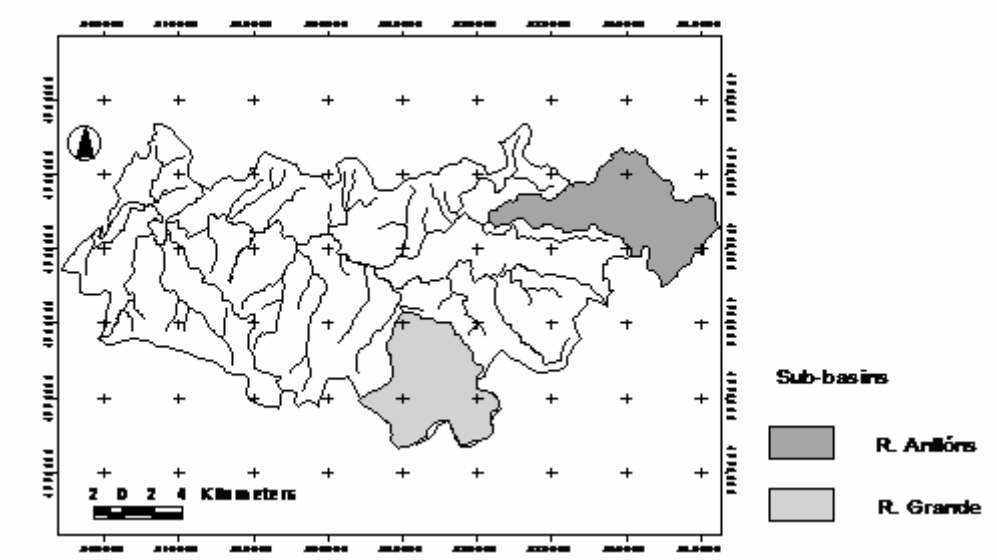

Figure 1: Sub-basin studied

Land use

The Upper Anllóns sub-basin is devoted to forest in a 58% of the total cover, whereas pastures and cultivation account for the 38% (Figure 2).

On the other side, the Grande sub-basin is devoted to scrublands in a 55% of the total cover. Cultivation accounts for the 35%, whereas forest is limited to the 9% of the total cover (

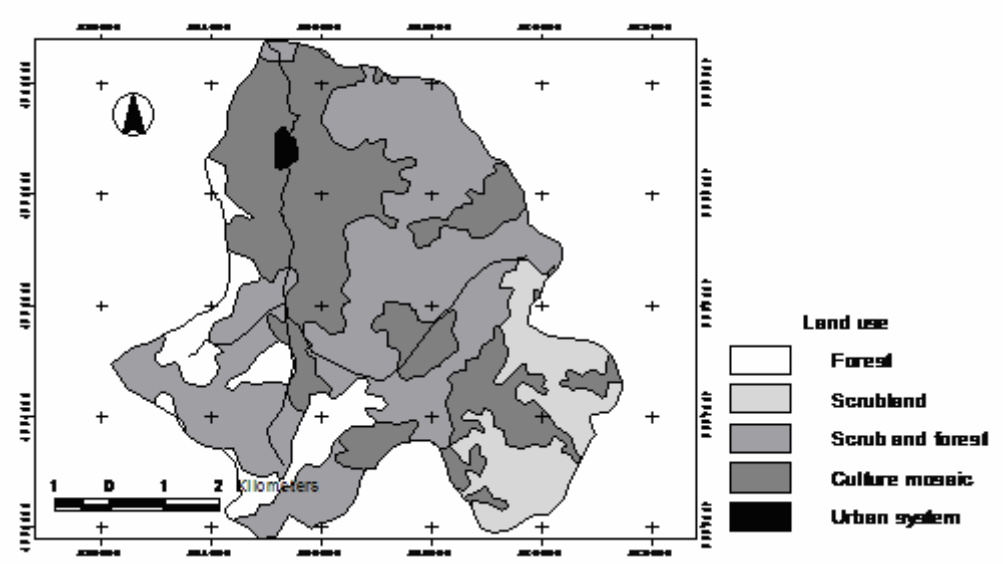

Figure 3)

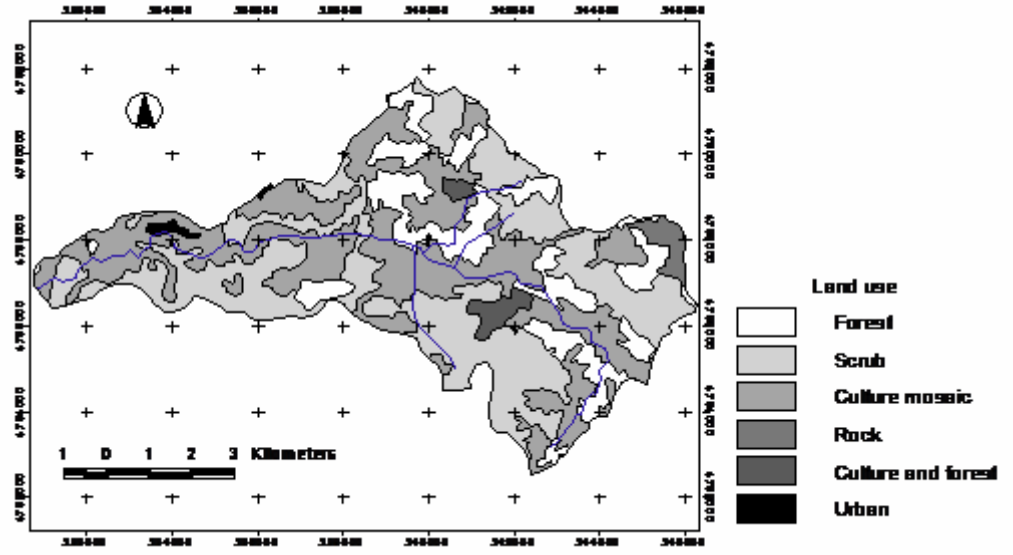

Figure 2: Land uses in river Anllóns sub-basin

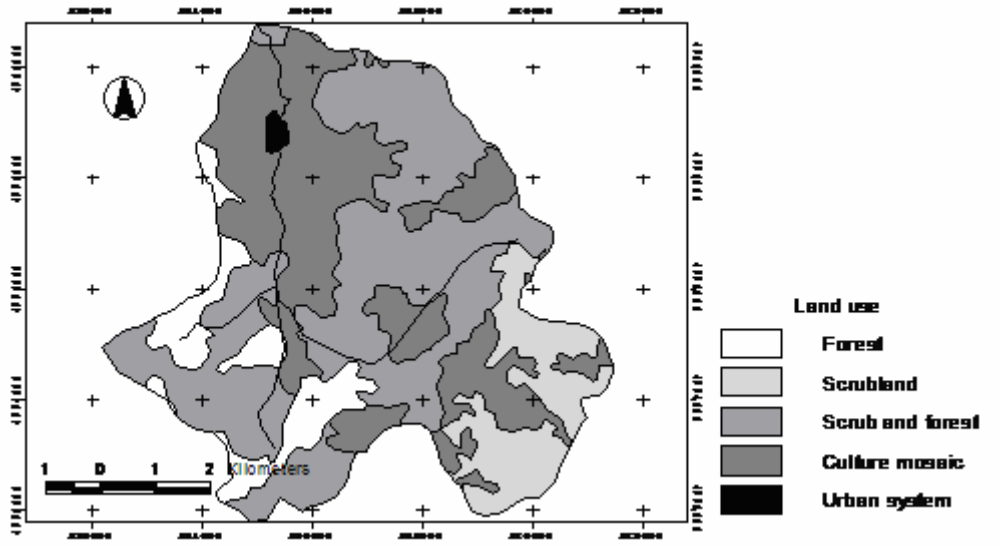

Figure 3: Land uses in river Grande sub-basin

Geology

The Upper Anllóns sub-basin shows a uniform lithology, constituted by acid rocks, with a predominance of schists and granodiorites (Figure 4). The Grande sub-basin is constituted by basic rocks, with a predominance of gabbros (Figure 5).

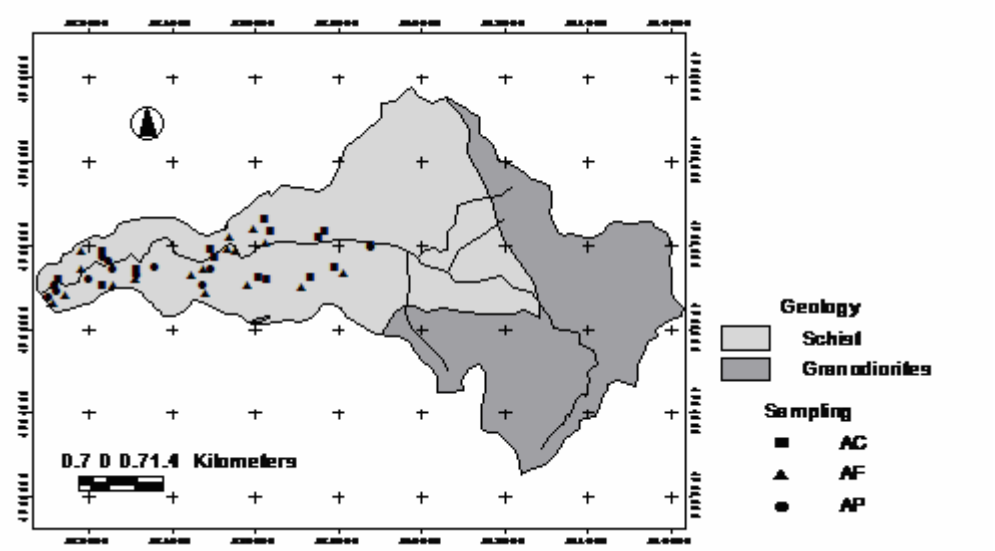

Figure 4: Sampling points and geology of river Anllóns sub-basin

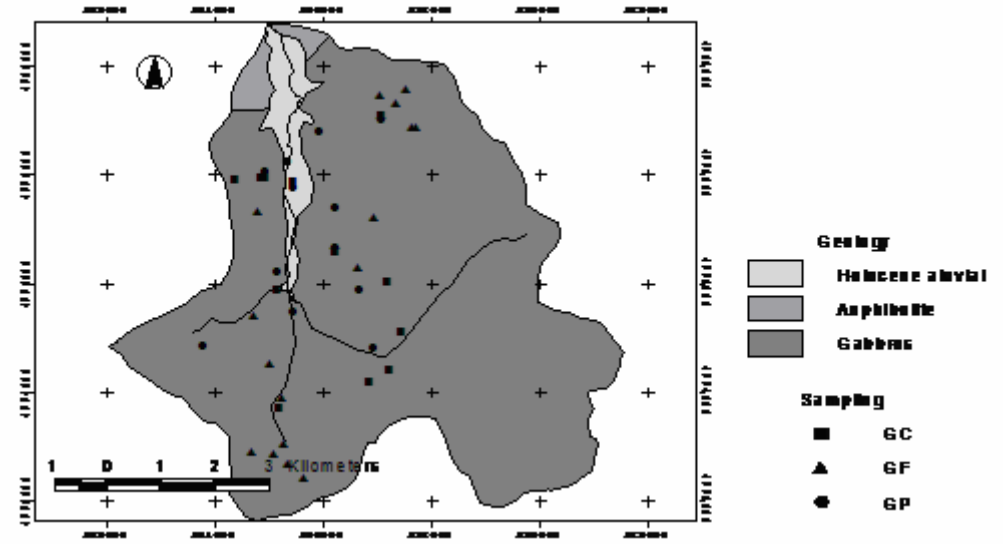

Figure 5: Sampling points and geology of river Grande sub-basin

Sampling and analytical methods

The sampling was realized between 2004 and 2005. 122 surface soil samples (0-2 cm) were taken from two sub-basins of the Anllóns river, a half from schist (the Anllóns upstream watershed), and the other half from gabbros (the river Grande basin). In each basin samples were distributed between culture soils (23%), forested soils (29%), pasture (20 %), road talus (14 %) and river banks (14 %). The samples were submitted to the following process:

- Once in the laboratory the samples were air dried and sieved by 63 µm.
- A representative fraction of each sample was measured by X-Ray Fluorescence (XRF) and the following elements determined: Rb, Cr, Mn, Cu, Zn, Nb, Zr, Ni, Al, Ga, Ti and Fe.
- A statistical procedure, including coefficients of correlation and discriminant analysis, was applied to the samples in order to determine the main factor that differentiates the distribution of the metallic elements in soils.

RESULTS AND DISCUSSION

The study carried out about the element concentration in the two sub-basins shows that Fe, Cr, Mn, and Ni are more abundant in the Grande River basin, whereas Al, Ni, Ga, As, Rb, Cr, Pb showed greater abundance in samples taken from the Anllons River basin. The other elements, like Ti, Cu, Zn, Se and Sr show similar concentrations in both basins. The observed differences and similarities observed in the Fig.6 are confirmed by a Student T test ($p < 0,05$, bilateral).

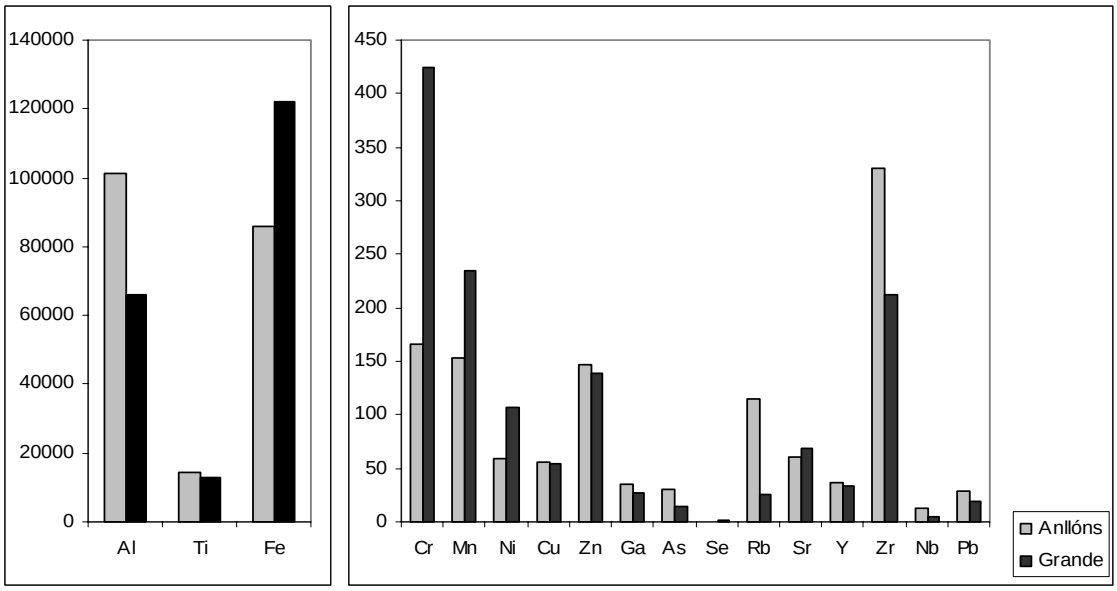

Figure 6: Element concentration (mg/kg) in both basins. By its abundance Mn concentration is divided by 10.

Elements like Al, Fe, Cr and Ni are more abundant in talus, as it is a B horizon; Zr shows the highest acumulation in the river. Other elements presents similars concentration in all uses. Duncan test don´t show a new and clear distribution of the elements about uses (Figure 7) Therefore, the land uses do not influence the element distribution, whereas lithology is the most influent parameter.

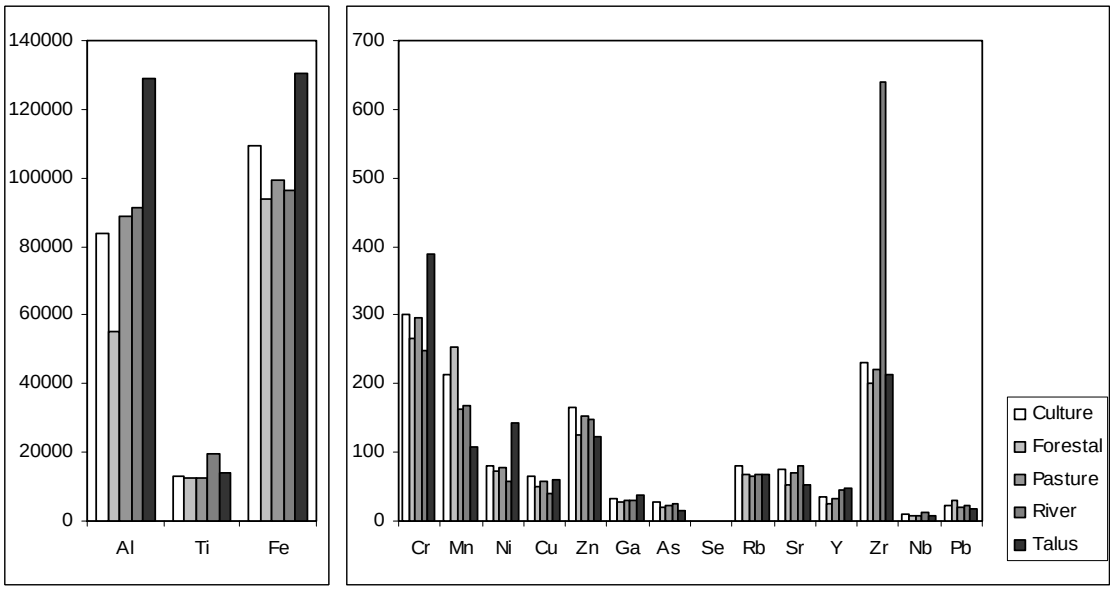

Figure 7: Element concentration (mg/kg) by uses. By its abundance Mn concentration is divided by 10.

Corrrelation analysis indicates that, in the two basins, some elements are positively related to Fe, they are: Al (0,36 in R. Anllóns and 0,56 in R. Grande), Cr (0,69 en R. Anllóns and 0,54 in R. Grande), Ni (0,60 in R. Anllóns and 0,39 in R. Grande), Cu (0,32 in R. Anllóns and 0,42 in R. Grande), Ga (0,36 in R. Anllóns and 0,80 in R. Grande). Additionally, Y (0,67) or Ti (0,60) are related to Fe in the the Grande basin and the Anllóns basin, respectively. All these correlations are significant to level 0,01, bilateral.

Discriminant analysis develops a function that allows to classify the samples in each one of the two subgroups previously established, the function gives a greater importance to Rb, Cr, Mn, Cu, Zn, Nb, Zr and Ni, in order to differenciate the basins, these elements are marked with an asterisk in Figure 8 . The relative importance is showed in the figure where the element coeficients in the function are represented. Discriminant analysis took the minimum number of elements wich permit the better differenciation then, some elements with a high coeficient are not used to the function because probably other element explain better the classification.

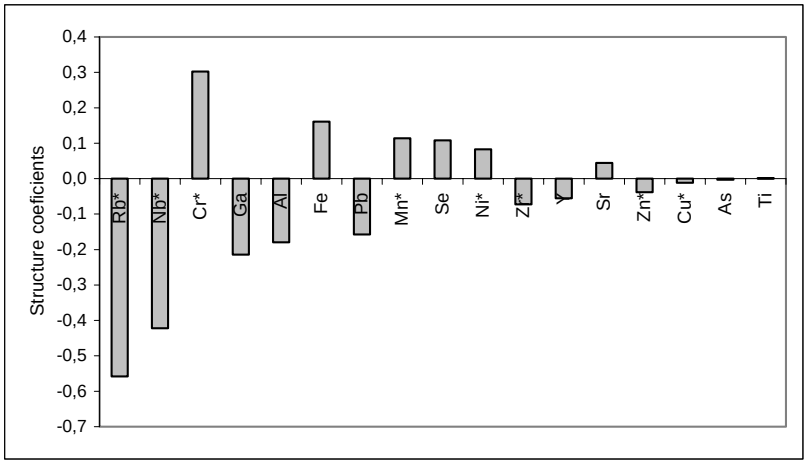

Figure 8: Structure element coeficients in discriminant analysis

With the objective of estimating the degree of contamination, the enrichment factor was calculated by using the following equation proposed by Hakanson (1980):

$$EF=(M/M_{reference})_{sample}/(M/M_{reference})_{crust}$$

Where $(M/M_{reference})_{sample}$ is the analyzed metal to a reference metal ratio in the sample and $(M/M_{reference})_{crust}$ is the analyzed metal to reference metal ratio in the crust. The element concentrations in the crust were taken from Wedepohl (1995). According to Szefer et al. (1999), EF values around 1.0 suggest anthropogenic sources. Several methods of normalization are in use and the constituent chosen must be correlated with the finer fraction and not show anthropogenic alteration. Among the most used are Al, Fe, total organic carbon, Cs, Rb and Li (Rubio, 2000). In this study, Nb was chosen as the reference element because is an element whose geogenic origin is much probably than the anthropogenic, being likewise not very mobile. In this case (Figure 9) As shows the higher EF in both basins, probably because there is some type of contamination. The other elements show a higher EF in R. Grande (EF values around 15) than R. Anllons (EF values around 5), this can be attributed to the lithology.

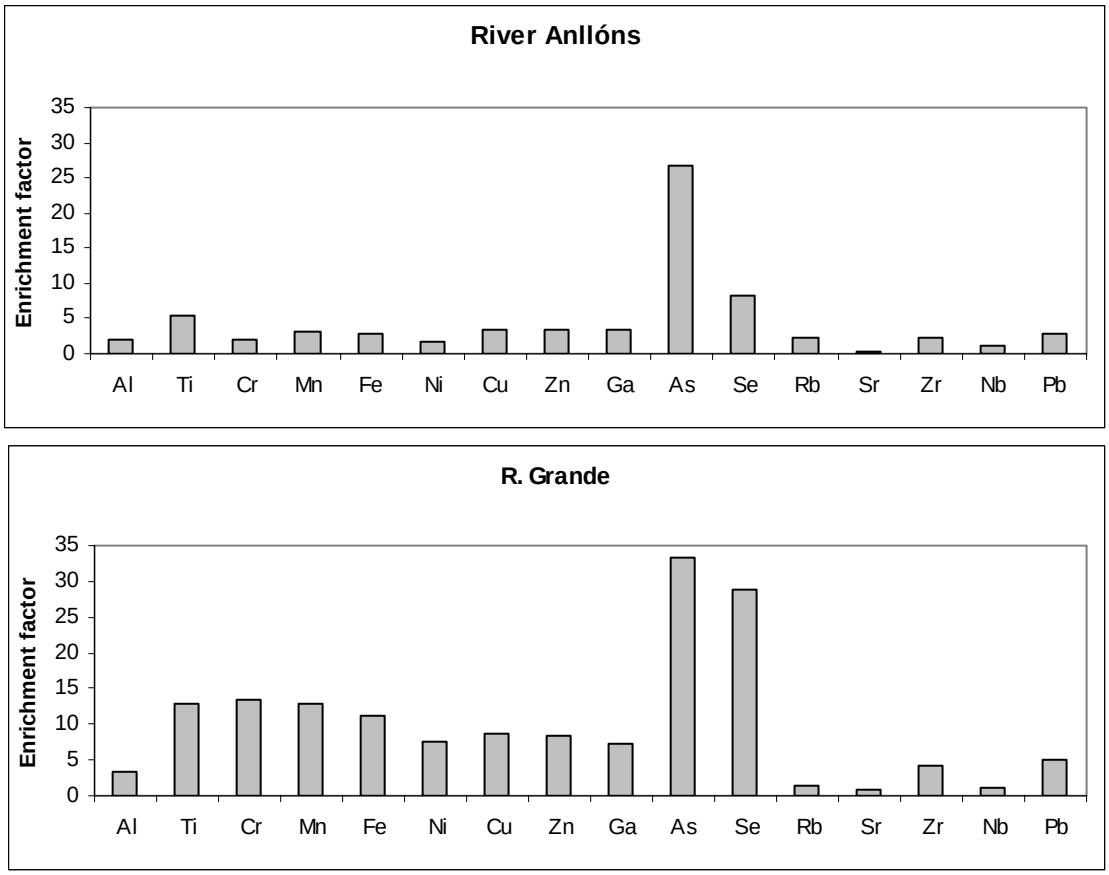

Figure 9: Enrichment factor in both basins

CONCLUSIONS

The Anllóns River basin has a more complex geochemical composition than the Grande River basin. After a complete statistical study, we can conclude that lithology is the main factor that differentiates the distribution of the metallic elements in soils, whereas the soil use does not affect the element distribution.

REFERENCES

Almeida, M.D., et al, 2005. Mercury loss from soils following conversion from forest to pasture in Rondônia, Western Amazon, Brasil. *Environmental Pollution* 137, 179-186.

Hakanson, L., 1980. An ecological risk index for aquatic pollution control. A sedimentological approach. *Water Res*., Vol 14,No 8, pp. 975-1001

Kabata-Pendias, A. & Pendias, H., 1984. *Trace elements in soils and plants*. CRC Press, Boca Ratón, Florida, USA.

Kempter, H. & Frenzel, B., 1999. The local nature of anthropogenic emission sources on the elemental content of nearby ombrotrophic peat bogs, Vulkaneifel, Germany. *The science of the total environment* 241, 117-128.

Luo, W., et al, 2007. Landscape ecology of the Guanting Reservoir, Beijing, China: Multivariate and geostatistical analyses of metals in soil. *Environmental Pollution* 146, 567-576.

Migaszewski, Z.M., et al, 2005. The use of the barbell cluster ANOVA design for the assessment of environmental pollution: a case study, Wigierski National Park, NE Pollan. *Environmental Pollution* 133, 213-223.

Navas, A. & Machín, J., 2002. Spatial distribution of heavy metals and arsenic in soils of Aragón (northeast Spain): controlling factors and environmental implications. *Applied Geochemistry* 17, 961-973.

Reimann, C., et al, 2007. Element concentrations and variations along a 120-km transect in sourthern Norway – Anthropogenic vs. geogenic vs. biogenic element sources and cycles. *Applied Geochemistry* 22, 851-871.

Rial, M.E., 2002. Caracterización hidrolóxica da bacía do río Anllóns. Universidad de Santiago de Compostela.

Rubio, B. et al (2000). Geochemistry of Major and Trace Elements in Sediments of the Ría de Vigo (NW Spain): an Assessment of metal Pollution. *Marine Pollution Bulletin* Vol. 40, No 11, pp. 968-980.

Sultan, K., 2006. Distribution of metals and arsenic in soils of Central Victoria (Creswick-Ballarat), Australia. *Archives of environmental contamination and toxicology* 52, 339-346.

Szefer, P., et al, 1999. Distribution of selected heavy metals and rare earth elements in surficial sediments from the polish sector of the Vistula Lagoon. *Chemosphere*, 39 (15), 2785-2798.

Wedepohl, K., 1995. The composition of the continental crust. Geochim. *Cosmochim. Ac*., 59 (7), 1217-1232.

GEOCHEMICAL CHARACTERISTICS OF BARREN AND MINERALIZED INTRUSIVES IN THE GEODO AREA, TAEBAEKSAN BASIN, SOUTH KOREA: IMPLICATIONS FOR ADAKITE MAGMATISM AND FE-CU(-AU) MINERALIZATION

[1]Jung Woo Park, [1]Seon-gyu Choi, [1]V.J. Rajesh, [1]Eun-mi Ko, [2] Se-Jung Chi

[1] Dept. of Earth & Environmental Sciences, Korea Univ., Seoul, 136 713
[2] Korea Institute of Geoscience and Minerals, Daejeon, 305-350
E-mail: parkjw@korea.ac.kr
Keywords: productive granitoids, adakite, Taebaegsan basin, Geodo skarn ore deposit, Fe-Cu(-Au) Mineralization.

ABSTRACT

The Taebaegsan basin within the Korean Peninsula encloses a variety of ore-deposit types such as veins, skarns, carbonate replacement ore, carlin-like ores and pegmatite from Early to Late Cretaceous. The Geodo Fe-Cu(-Au) skarn deposit in this basin hosts significant ore minerals such as magnetite, chalcopyrite, native gold and electrum. A range of intrusives (e.g. quartz-mozodiorite and granodiorite) are spatially related to this deposit which is noted for exclusive Cu mineralization in the Taebaegsan basin. The intrusives show features of I-type, magnetite series granite and have high Fe_2O_3/FeO ratio. The granodiorites display adakite-like geochemical signatures such as high Sr/Y (23-43) and La_N/Yb_N (16-40) ratios, low Y (13.0-23.7 ppm) and Yb (1.1-2.0 ppm), highly fractionated HREEs and absence of Eu anomaly. They also host significant Early Cretaceous (~ 100 Ma) Fe-Cu(-Au) mineralization. However, the quartz monzodiorite is less evolved than the granodiorite. In short, the granodiorite has adakite-like geochemical signatures and oxidized environment of magma generation. These geochemical features of the granodiorites are similar to many Fe-Cu(-Au) skarn related granites. The composition of skarn minerals in the Geodo Fe-Cu(-Au) deposit spatially associated with granodiorite also suggests the mineralization under oxidized environment. It is widely documented that the adakite-type magmas are often associated with Cu-Au mineralization under high oxygen fugacities. We interpret here that the significant Fe-Cu(-Au) mineralization in the Geodo area in the Taebaegsan basin is the effect of adakite-like magmatism of the granodiorite.

INTRODUCTION

Adakites are intermediate to felsic igneous rocks with genetic implication of slab melting in a subduction zone (Defent and Drummond, 1990). Slab melting-derived magma induces oxidized environment in mantle wedge by ferric ion input preventing the escape of SO_2 from adakitic, highly oxidized, sulfur-rich magma (Oyarzun *et al*., 2001, Mungall, 2002). These features of adakite result in the formation of porphyry Cu deposit and, in fact, it is reported that adakites are often associated with Cu-Au porphyry ore deposit (Mungall, 2002).
In the Geodo area, Fe-Cu(-Au) mineralization is hosted in skarnized Cambro-Ordovician carbonate rocks around the Cretaceous intrusives. The intrusives in the

Geodo area are divided into quartz monzodiorite and granodiorite (Chang & Park, 1982). Among them, the granodiorite shows geochemical characteristics similar to those of adakites, but quartz monzdiorite doesn't. A previous geochemical study by Yun (1986) has suggested that both quartz monzodiorite and granodiorite in the Geodo area were genetically related as fractionally differentiated rocks from a same magma source. There is also a time gap between the intrusions, the this paper we examine the petrographic and geochemical features of intrusives in the Geodo area and discuss the related granitoids of Geodo Fe-Cu(-Au) skarn deposit.older quartz monzodiorite and the younger granodiorite (Park *et al*., 1988).

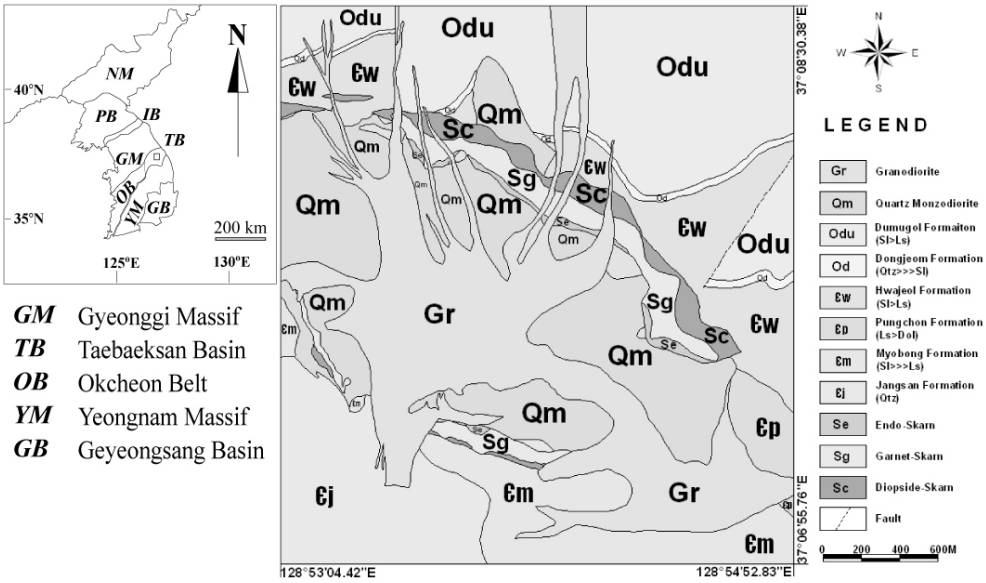

Figure 1: Geological map of South Korea and Geodo area.

GEOLOGICAL SETTING

The tectonic elements of South Korea consist of the Gyeonggi Massif, the Ogcheon Belt, the Yeongnam Massif and the Gyeongsan Basin from the north to south (Figure 1). The Ogcheon Belt, which is mainly composed of the Early Palaeozoic marine sedimentary rocks and the Late Paleozoic non-marine sedimentary rocks, was folded and metamorphosed during the Triassic and the Jurassic (Pak *et al.*, 2004). The Taebaegsan Basin is located in the northeastern part of the Ogcheon Belt and is divided into the Choseon Supergroup and the Pyongan Supergroup (Chough et al., 2000). The Choseon Supergroup is mainly composed of a succession of Cambrian-Ordovician quartzite, slate, limestone and shale (Yun, 1986) and the Pyeongan Supergroup comprises marginal marine to non-marine clastic successions (Pak *et al.*, 2004). The Geodo Fe-Cu(-Au) skarn deposit is located in the Choseon Supergroup. A range of intrusive rocks, quartz monzodiorite and granodiorite, are emplaced in the Geodo area. Available ages of both quartz monzodiorite and granodiorite range from 111 to 105 Ma (Kim, 1971; Farrar et al., 1978; Yun, 1986). However, Yun (1986) has reported relatively older age for quartz monzodiorite (108-111 Ma) and younger age for granodiorite (108-109).

PETROGRAPHY

According to quartz-alkali feldspar-plagioclase (QAP) diagram, the quartz monzodiorite ranges from monzodiorite to quartz monzodiorite and the granodiorite ranges from quartz monzodiorite to granodiorite.

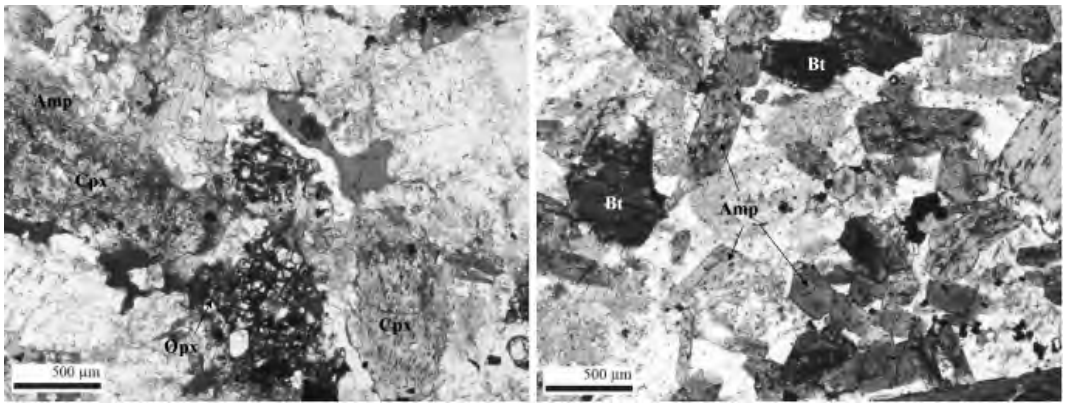

Figure 2: Microphotographs of quartz monzodiorite (SiO_2 54 wt. %) and granodiorite (SiO_2 55 wt. %). Both samples have similar SiO_2 contents, but show significantly different mineral assemblages.

The quartz monzodiorite and granodiorite in the Geodo area are characterized by medium grain size and high magnetic susceptibility (5.23-31.4×10^{-3} SI). Quartz monzodiorite shows equigranular texture and consists mainly of plagioclase, pyroxene, biotite, K-feldspar, quartz and amphibole (Figure 2). In more acidic varieties of quartz monzodiorite, an increase in the modal abundance of clinopyroxene, amphibole, K-feldspar and quartz have been observed. Uralitization is noticed along the grain margins of some pyroxenes. Plagiocalse grains are euhedral-subhedral with some sericitic alterations. Biotite grains are mostly subhedral granular with brownish color and at places they are entrapped in clinopyroxene grains.
Granodiorite shows mostly equigranular texture. However some samples also display porphyritic texture. Both equigranular and porphyritic granodiorite consist of plagioclase, K-feldspar, quartz, amphibole and biotite (Figure 2). Contrary to quartz monzodiorite, pyroxenes are virtually absent in granodiorites. In more acidic granodiorite amphibole contents are lower. Amphibole phenocrysts have high grade of idiomorphism and they are mostly euhedral. Biotites are subhedral granular with brown color.
On the basis of the variation in mineral assemblage with increase of SiO_2 contents among quartz monzodiorite and granodiorite, we infer that the two rocks have undergone different fractionation process.

GEOCHEMISTRY

Quartz monzodiorite and granodiorite in the Geodo area have the characteristics of high-K calc alkaline series magma and I-type peraluminous rocks. The SiO_2 contents of quartz monzodiorite and granodiorite range from 49.42 to 62.75 wt. % and from 55.63 to 64.80 wt. % respectively. Both are evidently rich in potassium; 1.53-4.70 wt. % for quartz monzodiorite and 2.49-3.55 wt. % for granodioirte. Hence, they show features of high-K calc alkaline-shoshonite magmatism. The Al_2O_3 contents of quartz monzodiorite (15.49-16.67 wt. %) are slightly higher than those of the granodiorites

(14.34-15.42 wt. %). The Na_2O contents of both quartz monzodiorite (3.10-3.88 wt. %) and granodiorite (3.19-3.91 wt. %) have positive correlation with SiO_2.
The trace element compositions of quartz monzodiorite and granodiorite are significantly different. Quartz monzodiorite have significantly high Sr (584-1209 ppm), Y (14.9-31.4 ppm), Yb (1.25-2.49 ppm), Th (27.0-93.2 ppm), Nb (13.1-37.1 ppm) and Zr (164-554 ppm). Nb, Zr, Rb, Ba contents show positive correlation with SiO_2. On the contrary, the granodiorites display Low Y (13.0-23.7 ppm), Yb (1.1-2.0 ppm), Th (8.76-29.6 ppm), Nb (9.4-13.5 ppm) and Zr (139-246 ppm) contents. Also Zr and Nb contents have negative correlations with SiO_2

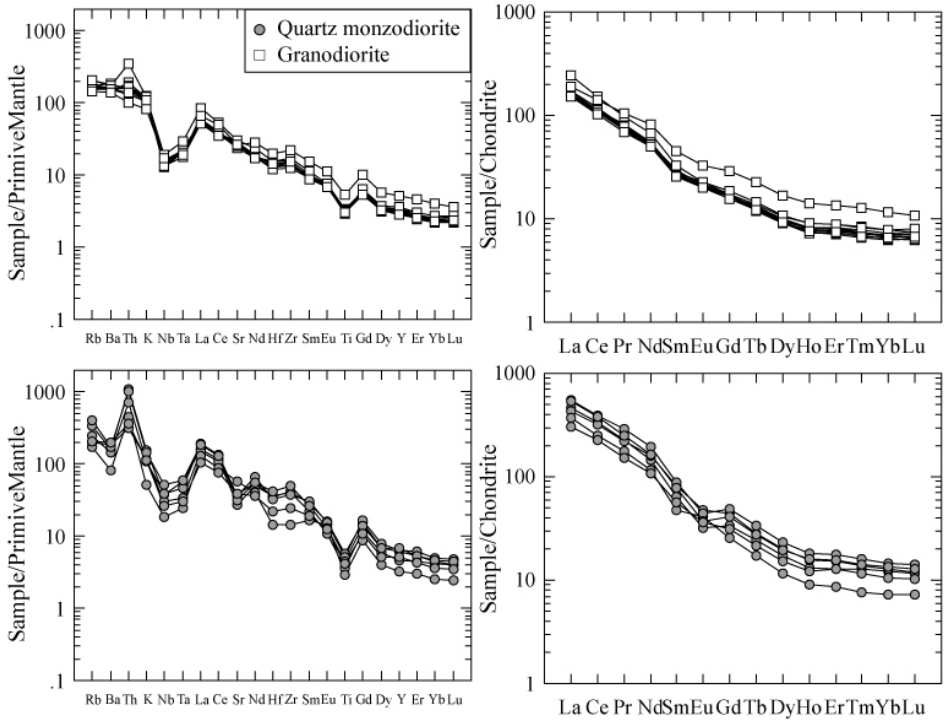

Figure 3: Primitive Mantle-normalized trace-element patterns and Chondrite-normalized REE patterns of quartz monzodiorite and granodiorite.

Primitive mantle-normalized trace element diagrams (Figure 3) illustrate the enriched LILE and depleted HFSE nature of both rock types. Also, they have strong negative anomalies for the elements Nb, Ta and Ti. These features are of typical magmatism in a subduction zone (Wilson, 1989). In general, the quartz monzodiorites have generally enriched trace element abundances than the granodiorites (Figure 3). The quartz monzodiorites show strong negative anomalies of Ba and Sr, and positive anomaly of Th, which are different from those of the granodiorites.
Chondrite-normalized rare earth element diagrams of both quartz monzodiorite and granodiorite show patterns of enriched LREEs and depleted HREEs (Figure 3). Their strong LREE/HREE fractionation (La_N/Yb_N=16-50) coincides with mantle magmatism (Wilson, 1989). The quartz monzodiorites, however, are different from granodiorites in the sense of its relative enrichment of REE contents and pronounced Eu negative anomaly.

DISCUSSION

Adakitic signatures of granodiorite in the Geodo area

Based on present geochemical data, it is likely that subducting slab-drived components play an important role in the magma genesis of the granodiorites. Enriched LILE and depleted HFSE (Nb, Ta, Ti) and depletion of HREE (Yb) are typical features of the magmatism in a subduction zone.

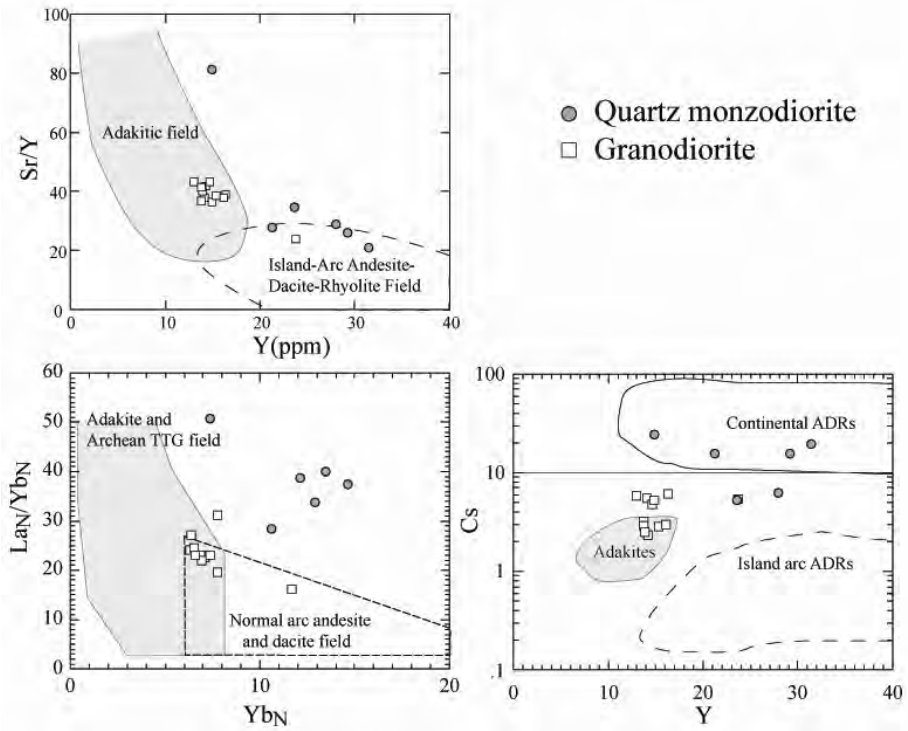

Figure 4: a) Sr/Y vs Y diagram (after Durummond & Defent (1990)). b) La_N/Yb_N vs Yb_N diagram (after Durummond & Defent (1990)). c) Cs (ppm) vs Y (ppm) diagram (after Durummond *et al*. (1996).

Slab melting has an important role in subduction zone magmatism (Yogodzinski et al., 1995). Kay (1978) named such slab melting-drived magmatic rocks as adakites and have the geochemical chracteristics of high Al_2O_3 (> 15 wt. %) and Sr/Y ratio (> 20-40), low HREE (Yb <1.9 ppm), Y (< 18 ppm), and lack of Eu anomaly. The granodiorites display the same features of adakites as described above. The Al_2O_3 contents range from 14.34 to15.42 wt. %. The Y contents range from 13.0 to 23.7 ppm with an average of 15.42 and the Yb concentrations vary from 1.1 to 2.0 ppm with an average of 1.27. Hence, the granodiorites have high Sr/Y ratios (23-43). Consequently in the Sr/Y vs Y (figure 4a) and La_N/Yb_N vs Yb_N (Figure 4b) diagrams, granodiorites are clearly plotted within the adakitic field except the most mafic ones. Again in the Cs vs Y diagram (Figure 4c) majority of the granodiorite data plot within the adakite field, whereas the quartz monzodiorites clearly falls in the field of continental arc andesite-dacite-rhyolite. From the aforementioned facts it can be concluded that Geodo granodiorites have features typical of adakites generated by melting of a subducted slab.

Relationship between Fe-Cu(-Au) skarn mineralization and granodiorites

Geodo Fe-Cu(-Au) ore deposits are hosted in the skarnized carbonate rocks. The compositions of skarn minerals such as garnet (andradite 40- 100%), pyroxene (diopside 59-91%), epidote (pistacite 28-33%) are coincident with the skarn mineral compositions of typical Fe-Cu-Au skarn and indicate oxidized environment of related magmatism. Meinert et al. (2005) suggest that igneous major and trace element composition might influence the behavior of ore constituents and skarn types. Cu skarn plutons are generally oxidized than the other skarn plutons. The chemical compositions of the related granitoids alone do not result in the formation of certain mineralization. The origin, differentiation mechanism, degrees of compositional evolution, oxidation state and physical parameters of related

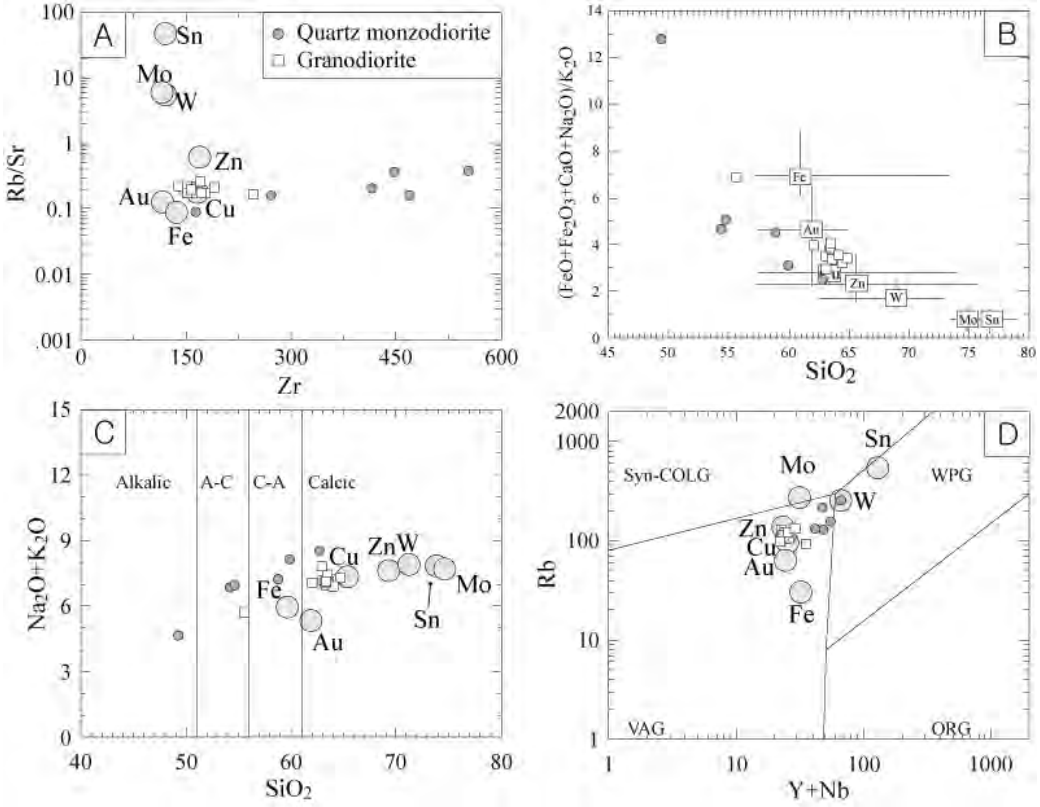

Figure 5: Average composition of plutons associated with different skarn types, Abbreviations= syn-collision: syn-Col, cocanic-arc: VA, within-plate: WP, oceanic-ridge: OR, diagram a,c and d from Meinert et al. 2005, b from Meinert, 1993

granitoids also have vital controls over the type and mineralogy of mineralization (Blevin, 2004). The majority of Cu skarn occurs in association with the calc-akaline granodiorites to quartz monzonite intrusives emplaced at shallow depths and have close spatial relation with felsic porphyry-textured stocks (Misra, 2000). According to Titley and Beane (1981), the productive porphyry Cu intrusives might not contain pyroxene, but conspicuous hornblende and biotite.

The petrological-geochemical characteristics of Geodo quartz monzodiorites and granodiorites undoubtedly suggest that they have different magma evolutionary

histories. The granodiorites have features of I-type, magnetite series granitoids with relatively high Fe_2O_3/FeO (0.29-0.74) and high magnetic susceptibility. The mafic mineral assemblage (hornblende and biotite) of the granodiorites is similar to those of productive Cu porphyries described by Titley and Beane (1981) whereas those of the quartz monzodiorites (mainly pyroxene and biotite) are identical to non-productive ones.
The geochemical composition of granodiorites shows strong consistency with Fe-Cu-Au skarn plutons (Figure 5). In the Figure 5a, the granodiorites are plotted close to the field of Cu skarn plutons, whereas the quartz monzodiorites are largely scattered because of their variable and high Zr contents. Also, from the figures 5b and 5c it is evident that the quartz monzodiorites are too less evolved to form Cu-Au mineralization.
Hence, it can be summarized that the granodiorites in the Geodo area clearly have adakitic features. It is well known that adakites are closely related with Cu-Au mineralization (Mungall, 2002). Hence, we envisage that owing to the adakitic signatures of the granodiorites, they are highly productive and are genetically related with Geodo Fe-Cu(-Au) skarn ore deposits.

ACKNOWLEDGEMENTS

This work was supported by a grant (No.: R01-2006-000-10553-0 and Year: 2006) from the Basic Research Program of the Korea Science and Engineering Foundation (KOSEF).

REFERENCES

Blevin P. L. 2004. Redox and Compositional Parameters for Interpreting the Granitoid Metallogeny of Eastern Australia: Implications for Gold-rich Ore Systems. *Resource Geology*, Vol. 54, 241-252.

Chang, H. W. & Pack, K.H. 1982. Petrogenesis of Fe-Cu Bearing skarn at Geodo. *Report of Geoscience and Mineral Resource KIER.* Vol. 14, 129-156.

Chough, S.K.,et al. 2000. Tectonic and sedimentary evolution of the Korean Peninsula: A review and new view: *Earth Science Reviews,* Vol. 52, 175-235.

Defant, M. J. & Drummond, M. S. 1990. Derivation of some modern arc magmas by melting of young subducted lithosphere. *Nature,* Vol. 347, 662-665.

Drummond, M. S. *et al*. 1996. Petrogenesis of slab-derived trondhjemite –tonalite - dacite / adakite magmas. *Transactions of the Royal Society Edinburgh: Earth Sciences*, Vol. 87, 205-215.

Farrar, E et al. 1978. Age of the Sangdong tungsten deposit, Republic of Korea, and its bearing on metallogeny of the southern Korean peninsula. *Economic Geology,* Vol. 73, 547-566.

Kay, R. W. 1978. Alutian magnesian andesites-melts from subducted Pacific ocean crust. *Journal of Volcanology and Geothermal research.* Vol. 4, 117-132.

Kim, O. J. 1971. Study on the intrusion epochs of younger granite and their bearing orogenesis in South Korea. *Journal of Korean Institute of Mining Geology,* Vol. 4, 1-10.

Meinert, L. D. et al. 2005. World skarn deposits. *Economic Geology. 100th Anniversary Volume,* 299-336.

Mungall, J. E. 2002. Roasting the mantle: Slab melting and the genesis of major Au and Au-rich Cu deposits. *Geology*, Vol. 10, 915-918.

Misra, K. C. 2000. Skarn Deposits. In: *Understanding Mineral Deposits,* Kluwer Academic Publishers, AH Dordrecht, The Netherlands, 414-449.

Oyarzun, R *et al.* 2001. Giant vs small porphyry copper deposits conozoic age in northern Chile: adakitic vs normal calc-alkaline magmatism. *Mineralium deposita,* Vol. 36, 791-798.

Park H. -I. et al. 1988. K-ar ages of mineral deposits in the Taebaeg mountain district. *Journal of Korean Institute of Mining Geology,* Vol. 21, 57-67.

Pak S. J. et al. 2004. Systematic mineralogy and chemistry of gold-silver vein deposits in the Taebaeksan district, Korea: Distal relatives of a porphyry system. *Mineralogical Magazine.* Vol. 68, 467-487.

Titley, S. R. & Beane, R. E. 1981. Porphyry copper deposits: Part I. Geological settings, petrology, and tectogenesis. *Economic Geology.* 75th anniversary Vol., 214-235.

Wilson, M. 1989. *Igneous Petrogenesis Uniwin Hyman*, London.

Yogodzinski et al., 1995 Magnesian andesite in the western Aleutian Komandorsky region: Implications for slab melting and processed in the mantle wedge. *GSA Bulletin*, Vol. 107, 505-519.

Yun, H. S. 1986. Petrochemical study on the Cretaceous granitic rocks in the southern area of Hambaeg Basin. *Journal of Korean Institute of Mining Geology,* Vol. 19, 175-191.

The Effect of the Kizilcaören Complex Mineralization (Fluorite-Barite-Thorium-Rare Earth Elements) on Groundwaters in Kızılcaören (Beylikova) Eskisehir, NW,Turkey

Örgün Y. and Çelik Balcı N.

Istanbul Technical University (ITU), Faculty of Mines, Department of Geology Engineering, Ayazaga Kampusu, 34469-Istanbul, Turkey
E-mail: orgun@itu.edu.tr
Keywords: Fluoride, dental fluorosis; groundwaters, REE, radioactivity

ABSTRACT

The current study is carried out to investigate the effect of the Kızılcaören complex mineralization (Fluorite-Barite-Thorium-Rare Earth Elements) on the groundwaters in the Kızılcaören area. 32 groundwater samples were taken from the mining district and its vicinity. The samples were analyzed for major and minor hydrogeochemical parameters along with natural radioactivity levels (gross-alpha (α) and -beta (β)). The results indicate that the groundwaters in the region can be classified as Ca-HCO_3, Ca-Mg-HCO_3, Mg-HCO_3, Ca-Mg-Na-HCO_3, type of water in the decreasing order, respectively. The concentration of Ba, F, U, Rare Earth Elements (La, Ce, and Y) in the groundwater from the mining district are significantly higher than those taken from the pristine water samples. This is especially true for the fluoride concentration. The fluoride concentration of the samples from the mining district and its near vicinity are higher than 1.0 mg/l. The gross-α and -β activity concentrations ranged from 0.006 to 0.12 Bq/l and from 0.01 to 0.24 Bq/l, respectively; the highest activity values were determined in the mining district. Our results suggest that the mineralization dominantly controls the F, Ba, U, La, Ce, Y concentrations and gross-α activities in the groundwaters.

INTRODUCTION

The major anion (Cl^-, $SO4^{2-}$, F^- etc.), cation (Ca^{2+}, Mg^{2+} etc.), trace elements and natural radionuclide concentrations in groundwater depend on the mineralogical and geochemical composition of the aquifer rocks, degree of weathering of the rocks, the chemical composition of the water, redox conditions, and the residence time of the groundwater in soil and aquifer. Fluoride is one of the important constituents in drinking water and fluoride is derived from both natural sources (rocks, soil or mine areas) and anthropogenic activities such as phosphatic fertilizers containing fluoride as an impurity. Through weathering of the F-bearing minerals that occur in almost all rock types, especially granites, granite gneisses, pegmatites and alkaline and acidic volcanic rocks, fluoride is released into the groundwater or soil. Therefore, high fluoride concentration in

groundwater is generally associated with these type rocks (Handa, 1975; Wenzel & Blum, 1992; Banks *et al*., 1998; Mahlknecht *et al*., 2004).
The activity concentrations of natural radionuclides in groundwater are connected to the activity concentrations of uranium (U), thorium (Th) and potassium (K) and their decay products in soil and granitic and alkaline volcanic- bedrocks. Thus, natural radioactivity levels of groundwaters derived from these rocks may exceed recognised drinking water norms (Reimann *et al*., 1996; Banks., *et al*., 1998; Örgün *et al*., 2005). The gross-alpha (α) activity in the groundwater samples dominantly originated from the ^{238}U and its daughter ^{226}Ra, while gross -beta (β) activity is principally from ^{232}Th and its daughter products such as ^{228}Ra and ^{228}Ac, and ^{40}K (Conthern & Rebers, 1990). Limit values for gross-α and -β radioactivity concentrations in drinking water are 0.1 and 1.0 Bq/l, respectively (WHO, 1996). These guidelines ensure an exposure lower than 0.1 mSv/yr assuming a water consumption rate of 2 L/day.
Kızılcaören complex mineralization (Fluorite-Barite-Thorium-Rare Earth Elements) is located at approximately 2 km south of the Kizilcaören village (Fig. 1 and Fig. 2). There has not been any mining operation in the mine area since present. The rural population use groundwater for drinking, domestic and irrigation purposes. Elevated concentrations of fluoride in groundwaters have been reported in the Kizilcaören district and the endemic fluorosis in the village is unfortunately more prevalent (Fidanci *et al.,*1994). This article examined the mineralogical and chemical characteristics of the Kizilcaören mining district, chemistry of the groundwaters, and the impact of the Kizilcaören F-Ba-Th-REE mine on the groundwater.

Geology, topography and climate of the study area

The Kizilcaören fluorite-barite-thorium-rare earth element deposit is located in Beylikova, Eskisehir region, in northwestern Anatolia. In the Kizilcaören district and near vicinity, the main rock types are Mesozoic metamorphic rocks, phyllites and partly metamorphosed clastic rocks (metaarkose, metagreywacke, sandstone and massive and partly metamorphosed limestone blocks), Cretaceous serpentinized ultrabasic rocks, Oligo-Miocene volcanic unite, Pliocene unconsolidated sand, clay and pebble and alluvium (Fig. 1). Weathering, alteration and fracturing are common in the magmatic and metamorphic rocks; however their degrees range from one spot to another. Oligo-Miocene volcanic unite consist of silicified trachytic tuff, alkaline trachyte and phonolite, breccia zones and ore veins (Özgenç, 1993). The Triassic clastic rocks and Oligo-Miocene volcanic rocks host the ore veins, also. The Kızılcaören district is transversed by closely spaced normal faults (Fig. 1). Three fault systems define the geometry of the fluorite-barite-REE deposits and the deposits seem to be related to these faults (Özgenç, 1993; Gültekin *et al*., 2003).

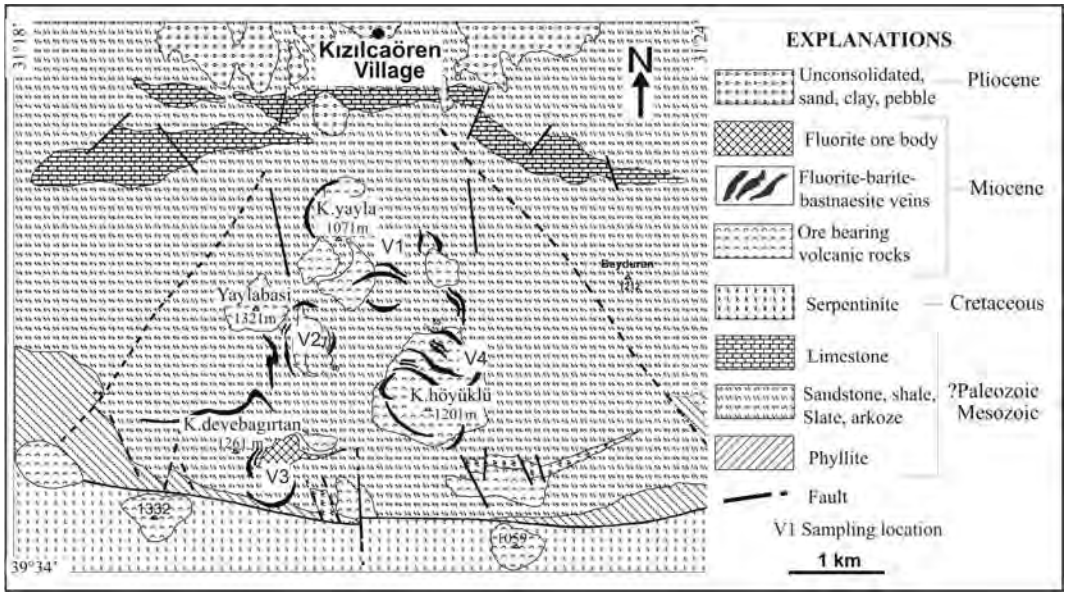

Figure 1: Geological map of the Kizilcaören mine district (modified from Özgenç, 1993). The thickness of the ore veins is exaggerated.

The study area lies at an altitude of 1330-800 m and is dissected hilly topography. Mountains in the south and south-east part of the study area reach 1500 m. Further north the topography is smoother and gentler with an approximately altitude of 800 m. The main aquifers that have low and locally high discharge are limestone, sandstone, greywacke, unconsolidated sand, clay, pebble and altered or non altered volcanic rocks in the study area. The area is drained mainly by Porsuk river that is major perennial river in the region. However, the majority of the streams are ephemeral, except Okcu stream. The general direction of groundwater flow is from mine district to Porsuk river, which flows in north direction (Figure 2). The region has a semiarid-type climate with dry summers and cold and wet winters dominant. July and August are the hottest months with average temperatures around 35 ^{o}C, whereas January and February are the coldest with temperatures around 0^{o}C. The annual precipitation is average 400 mm. The area is covered mainly bush and scrub. Cultivation is restricted to wheat and fruit.

Mineralogical and chemical characteristics of the Kizilcaören Mine area

The Kizilcaören F-Ba-Th-REE deposit is the most important fluorite, barite, thorium and Rare Earth Element resource in Turkey. Mineral Research and Exploration Institute of Turkey (MTA) identified a geological reserve of 0.4 Mt grading at 0.2 % ThO and 4 Mt grading at 0.3% Ce+La+Y, in additional 2 Mt of fluorite (proven reserves) with estimated ore reserves of over 10 Mt and a total reserve of the commercial barite of about 40 Mt. The Kizilcaören district consists of four separate mineralized areas (as shown in V1-V4, Fig.1) in which the concentrations of fluorite-barite-REE are probably of sufficient size

to merit production. The chemical analyses of the samples taken from the mine district are given in Table 1. In the Kizilcaören deposit the main ore minerals are fluorite, barite and bastnaesite. In general, bulk paragenesis is from fluorite through REE-carbonates to barite. The fluorite occurs typically as subhedral, coarse-grained aggregates in the fault zones, sometimes as fluorite masses. The mineralogical studies have revealed the presence of four REE-bearing phases accompanied by fluorite and barite. These are: bastnaesite, brockite, flurencite and monazite (Özgenç, 1993; Stumbfl & Kırıkoglu, 1985; Gültekin *et al.,* 2003). Of these, bastnaesite is the main Ce-bearing phase. Other members of the Kizilcaören mineral assemblage are quartz, calcite, pyrolusite, psilomelane, hematite, pyrite, phlogopite, plagioclase, feldspar, goethite, braunite and rutile in decreasing order of abundance.

Sample location	V1	V2	V3	V4
SiO_2	20.44	10.93	9.48	12.36
Al_2O_3	4.18	5.53	3.73	3.08
TiO_2	0.10	0.27	0.15	0.05
Fe_2O_3	4.19	4.68	3.90	1.92
MgO	1.97	2.89	2.66	2.10
CaO	5.25	3.90	3.85	2.88
Na_2O	0.05	0.05	0.05	0.05
K_2O	0.10	0.30	0.30	0.10
MnO	1.63	3.45	2.67	0.67
P_2O_5	0.60	0.28	0.56	0.43
$BaSO_4$	22.95	30.49	28.46	38.47
CaF_2	30.16	32.07	37.13	32.19
La+Ce+Y	3.77	2.54	1.76	1.94
Th	0.30	0.25	0.12	0.13

Table 1.The chemical analysis of the ore veins from the Kizilcaören mine district (wt%)

Sampling and Analytical Methods

In this study, 32 groundwater samples taken from wells, fountains and springs were analyzed. The samples were taken from 10 villages and the mine district (Fig. 2). The samples were collected in September

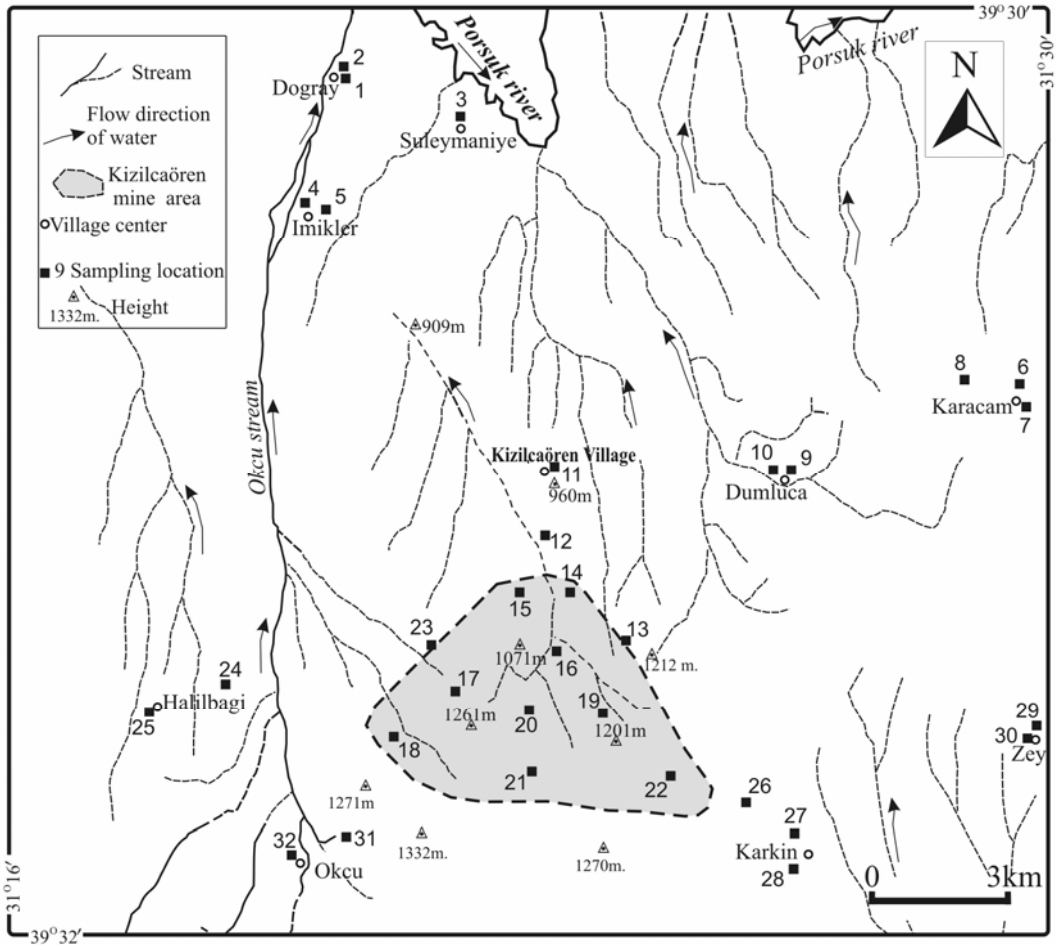

Figure: 2 The Kizilcaören mine area, Stream system of the study area and water samples locations

2002 (dry season). The 50-ml acidified samples were analyzed for major cations and trace element contents. 50-ml unacidified samples (2 % HNO_3) were analyzed for F^- and major anions content. All the analyses were performed based on the strict protocol. The fountains were run for 10 minute before drawing the samples. All polyethylene bottles used for the sampling were rinsed thoroughly three times with groundwater and the water samples were filtered by using 0.45 μm membrane filter for the analysis. pH and electrical conductivity (EC) were measured in-situ with portable devices (pIONeer 65, Portable Multi-parameter Instrument); alkalinity was measured by titration using Aquamerck 1.11109.0001 Alkalinity Test, in the field. The major cations (Ca, Mg, Na, K) and other trace element (As, U, Fe, La, etc.) concentrations were analyzed by using the ICP MS technique at ACME Laboratories (Canada). The WASTWATRB7 was used as a standard for ICP-MS analyses with detection limits of 0.02 μg/l for U and 0.05 μg/l for Th. The major anions (F, Cl^-, SO_4^{2-}) were determined by using the Photometer MPM 3000 using Merck Cell Tests 1.14547, 1.14548 and 1.14730, respectively, at Istanbul Technical University, in laboratories of Faculty of Mines.

In order to determine the activity concentrations (gross-α and gross-β) of the groundwaters, total 10 samples were used; 4 samples from the mine district and the rest (totally 6 samples) was from the pristine water. For this purpose, 1000-ml acidified samples were stored in polyethylene bottles. The gross- α and gross- β activities were measured using a low-level LB 770 counter. The sample preparation and all radioactivity measurements were made in Cekmece Nuclear Research and Training Center, Department of Health Physics counting laboratory (Istanbul-Turkey). The details of the sampling, sample preparation and the analyses were published in Örgün et al., (2005).

RESULT AND DISCUSSIONS

Chemical characterization of the groundwaters

The physicochemical parameters of the groundwater samples are presented in Table 1. The groundwaters used for drinking and irrigations purposes by rural population are general moderately hard in character (from 44.50 to 20.11 F^o, in French Hardness). The waters have pH values ranging from 6.98 to 8.29. The lowest pH (sample 16, Table 2) value belongs to the sample taken from the mine district. The conductivity (EC) values vary from 1067 to 334 µS/cm. In the mine district EC values are low, ranging from 446 to 359 µS/cm.

In general, Ca values are higher than Mg, and Ca is the dominant cation in the groundwater (Table 2). The Ca and Mg values vary from 21.1 to 138.4 mg/l and 116.6 to 4.2 mg/l, respectively. The K values are very low and vary from 0.1 to 3.2 mg/l. Na is higher than K in the all samples and the values very from 0.5 to 23.5 mg/l. The highest Na+K value was obtained in the sample (sample 16, Fig. 2, Table 2) taken from the mine area, as 24.3 mg/l. As seen from Table 2, in the mine district major cation values of the samples are very homogeny than those of the samples taken from the other parts of the study area. It is know that chemical composition of the groundwaters depend on the mineralogical and geochemical composition of catchment area and aquifer rocks. As mention above there are several different rock type in the study area and their mineralogical and chemical composition are different from the each other. The Kizilcaören village and the mine district are located on the clastic rocks (metaarkose, metagreywacke, sandstone and massive and partly metamorphosed limestone blocks) and volcanic rocks (silicified trachytic tuff, alkaline trachyte and phonolite) (Fig.1). The limestone blocks are commonly observed on the northern part of the mine district and southern of the

Sam.	pH	EC[1] µS/cm	Ca mg/l	Mg mg/l	Na mg/l	K mg/l	HCO_3 mg/l	Cl mg/l	SO_4 mg/l	F mg/l	As µg/l	Ba µg/l	Cr µg/l	Cu µg/l	Fe µg/l	Mn µg/l	U µg/l	Th µg/l	Ce µg/l	La µg/l	Y µg/l
1	7,65	610	87,2	32,2	18,8	1,1	420,3	19	18	0,61	<0,05	46,2	4,2	0,9	45	0,1	0,05	<0,05	<0,01	<0,01	0,01
2	7,37	583	65,6	70,4	20.7	1,8	256,4	147	63	0,55	<0,05	57,3	4,3	0,9	20	0,1	0,05	<0,05	<0,01	<0,01	0,01
3	8,29	847	19,3	116,6	1,8	0,1	558,3	21	38	0,57	<0,05	63,8	5,1	0,8	52	0,1	0,03	<0,05	0,01	<0,01	0,01
4	8,08	398	112,4	31,4	2,1	0,8	436,2	22	25	0,53	<0,05	52,8	4,8	0,5	69	0,1	0,04	<0,05	<0,01	<0,01	0,01
5	8,20	636	103,4	8,7	2,5	0,2	318,1	9	21	0,56	<0,05	78,4	5,1	1,2	112	0,1	0,08	<0,05	<0,01	<0,01	0,01
6	7,39	660	69,3	81,5	15,6	0,5	465,2	39	82	0,60	<0,05	46,8	7,3	7,0	23	1,2	0,07	<0,05	<0,01	<0,01	0,01
7	7,72	850	57,7	93,3	2,7	0,3	453,6	27	114	0,49	<0,05	56,4	2,5	0,1	89	0,9	0,09	<0,05	<0,01	<0,01	0,01
8	8,01	1067	66,9	8,3	2,4	0,1	459,7	38	99	0,50	<0,05	55,3	4,6	0,9	45	0,1	0,09	<0,05	0,01	<0,01	0,01
9	7,53	425	117,6	5,6	1,1	0,1	299,2	21	37	0,37	<0,05	68,5	6,1	3,0	178	0,6	0,58	<0,05	<0,01	<0,01	0,01
10	7,33	476	116,4	4,2	0,9	0,1	328,3	24	4	0,70	<0,05	75,2	4,3	0,2	33	0,2	0,51	<0,05	0,01	<0,01	0,02
*11**	*8,12*	*688*	*97,6*	*25,7*	*2,2*	*0,1*	*425,7*	*19*	*15*	*0,75*	*0,05*	*85,2*	*1,9*	*0,7*	*269*	*0,3*	*1,01*	*<0,05*	*0,01*	*0,02*	*0,02*
*12 **	*7,78*	*554*	*99,3*	*21,8*	*23,5*	*0,2*	*398,2*	*23*	*26*	*0,97*	*0,5*	*104,6*	*3,5*	*1,8*	*293*	*0,3*	*2,78*	*<0,05*	*0,01*	*0,02*	*0,03*
*13**	*7,93*	*521*	*73,8*	*19,2*	*19,3*	*2,1*	*306,6*	*21*	*24*	*1,10*	*1,2*	*98,2*	*3,1*	*1,1*	*98*	*0,3*	*3,29*	*<0,05*	*0,01*	*0,30*	*0,11*
*14 **	*7,87*	*422*	*53,3*	*18,4*	*15,5*	*1,2*	*258,7*	*18*	*6*	*1,94*	*2,3*	*212,5*	*2,4*	*0,9*	*171*	*0,4*	*3,20*	*<0,05*	*0,02*	*0,09*	*0,13*
*15 **	*7,76*	*372*	*69,3*	*24,6*	*16,3*	*2,2*	*306,1*	*29*	*18*	*2,32*	*3,0*	*196,4*	*2,3*	*0,7*	*243*	*0,1*	*2,14*	*<0,05*	*0,03*	*0,30*	*0,22*
*16 **	*6,98*	*423*	*25,5*	*34,7*	*21,1*	*3,2*	*280,3*	*14*	*8*	*2,50*	*12,0*	*154,3*	*2,1*	*0,4*	*148*	*19,2*	*1,41*	*<0,05*	*0,53*	*0,41*	*0,25*
*17 **	*7,67*	*365*	*67,8*	*21,3*	*14,3*	*1,5*	*301,9*	*24*	*5*	*2,32*	*6,1*	*239,1*	*3.5*	*0,8*	*151*	*3,6*	*2,39*	*<0,05*	*0,32*	*0,40*	*0,24*
*18**	*8,06*	*372*	*87,3*	*22,5*	*17,1*	*2,2*	*357,7*	*32*	*10*	*2,41*	*5,4*	*208,3*	*2,8*	*0,5*	*241*	*2,4*	*1,87*	*<0,05*	*0,08*	*0,20*	*0,18*
*19 **	*8,03*	*372*	*43,3*	*17,8*	*16,8*	*1,8*	*238,2*	*14*	*6*	*2,60*	*3,2*	*212,1*	*2,2*	*0,8*	*235*	*1,2*	*2,36*	*<0,05*	*0,03*	*0,09*	*2,26*
*20 **	*8,21*	*446*	*26,7*	*35,3*	*21,1*	*2,5*	*273,9*	*14*	*13*	*2,80*	*4,9*	*369,7*	*1,7*	*1,3*	*192*	*1,1*	*5,53*	*<0,05*	*0,04*	*0,08*	*0,27*
*21 **	*8,27*	*359*	*74,5*	*20,7*	*16,5*	*1,0*	*343,5*	*15*	*5*	*2,70*	*1,6*	*376,5*	*3,0*	*0,9*	*261*	*1,2*	*8,63*	*<0,05*	*0,03*	*0,09*	*0,27*
*22 **	*7,86*	*422*	*41,8*	*20,9*	*8,3*	*1,7*	*216,8*	*13*	*10*	*2,60*	*3,9*	*223,6*	*1,9*	*1,1*	*212*	*2,1*	*4,29*	*<0,05*	*0,01*	*0,10*	*0,21*
*23**	*7,93*	*612*	*78,2*	*21,1*	*10,8*	*1,1*	*315,5*	*14*	*27*	*0,85*	*2,1*	*183,1*	*2,3*	*0,4*	*186*	*0,9*	*2,49*	*<0,05*	*0,02*	*0,06*	*0,09*
24	7,53	427	72,2	11,5	4,7	0,3	241,7	16	21	0,48	1,1	20,1	2,1	1,1	64	0,5	0,53	<0,05	0,01	0,01	0,03
25	7,62	436	82,1	13,7	4,9	1,0	308,4	9	16	0,50	<0,5	56,8	2,9	1,3	85	n.d	0,24	<0,05	0,01	0,01	0,01
26	7,70	597	99,3	21,4	22,7	0,2	433,6	22	21	0,93	<0,5	45,3	3,5	1,6	296	0,2	2,53	<0,05	0,01	0,02	0,01
27	7,49	596	88,5	21,2	10,1	2,7	357,3	15	20	0,53	<0,5	39,4	4,9	1,5	241	0,8	1,96	<0,05	<0,01	0,02	0,01
28	7,52	584	96,6	22,8	17,8	3,2	403,3	12	27	0,60	<0,5	18,6	4,2	1,6	151	0,7	0,56	<0,05	<0,01	0,04	0,01
29	7,29	613	138,4	6,6	1,4	0,2	385,2	17	29	0,42	<0,5	24,2	0,8	0,3	15	0,6	<0,02	<0,05	<0,01	0,01	0,01
30	7,87	334	126,2	4,3	0,5	0,1	374,4	2	19	0,41	<0,5	25,3	0,5	0,4	20	0,7	<0,02	<0,05	<0,01	<0,01	0,01
31	8,22	443	21,8	33,3	0,7	0,1	236,5	4	10	0,37	<0,5	12,9	9,7	0,3	108	0,7	<0,02	<0,05	0,01	0,02	0,01
32	8,24	403	20,1	35,4	0,8	0,1	215,3	15	4	0,10	<0,5	12,1	8,6	0,2	124	0,8	0,3	<0,05	0,01	<0,01	0,01

*[1]: EC :Conductivity *:The samples taken from the mine district*

Table 2. The chemical analyses of the groundwaters

Kizilcaören village and volcanic rocks are also in the mine district. Both of these type rocks contain a high percentage of Na-K-bearing minerals such as orthoclase and plagioclase, and carbonate bearing minerals such as calcite and dolomite. Thus, HCO_3, calculated from alkalinity, is dominant anion in the samples and its concentration ranges from 558.3 to 215.3 mg/l. All of the water samples showed that ratio of HCO_3 to SiO_2 is greater than 10, indicating that carbonate weathering could be the major water-rock interaction in the groundwater system. The concentrations of Cl^- and SO_4^{2-} in the samples vary from 2 to 147 mg/l and 4 to 114 mg/l, respectively. The concentrations of Cl^- and SO_4^{2-} of the samples taken from the mine area range from 13 to 29 mg/l and from 5 to 27 mg/l, respectively (Table 2). All of these values are below the recommended value by WHO (1996).

The cation permutation of the samples are mostly in rCa> rMg> r(Na+K) with rarely rMg >rCa> r(Na+K) arrangements. Piper plots created by using the major dissolved ionic constituents of waters show that the groundwater compositions in the region are spread among the Ca-HCO_3, Ca-Mg-HCO_3, Mg-HCO_3 and Ca-Mg-Na+K-HCO_3 type waters; however, Ca-HCO_3 and Ca-Mg-HCO_3 type waters are common (figure is not given). The Ca-Mg-Na+K-HCO_3 type waters are essentially determined in the mine district. The water type in the region reflects that most of the groundwaters may be located within limestone, conglomerate, sandstone, shale, phyllite, volcanic rocks and alluvium.

The trace metal contents of the samples were also analyzed and the results were given in Table 2. As seen from the table, although the trace element concentrations of the samples are generally lower than drinking water guidelines of WHO (1996). The samples taken from the mine district shows the high element content relative to the pristine waters.

Although the Th content of the Kizilcaören complex mineralization is fairly high, Th concentration of the water samples (< 0.05 μg/l) is very low compared to U (varying from 0.02 to 8.60 μg/l). This is consistent with the fact that Th is very insoluble and immobile at least for pH >3-4 and also Th is highly reactive with mineral surface, and is much more strongly sorbed than U (Porcelli & Swarzenski, 2003). On the basis of this knowledge, the low Th content of the groundwaters from Kizilcaören region can be explained.

Similar to the U concentrations, Ba, Ce, La and Y content of the samples (from sample 12 to sample 23) are higher (Table 2). All of the results are consistent with the chemical analysis of the host rocks of the Kizilcaören complex mineralization and indicate that the source of Ba, Ce, La and Y in the groundwater is the mineralization.

Fluoride concentration of the groundwaters

The fluoride concentrations of the groundwaters range from 0.10 to 2.85 mg/l. As seen from Table 2, the higher F^- values belong to the mine district, and the values range from 1.10 to 2.85 mg/l (from 13 to sample 22) (Fig. 3). As stated previous, the higher Na + K values belong to the groundwater derived from the mine area. Moreover, these groundwaters are alkaline in pH (7.67 - 8.27; except sample 16, Table 1) and their EC, Ca^{2+} and HCO_3^- values range from 359 to 521 μS/cm, 25.5 to 87.3 mg/l and 216.8 to 357.7 mg/l, respectively. All of these conditions are favourable physico-chemical conditions for the decomposition and dissolution of the fluorite (Saxena & Ahmed, 2003).

As seen from Fig. 2, the general direction of groundwater flow is from the mine area (south) to the Kizilcaören village. However, the samples (4, 5, 9 and 10) do not show significant F concentration (Table 2). Low F concentration in the northern and eastern part of the Kizilcaören village may be due to different rock types. These parts of the study area consist of different rock types such as peridotite, claystone, sandstone, conglomerate, limestone and alluvium having very low F contents.

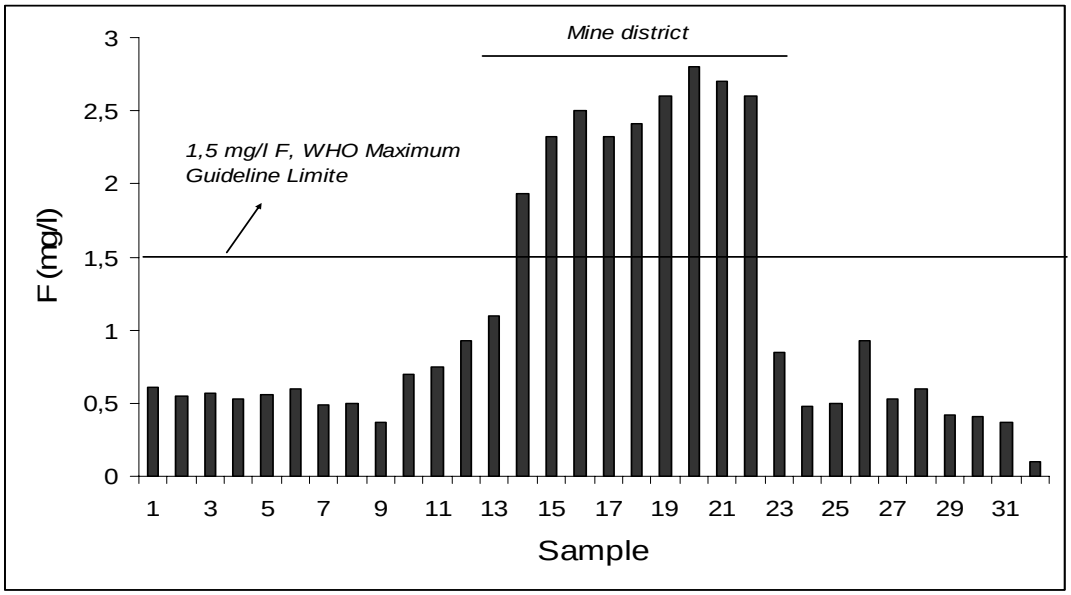

Figure: 3 Fluoride levels around the mine district and its vicinity

The World Health Organization has set an upper guideline limit for drinking water fluoride of 1.5 mg/l. As mentioned previous, the region is very hot especially summer (from May to September) and thus, daily water consumption is high. Climatic condition and dietary habits of the Kizilcaören village and the near vicinity population suggest that individual adult daily water consumption is on order of 3 to 3.5 liter. People in Kizilcaören village have been used groundwater derived from the mine district for drinking and domestic purposes until 1990. After that, the peasants of the Kizilcaören have begun to use another water source derived from out of the mine district; F content of the new water source is 0.75 mg/l. Dietary habits in this region may also increase F^- levels above WHO food intakes of 0.2-0.5 mg / day. Because the mine area and its near vicinity is arable fields of the village and also F-bearing waters is used for irrigation. So, cereal, vegetable, fruit and animals are indirectly influence by the mine. In present, 10-15 people live in the Kizilcaören village and dental fluorosis are very common among those people. Deficiency of the fluoride in drinking water (< 0.6 mg/l) causes dental caries but more than the permissible limit of 1.5 mg/l causes skeletal and dental fluorosis (Susheela *et al.,* 1999).

Natural radioactivity levels of the samples

For determine the natural radioactivity levels in the groundwaters, total 10 sample were chosen; 4 sample (19, 20, 21 and 22) from the mine area and 6 samples from the villages (7, 9, 24, 27, 30 and 31). The gross-α and gross-β activity concentrations

vary from 0.004 to 0.12 Bq/l and 0.01 to 0.24 Bq/l, respectively. As seen from Fig. 4, the highest gross-α and gross-β values belong to the mine district.

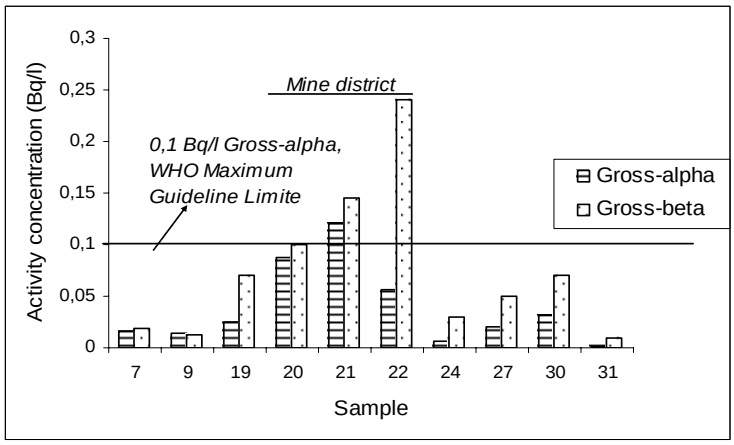

Figure: 4 The gross-α and gross-β activity concentrations

In the mine district, the gross-α and gross-β values vary from 0.025 to 0.12 Bq/l and 0.07 to 0.24 Bq/l, respectively. The sample having the highest gross-α value (0.12 Bq/l) was taken from a spring that was used for irrigation in the mine area. All of the activity concentrations are consist with the U and Th content of the groundwaters in the region.

CONCLUSIONS

The groundwaters are general moderately hard in character. The waters in the region are Ca- HCO_3, Ca-Mg-HCO_3, Mg-HCO_3 and Ca-Mg-Na+K-HCO_3 type; however, Ca-HCO_3 and Ca-Mg-HCO_3, type waters are common. The Ca-Mg-Na+K-HCO_3 type waters are essentially determined in the mine district. The major cation and anion concentrations of the samples are below the WHO drinking water guidelines.
The concentration of As, Ba, F, U, Rare Earth Elements (La, Ce, Y) in the groundwater from the mining district are significantly higher than those taken from the pristine water samples. The F concentrations in the mining district are higher than 1.0 mg/l. The highest activity concentrations were determined in the samples from the mining district to be 0.12 Bq/l gross-α and 0.24 Bq/l gross-β. Our results suggest that the mineralization dominantly controls the F, Ba, U, La, Ce, Y concentrations and gross-α activities relative to As, Cu, Fe and Mn in the groundwaters.

ACKNOWLEDGEMENT

This study is financially supported by Scientific Research Projects Unite of Istanbul Technical University (ITU) (Project Number: 1698).

REFERENCES

Banks, D. *et al.* 1998. The chemistry of Norwegian groundwaters: I. The distribution of radon, major and minor elements in 1604 crystalline bedrock groundwaters. *Science of the Total Environment, Vol.* 222, 71-91.

Conthern, C.& Rebers, P. 1990. Radium, radon and uranium in drinking water. *Lewis Publishers,* Michigan.

Fidancı, UR. *et al.* 1994. The fluorid content of water sources in Kızılcaören village in Eskişehir. *Turkish Journal Of Medical Sciences,* Vol. 20, 15-17.

Gültekin, AH**.** *et al.* 2003. Geology, mineralogy and fluid inclusion data of the Kızılcaören fluorite-barite-REE deposits Eskişehir-Turkey, *Journal of Asian Earth Science,Vol.* 21/4, 365-376.

Handa, BK. 1975. Geochemistry and genesis of fluoride containing groundwater in India. *Ground Water* Vol. 13, 275-281.

Mahlknecht, J. *et al.* 2004. Groundwater chemistry and mass transfers in the independence aquifer, central Mexico, by using multivariate statistics and mass-balance models. *Environmental Geology*, Vol, 45, 781-795.

Örgün, Y. *et al.* 2005. Natural Radioactivity Levels in Granitic Plutons and Groundwaters in Southeast Part of Eskisehir, Turkey, *Applied. Radiation Isot*ope, Vol.63, 267-275.

Özgenç, I. 1993. *Kizilcaören (Sivrihisar-Eskişehir) karbonatit, bastnezit-fluorit-Barit yatagının jeolojisi ve nadir toprak element jeokimyası.* Türkiye Jeoloji Bülteni, Vol.36, 1, 1-11 (in Turkish).

Porcelli, D & Swarzenski, PW. 2003 The behavior off U- and Th-series nuclides in groundwater. In: *Uranium-Series Geochemistry. Bourdon, B., Henderson, G. M., Lundstrom, C. C., Turner, S.P., Eds., Reviews in Mineralogy & Geochemistry*, Vol. 52**.** p.317-361.

Reimann, C, *et al.* 1996. Radon, flouride and 62 elements as determined by ICP-MS in 145 Norwegian hard-roch groundwater samples. *Science of the Total Environment*, Vol,192, 1-19.

Saxen VK and Ahmed S. 2003 Inferring the chemical parameters for the dissolution of fluoride in groundwater. *Environmental Geology,* Vol, 43, 731-736.

Stumbfl, E.F & Kırıkoğlu, M.S. 1985. Fluorite-barite-rare earths deposits at Kızılcaören, Turkey. Mitt. Österr. Geol. Ges. , Vol,78: 193 – 200.

Wenzel, WW & Blum, WEH. 1992. Fluoride speciation and mobility in fluoride contaminated soil and minerals. *Soil Science, Vol,* 153, 357-364.

US EPA 2000 December 7, 2000, Federal Register, Part II Environmental Protection Agency 40 CFR Parts 9, 141, and 142 National Primary Drinking Water Regulations; Radionuclides; Final Rule.

WHO 1996 Guidelines for Drinking Water Quality. Recommendations, Vol. 2, Health Criteria and other Supporting Information, Geneva.

Air pollution prediction models of particles, As, Cd, Ni and Pb in a highly industrialized area.

[1]Vicente-Fortea, A. B., [3]Sánchez-Barbie, A., [2]Jordan-Vidal, M. M., [1]Sanfeliu-Montolio, T. and [3]Esteban-Lefler, Mª D.

[1] Dpto. de Ciencias Agrarias y de Medio Natural. Universidad Jaume I de Catellón. Campus Riu Sec s/n 12071 Castellón.
E-mail: avicente@sg.uji.es.
[2] Dpto. de Agroquímica y Medio Ambiente. Universidad Miguel Hernández de Elche. Avda. de la Universidad s/n. 03202 Elche (Alicante).
[3] Dpto. de Estadística, Matemáticas e Informática. Instituto Universitario Centro de Investigación Operativa. Universidad Miguel Hernández de Elche. Avda. de la Universidad s/n. 03202 Elche (Alicante).
Keywords: Air Pollution, Ambient Air, Prediction Models, Public Health, TSP, PM10, Heavy Metals.

ABSTRACT

A study was carried out of TSP (Total Suspended Particles), PM10, As, Cd, Ni and Pb concentration levels in ambient air, in a highly industrialized area in the ceramic cluster of Castellón during five years (2001-2005). The origin of the contamination in this area is both natural and anthropogenic. The natural origin is due to the resuspension of mineral materials from the surrounding mountains and from the long-range transport of materials from North Africa. The anthropogenic contamination sources that stand out include the non-metallic mineral material industries (ceramic production), chemical industries (color, frit and enamel manufacturing) as well as vehicular traffic. The objective of this study was the elaboration of a series of mathematical models with the aim of short-term prediction of these contaminants that depend on some known variables. The goal is to provide a useful instrument to alert the population facing possible episodes of high concentrations of atmospheric pollution.

INTRODUCTION

The high development reached by our society, due to a constant increase in the demand of consumer goods and from the requirements of technological advances, brings as a consequence the use of raw materials and their subsequent industrial transformation. All this introduces large quantities of chemical substances into the atmosphere, whose behavior in the natural environment and the effects upon living organisms and material goods are unknown in some cases. Atmospheric pollution is

in part formed by industrialized life, and a consequence of industrialized areas' constant development (Boix *et al*., 2001; Gómez *et al*., 2005; Jordan et al., 2005).
The requirement for clean and pure air comes from treating it as a limited and common good, indispensable for life. Earth's atmosphere is finite and its self-cleansing capacity has limits. As such its utilization must be subjected to practices that prevent the deterioration of its quality, from either use or abuse, in such a way that its purity is preserved for a guaranteed normal development of living beings.
In the present study an assessment of atmospheric air quality was conducted, keeping in mind the atmospheric particulate (TSP, PM10, As, Cd, Ni and Pb) in the municipality of Vila-real (Fig. 1), during 5 years, from 2001 to 2005. The objective was the elaboration of a series of mathematical models with the aim of short-term prediction of these contaminants that depend on some known variables. The goal is to provide a useful instrument to alert the population facing possible episodes of high concentrations of atmospheric pollution.

Fig. 1 Location of studied area.

DESCRIPTION OF THE STUDIED AREA

The general study zone is located in an important ceramic industrial area in the province of Castellón (Spain). This area produces approximately 93% of the Spanish ceramic tiles, and 95 % of frits, enamels and colors. It is at the E-SE part of the province, and is approximately 1000 Km2. One place has been chosen in this ceramic cluster: the municipality of Vila-real (Castellón), which possesses a high industrial density. The area of the atmospheric study is located in the southwest of the municipality of Vila-real. This industrial city is located in the east of the province of Castellón, and is 46 meters above sea level in the "Plana Baixa" Community. The population nucleus resides between two fluvial basins, the River Millars to the north and the Riu Sec to the south. The population of the municipality, according to the Vila-real Council, numbers approximately 49,000 inhabitants.
There is also a high traffic density in the area, a consequence of the proximity of the population to various community roadways, the AP-7 toll motorway and also the N-340 highway. These two factors cause punctual high concentration peaks of atmospheric particle contaminants.

The main emission sources of the area (Fig.2) are the traffic (mobile sources), the manufacturers of ceramic tiles and frits, enamels and ceramic colors (both fixed sources).

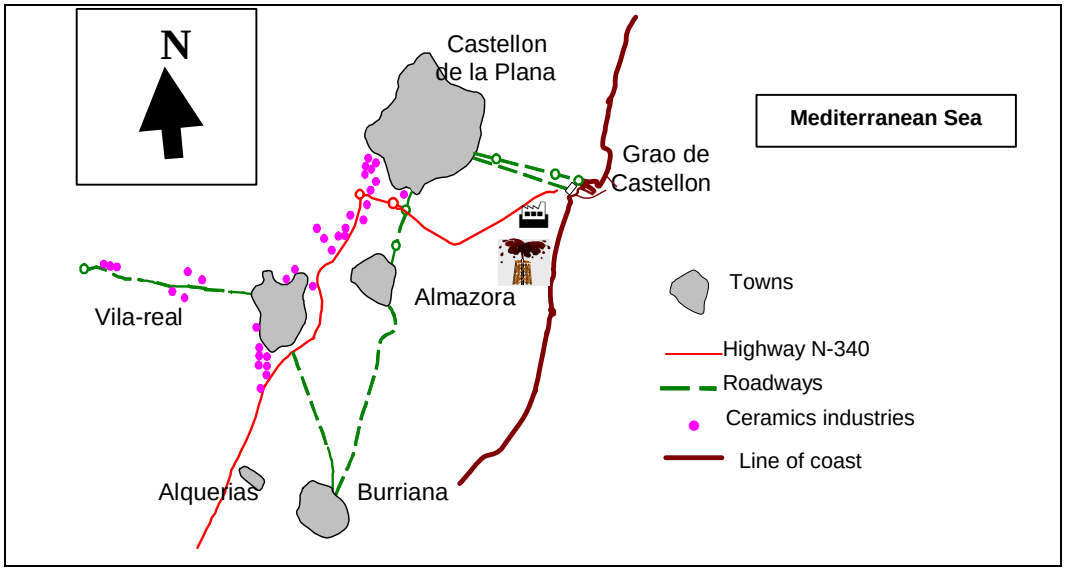

Fig. 2 Location of the primary emission sources in the studied area.

SAMPLING CONDITIONS

The sampling station was installed, conforming to the guideline of the implantation of Directive 1999/30/CE, in the southwestern portion of Vila-real, specifically within the municipal warehouse installations of this locality (UTM coordinates: X 746.543 Y 4.424.906).

In order to avoid measuring microclimates the sampling station was located in an open area containing al least 500 m2. There were no restrictions to the airflow around the sampling entrance point, established approximately 3 meters above ground level on a special metallic platform. There were no local emission sources nearby, in this way avoiding a distortion of the sample due to the influence of smoke plums of specific contaminants.

The technology of the equipment used consists in blowing air through an inlet with a vacuum pump. According to the characteristics of the inlet, different types of atmospheric particles were collected, TSP or PM10 (Vicente et al., 2007). Particles were trapped on a permeable support, being a 47mm diameter filter. Quartz fiber filters were used in the sampling. They are made of a pure SiO_2 base, with a total absence of additives. Polystyrene cassettes were used to protect the filters during transport and storage.

A PM10 medium volume sampler was used, model IND-LVS3, manufactured by Kleinfiltergerät. This device is considered as a reference according to the European regulations (Directive 1999/30/CE; UNE-EN 12341:1999) for the sampling of PM10 particles. The particulate matter was blown in through the opening circumference between the frame and round cover mounted on top. Within the sampler inlet the

airflow was accelerated by eight impactor nozzles and then directed toward the impacting surface. The device contains a temperature sensor, with a radiation protector that eliminates deviations in the reading due to solar radiation, and also a pressure sensor. The sampling volume of flow was 2.3m^3/h during 24-h periods. 887 samples of the PM10 were collected.
For TSP sampling, the captor used was a high-volume MCV-8D sampler, according to Directive 80/779/CEE. The volume of flow was 1.5 m3/h during 24-h periods. 1003 samples of the TSP were collected.
Meteorological dates were also obtained from an automatic meteorological station (Weather Monitoring II-DAVIS), belonging to the Vila-real municipality. Daily dates were used to built a matrix for each sampling period with the following parameters: daily mean temperature, daily mean atmospheric pressure, daily mean humidity, wind direction, wind speed and daily total precipitation.

METHODOLOGY

Once the samples were collected, particle concentration levels were determined gravimetrically. This method consists in first weighing the empty filters and then with sample. The filters must be kept for at least 48-h in a special camera. The conditions inside the camera are 50% humidity and 20ºC temperature, according to normative UNE –EN 12341:1999.

Fig. 3. Camera

Fig. 4. Filters inside the weight camera

Fig. 5. Analytical precision set.

The weights of the collected samples are obtained with the use of an analytic scale having a precision of 0.1 mg. The PM10 concentration levels are determined from the sample quantities obtained and the volume of air pumped using the expression:

$$C_{PM} = (Pm-Pv)\ 10^6/V_{air}$$

Being:

- C_{PM}: particle concentration in µg/m^3
- Pm: Weight of the sampled filter in g

- Pv: Empty weight of the filter in g
- V_{air}: Volume of air pumped in m^3

The As, Cd, Ni and Pb levels in the PM10 samples were determined by ICP-MS. The equipment utilized is a PerkinElmer model Elan-6000, with a 3600 lines/mm holographic network, 1 meter focal distance, 0.26nm/mm linear dispersion, 27.12 MHz frequency and 1.60 kw maximum power. The instrumental technique allows a rapid form of determining the As, Cd, Ni and Pb levels after dissolution of the sample. The dissolution is obtained by acid digestion in hermetic Teflon recipients. This methodology has been used by many authors (Kubilay et al., 1995 and Querol et al., 2000).

To determine the possible As, Cd, Ni and Pb traces that the reagents and quartz filter fibers might contain, giving rise to sample contamination, digestions with only reagents (blank reagents) and filters without a sample (blank filters) are performed. In the validation of the results the SRM 1648 “urban particulate matter” pattern was used, whose composition is particulate matter of anthropogenic origin collected in an industrialized urban atmosphere and adequate for use as a reference standard.

With the values obtained in ppb from the aforementioned technique described, the As, Cd, Ni and Pb concentration levels were determined, keeping in mind the possible traces that the reagents and quartz fiber filters utilized in the collection of samples may contain. The values are expressed in micrograms of As, Cd, Ni and Pb in PM10 per cubic meter of air.
As available data is time dependent, predictive models have been constructed by using Multiple Regression Analysis (Rencher, 2000) together with Time Series Models (Wei, 1990). We recall that one of the standard hypotheses in Multiple Regression Analysis is the independence of the residual errors. However if variables are periodically observed over time, lack of independence occurs and therefore straightforward linear regression predictions are inefficient. To avoid this difficulty, Time Series analysis, and more concretely ARIMA models, is used for modeling the behavior of residual errors. The SPSS 14.0 statistical software has been employed to analyze the obtained experimental data.

ATMOSPHERIC POLLUTING AGENTS PREDICTION MODELS

The target of this study is to construct a model to obtain predictions of a dependent variable based on several independent variables with information over time. The dependent variables are: TSP, PM10 in µg/m3, and As, Cd, Ni, and Pb in ng/m3. Independent variables are the following meteorological variables: average wind speed (Vmed, m/s), maximum wind speed (Vmax, m/s), wind direction (DirDomi, degrees), average temperature (TMedia, degrees Celsius), relative humidity (HR in %) and Pressure (Presion, milibares). All the independent variables are initially considered in the model, but only the significant ones are finally used to obtain predictions.

Modeling TSP variable based on meteorological variables.

The TSP model is:

$$PST = -1256.970 + 2.545 \times TMedia - 0.055 \times DirDomi + 1.282 \times \Pr esion + \varepsilon_t =$$

$$= -1256.970 + 2.545 \times TMedia - 0.055 \times DirDomi + 1.282 \times \Pr esion + 0.451\varepsilon_{t-1} - 0.316\varepsilon_{t-2} + a_t$$

ε_t is the prediction error, and is estimated as the difference between the observed and the predicted value in the model. a_t is a white noise with standard normal distribution.

TSP are solid or liquid particles with high sedimentation velocities and relatively short residence periods in the atmosphere. Their size range is between 0.1 and 32µm. Temperature increases cause the dryness of the substrate in the area and favor resuspension of these particles (Colombo *et al*., 1999; Gómez *et al*., 2001), and due to an increase of the TSP concentration in the atmosphere. On the other hand, TSP has short residence periods; their concentration is influenced by the wind direction. The relationship between TSP and the dominant direction is inverse, which is to say the TSP increases under low degree directions, for example NE (45º) winds, and decreases if the predominant wind is W (270º) or NW (315º). This behavior is logical when keeping in mind that the greatest sources of TSP are the ceramic sector businesses located between the SW (225º) and NW (315º) relative to the sampling point. The atmospheric pressure presents a direct relationship with TSP; with greater pressure there is less expansion of the lowest level layers in the atmosphere, decreasing as such the dispersion of the contaminants (Wark *et al*., 2000), which as a result brings a greater increase in the concentration. In this case it gives rise to an increase in the TSP concentration levels.

Modeling PM10 variable based on meteorological variables.

The PM10 model is:

$$PM10 = -1110.954 + 1.168 \times TMedia - 0.024 \times DirDomi + 0.257 \times HR + 1.112 \times \Pr esion + \varepsilon_t =$$

$$= -1110.954 + 1.168 \times TMedia - 0.024 \times DirDomi + 0.257 \times HR + 1.112 \times \Pr esion + 0.448\varepsilon_{t-1} - 0.342\varepsilon_{t-2} + a_t$$

Like in the TSP model, PM10 particles (particles between 0.1-10µm) depend in the same way upon the meteorological variables of average temperature, dominant wind direction and atmospheric pressure. The explanation is the same for TSP. With high temperatures there is greater terrain dryness, favoring resuspension (Colombo *et al.*, 1999; Gómez *et al.*, 2001), and giving rise to higher PM10 concentrations. When the pressure increases there is less expansion in the lowest layers of the atmosphere, carrying less dispersion of the contaminants with it, and increasing their concentration (Wark *et al.*, 2000). In the case of PM10 the two predominant sources of this contaminant are the ceramic sector business and traffic. The influence of the ceramic sector businesses is presented in the model with the inverse relationship between the PM10 concentration levels and the predominant wind direction, just as was described in the preceding section of the TSP, due to the location of the industrial parks between the SW (225º) and NW (315º) relative to the sampling point. However, unlike the TSP model, in that of the PM10 a direct relationship appears between this contaminant and the relative humidity (HR). This new variable introduces the influence of traffic upon the PM10 contaminant. The particles that contribute to the PM10 from traffic present a small particle size, which is to say, within the PM10 range are in the smallest region, around 1-2µm. These particles are

seen influenced by condensation processes, which at the same time are governed by the environmental humidity. With greater humidity there is greater condensation (McGregor, 1999), and greater concentrations of these particles.

Modeling As variable based on meteorological variables and PM10.
The As model is:

$$As = 13.104 + 0.064 \times PM10 - 0.333 \times TMedia + \varepsilon_t =$$

$$= 13.104 + 0.064 \times PM10 - 0.333 \times TMedia + 0.424\varepsilon_{t-1} - 0.239\varepsilon_{t-2} + a_t$$

Arsenic is a very volatile element that is presented in the lowest grain size fractions of PM10, 74.8% of arsenic is found in the fraction < 0.6µm (Fernández *et al*., 2001). It depends upon the temperature in an inverse fashion. Arsenic oxides, from different local sources, condense upon contact with the atmosphere; the aerosol-vapor equilibrium depends on the temperature. At low temperatures the aerosol phase is favored and at high temperatures the vapor phase (Pallarés *et al*., 2007). From this, the arsenic concentration increases at low temperatures just as the model demonstrates. Arsenic is shed by various previously cited sources, it must be noted that it stems from the combustion of combustible fossils, and these are used in many fields. From here on it does not depend upon meteorological factors besides that of wind direction.

Modeling Cd variable based on meteorological variables and PM10.
Obtained model for Cd is:

$$Cd = 1.541 + 0.034 \times V\max + \varepsilon_t$$

Cadmium, according to the proposed model, is related with the maximum wind velocity. Remember that this element is the chemical element studied that appears in lesser concentrations in PM10. Cadmium is found in 61.3% of that associated with the fraction < 0.6µm (Fernández *et al*., 2001), from which it has long residence times in the atmosphere (Röösli *et al*., 2001). The main source of this contaminant is the power station located at the El Serrallo industrial park (Grao de Castellon), and the ceramic sector businesses also contribute to a smaller degree. The power station is located farther away from the sampling point, some 15 km, than the ceramic sector industrial parks that are located in the same municipality, so the cadmium concentration levels increase as the velocity of the wind. It disperses the particles in a great measure, causing them to arrive to the sampling point in greater quantities from the main source.

Modeling Ni variable based on meteorological variables and PM10.

The *Ni* model is:

$$Ni = -2.682 + 0.045 \times PM10 + 0.083 \times TMedia + 0.009 \times DirDomi + 0.044 HR + \varepsilon_t =$$

$$= -2.682 + 0.045 \times PM10 + 0.083 \times TMedia + 0.009 \times DirDomi + 0.044 HR + 0.46 \varepsilon_{t-1} - 0.256 \varepsilon_{t-2} + a_t$$

Nickel, like the previous chemical elements, is found in a high percentage in the fraction < 0.6µm, at 57.5% (Fernández *et al*., 2001). The main origin of nickel is the combustion of combustible fossils, as it is found in petroleum in traces. The main sources of this contaminant are the power station and the petrochemical plant in the Grao de Castellón, located to the SE of the sampling point. This is the motive from which the model presents a direct relationship with the dominant wind direction. At directions between SW (225º) and NW (315º), the arrival of contaminants from the Grao del Castellón is favored and the nickel concentration levels increase at the sampling point. Nickel also presents a direct relationship with the temperature. The main emission sources of nickel, the power station and petrochemical plant, emit this contaminant in the form of airborne ashes and not in a gaseous state (Boix *et al*., 2001). These airborne ashes have a very fine grain size and the temperature influences their dispersion. At high temperatures there is greater atmospheric turbulence (Wark *et al*., 2000), and this fact due to a greater dispersion, making that these ashes arrive farther, and the nickel concentration levels increase in the sampling point, just as the model presents. Relative humidity is another significant variable in this model; it presents a direct relationship with the nickel. Higher relative humidity means greater condensation (McGregor, 1999), and increases the contaminant concentration levels.

Modeling Pb variable based on meteorological variables and PM10.
The *Pb* model is:

$$Pb = -5072.687 + 1.474 \times V\max - 0.175 \times DirDomi + 1.651 \times HR + 5.105 \times \Pr esion + \varepsilon_t =$$

$$= -5072.687 + 1.474 \times V\max - 0.175 \times DirDomi + 1.651 \times HR + 5.105 \times \Pr esion + 0.445 \varepsilon_{t-1} - 0.297 \varepsilon_{t-2} + a_t$$

Lead is the element that has greater concentration levels in PM10 than the other studied elements. Notwithstanding, the variation of its concentration levels with the PM10 variation is not sufficiently significant for this variable to appear in the proposed model. Just like the other chemical elements it is found to be associated with the finest PM10 fraction, 69.0% is found in the fraction < 0.6µm (Fernández *et al*., 2001). The main emission sources of lead are the ceramic industries located between the NW (315º) and SW (225º) from the sampling point. This contaminant presents an inverse relationship with the dominant wind direction and a direct relationship with the maximum wind velocity. It must be remembered that this element is heavier than those previous and in greater concentration, and although its emission source is closer than the previous elements, greater wind velocities will be necessary in order to displace it. This model also presents a direct relationship between the lead and the relative humidity and the atmospheric pressure. As was explained in the previous models, higher relative humidity favors condensation (McGregor, 1999), and with it an increase of the concentration levels of this contaminant. In the same way an increase in the pressure reduces the expansion of the lowest atmospheric layers,

and contaminant dispersion decreases (Wark *et al*., 2000), bringing concentration increases of them.

CONCLUSIONS

Some prediction models of the studied atmospheric contaminants have been developed, of easy application, and are presented as a useful tool in times of alerting the population from possible episodes of high contamination.
The independent variables, considered to be significant in the final prediction models, mark the importance of the types of anthropogenic emissions that occur in the study area, and the influence they exercise upon the concentration levels of the different atmospheric contaminants. Therefore, the variables of predominant direction and maximum wind velocity signal from which industrial park the contamination comes; the average temperature indicates the relationship with the types of industrial processes developed in the area, and this variable along with the atmospheric pressure and relative humidity mark the convective dynamic of the atmosphere that carry with them greater or lesser dispersion of the contaminants.

REFERENCES

Boix A.; Jordán M.M.; Querol X.; Sanfeliu T. (2001) Characterization of total suspended particles around a power station in an urban coastal area in eastern Spain". Environmental Geology 40:891-896.

Colombo J.C.; Landoni P.; Bilos C. (1999) "Sources, distribution and variability of airborne particles and hydrocarbons in La Plata, Argentina". Environmental Pollution 3:26-31.

Fernández A.J.; Ternero M.; Barragán F.; Jiménez C. (2001), "Size distribution of metals in urban aerosol in Seville (Spain)". Atmospheric Environment 35:2595-2601.

Gómez E.T.; Sanfeliu T.; Rius J.; Hernández D. (2001), "Caracterización granulométrica y mineralógica de la materia particulada atmosférica en el área cerámica de Castellón". Boletín de la Sociedad Española de Cerámica y Vidrio. (40) N3:185-194.

Jordan M.M.; Almendro, M.B.; Rimero, M.; Rincón, J.M. (2005). "Application of sewage sludge in the manufacturing of ceremic tile bodies". Applied Clay Sciences 30(3-4): 219-224.

Kubilay N.; Saydam A.C. (1995), "Trace elements in atmospheric particulate over the eastern Mediterranean; concentrations, sources and temporal variability". Atmospheric Environment 29:1352-1310.

McGregor G.R. (1999) "Basic Meteorology". In: air pollution and health. Eds. Holgate S.T.; Samet J.M.; Maynard R.L. Ed. Academic Press pp.21-49.

Pallarés S., Vicente A.B.; Jordán M.M.; Sanfeliu T. (2007). “Study of the levels of concentrations of As, Cd and Ni in a ceramic cluster”. Water, air and soil pollution. 180:51-64.

Querol X.; Alastuey A.; López-Soler A. Plana F. (2000) “Levels and chemistry of atmospheric particulates induced by spill os heavy metal minig wastes in the Doñana area Southest Spain”. Atmospheric Environment 34:239-253.

Rencher A.C. (2000). Linear models in Statistics. John Wiley.

Röösli M.; Theis G.; Künzli N.; Staenhelin J.; Mathys P.; Osglesby L.; Camenzind M.; Braun-Fahrländer Ch. (2002). “Temporal and spatial variation of the chemical composition of PM10 at urban and rural site in the Basel area, Switzerland”. Atmospheric Environment 35:3701-3713.

UNE-EN 12341:1999 Determinación de la fracción PM10 de la materia particulada en suspensión. Método de referencia y procedimiento de ensayo de campo para demostrar la equivalencia de los métodos de medida de referencia.

Vicente A.B.; Jordan M.M.; Pallarés S.; Sanfeliu T. (2007), “PM10 and Pb evolution in an industrial area of the Mediterranean basin”. Environmental Geology 51:1413-1424.

Wark K.; Warner C.F. (2000) “Contaminación atmosférica. Origen y control”. Ed. Limusa S.A.

Wei W.W.S. (1990). Time series analysis. Univariate and multivariate methods. Addison-Wesley.

Ecosystems health and geochemistry: concepts and methods applied to abandoned mine sites

[1]Hernández, A. J. and [2] Pastor, J.

[1] Dpto. Ecología, Universidad de Alcalá (Madrid). Edificio Ciencias, Campus Universitario. E-mail: anaj.hernandez@uah.es.
[2] Dpto. de Ecología de Sistemas. IRN, CCMA, CSIC, C/ Serrano 115, Madrid 28006. E-mail: jpastor@ccma.csic.es

ABSTRACT

This study is based on the premise that the good health of an ecosystem is essential for its sustainable development, introducing a new terminology for understanding pollution. Thus, the health of ecosystems is defined as an emerging science, or systemic approach, to prevent, diagnose and predict management features and establish relationships between the health of ecosystems and humans. It is within this framework that our experimental study was conducted on three sites situated in abandoned mines in the central Iberian Peninsula. The ecosystems present are mainly those of grazing pastures although cereals are also cultivated. In each of these settings, we find that soils contain more than one heavy metal in their top layers, particularly Cu, Zn, Pb and Cd. This pollution is punctate and affects both the plant populations of the sites and their consumers, with the possible transfer of pollutants to the river or groundwater systems, depending on the type of soil and geomorphological factors. We describe the protocol used to evaluate the health status of these ecosystems in terms of effects involving the geochemistry of the heavy metals they contain.
Keywords: heavy metals, pastures, punctate pollution.

INTRODUCTION: ECOSYSTEMS HEALTH IN THE CONTEXT OF SUSTAINABLE DEVELOPMENT

Thirty years ago, research into geochemistry and health commenced as one of the lines of Unesco's MAB (Man and Biosphere) programme (1978). However, we feel that in relation to ecosystems health, this line of research is practically new.
This study was not envisaged to only explore the response of plants to heavy metals (Barceló and Poschenrieder, 1992; Liphadzi and Kirkham, 2006), but to also address the so-called "ecodiseases" that heavy metals cause (Pérez, 2001). Many authors claim that there is currently a "silent pandemic" due to environmental pollutants, whose effects on persons are real yet difficult to measure (Ortega et al., 2005).
Here, we present the results obtained concerning pollution transfer via the food chain, along with a summary of related possible ecodiseases and a

proposed protocol for assessing this type of issue for use on abandoned mine areas.

MATERIALS AND METHODS

a) Study sites

Scenario 1: Garganta de los Montes. "Fernandito" is a copper mine in the Sierra de Guadarrama (Garganta de los Montes, Madrid) abandoned some 40 years ago, whose current landfill covers around 3500 m^3. The soils of the zone lie at heights of 1180 to 1200 m and have been classified by the FAO as humic and distric Cambisols. Given that the mine's main mineral is chalcopyrite, some of its Cu forms are due to its presence as mineral sulphur (Encabo et al., 1997). The main metals found are Cu, Zn, Cd and Pb.

Scenario 2: Guajaraz. This site includes the silver mine "La Económica" close to the Guajaraz River (Toledo, Spain). The site comprises the two geological domains: the migmatite domain of Toledo (in the N), mainly composed of homogenous granitoids and migmatites, and the Montes de Toledo domain (mainly in the S), harbouring Palaeozoic deposits of granitic influence. According to the FAO, the soils of the region are mainly distric Leptosols, although distric Cambisols close to the river and a poorly developed rendzic Leptosol also appear.

The orography of the mine site is flat with heights of 660 to 750 m. The mine was worked to a depth of 150 m and was exploited until 1990. Its landfills have volumes of around 25000 m^3. Pb and Zn appear at greatest concentrations in soils and alluvions.

Figure 1

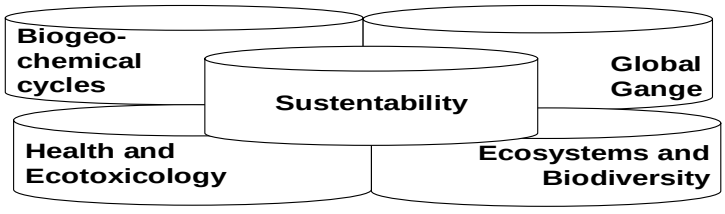

The site contains poor pastures, characteristic of this semiarid region. There are no trees, only shrub vegetation, and most of the land is used to cultivate cereals.

Scenario 3: Navas del Rey. The old "La Asturiana" barium mine situated north of the village Navas del Rey (SW Madrid province). It is one of the many mines existing in the Central System, north of Madrid exploited during the XIXth and XXth centuries. The legacy left behind by these mines is a series of dispersed landfills that act as a fairly unknown constant source of pollution. The mine was used to extract barite as ore until 1945. It occurs at the contact between a granite massif and the Escorial-Villa del Prado metamorphic complex (Peinado, 1970). Generically speaking, it is a biotite granite with feldspar phenocrystals. Barite sulphate appears in quartz seams at the highest altitudes, which appear tortuous and irregular and extend in depth and length up to a thickness of 1 m alongside bands of kaolin and clay that attain a thickness of 15 cm. The barite seams have associated sulphides, mainly zinc blende, calcopyrite and galena (Gutierrez et al., 1986). Besides the metals in the paragenesis (Pb, Zn, Cu, Ba and Fe), Cd is commonly found although in scarce quantities from isomorphic replacements in blende rich in galena and calcopyrite. The open mine was a 20 m–long, 2.5 m–wide and 2 m–high trench in the granite itself exploited through a well deeper than 30 m. Until the 1980s, medium-sized landfills were derived from the main well and its channels. From a perspective of landscape, the La Asturiana mine and its surroundings occupy a plain crossed by a stream. This promotes the dispersion of mine tailings through the actions of water and wind that interrupt natural cycles. The abundance of sulphides may have resulted in the dissemination of heavy metals via the drainage network (Gutierrez-Maroto et al., 1989).

b) Sampling and chemical analyses

The soils and plants of the mine sites were sampled by stratifying according to affected landfills and ecosystems. At each established sampling point, a mean soil sample was collected at random from the topsoil layer (0-10 cm) using a hoe. At the Garganta site, 38 sampling points were established in the mine area and adjacent zones. Total and bioavailable elements in the soil and plants were determined by inductively coupled plasma-optical emission spectroscopy (ICP-OES). For soil determinations, the samples were ground in an agate mortar and acid digests prepared using a 4:1 mixture of HNO3 and HClO4. Soil analyses (pH, OM, total N and soil anions) were performed according to Hernández and Pastor (1989). Metals were determined after grinding the soil in an agate mortar by X-ray fluorescence (XRF), plasma emission spectroscopy (PES) and through the action of acid using a 4:1 mixture of HNO_3 and $HClO_4$. Available metals were determined by the acetate-EDTA method (Lakanen and Ervio, 1971). Log-transformed data were analysed by calculating Pearson correlation coefficients (using SPSS 13.0 software).

RESULTS AND DISCUSSION

The Garganta site is crossed by a droving route. Its pastures, which are mainly grazed by cattle, show the most polluted soils of the entire mine site (Table 1). Plant cover is generally high (95% in pastures), and lower in the landfills (40% at the base) (Table 2). Of 32 pasture species examined (above-ground parts), all showed notable levels of Cu; half showed Ni; 14 species Cd; 10 species Cr and three Pb. Most species exhibited more than two heavy metals. Thus, although plant diversity is reduced by soil pollution, the behaviour of these grassland species is generally tolerant towards these metals with the consequent repercussions on the food chain. The distribution of metals in the superficial layer of soils from other two scenarios, neither is homogeneous (Table 3 and 4). Table 5 show 22 plant species that grow on Site 1 of the "La Económica" mine whit high concentrations of Zn, Pb and Cd.

Sites Garganta Mine	Zn	Cu	Pb	Ni	As	Cd
Reference Soil	103	46,5	99	8,0	-	<3
1	157	180	108	11,5	-	<3
2	110	135	70	8,5	-	<3
3 Refuse dump	147	150	107	10,5	23	<3
3	150	185	104	11,5	-	<3
4 Ash-trees plantation-a)	166	325	120	12,5	45	<3
5	204	845	190	18,0	-	10,5
6 Ash-trees plantation-b)	133	680	199	21,5	42	<3
7 Wet grassland 200m	118	770	135	15,0	21	<3
8 Wet grassland 430m	166	910	133	12,5	30	<3
9	133	225	136	16,0	-	7,5
10	246	3500	181	14,0	-	8,5
11 Wet grassland 420m	478	1950	123	13,0	-	18
12	149	295	118	17,5	-	<3
13	159	750	145	16,5	-	4
14	95	55	118	13,5	-	<3
15	70	30	134	15,0	-	<3
16 Wet grassland	361	1000	120	15,0	-	11,5
17 Wet grassland	202	1800	160	25,5	-	3,5
18	134	950	162	17,5	-	3,5
19	139	1000	165	14,0	-	<3
20	104	680	97	19,5		<3
21	100	385	115	14,0		<3

Table 1. Heavy metal levels on the "Fernandito" Mine area grasslands.

Logically, there are also differences between the values of total metals and available ones (see Table 6). Nevertheless, enough correlations have

been observed between metal levels in the superficial layer of the soils analyzed and diverse biodiversity parameters related with plant communities growing there. In the Table 7 can are shown a results for the scenario 3.

Botanical Family (Species No.)	Site 3	Site 4	Site 7	Site 11
Grasses	8	6	2	2
Legumes	2	7	3	2
Composites	6	6	2	0
Others	14	9	4	3
Total	30	28	11	7
Plant cover %	60	95	57	100

Table 2. Number of species of main botanical families found in inventories carried out in plant communities on the location of the "Fernandito" mine (Garganta de los Montes, Madrid).

Sites	Zn	Cu	Pb	Cd
1	5095	85	3855	37
2	2865	50	2430	11
3	835	19	1420	0
4	2940	46	2250	15
5	2290	22	1635	0
6	820	13	1205	0
7	1490	10	180	0
8	1005	20	1845	0
9	1585	23	1770	0
10	855	17	1220	0
Ref. Level	**200**	**50**	**50**	**1**

Table 3. Levels of heavy metals in different areas of the location of the "La Economica" mine (Guajaraz).

Descriptors	Soil 1	Soil 2	Soil 3	Soil 4	Soil 5	Soil 6	Soil 7	Soil 8	Soil 9 (C)
Zn XRF	796	469	134	223	191	169	106	104	55
Zn PES	771	237	96	158	133	104	72	75	37
Zn L&E	198	46	14	7.1	13	14	2.5	2.4	0.2
Pb XRF	618	75	290	80	92	89	57	67	29
Pb PES	105	2.4	249	115	91	13	111	122	11
Pb L&E	52	0.7	82	12	20	0.0	0.0	0.0	0.0
Cu XRF	215	47	35	55	43	48	19.7	21	25
Cu PES	170	26	14	33	18	26	5.0	4.6	12
Cu L&E	100	3.3	2.3	2.3	3.3	3.3	1.4	0.7	1.0
Cd XRF	17	2.7	1.1	0.3	1.1	2.4	0.0	0.0	0.0
Cd PES	5.5	1.4	1.1	0.7	0.7	1.1	0.0	0.0	0.0
Cd L&E	2.5	0.3	0.0	0.0	0.0	0.3	0.0	0.0	0.0
Ba XRF	74676	1140	1501	1608	1737	1193	673	686	602

Table 4. Levels of heavy metals (ppm) in different soils of the "La Asturiana" mine.

(C) Control Soil; XRF, X-ray fluorescence; PES, plasma emission spectroscopy; L&E: Lakanen and Ervio method.

Metals can be absorbed by plants or may be lost by leaching at greater soil depths and eventually reach groundwater sources. Moreover, soil erosion may determine that metals reach surface water courses. The importance of the different routes of transfer of these elements to other compartments of the food chains varies according to the metal, species present, or the use of the pasture land (plants consumed in situ by livestock or collected for forage or preparing feeds). Several studies have shown that animals reflect the concentrations of toxic elements when they graze on plants growing in polluted soils (Ronneau and Cara, 1984, Morcombe et al., 1994, Petersson et al., 1997). This highlights the need to control metal levels in terrestrial ecosystems. The FAO (2000), established threshold limits for Pb and Cd that were later adopted by the USA. It is generally admitted that Cd is highly toxic; Cu and Pb are considered toxic although the latter is moderately toxic for plants and highly toxic for animals; and Ni, Zn and Cr add to the list of metals causing toxicity. However, the knowledge we have of these issues is still scarce (Hapke, 1996), especially related to wild plant species. Ecotoxicological data on pastures are also scant.

Descriptors	Soil 1	Soil 2	Soil 3	Soil 4	Soil 5	Soil 6	Soil 7	Soil 8	Soil 9
Species No.	13.7	16.3	15.3	27.0	19.7	17.0	17.3	17.3	25.3
Plant cover %	40.3	47.7	64.5	59.7	127.8	46.2	51.2	41.8	84.0

Table 4. Biodiversity and plant cover mean values of plant communities (750 cm^2 plots) in the location of "La Asturiana" mine.

Species	
Agrostis castellana	*Dactylis glomerata*
Elysum granatense	*Diplotaxis catholica*
Andriala integrifolia	*Hirschfeldia incana*
Asparagus sp	*Melica cilliata*
Bellardia trixago	*Mentha rotundifolia*
Bromus rubens	*Plantago lagopus*
Cardus tenuiflorus	*Rumex bucephalophorus*
Cardus sp.	*Spergularia rubra*
Centaurea mellitensis	*Stipa sp.*
Chondrilla juncea	*Thymus zigis*
Crepis vesicaria	*Trifolium gemellum*

Table 5. Plant species growing in the site 1 of "La Económica" mine.

Specific heavy metals should be monitored since the results obtained for each of the mines indicate that they could pass to the food chain, from plants to herbivores, and to the humans that consume these animals (Hapke, 1976, 1991).

A pursuit will be made of concrete heavy metals that according to the obtained results for each one of the mines, can reach the trophic chain, from the plants to the herbivores and human populations that feed of them (Hapke, 1976).

Total Metals	Al	Fe	Mn	Zn	Cu	Cd	Ni	Pb
Scenario 1	28407	16100	515	190	1120	4,5	15,1	47,2
Scenario 2	25097	22600	1190	4675	404	25,4	29,9	6925
Available Metals								
Scenario 1	0,42	7,2	9,5	5,7	71,4	0,56	0,13	1,1
Scenario 2	0,12	6,4	7,4	129,2	34,7	0,98	0,36	137,6

Table 6. Total and available metals (ppm) in two soils of 1 and 2 Scenarios.

Metals	Species No.	Leguminosae No.	Compositae No.	Plant cover %
Zn XRF	- 0.430 (*)	- 0.182	- 0.349 (R)	- 0.349 (R)
Zn PES	- 0.448 (*)	- 0.294	- 0.295 r	- 0.328 (R)
Zn L&E	- 0.557 (**)	- 0.210	- 0.431 (*)	- 0.301
Pb XRF	- 0.600 (**)	- 0.427 (*)	- 0.323 (R)	- 0.275
Pb PES	- 0.113	- 0.262	0.032	- 0.069
Pb L&E	- 0.213	- 0.113	- 0.191	- 0.227
Cu XRF	- 0.313 (R)	- 0.224	- 0.139	- 0.226
Cu PES	- 0.241	- 0.120	- 0.117	- 0.181
Cu L&E	- 0.435 (*)	- 0.362 (R)	- 0.166	- 0.274
Cd XRF	- 0.533 (**)	- 0.326 (R)	- 0.284	- 0.313 (R)
Cd PES	- 0.348 (R)	- 0.209	- 0.229	- 0.272
Cd L&E	- 0.412 (*)	- 0.424 (*)	- 0.049	- 0.299
Cr XRF	- 0.332 (R)	- 0.371 (R)	- 0.047	0.201
Ni PES	- 0.289	- 0.134	- 0.089	- 0.171
Ba XRF	- 0.389 (*)	- 0.387 (*)	- 0.113	- 0.214

Table 7. Correlations between several biodiversity markers and plant cover for the plant communities and pseudototal (2) and bioavailable metal contents of the soils from the abandoned barium mine site.

*** significant at the level 0.001; ** significant at the level 0.01;
* significant at the level 0.05; R reliable at the 90% significance level

In the following section, using the terminology employed by Pérez (2001) we discuss the "ecodiseases" caused by metals that were found to be most closely related to the geochemistry of the soils examined.

Cadmium in nature, is found associated with other elements, especially Zn, Pb and Cu. It is among the most toxic elements, passing through plants to the food chain. Cd is a cumulative metal. In plants, Cd has effects on chlorophyll function (wilting, necrosis, leaf chlorosis), inhibiting photosynthesis and carbon dioxide fixing, which leads to the short-term death of species. In agricultural practice in this region, P fertilizers are used, and although it is known that these reduce the bioavailability of heavy metals, this is not true for Cd. Moreover, plants take up this metal more when the soil Zn content is low (Liphadzi and Kirkhan, 2006).
The toxic effects of Cd are much worse in plants and herbivores, with no Cd-related ecodiseases in carnivores detected to date. In humans, Cd can persist in the body and accumulate after many years of exposure to low levels. Eating foods containing Cd severely irritates the stomach, leading to vomiting and diarrhea. Its build-up in the body can cause damage to the kidneys, lungs and bones (Hapke, 1991).

Lead is a significant toxic element owing to its dispersion in nature. Pb is mainly generated during soil degradation and weathering of mineral deposits, although the most notable Pb pollution is provoked by anthropogenic actions. Transport of soil Pb to groundwater depends on the type of Pb compound and the characteristics of the soil. Plants may absorb this metal relatively easily and mainly store it in the roots. Thus, the risk of Pb poisoning is particularly evident when it affects certain bulbs, beetroot, potatoes, onions etc. Some animals have a special capacity to accumulate Pb with no detectable effects including the earthworm. This determines that the current use of this species, for instance, to prepare feeds in fish and poultry farms, is a dangerous practice.
Both in humans and animals, chronic Pb poisoning manifests as a reduction in body growth (reduced height). As an ecopathogen, its effects on both the peripheral (extensor muscle damage, sensory disorders, increased pain sensitivity) and central nervous system, (mainly memory loss and encephalopathy), particularly in children, are well known. However, this heavy metal may affect almost every organ of the body (especially the kidneys and male reproductive system).

Zinc is an essential micronutrient, considered non-dangerous, although it may become toxic; its toxicity may increase in the presence of arsenic, lead and cadmium. On the contrary to other heavy metals, Zn is usually gradually lost throughout the food chain. Its toxic effects on plants include

chlorosis, which can in turn cause deficiencies in Mg or Fe, essential nutrients for all organisms.

Copper is another essential trace element well known for its toxic effects on beans and legumes in general. Its detrimental effects include cytoplasm membrane damage in plant and animal cells. According to the literature, Cu has been recently the most widely investigated metal in relation to its toxic effects on legumes (Bunzl et al., 2001; Cuypers et al., 2005). A study by Hernández et al. (2006) demonstrated high Cu levels in the fruits of cultivated legumes. The Zn contents of these fruits were also high, and the dry weight of the plant reduced. This latter finding has also been reported by Miyazawa et al. (2002). According to Adriano (2001), a Cu level of 2 to 250 ppm can be toxic for cultivated plants and given that, along with Zn, this nutrient is supplied in the diet by legumes, levels reached in their fruits could provoke toxic effects.

Manganese toxicity is due to its absorption by plants in soils of low pH containing Al (Hernández, 1986 and 1987). Although the soils of the present study area are basic, their Al contents are high such that we propose further work should be conducted on the possible toxic effects of both these metals.

The water-soluble components of **Cr VI** are highly toxic. Chromium tends to accumulate in roots, although toxic effects on the respiratory tract have been reported (INERIS, 2004), since this metal builds-up in the food chain.

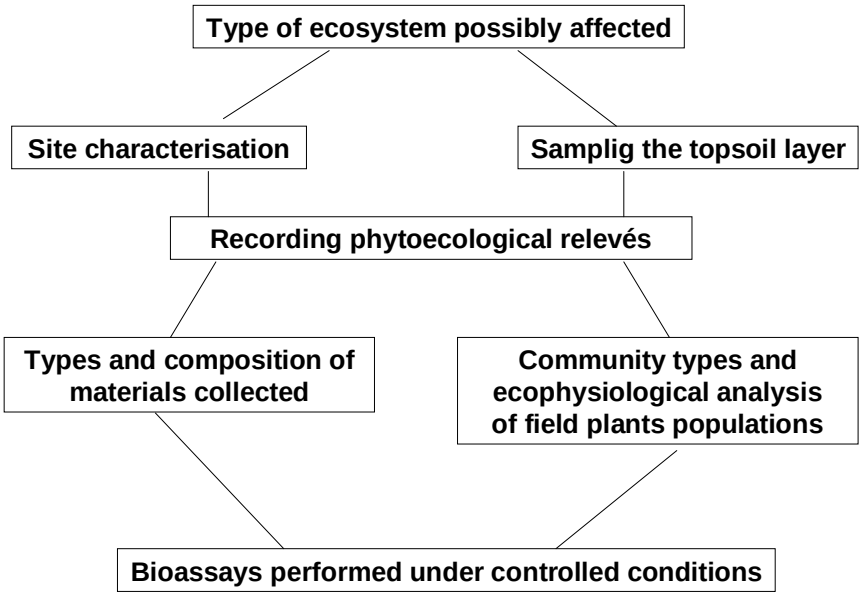

Figure2. Protocol

Nickel, which is produced by the build-up of urea in legumes, may be toxic at plant levels above 10 ppm. Ni inhibits meristem cell division and limits the spreading of roots (Liphadzi & Kirkhan, 2006).

Arsenic is used in pesticides and slowly accumulates since although highly absorbed it is excreted in the urine. In conditions of humidity, moulds in soil convert As into highly toxic gasses. According to the EPA (USA Environmental Protection Agency), the dangers of As for humans may be linked to waters and fish but rarely to soils or to domestic animal excretory products. Although most plants tend to exclude As from their above-ground mass, they accumulate the metal in their roots (Landis & Ming-HoYu, 1999). The ecodisease due to this metal produces vomiting, abdominal pain and even death. Epidemiological evidence for its carcinogenicity has been obtained in experimental animals (lung tumours produced by inorganic As compounds).
Lastly, in the figure 2, is shown the protocol that has been deduced as important to carry out the study of the relationship between the geochemistry and the health of ecosystems.

CONCLUSIVE ASPECTS

The diagnosis of soil pollution in relation to the most commonly used remediation methods is an innovative way of tackling this problem. To this end, the theoretical framework of Ecosystems Health has been instrumental, since this area is presently emerging as a new language for general discourse on pollution. For example, the use of the term stressor

for a pollutant implies the study of behavior responses in living organisms (at different levels of organization, from the cell to ecosystem) both in terms of impacts (toxicity) and tolerance towards the pollutant (their adaptation).
We focused on the autotrophic component of the affected ecosystems for several reasons: toxicity tests could be used to examine the physiological and behavioral responses of organisms (mortality, injury, metabolic changes) as well as population (population density, risk of extinction) or community (structure, diversity, biomass, nutrient flow changes) variables. The build-up of a heavy metal in the above-ground part of a plant (phytoaccumulation) consumed by herbivores is also detrimental for health, due to transfer to the trophic network. Root systems may play a role in phytostabilizing heavy metals and in preventing them from passing to deeper soil layers. Finally, given the erosion problems of fine materials in landfills and waste tip slopes, vegetation helps avoid the movement of topsoil layer pollutants to other ecosystems.
The methodological approaches validated by results obtained over the last twenty years can be summarized as: studies of polluted sites based on phytoecological sampling, analysis of soil chemical and physical properties, georeferencing of the heavy metals they contain for further sampling in areas showing the highest levels, collecting and chemically analyzing plants at these sites, and the use of soils with their seed banks to perform experiments on microcosms in controlled conditions. The idea is to use a combination of field and laboratory methods that simulate real scenarios in which soil pollution occurs.

***Agradecimientos**:* al Programa EIADES de la CM y Al Proyecto CTM2005-02165/TECNO del MEC.

REFERENCES

Adriano, D. C. 2001. *Trace elements in the terrestrial enviroment*. Springer Verlag.
Barceló, J. & Poschenrieder, Ch. 1992. Respuestas de las plantas a la contaminación por metales pesados. *Suelo y Planta*, 2, 345-361.
Bunzl, K. *et al.* 2001 Availability of Arsenic, Copper, Lead, Thalium and Zinc to various Vegetables Grown in Slang-Contaminated Soils. *Journal of Environmental Quality* 30, 934-939
Calow, P. 1995. Ecosystem Health. A critical analisis of concepts. In: *Evaluating and Monitoring the Health of Large-Scale Ecosystems.* NATO ASI Series, vol. 138, Springer-Verlag, Berlín, 33-41.
Cuypers, A. *et al.* 2005. Analysis of bean (*Phaseolus vulgaris* L.) proteins affected by copper stress. *Journal of Plant Physiology*, 162,383-392.
Di Gulio, R. T.& Monosson, E. 1996. *Interconnections between Human and Ecosystems Health.* Champman & Hill.
Encabo, C. *et al.* 1997. Evaluación de la dispersión de metales pesados del entorno de una mina, mediante el método de especiación secuencial

química. Boletín geológico y minero, Instituto Tecnológico Geominero de España.
Gutierrez, A. *et al.* 1986. Mineralizaciones de baritina y fluorita con sulfuros asociados del SO de la Sierra del Guadarrama. *Mat. Proc. Geol.* IV. 103-126.
Gutierez-Maroto, A. *et al.* 1989. Dispersión de elementos pesados y su incidencia en el medio natural. *Boletín Geológico y Minero*, 100-105, 886-896.
Hapke, H. J. 1976. Heavy metals transfer in the food chaín to humans. C. R. Barrueco (ed). *Fertlilizers and Enviroment*Kluwer Acad Publ, 431-436.
Hapke, H. J. 1991. Metal accumulation in the food chain and load of feed and food. In: E. Merian, Ed., *Metals and their Compounds in the Environment*, VCH, New York, USA, 469–489.
Hernández A. J. & Pastor, J. 1989. Técnicas analíticas para el estudio de las interacciones suelo- planta. *Henares, Rev. Geología,* 3, 67–102.
Hernández, A. J. *et al.* 2006. Estudio de la nutrición mineral de *Phaseolus vulgaris* L. en suelos de cultivo que contienen metales pesados. En: *Nutrición Mineral. Aspectos fisiológicos, agronómicos y ambientales,* C. Lamsfus, Ed. Universidad Pública de Navarra, Pamplona, 573-580.
Koptsik, S. *et al.* 2003. Heavy metals in soils near the nickel smelter: Chemistry, spatial variation and impacts on plant diversity. *Journal of Environmental Monitoring*, 5. 441-450.
Lakanen, E. & Ervio, R. 1971. A comparison of eight extractants for the determination of plant available micronutrients in soils. *Acta Agriculturica Fennica* 123, 223-232.
Liphadzi, M. S. & Kirkhan, M. B. 2006. Physiological Effects of Heavy Metals on Plant Growth and Function. In: *Plant-Environment Interactions*. B. Huang (ed). Taylor and Francis, New York, 243-269.
Morcombe, P. W., *et al*.1994. Cadmium concentrations in kidneys of sheep and cattle in Galicia (north-western Spain*). Veterinary Journal*, 160, 259-266.
Miyazawa, M. *et al.* 2002. Absorption and toxicity of copper and zinc in bean plants cultivated in soil treated with chicken manure. *Water, Air, and Soil Pollution* 138, 211-222.
Ortega, J. A. *et al.* 2005. Neurotóxicos medioambientales (II). Metales: efectos adversos en el sistema nervioso fetal y posnatal. *Acta Pediatrica Española*, 63, 182-192.
Peinado, M. 1970. Carácter del metamorfismo en el macizo metamórfico El Escorial-Villa del Prado (Sistema Central Español*). Estudios Geológicos* 26, 323-326
Pérez, F. 2001. Ecopatologías: influencia en la salud pública y sanidad animal. *Anales de la Real Academia Nacional de Medicina,* CXVII, 137-170.
Pérez, L. *et al.* 2004. Índices de acumulación de metales pesados en granos y hojas de trigo. *www.schironia.com Nº 3-Julio.*
Petersson, K. P. *et al.* 1997. Cadmium levels in kidneys from swedish pigs in relation to environmental factors-temporal and spatial trends. *Science of the Total Environmen*t, 208,111-122.

Rapport, D. J. et al. (Eds.) 2003. *Managing for Healthy Ecosystems.* Lewis Publishers USA.
Ronneau, C. & Cara, J. 1984. Correlations of element deposition on pastures with analysis of cows´ hair. *Science of the Total Environment*, 39, 135-142.
UE 2004. Proposal for a directive of the European Parliament and of the Council establishing a framework for the protection of soil and amending Directive 2004/35/EC. Commission of the European Communities, Brussels.
UNESCO, 1978. *"La Naturaleza y sus Recursos":* Boletín del programa MAB XIV, 1-14.